Anal. Methods Environ. Chem. J. 7 (3) (2024) 5-20

AMECJ

Research Article, Issue 3
Analytical Methods in Environmental Chemistry Journal
Journal home page: www.amecj.com/ir

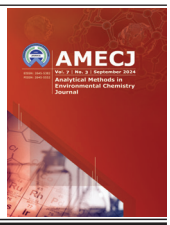

Bioanalytical Method: Determining pesticide residues in tomatoes and mushrooms by a bioactive membrane-based sensor, enzyme inhibition, and UV-Vis Spectrophotometry

Geetu Gambhir[a,*], Sunita Hooda[b], Ms. Laishram Saya[c] , and Ms Drashya[d]

[a*]*Associate Professor in Chemistry, Acharya Narendra Dev College, University of Delhi, New Delhi, India.*
[b]*Professor in Chemistry, Acharya Narendra Dev College, University of Delhi, New Delhi, India.*
[c]*Assistant Professor in Chemistry, Sri Venkateswara College, University of Delhi, New Delhi, India.*
[d]*Research Scholar, Polymer Chemistry Laboratory, Acharya Narendra Dev College, University of Delhi, New Delhi, India.*

ARTICLE INFO:

Received 1 May 2024
Revised form 15 Jul 2024
Accepted 12 Aug 2024
Available online 30 Sep 2024

Keywords:
Bioanalytical method,
Bioactive membrane based sensor,
Pesticide residues,
Tyrosinase and pyrocatechol,
Enzyme inhibition,
UV-Vis spectrophotometry

ABSTRACT

Pesticides play a vital part in crop production. The present study intends to develop a bioactive membrane-based sensor based on enzyme inhibition for determining pesticide residues. The absorbance (AU) of samples is determined by UV-Vis spectrophotometry. It also aims to study the stability of the enzyme extract at various concentrations. To immobilize the enzyme, different mediums like cellulose, chitosan, guar gum, and cellulose with guar gum are considered for finding an effective membrane. Findings reveal the efficiency of the biosensor in detecting the pesticide residues from tomatoes and mushrooms by finding tomatoes with 0.01M Malathion showed a high absorbance rate of 0.97, 20 times diluted Tyrosinase extract from mushrooms showed maximum absorption of 0.55, and aluminum oxide in tomatoes has explored an absorbance rate of 0.96 at 0.1M concentration. So, the aluminum oxide in tomatoes has explored a high absorbance rate. The LOD, LOQ, RSD, linear range and sensor recovery were obtained for different pesticides. The RSD (%), LOD, and LOQ for these pesticides are obtained at (1.155, 1.81, 2.09 mmol L^{-1}), (3.81, 5.973, 6.897 mmol L^{-1}), and (11.55, 18.8, and 20.9 mmol L^{-1}), respectively. The linear ranges are 2, 6, and 20 mmol L^{-1}. Then, the outcomes of Tyrosinase activity inhibition were obtained through absorbance of different pesticides.

1. Introduction

Pesticide is the common term for the substances utilized for poisoning pests like insects, rodents, weeds, etc. Pesticides that are harmful to human beings are rodenticides and insecticides. Farmers generally use synthetic pesticides due to their simple application, widespread availability, efficiency, and economic returns with more environmental costs. Recently, the residues of toxic pesticides in food samples and groundwater have enhanced public concerns, particularly in association with children's health [1]. Due to the increased utilization of pesticides over the last few years, the possibility of disclosing these toxic chemicals has also found considerable improvement. Currently, the use of pesticides has found significant enhancements in satisfying the demands of people due to rapid population development. This is because more

*Corresponding Author: Geetu Gambhir
Email: geetugambhir6@gmail.com
https://doi.org/10.24200/amecj.v7.i03.255

food has to be produced due to an increase in the number of pesticides used in agriculture in the community It resulted in high farm productivity for which the farmers employed pesticides. Various reports stated the prime pesticide levels in the food could lead to the improvement of diseases such as kidney, lung, and cancer ailments. Based on the reports of the WHO (World Health Organization), every year, nearly 30,00,000 cases of people are getting poisoned by pesticides with 2,20,000 deaths, especially in developing countries [2]. Moreover, 2.2 million individuals, mainly from evolving countries have been exposed to a high risk of pesticides [3, 4]. Traditional research tried to study the detection of pesticide residues. Accordingly, a perspective on using pesticides in the agricultural area has been afforded to find the pesticide's impact on the environment and food production. Hence, it has been vital to emphasize the significance of finding the residues of pesticides in food aiming to confirm food safety as these compounds could indicate the risks associated with the environment and human health [5, 6]. It has also been exposed that the mass spectrometry and chromatographic methods support finding the pesticide residues for assessing the food quality which reached customers along with MRLs (Maximum Residue Limits) laid by each country's legislation, these instrumentations turn to manage the population exposure to pesticides [7]. Though MRL has been utilized as the food quality parameter, global variations in the pesticide legislation do not guarantee the safety of consumers. For the diet of human beings, vegetables, and fruits have been an essential part as they possess essential nutrients needed for a normal human to react to several reactions within their body. Persisting pesticide usage has resulted in several issues including the health of humans. To maintain losses and manage the standardization of these vegetables and fruits, harvest pesticides have been used. The main intention of the conventional research has been to find the quality of pesticides existing in these foods by computing the normalized variation of vegetation index through the sensor. The process has been undertaken in two fragments. The initial part identifies the vegetables and fruits through the usage of a Convolutional Neural Network (CNN) by training it with the image feature sets like shape, texture, and color. In the subsequent module, the pesticides in these vegetables and fruits have been detected through three manners for computing its Normalized Difference Vegetation Index (NDVI) through the usage of a gas sensor and IR sensor. Then, the comparison has been undertaken. Arduino program afforded the output. Information that has been detected will be shown on the screen. Following this, the graph has been plotted. It has been concluded that the gas sensor provides high accuracy for pesticide detection [8]. Analysis has been undertaken to review rapid pesticide detection approaches involving enzyme inhibition, fluorescence sensor, biosensor detection, spectrophotometric and chromatographic analysis, which has examined the progressive status. It has been summarized that the rapid detection method has become faster and highly extensive [9, 10]. A Fluorometric-atrazine assay relying on N-GQDs and Tyrosinase inhibition has been developed. This Tyrosinase includes a copper-comprising enzyme of the animal and plant tissues that catalyzes melanin production and supplementary pigments from the Tyrosine through oxidation like the blackening of sliced or peeled potatoes that have been exposed to air. It has been found within the Melanosomes. In the molecular-biology, Tyrosinase indicates an oxidase that indicates the enzyme limited by rate to manage melanin production [11]. Tyrosinase carries phenol oxidation, such as pyrocatechol, using di-oxygen and Tyrosine. In Tyrosinase existence, benzoquinone has been formed from the Cathecol, and the structure of Tyrosinase is shown in Figure 1.

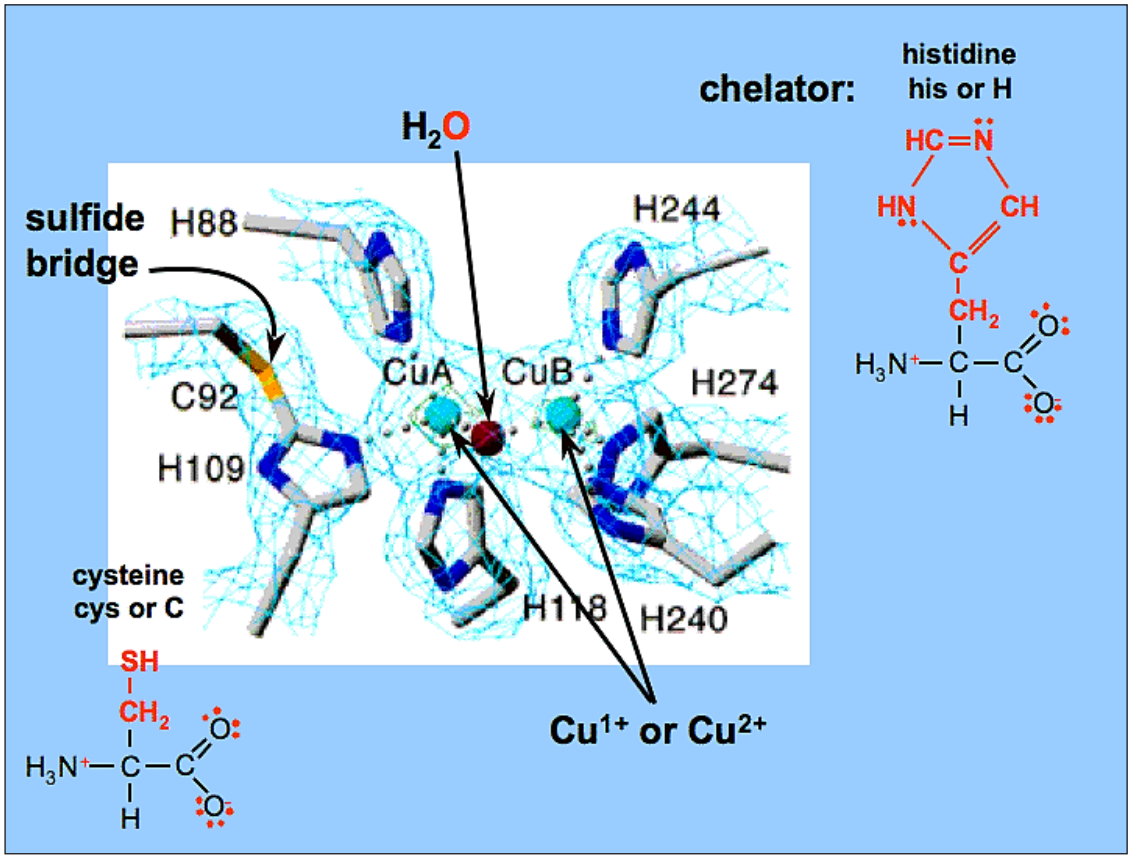

Fig.1. Structure of Tyrosinase

NGQDs have been synthesized through hydrothermal reaction by applying ammonia and citric acid. The tyrosinase-driven dopamine oxidation reaction produced dopaquinone, which could effectively reduce N-GQDs fluorescence by the dynamic quenching method. Tyrosinase inhibitor named atrazine could alleviate enzymatic reaction by declining the Dopaquinone generation resulting in fluorescent recovery that depends on the atrazine concentration. The recent identification of the metabolite or parent compounds has impacted the pesticide analysis rate, thus instigating the request for methods to compute minimum concentration levels [12].

In addition, current knowledge regarding the detection and isolation of pesticides in fatty commodities has been analyzed. Several isolation methods have been discussed such as solvent partitioning, dispersive solid-phase, and solid-phase, matrix solid-phase dispersion, gel-permeation chromatography, accelerated-solvent extraction, micro-extraction methods, Soxhlet extraction, and QuEChERS-based methods. The chromatographic techniques pre-dominate the pesticide residue analysis in the fatty matrices. Due to this, the analysis concentrates on these methods, especially those integrated with mass spectrometry. Still, analytical chemists face issues in determining pesticide residues in the fatty matrices to develop quick and simple ways that consume minimum organic solvents. Until now, various methods have been introduced to extract and detect pesticides from conventional to progressive detection methods [13-15]. A comprehensive review of accessible traditional methodologies (liquid chromatography integrated with several detectors and gas chromatography) to advanced pre-treatment (magnetic nano-particle coated with polystyrene) and detection (nano-technology and sensor development) methods utilized in pesticide residue analysis in several vegetables and fruits have been analyzed.

Though the detection and extraction systems options remain similar, these methods have been expensive and time-consuming [16]. In recent years, advanced methodologies like biosensors [17], nanotechnology, and molecular-imprinted polymers have been used as an alternative to detect pesticides. Progressive enhancement of biosensors has been explored to detect dichlorvos pesticides, from the usage of traditional immobilizing assistances to highly promoted composite or hybrid nanomaterials. Further, biosensor development has been summarized through enzyme inhibition methodologies wherein enzymes like Tyrosinase, AChE (Acetylcholinesterase), etc have been immobilized on transducer by conventional immobilization methodologies or applying advanced nanomaterial to integrate in a better manner [18]. A six-stage method has been explored for designing the enzyme sensors aimed at evaluating the complex matrix quality. This has to be followed to accomplish maximum probable biosensor sensitivity to probable toxic substances for reducing the impact of uncontaminated complex mixture elements on the biosensor activity. Testing has been performed with the endorsed approach to outline a bio-luminescent biosensor to integrate rapid evaluation of vegetables and fruit safety. Techniques and methods have been described to attain the desired outcome in the individual stage. It has been found that the six-stage technique to design the bio-luminescent enzyme biosensors could be utilized for designing the enzyme-based sensors relying on several other enzymes [19]. Traditional studies were undertaken on biosensors to inhibit enzymes to find the carbamate pesticides and organophosphorus compounds, which have been reviewed [10, 20, 21]. Biosensor sensitivity has been enhanced by including effective immobilization methodologies like thin-polymer films and self-assembled monolayers. Additionally, a computational model framed from perceived data relies on varied inhibition approaches with diverse inhibitors that assist to classify and find pesticides in real-time samples concurrently. Likewise, critical analysis has been emphasized between 2015 and 2019 along with to date overview of analysis methodologies and extraction techniques in detecting the residues of pesticides in several food samples [22]. Theoretically, pesticide residues existing in food might metabolize and generate new chemical substances while processing food. Thus, research is essential for biosensor development that could be utilized for detecting the pesticide's existence during the pre-processing stage [23]. Consequently, pesticide detection through biosensor technology has been a promising area, and efficient products are expected to be developed for huge employment in the future [24, 25]. It has also been vital to estimate the existence of these toxic chemicals in daily food constituents beyond the tolerable limit. Also, the organic compounds such as VOCs and pesticides can be determined by different techniques such as gas chromatography, UV-Vis and HPLC in different matrixes [26-31]. To attain efficient knowledge, the present study aims to generate enzyme-based bioactive sensors for sensing the existence of pesticides in fruits and vegetables consumed regularly. To accomplish this, the study considers extracting Tyrosinase (enzyme) from food samples. In this study, tomatoes and mushrooms are considered as samples and the enzyme inhibition rate with various metal inhibitors and pesticides is researched to find the effectiveness of the system in the detection of pesticide residues.

2. Experimental

The research aims to develop bioactive membrane-based sensors to determine pesticide residues. Though conventional works attempted to detect pesticide residues, they have been ineffective and time-consuming. Thus, the present work performs experiments based on the below steps to prepare the membrane. Absorbance (AU) and transmittance (%) are measurements used in spectrophotometry (Cary 4000, Agilent, USA). Spectrophotometry UV-Vis measures how much radiant energy a sample absorbs at varying wavelengths of light between 175-900 nm. The UV-Vis technique determined the concentration of pesticide residues in solutions after calibration by standards.

2.1. Experimental procedure to prepare membrane

In this section, tyrosinase from two detected sources tomato and mushroom were extracted. The stability of enzyme extraction at varied pH and temperatures was also studied. In addition, immobilizing the enzyme extracts on different mediums such as chitosan, guar gum, and cellulose was done and the integration of the two in diverse ratios as well as its standardization to use further. The enzyme activity with diverse indicators utilizing the colorimeter studied and enzyme inhibition through different metal ions and pesticides with the utility of standardized indicators was obtained. Casting an immobilized enzyme membrane on ideal solid support was evaluated.

2.1.1.Extraction of Tyrosinase

2.1.1.1.Extraction of Tyrosinase from tomato

First, 300 g of tomatoes are added to a blender with 300 mL of sodium fluoride (NaF). Then, a tomato is peeled and cut into 1-inch squares. After this, it is homogenized for one minute at high speed. The mixture (homogenate) is poured through various cheesecloth layers into the beaker. The volume of the obtained mixture is measured. Following this, an equal amount of aluminum sulphate is added. This led to the appearance of a fluffy white precipitate as several early soluble proteins of tomato became insoluble. A tyrosinase enzyme is one of these proteins, thus, it is found later in the precipitate [32]. The above mixture is partitioned into chilled centrifuge tubes. This is then centrifuged at 3000rpm at 4°C. Subsequently, centrifuge tubes are carefully collected and poured off. Then, the fluid is discarded and the pellets are saved. All pellets are integrated into a 100ml beaker. A citrate buffer of 60 mL is integrated into the pellets. Contents are stirred well. Following this, a glass rod is utilized for breaking the pellet to preserve its coolness. This solution is again partitioned into the centrifuge tubes. This is again centrifuged at 3000 rpm for five minutes at 4°C. The supernatant is gathered and then saved. It includes the extracts of the enzyme. This is then positioned in volumetric flasks and the enzyme extracts are labelled and placed in the ice bucket.

2.1.1.2.Extraction of Tyrosinase from Mushrooms

Mushrooms are dissected into small parts. It is then weighed for 30 g. Each mushroom cube is wrapped into a separate [33] Aluminium foil. After some time all the foils are removed and the mushrooms are put into a blending flask. 50 ml of the Tris solution containing NaF is added and blended for 1 minute and 3 times. The blended mixture is filtered through a fritted funnel and the filtrate is fed into a conical flask. The mouth of the flask is covered with Aluminium foil and immediately put into an ice bucket full of ice.

2.1.2.Study of enzyme extraction stability at varied pH

To study the stability of enzyme extraction at different pH and temperatures, a Tris buffer is made with NaF solution based on the below procedure[34]. We used this powder (0.605 g), HCl (1 N), NaF solution (0.1 M), and distilled water. To prepare 1 N HCl, we added 11 ml distilled to 1 mL HCl. The preparation of 0.1 M NaF solution was done by adding 0.295 g of NaF to 50 ml of distilled water. So, the tris solution prepared by 2 gm of tris dissolved in 50 ml distilled water and the final tris solution containing NaF prepared by 12 ml HCl solution is added to the prepared Tris solution. The above mixture is Tris buffer. Then, 25 ml of Tris buffer and 25 ml of 0.1 M NaF solution are taken in a conical flask and mixed correctly. This has given 50 ml of the above solution.

2.1.3.Preparation of membranes

Due to Schema 1, membranes like guar gum, cellulose, chitosan, and a silica gel layer are also prepared to stabilize the enzyme activity. This preparation is achieved using the procedure below.

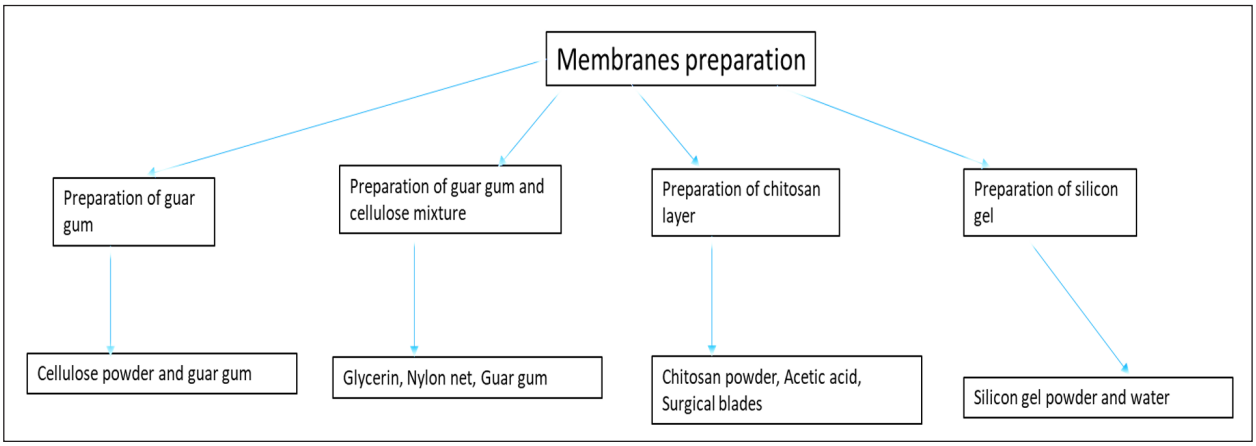

Schema 1. Preparation of membranes like guar gum, cellulose, chitosan, and silica gel layer

2.1.3.1. Preparation of guar gum

The guar gum is prepared with 2 g of guar gum powder which is weighed and put in a 400 ml beaker and 4 ml of Isopropanol is added to it and stirred properly. Then, 200 ml of distilled water is added and stirred vigorously until dispersed uniformly. The mixture is divided into two parts into two separate beakers. One beaker is placed in a water bath for 10 minutes. After ten minutes, it is labelled as a heated one and another mixture remains as such.

2.1.3.2. Preparation of guar gum and cellulose mixture

In the mixtures, the cellulose powder is added and it is mixed well so that the cellulose gets mixed completely with guar gum. The consistency is checked according to the below procedure.

2.1.3.3.Preparation of guar gum – cellulose membrane

The guar gum-cellulose membrane is prepared by a ratio of 3:2. A few glass slides are taken, and the nylon net is cut into small pieces of slide dimensions. Then, some glycerin is spread over the glass slides completely. The nylon net is kept on each slide and the guar gum and cellulose mixture are spread over the slides containing the nylon net. Then, it is left for 24 hours to dry, and the formed membrane is finally removed.

2.1.3.4. Preparation of chitosan layer

The chitosan layer is prepared with 2 g of chitosan powder is weighed and put into the beaker. Then, 50 ml of the distilled water is added and the chitosan powder is dissolved properly in it and 1 ml of Acetic acid is added to it which makes the mixture viscous. At that moment, it is stirred for half an hour until all the bubbles are removed from it. Then, the mixture is spread in a petri dish and left undisturbed for 24 hours for drying. Finally, it is removed through surgical blades from a Petri dish.

2.1.3.5.Preparation of silica gel layer

The silica gel layer is prepared using some amount of silica gel powder and added to distilled water. It has been mixed until the required consistency is obtained. If required, silica gel or water is added to it. Then, the above mixture has been spread over the glass slides. It is kept undisturbed until it dries completely. Finally, the silica gel layer is ready for further tests [35]

2.1.4. Immobilization of the enzyme extracts

Immobilization indicates the enzyme attachment [36] onto an inert and insoluble material that could afford high resistance to alterations in different conditions like temperature or pH. This permits enzymes to hold it throughout the reaction, this is followed by easy separation from corresponding products that might be utilized again. It is an effective method and is widely employed in industries for catalyzed reactions of the enzyme. The immobilized enzymes are highly significant for commercial usage due to their benefits for

processing reactions. The main advantages of these enzymes are economy, convenience and stability. As an economic advantage, the immobilized enzyme could be easily partitioned from the reaction making it easy to recycle the bio-catalysts. For convenience, the small quantities of protein get dissolved in reactions so that the workup could be easier. After completion, the reaction mixture usually comprises only the reaction and solvent products. As a stability advantage, the immobilized enzymes possess high operational and thermal stability in comparison to soluble immobilization which indicates the enzyme attachment to the inert and insoluble material. It could afford enhanced resistance to alterations in conditions like temperature or pH. This permits enzymes to be detained in a position throughout the entire reaction. Then, these are separated easily from products and enzyme forms. Also, three effective approaches exist for enzyme immobilization adsorption, entrapment and cross-linkage. Due to adsorption, attachment of enzyme to the exterior of inert material occurred. Generally, this methodology is slower than the entrapment and entrapment process. As absorption is not a chemical reaction, the active site corresponding to the immobilized enzyme might be blocked through a bead or matrix greatly minimizing the enzyme activity. The structure of Tyrosinase exploring its active site is shown in Figure 2.

Two copper atoms within the active site of the Tyrosinase enzymes communicate with the di-oxygen to form highly reactive chemical intermediation that oxidizes the substrate. Tyrosinase activity is identical to the catechol oxidase that is associated with the copper oxidase class which is collectively called polyphenol oxidase. The other effective approach for enzyme immobilization is entrapment. In the entrapment, the enzyme is confined to the microspheres or insoluble beads, such as a calcium alginate reaction. Nevertheless, this insoluble material hinders the substrate arrival and product exit. Also, cross-linkage is another effective approach for enzyme immobilization.In the cross-linkage, covalent bonding of enzyme to the matrix is performed by a chemical reaction. It is more

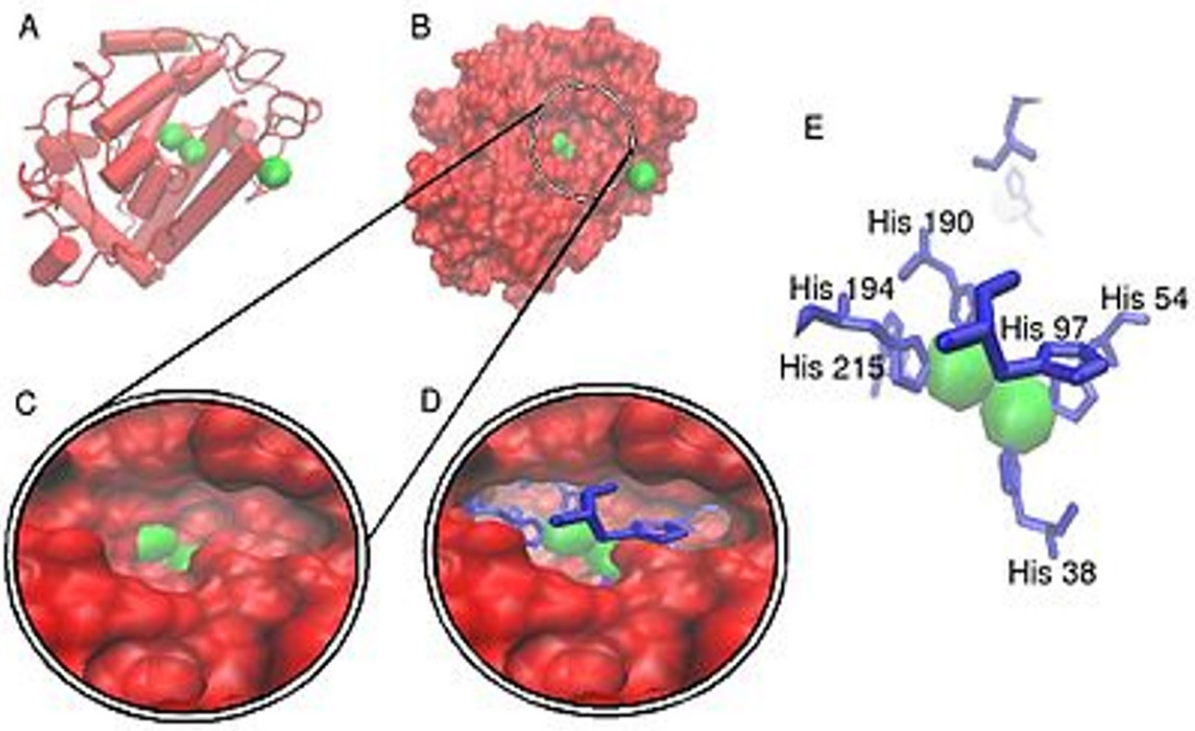

Fig. 2. Active sites of tyrosinase structure

efficient than entrapment and absorption. Chemical reaction confirms that the binding site does not cover the active site of the enzyme, enzyme activity is only impacted by immobility. Nonetheless, covalent bond inflexibility impedes self-healing features explored through the chemo-absorbed and self-assembled monolayers.

2.1.5.Immobilization of the Tyrosinase extract on the different layers

The layers prepared (chitosan, guar gum, cellulose, and integration of two in diverse ratios) are then embedded with Tyrosinase by pouring the enzyme extract of the most active concentration over them [37]. It has been left undisturbed at a low temperature for 10 -12 hrs. The enzyme gets adsorbed over the layer to retain its properties. So, chitosan, guar gum, and cellulose are explained below.

Chitosan is a functional linear polysaccharide that can be produced from the N-Deacetylation of chitin. It is a biopolymer comprised of N-acetyl glucosamine and glucosamine units comprised of glycosidic linkages. Due to the amino groups on the polysaccharide chain, the chitosan could be positively charged and solubilized when the pH of the solution is below 6, thus turning into a polycationic polymer. The chitosan gets despoiled into the non-toxic product in the Vivo. Hence, it is widely utilized for several biomedical applications. The feasibility of using an acid solution such as acetic acid for chitosan dissolution and the subsequent homogeneous, porous membrane is produced.

Chitosan membrane works as a very good adsorptive platform for the enzyme Tyrosinase and is cross-linked with it. Tyrosinase is stable in the membrane for more than 15 days at 4°C (in the fridge). On reacting with Pyrocatechol, the immobilized enzyme in the chitosan membrane turned dark due to Ariel oxidation. The molecular structure of chitosan is shown in Figure 3 and the formation of chitosan from chitin is explored in Figure 4.

Cellulose is a polysaccharide comprised of long chains of the linked with the units of D-glucose. This is utilized in huge application ranges that need a structured backbone. It is employed in preparing the chromatographic structural media in the gels to process like ionic separations and electrophoresis as well as a substrate for identifying and studying the cellulosic systems. The molecular structure of cellulose is shown in Figure 5.

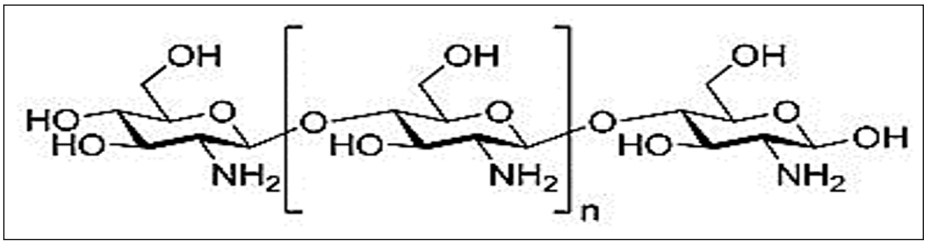

Fig. 3. Molecular structure of chitosan

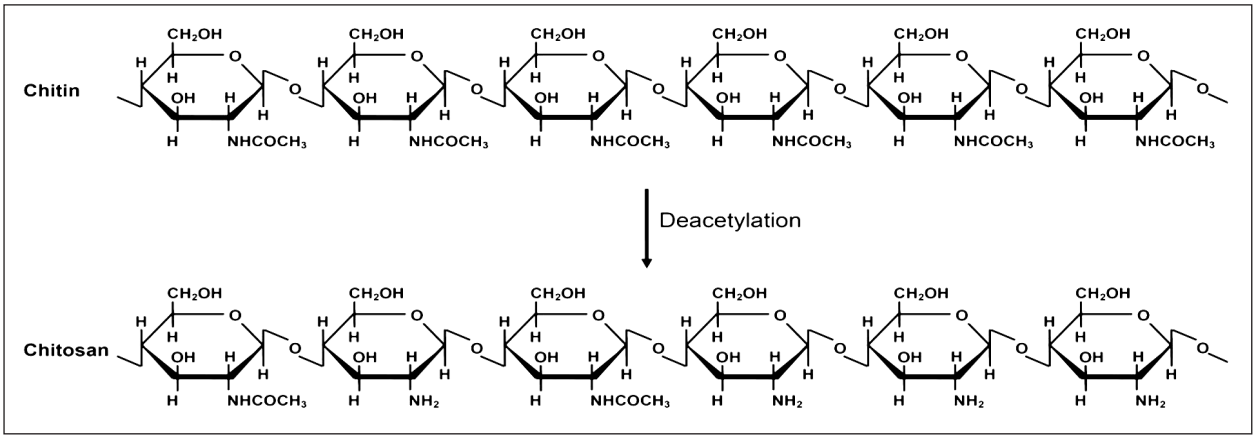

Fig. 4. Formation of chitosan from chitin

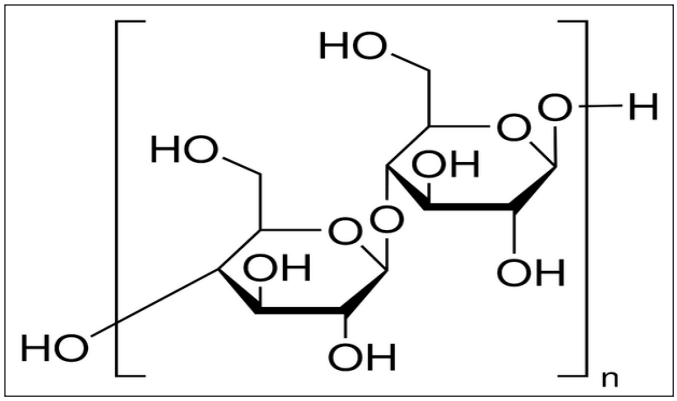

Fig. 5. Molecular structure of cellulose

The paper-based product features usually comprise the cellulose fibres of 90 to 99% that are the fundamental structural component with significant components impacting the properties of end usage. A Paper network is comprised of the laid fibrous and non-fibrous materials that comprise complicated cavity pore channel sets with several capillary dimensions. Thus, it is possibly permeable to the liquids. Nevertheless, the paper structure could be altered during the liquid contact as it interrupts the hydrogen bonds, and fibre relaxation and generates dimensional alterations in the capillaries and pores. So, cellulose can be used to make a membrane on which enzymes can get adsorbed and can be checked for its activity. The drawback of cellulose powder is, that it doesn't bind easily to form a membrane, thus, guar gum is prepared to add viscosity and bind cellulose powder. It makes the formation of the membrane possible and provides a white background to it. To make the film stiff, guar gum and cellulose solution are transferred to nylon mesh.

2.1.6.Inhibition of the enzyme by the pesticide

The presence or absence of the pesticide could be tested only if the immobilized enzyme on the membrane gets inhibited by the known pesticide [38]. Solutions for different pesticides like Malathion, Carbofuran, and aluminium phosphide in different concentrations are prepared and the membranes are dipped in these solutions for various recorded times. These are then taken out at the noted time intervals and tested for enzyme activity using the indicator (developer). The inhibition of the enzyme is more with lesser qualitative color intensity produced with the indicator. In this work, Pyrocatechol is utilized as an indicator for Tyrosinase activity as it oxidizes the Tyrosinase thereby showing the color change.

2.1.7.The casting of the membrane

The immobilized Tyrosinase on different layers is then cast into a stable membrane by initially pouring the solution of these inert layers on the fine nylon mesh. It is made to dry completely and the extract of Tyrosinase is adsorbed over the membrane for 10-12 hrs. Finally, the casted membrane [39] is ready to use.

3. Results and Discussion

Observations on absorption rate at various concentrations of a complex formed by Tyrosinase, enzyme activity at different concentrations, the activity of Tyrosinase membrane with various metal inhibitors, absorption of tomato extracts with pesticides with Tyrosinase membrane using Pyrocatechol as an indicator, and inhibition of Tyrosinase activity by different pesticides absorbance are discussed in this section. Pyrocatechol has been used as an indicator in this context. Initially, the results were obtained for the absorbance of Pyrocatechol at various concentrations of 1M Pyrocatechol solution, 0.1M Pyrocatechol solution, 0.2M Pyrocatechol solution, and 0.3M Pyrocatechol solution are shown in Table 1 and Figure 6.

Table 1. Pyrocatechol and its absorbance rate at various concentrations

Solutions	Absorbance
1M Pyrocatechol solution	a.u 0.1
0.1M Pyrocatechol solution	a.u 0.17
0.2M Pyrocatechol solution	a.u 0.06
0.3M Pyrocatechol solution	a.u 0.02

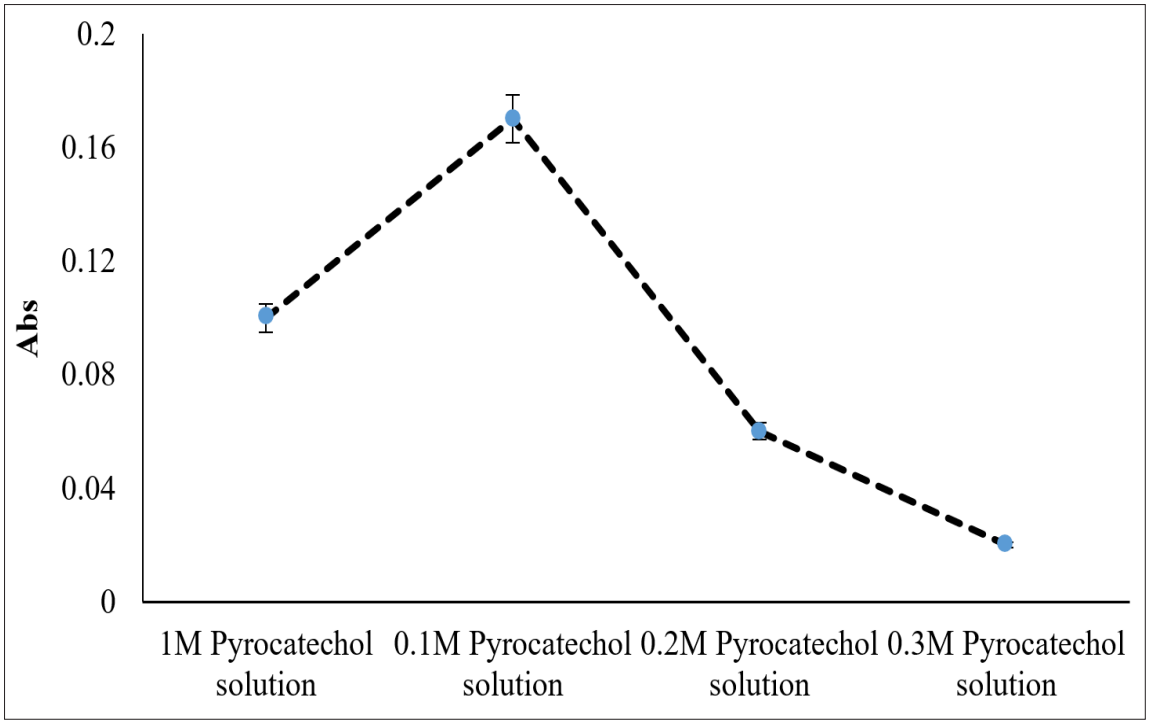

Fig. 6. The absorbance of Pyrocatechol at different concentrations

From Figure 6, the maximum absorption was observed for a 0.1M solution of Pyrocatechol with the enzyme extract. Henceforth, this indicator concentration would be used to study the enzyme activity at several concentrations. The obtained outcomes are shown in Table 2 and Figure 7. The absorbance of the sensor must be checked with a high instrument for the first time. The SD value is 1.155 and the LOD (limit of detection) and LOQ (limit of quantity) values are 3.8115 and 11.55 mmol L^{-1}.

From Figure 7, the absorbance curve for commercial and extracted Tyrosinase gave a better concentration estimate when extracted from the mushroom. That is, 20 times diluted Tyrosinase extract from mushrooms showed a maximum absorption of 0.55 and hence it could be considered for further use. Further, the activity of the Tyrosinase membrane with different metal inhibitors has been studied using the Pyrocatechol indicator. Obtained results are shown in Table 3 and Figure 8. The SD value is 1.81 and LOD (limit of detection) and LOQ (limit of quantity) values are 5.973 and 18.1 mmol L^{-1}

Lead acetate, lead nitrate, and aluminum sulphate are metal inhibitors. It has been concluded that a major change in the colour of the Tyrosinase membrane indicated the inhibition of the Tyrosinase by the salts of Aluminium and Lead. Tyrosinase produces a brown colour when reacted with Pyrocatechol. However, the colour formation (activity of the enzyme) was inhibited by different

Table 2. Study of enzyme activity at different concentrations using 0.1 M Pyrocatechol in mushroom

Tyrosinase concentrations	Absorbance
Stock Solution (0.1M)	0.66 a.u
0.001M Tyrosinase(commercial)	0.6 a.u
0.002M Tyrosinase	0.04 a.u
0.003M Tyrosinase	0.01 a.u
Mushroom Tyrosinase (40 times diluted)	0.34 a.u
Mushroom (30 times diluted)	0.43 a.u
Mushroom (25 times diluted)	0.49 a.u
Mushroom (20 times diluted)	0.55 a.u

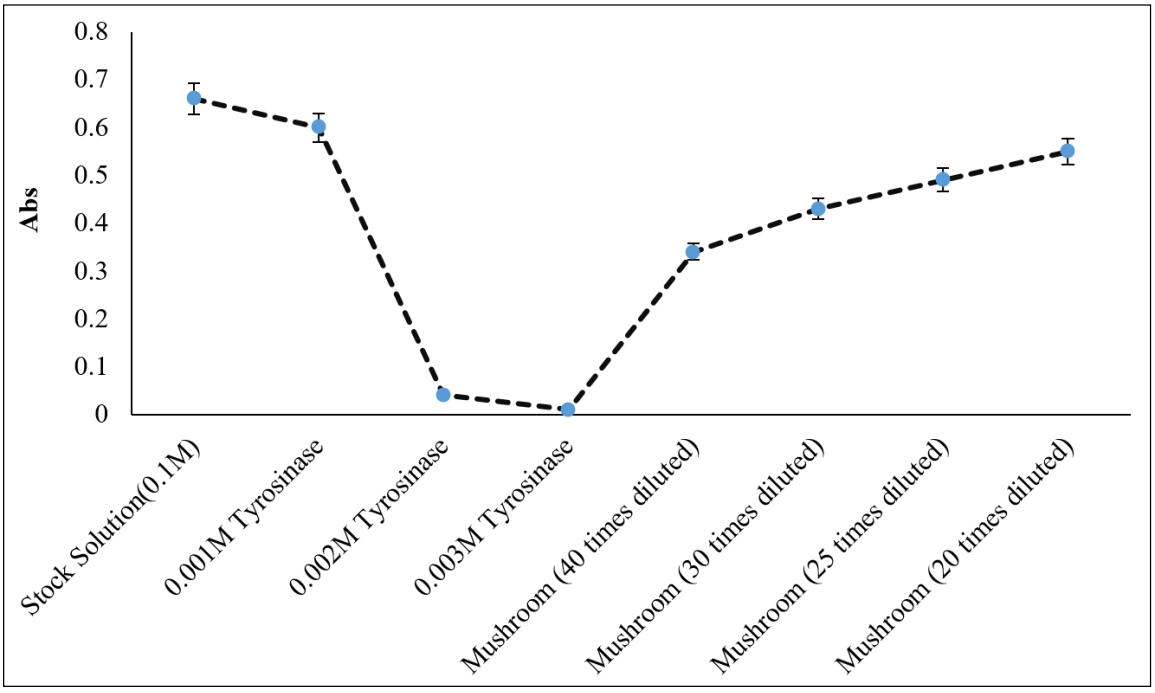

Fig. 7. Absorbance rate at different concentrations of the Tyrosinase

Table 3. The activity of the Tyrosinase membrane with various metal inhibitors using the Pyrocatechol (indicator)

Pyrocatechol + TM	Dark Purple
Pyrocatechol+ TM+ lead acetate	Green
Pyrocatechol +TM +lead nitrate	Light green
Pyrocatechol + TM + aluminum sulphate	Brown
TM: Tyrosinase Membrane*	

pesticides. Malathion inhibited the enzyme's activity when it was added to the film embedded with Tyrosinase which produced no colour with the addition of Pyrocatechol. Moreover, outcomes were attained through the addition of Malathion on Tyrosinase. Carbofuran also inhibited the activity of the enzyme as it also did not produce any colour change with Pyrocatechol. Aluminum oxide also inhibited the activity of the enzyme as it also did not produce any colour with Pyrocatechol. Further, a chitosan membrane was prepared which proved to be a perfect immobilization material for Tyrosinase, but the problem was the lack of a light background. And the membrane once air-dried became very stiff. Once the enzyme gets embedded in the addition of Pyrocatechol it turns dark in colour (blackish). While inhibition of enzymes with pesticides showed no colour change. Then, silica gel mesh was prepared on glass slides, on which Tyrosinase was embedded, it provided a very fine background and colour change was observed with the addition of Pyrocatechol in the immobilized enzyme as yellow which showed brown colour when inhibitor (pesticides) were present as shown in Figure 8. However, the enzyme was not stable for more than three days.

Then, attempts were made to work with cellulose, as its light colour gives a good background and enzyme easily and on the addition of indicator it showed a dark purple colour. While, in the presence of pesticides, it gives a brown colour. The drawback of cellulose was, the inability to bind. Thus, it was mixed with guar gum solution to make a good quality membrane. So, the guar gum–cellulose membrane was found to be effective. Then, the results of the absorption rate of tomato extracts with different pesticides are shown in Table 4 and Figure 8.

Table 4. Study of absorption of tomato extracts with different pesticides with Tyrosinase Membrane using Pyrocatechol as an indicator

Solutions	Absorbance
Fresh Tomato	a.u 0.35
Tomato in Carbofuran (0.1M)	a.u 0.46
Tomato in Malathion (0.01M)	a.u 0.32
Tomato in Al_2O_3 (0.1M)	a.u 0.96

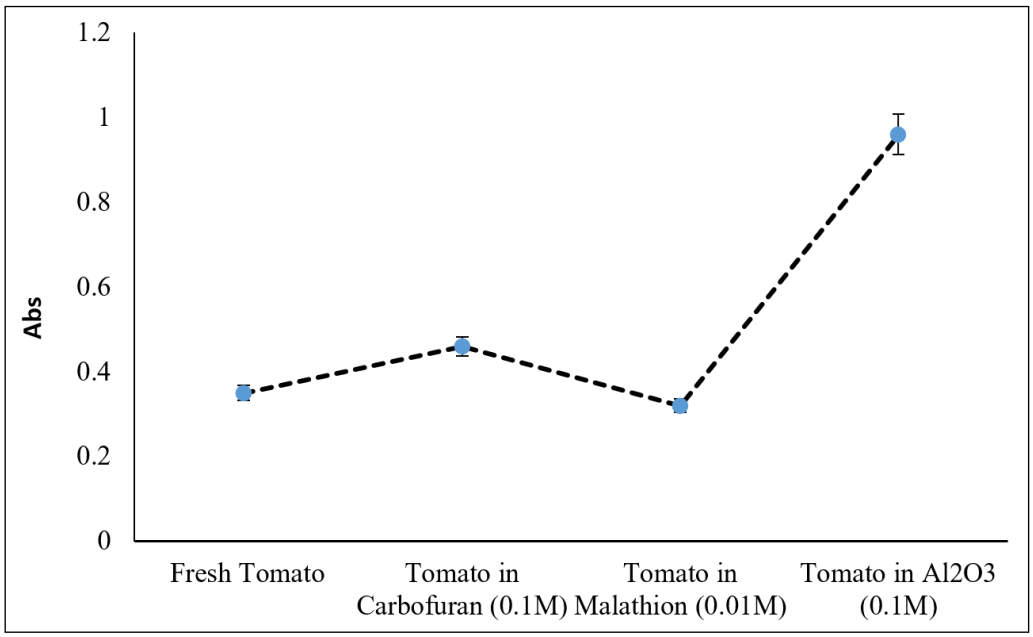

Fig. 8. The absorption rate of tomato extracts with different pesticides

The absorbance of tomato extract with different pesticides was determined using a biosensor. According to Figure 8, it is found that tomatoes in aluminum oxide have explored a high absorbance rate of 0.96 at 0.1M concentration. Then, the outcomes obtained for inhibition of Tyrosinase activity through absorbance of different pesticides are shown in Table 5 and Figure 9. The SD value is 2.09 and LOD (limit of detection) and LOQ (limit of quantity) values are 6.897 and 20.9 mmol L^{-1}. The absorbance of the sample using UV-Vis is shown in Table 5.

The inhibition of Tyrosinase activity in different pesticides is identified using biosensors. 0.01546 mmol L^{-1} is the value for absorbance 0.3, 0.7 absorbance attained 0.0608 mmol L^{-1}, absorbance of 0.97 value has 0.05000 mmol L^{-1}, 0.69 absorbance value obtained 0.03557 mmol/L and 0.66 absorbance attained 0.03402 mmol L^{-1} for cell length 1 and molar absorptivity 19400 for all the absorbance.

From Figure 9, it is found that the extract of tomato with 0.01M Malathion showed a high absorbance rate of 0.97, while, Tyrosinase + Tomato extract with pesticide (Malathion)+ Pyrocatechol showed a minimum absorbance rate of 0.66. Thus, it could be concluded that 20 times diluted Tyrosinase extract from mushrooms showed maximum absorption of 0.55, and tomato in Aluminium oxide has explored a high absorbance rate of 0.96 at 0.1M concentration. The 0.01 molar value in mg L^{-1} is 980 for a density of 0.001 and molecular weight of 98 mg.

4. Conclusion

The research aimed to develop bioactive membrane-based sensors through enzyme inhibition for to determine pesticide residues, especially in tomatoes and mushrooms. The stability of the

Table 5. Inhibition of Tyrosinase activity through the absorbance of different pesticides

Solutions	Absorbance
Tyrosinase + Pyrocatechol	a.u 0.3
Extract Tomato without Pesticide	a.u 0.7
Extract Tomato with 0.01M Malathion	a.u 0.97
Tyrosinase + Tomato extract without pesticide + Pyrocatechol	a.u 0.69
Tyrosinase + Tomato extract with Malathion+ Pyrocatechol	a.u 0.66

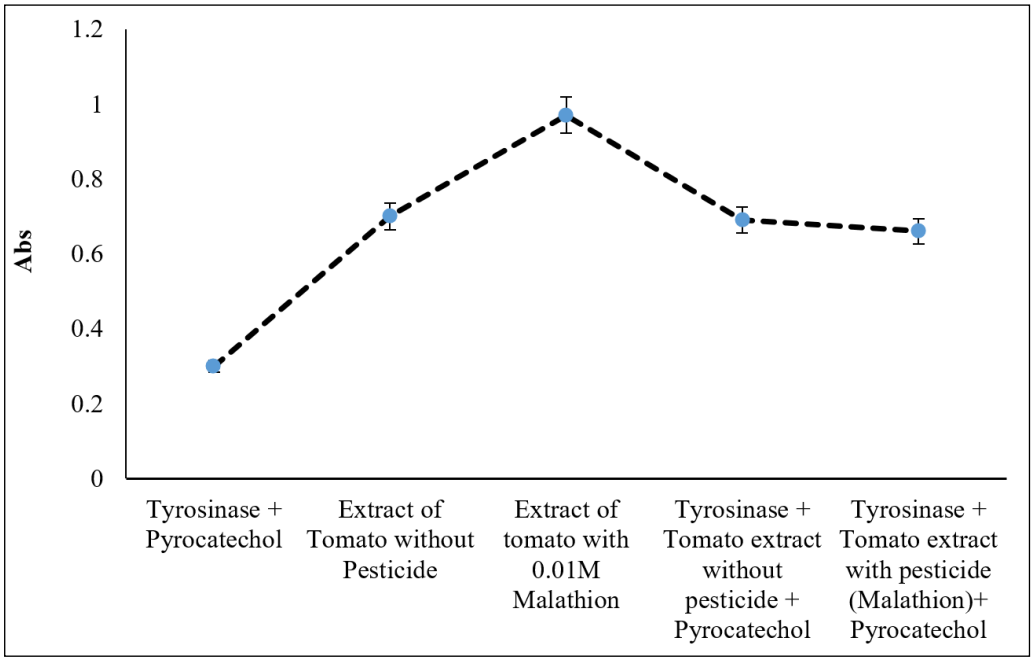

Fig. 9. Inhibition of Tyrosinase activity by different pesticides

enzyme extract at different concentrations was studied. Immobilization of the enzyme extract on different mediums like cellulose, chitosan, guar gum, and a combination of guar gum and cellulose was tested. Due to the effective binding and stable nature of guar gum and cellulose, it was integrated and considered a membrane. Pyrocatechol was used as an indicator for Tyrosinase activity as it oxidizes Tyrosinase by showing the colour change. The maximum absorption was observed for a 0.1M solution of Pyrocatechol with the enzyme extract. Thus, this concentration of the indicator was used to study the enzyme activity at several concentrations. Finally, the study was undertaken for the inhibition of an enzyme by different pesticides and metal inhibitors with the use of 0.1M Pyrocatechol. It was found that 20 times diluted Tyrosinase extract from mushrooms showed maximum absorption of 0.55. Meanwhile, tomatoes with aluminum oxide had a high absorbance rate of 0.96 at 0.1M concentration. This maximum rate of absorption indicates the efficiency in detecting the pesticide residues. The LOD, LOQ, RSD%, and linear range (LR) and recovery of the sensor were discovered for every different pesticide. The RSD for all these pesticides is 1.155, 1.81, and 2.09, LOD is 3.81, 5.973, 6.897 mmol L^{-1}, LOQ is 11.55, 18.8, and 20.9 mmol L^{-1} respectively. The LR are 2.6 and 20 mmol L^{-1}. The pesticide residues found are accurate.

5. Acknowledgment

The authors would like to thank the Acharya Narendra Dev College, University of Delhi, New Delhi, India, and the authors declare that they have no competing interests

6. References

[1] R. Kaur, G. K. Mavi, S. Raghav, I. Khan, Pesticides classification and its impact on environment, Int. J. Curr. Microbiol. Appl. Sci., 8 (2019) 1889-1897. https://doi.org/10.20546/ijcmas.2019.803.224

[2] V. Rathee, A. Kumar Dubey, M. Kaur, Effects of pesticides on human health, J. Forensic Sci. Res., 7 (2023) 034-039. https://doi.org/10.29328/journal.jfsr.1001047

[3] B. Hicks, Agricultural pesticides and human health, geology, and human health, teach the earth, 2012. https://serc.carleton.edu/NAGTWorkshops/health/case_studies/pesticides.html

[4] V. Philippe, A. Neveen, A. Marwa, A. Y. A. Basel, Occurrence of pesticide residues in fruits and vegetables for the Eastern Mediterranean Region and potential impact on public health, Food Control, 119 (2021) 107457. https://doi.org/10.1016/j.foodcont.2020.107457

[5] H. D. O. Gomes, J. M. C. Menezes, J. G. M. da Costa, H. D. M. Coutinho, R. N. P. Teixeira, R. F. do Nascimento, A socio-environmental perspective on pesticide use and food production, Ecotoxicol. Environ. safe., 197 (2020) 110627. https://doi.org/10.1016/j.ecoenv.2020.110627

[6] D. Kumari, S. John, Health risk assessment of pesticide residues in fruits and vegetables from farms and markets of Western Indian Himalayan region, Chemosphere, 224 (2019) 162-167. https://doi.org/10.1016/j.chemosphere.2019.02.091

[7] A. Verdian, Apta-nanosensors for detection and quantitative determination of acetamiprid–A pesticide residue in food and environment, Talanta, 176 (2018) 456-464. https://doi.org/10.1016/j.talanta.2017.08.070

[8] B.S. Aradhana, R. Aiswarya, K.G. Praveena, M. Joshy, B.S.Reshmi, Quality and pesticides detection in fruits and vegetables, J. Emerg. Technol. Innov. Res., 8 (2021) g227-g230. https://www.jetir.org/papers/JETIR2105829.pdf

[9] V. V. Sarbhukan, L. Ragha, Establishing secure routing path using trust to enhance security in MANET, Wirel. Pers. Commun., 110 (2020) 245-255. https://doi.org/10.1007/s11277-019-06724-0

[10] C. Pundir, A. Malik, Bio-sensing of organophosphorus pesticides: A review, Biosens. Bioelectron., 140 (2019) 111348.

https://doi.org/10.1016/j.bios.2019.111348

[11] D. Wang, P. Wang, D. Liu, Z. Zhou, Fluorometric atrazine assay based on the use of nitrogen-doped graphene quantum dots and on inhibition of the activity of tyrosinase, Microchim. Acta, 186 (2019) 1-7. https://doi.org/10.1007/s00604-019-3648-6

[12] S. Muehlwald, N. Buchner, L. Kroh, Investigating the causes of low detectability of pesticides in fruits and vegetables analysed by high-performance liquid chromatography–Time-of-flight, J. Chromatogr. A, 1542 (2018) 37-49. https://doi.org/10.1016/j.chroma.2018.02.011

[13] K. Madej, T. K. Kalenik, W. Piekoszewski, Sample preparation and determination of pesticides in fat-containing foods, Food Chem., 269 (2018) 527-541. https://doi.org/10.1016/j.foodchem.2018.07.007

[14] A. Samsidar, S. Siddiquee, S. M. Shaarani, A review of extraction, analytical and advanced methods for determination of pesticides in environment and foodstuffs, Trend. Food Sci. Technol., 71 (2018) 188-201. https://doi.org/10.1016/j.tifs.2017.11.011

[15] M. V. Navarro, M. A. Cabezon, P. C. Damiani, Simultaneous determination of pesticides in fruits by using second-order fluorescence data resolved by unfolded partial least-squares coupled to residual bilinearization, J. Chem., 2018 (2018) 217465. https://doi.org/10.1155/2018/3217465

[16] S. Narenderan, S. Meyyanathan, B. Babu, Review of pesticide residue analysis in fruits and vegetables. Pre-treatment, extraction and detection techniques, Food Res. Int., 133 (2020) 109141. https://doi.org/10.1016/j.foodres.2020.109141

[17] Y. V. Plekhanova, A. Reshetilov, Microbial Biosensors for the determination of pesticides, J. Anal. Chem., 74 (2019) 1159-1173. https://doi.org/10.1134/S1061934819120098

[18] A. Mishra, J. Kumar, J. S. Melo, B. P. Sandaka, Progressive development in biosensors for detection of dichlorvos pesticide: A review, J. Environ. Chem. Eng., 9 (2021) 105067. https://doi.org/10.1016/j.jece.2021.105067

[19] E. N. Esimbekova, V. P. Kalyabina, K. V. Kopylova, I. G. Torgashina, V. A. Kratasyuk, Design of bioluminescent biosensors for assessing contamination of complex matrices, Talanta, 233 (2021) 122509. https://doi.org/10.1016/j.talanta.2021.122509

[20] B. Rajangam, D. K. Daniel, A. I. Krastanov, Progress in enzyme inhibition based detection of pesticides, Eng. Life Sci., 18 (2018) 4-19. https://doi.org/10.1002/elsc.201700028

[21] H. Patel, D. Rawtani, Y. Agrawal, A newly emerging trend of chitosan-based sensing platform for the organophosphate pesticide detection using Acetylcholinesterase-a review, Trend. food Sci. Technol., 85 (2019) 78-91. https://doi.org/10.1016/j.tifs.2019.01.007

[22] N. S. Sulaiman, K. Rovina, V. M. Joseph, Classification, extraction and current analytical approaches for detection of pesticides in various food products, J. Consum. Prot. Food Safe., 14 (2019) 209-221. https://doi.org/10.1007/s00003-019-01242-4

[23] M. Fuyal, B. Giri, A Combined system of Ppaper device and portable spectrometer for the detection of pesticide residues, Food Anal. Method., 13 (2020) 1492-1502. https://doi.org/10.1007/s12161-020-01770-y

[24] N. Kalyani, S. Goel, S. Jaiswal, On-site sensing of pesticides using point-of-care biosensors: a review, Environ.l Chem. Lett., 19 (2021) 345-354. https://doi.org/10.1007/s10311-020-01070-1

[25] L. Karadurmus, S. Kaya, S. A. Ozkan, Recent advances of enzyme biosensors for pesticide detection in foods, J. Food Meas. Charact., 15 (2021) 4582-4595. https://doi.org/10.1007/s11694-021-01032-3

[26] M. Arjomandi, H. Shirkhanloo, A review: analytical methods for heavy metals determination in environment and human samples, Anal. Methods Environ. Chem. J., 2 (2019) 97-126. https://doi.org/10.24200/amecj.v2.i03.73

[27] S. Teimoori, H. Shirkhanloo, A. H. Hassani, M. Panahi, N. Mansouri, An immobilization of aminopropyl trimethoxysilane-phenanthrene carbaldehyde on graphene oxide for toluene extraction and separation in water samples, Chemosphere, 316 (2023) 137800. https://doi.org/10.1016/j.chemosphere.2023.137800

[28] S. Teimoori, H. Shirkhanloo, A. H. Hassani, M. Panahi, N. Mansouri, Rapid extraction of BTEX in water and milk samples based on functionalized multi-walled carbon nanotubes by dispersive homogenized-micro-solid phase extraction, Food Chem., 421(2023) 136229. https://doi.org/10.1016/j.foodchem.2023.136229

[29] S. Teimoori, H. Shirkhanloo, A. Hassani, M. Panahi, and N. Mansouri, New extraction of toluene from water samples based on nano-carbon structure before determination by gas chromatography, Int. J. Environ. Sci. Technol., 20 (2023) 6589-6608. https://doi.org/10.1007/s13762-023-04906-9

[30] R. Ashouri, H. Shirkhanloo, A. Rashidi, S. Mirzahosseini, N. Mansouri, Dynamic and static removal of benzene from air based on task-specific ionic liquid coated on MWCNTs by sorbent tube-headspace solid-phase extraction procedure, Int. J. Environ. Sci. Technol., 18 (2021) 2377-2390. https://doi.org/10.1007/s13762-020-02995-4

[31] J. Rakhtshah, H. Shirkhanloo, N. Esmaeili, A rapid extraction of toxic styrene from water and wastewater samples based on hydroxyethyl methylimidazolium tetrafluoroborate immobilized on MWCNTs by ultra-assisted dispersive cyclic conjugation-micro-solid phase extraction, Microchem. J., 170 (2021) 106759. https://doi.org/10.1016/j.microc.2021.106759

[32] O. V. Omotoyinbo, E. O. Awojulu, D. M. Sanni, Phytochemical screening, antioxidant and tyrosinase inhibitory studies of methanol leaf extracts of two tomato varieties, Highligh. BioSci., 3 (2020) 20216. https://doi.org/10.36462/H.BioSci.20216

[33] P. Angelini, R. Venanzoni, G. Angeles Flores, B. Tirillini, G. Orlando, L. Recinella, Evaluation of antioxidant, antimicrobial and tyrosinase inhibitory activities of extracts from Tricholosporum goniospermum, an edible wild mushroom, Antibiotics, 9 (2020) 513. https://doi.org/10.3390/antibiotics9080513

[34] T. J. Al-Khafaji, F. Wong, P. S. Fleming, N. Karpukhina, R. Hill, Novel fluoride and strontium-containing bioactive glasses for dental varnishes-design and bioactivity in Tris buffer solution, J. Non-Crystalline Solids, 503 (2019) 120-130. https://doi.org/10.1016/j.jnoncrysol.2018.09.037

[35] P. Pushankina, G. Andreev, I. Petriev, Hydrogen permeability of composite Pd–Au/Pd–Cu membranes and methods for their preparation, Membranes, 13 (2023) 649. https://doi.org/10.3390/membranes13070649

[36] A. K. Singh, I. Tiwari, Nanomaterial synthesis and mechanism for enzyme immobilization: part II, Nanomaterials in biofuels research book, Springer publisher, pages191-212, 2020. https://doi.org/10.1007/978-981-13-9333-4_8

[37] S. Aggarwal, A. Chakravarty, S. Ikram, A comprehensive review on incredible renewable carriers as promising platforms for enzyme immobilization and thereof strategies, Int. J. Biol. Macromol., 167 (2021) 962-986. https://doi.org/10.1016/j.ijbiomac.2020.11.052

[38] T. Rasheed, Carbon dots as robust class of sustainable and environment friendlier nano/optical sensors for pesticide recognition from wastewater, TrAC Trend. Anal. Chem., 160 (2023) 116957. https://doi.org/10.1016/j.trac.2023.116957

[39] T. Ban, M. Guo, Y. Wang, J. Ma, X. Wang, Z. Wang, Efficient and durable vanadium flow batteries enabled by high-performance fluorinated poly (aryl piperidinium) membranes, J. Mater. Chem. A, 11 (2023) 24013-24025. https://doi.org/10.1039/D3TA05382B

Anal. Methods Environ. Chem. J. 7 (3) (2024) 21-33

AMECJ

Research Article, Issue 3
Analytical Methods in Environmental Chemistry Journal
Journal home page: www.amecj.com/ir

Determination and evaluation of pesticide residues in vegetables using gas chromatography-mass spectrometry

Mona Sharififard[a,b], Farhad Safdari[c], Ali Faghihi-Zarandi[d], Afshin Takdastan[b,c], and Ismaeil Alizadeh*[, E]

[a] *Department of Medical Entomology and Vector Control, School of Public Health, Ahvaz Jundishapur University of Medical Sciences, Ahvaz, Iran*
[b] *Environmental Technologies Research Center, Ahvaz Jundishapur University of Medical Sciences, Iran*
[c] *Department of Environmental Health Engineering, School of Public Health, Ahvaz Jundishapur University of Medical Sciences, Ahvaz, Iran*
[d] *Department of Occupational Health Engineering and Safety at Work, Faculty of Public Health, Kerman University of Medical Sciences, Kerman, Iran*
[e] *Department of Vector Biology and Control of Diseases, School of Public Health, Tehran University of Medical Sciences, Tehran, Iran*

ARTICLE INFO:

Received 4 May 2024
Revised form 10 Jul 2024
Accepted 19 Aug 2024
Available online 29 Sep 2024

Keywords:
Pesticide residues,
Vegetables,
Gas chromatography-mass spectrometry,
Health risk assessment,
Maximum residue limits

ABSTRACT

This study aimed to determine and evaluate the pesticide residues (mg kg^{-1}) in the most commonly consumed vegetables and their health risk assessment in Ahvaz City, southwest Iran in 2022. Gas-chromatography-mass spectrometry (GC-MS) was employed to analyze and identify the presence of pesticide residues in the vegetable samples. The analysis of pesticide residues in the vegetable samples revealed the presence of fifteen pesticides, including commonly used insecticides from the organophosphate class. In some samples, the levels of pesticide residues exceeded the national MRLs. Most pesticides' calculated hazard index (HI) was below 100, indicating a lower risk of adverse health effects. However, in the case of oxydemeton-methyl in tomatoes, the HI was found to be 190, suggesting a higher potential for health risks. The cumulative risk index of pesticide residues, measured as the pesticide toxicity index (PTI), was determined for tomatoes, cucumbers, and potatoes by GC-MS (recovery of more than 95%). The PTI values were 15.2, 11.7, and 12.6, respectively, which exceeded the standard value of 1. This indicates that long-term consumption of these vegetables, containing various pesticide residues, may pose a chronic health risk to humans. While most pesticides had a relatively lower risk of adverse health effects, the elevated PTI values in all three vegetable types indicate a potential chronic health risk associated with the long-term consumption of these contaminated vegetables. Sample preparation and determination of pesticide residues in vegetables by GC-MS helps continuous monitoring to maintain the safety and quality of vegetables in the local market.

1. Introduction

Food security is one of the most important issues of human life, and along with it, food safety has also been the focus of the consumers of agricultural products. Most agricultural products that have been exposed to pesticides are presented to the consumer market for a short period after spraying, contain some pesticide residues [1-3]. The excessive use of pesticides in crops causes the emergence of phenomena called toxic residues, which are considered risk factors for human health and environmental pollution [1, 3].

*Corresponding Author: Ismaeil Alizadeh
Email: ismaeil.alizadeh@yahoo.com
https://doi.org/10.24200/amecj.v7.i03.349

The residues of chemical compounds in foodstuffs have a wide spectrum of origins, which include natural poisons, chemicals used in agriculture, veterinary drugs, industrial-biological pollutants, and chemicals from food processing and packaging [4]. If pesticides are not used, the losses of agricultural products are estimated to be about 46% in some countries [5, 6], so, they are considered one of the important environmental pollutants and harm the health of living beings, including humans [7] directly and through chemical residues in food products [8]. Approximately, 2 million tons of pesticides are used annually worldwide. China, the USA, and Argentina have the most usage, which is increasing rapidly. However, by the year 2020, global pesticide usage has been estimated to increase up to 3.5 million tons [9]. The use of these chemical compounds causes many adverse health effects on humans and the environment. In addition to acute toxicity, the increasing prevalence rate of dangerous and non-exclusive diseases, for instance, cancer is related to the consumption of pesticides and fertilizers and their residues in agricultural products [10, 11]. Out of about 800 pesticides used worldwide, 211 types of chemical compounds with different formulations and applications have been recorded in Iran. The production of greenhouse and garden products also requires the use of pesticides [12, 13]. To guarantee food safety, promote global trading, and prevent outlawed or improper use of pesticides, MRLs are also established for pesticide residues in food and feed within the FAO/WHO Codex Alimentarius. The rate of pesticide consumption varies under different agricultural, weather, and climate conditions in different countries and between different regions of the same country [14]. The standards of pesticide residues, including MRLs and ADI (Acceptable Daily Intake), must be followed when using agricultural products. MRLS depends on various factors, including the variety of pesticide consumption, the food basket of each country, and the daily limit of the poison that can enter the human body [11]. Although the use of pesticides in agriculture increases crop production, due to environmental problems and the consequences of pesticide residues in consumers' food, reducing the use of these compounds has attracted everyone's attention recently. Of course, it should be noted that the type, pesticide concentration, the stored time the product is kept after harvesting, the thickness of the skin, etc. affect the amount of poison left in the product [8, 15]. More than 80% of the pesticide residue in humans, especially in children, causes serious health risks. Also, approximately 20% of pesticides may cause cancer [16, 17]. Generally, the accumulation of pesticide substances in food, water, land, and air is one of the most important debates in human health and the environment. An important factor in the chronic toxicity of pesticides is their ability to accumulate in the body, which occurs in all people through direct and even indirect exposure through food, breathing, or skin absorption [18]. Monitoring the pesticide and mineral residues in foodstuffs is carried out continuously in many countries to ensure the MRLs [17]. There is little information on pesticide residue levels and their health risks in vegetables in southwest Iran. To partially address this gap, we performed a cross-sectional study to assess levels of pesticide residues in the most commonly consumed vegetables, including tomatoes, potatoes, and cucumbers, from major wholesale markets in Ahvaz city during 2022. Moreover, in this study, the pesticide residues in vegetables were determined using GC-MS and the health risk assessment was used to characterize potential dietary exposure risks to obtain more comprehensive and reliable predictions of risks and uncertainties. To the best of our knowledge, this was the first study to provide basic information on the occurrence of pesticide residue in selected vegetables from Ahvaz city, located in southwest Iran.

2. Material and Methods

2.1. Study areas

The research was undertaken in Ahvaz city (Khuzestan province), southwest Iran (Fig.1). Vegetable samples were collected from the main wholesale fruit and market between spring and summer in 2022 in Ahvaz city. The region is one of the metropolitan cities in the southwestern of Iran, with a population of 1.3 million. It is located in a dry area with a subtropical hot desert climate [19, 20].

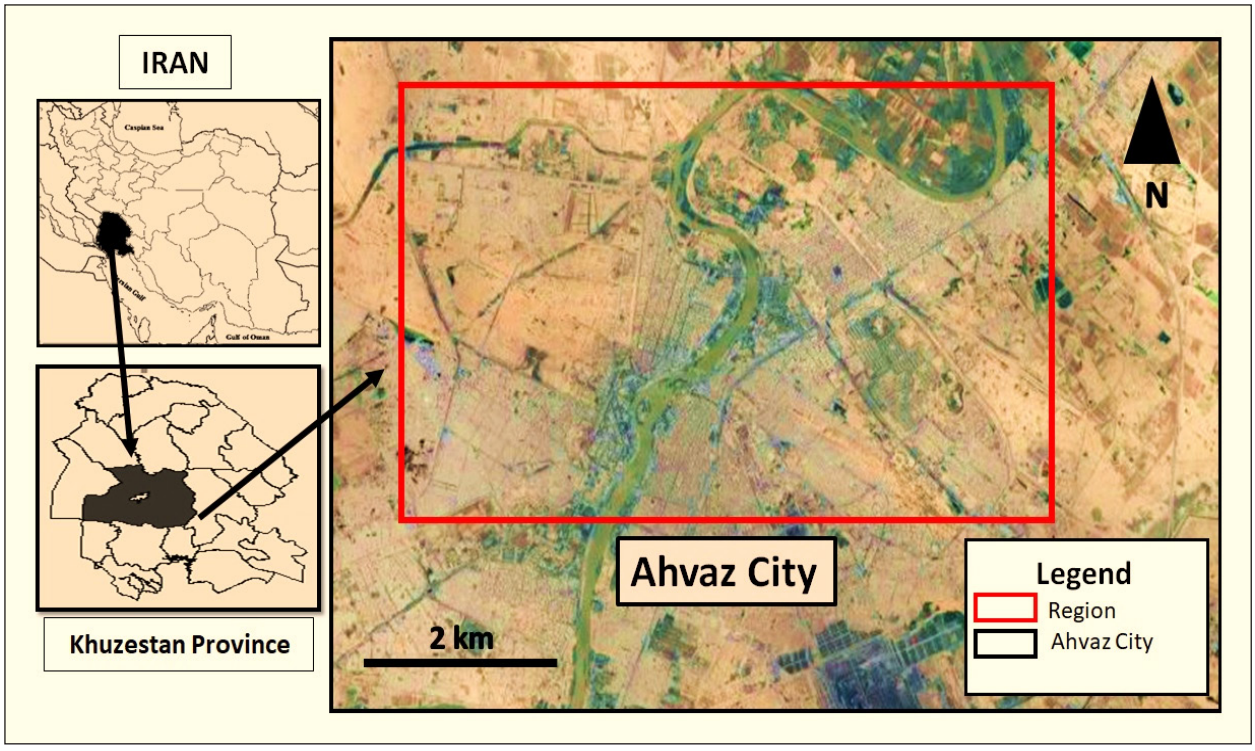

Fig. 1. Location of the study areas in Ahvaz city, southwest Iran.
(Images provided through Google Earth Professional (https://www.google.com/earth/versions/#download-pro).

2.2. Sample collection

The samples in this study were the most commonly used and locally cultivated vegetables in Ahvaz city. Three ready-to-eat fresh vegetables including cucumbers, tomatoes, and potatoes weighing 1kg each, were collected. Sampling was completely randomized every two weeks a month in two seasons (spring and summer). All samples were carefully collected, sealed in polyethylene bags, and labelled. Then placing them in a container containing ice, and transferred to the chemistry laboratory of Ahvaz city for analysis.

2.3. Chemicals used

Sodium sulfate and dichloromethane were purchased from Sigma Aldrich, Germany.

2.4. Preparation and Extraction

Measurement of pesticide residues in vegetables was done according to the QuEChERS method [11]. To prepare the samples, they were firstly washed and cut into pieces, and then 10 grams of each sample was mixed with acetonitrile (repeated twice with 60 mL) in a blender. The resultant mixture was then passed through the Buchner funnel and poured into the decanter. Then 150 mL of 2% sodium sulfate was added to this sample. Sixty mL of dichloromethane (3×20 mL) was added to the above solution and shaken vigorously. Dichloromethane was collected in another container each time. All the contents of the dichloromethane were passed through the Buchner funnel (containing sodium sulfate) then, the samples were distilled using a freeze-drier and a vacuum distillation device. The dried samples were transferred to polyethylene containers (Falcom) wrapped with aluminum and kept at -18º C until they were sent to a laboratory to perform GC-MS. Samples analyses were carried out either immediately upon their arrival at the laboratory or stored at –5°C for 4 days before analysis. The schematic of study stages including the sampling, the QuEChERS method, and analysis of pesticides by GC-MS are illustrated in Figure 2.

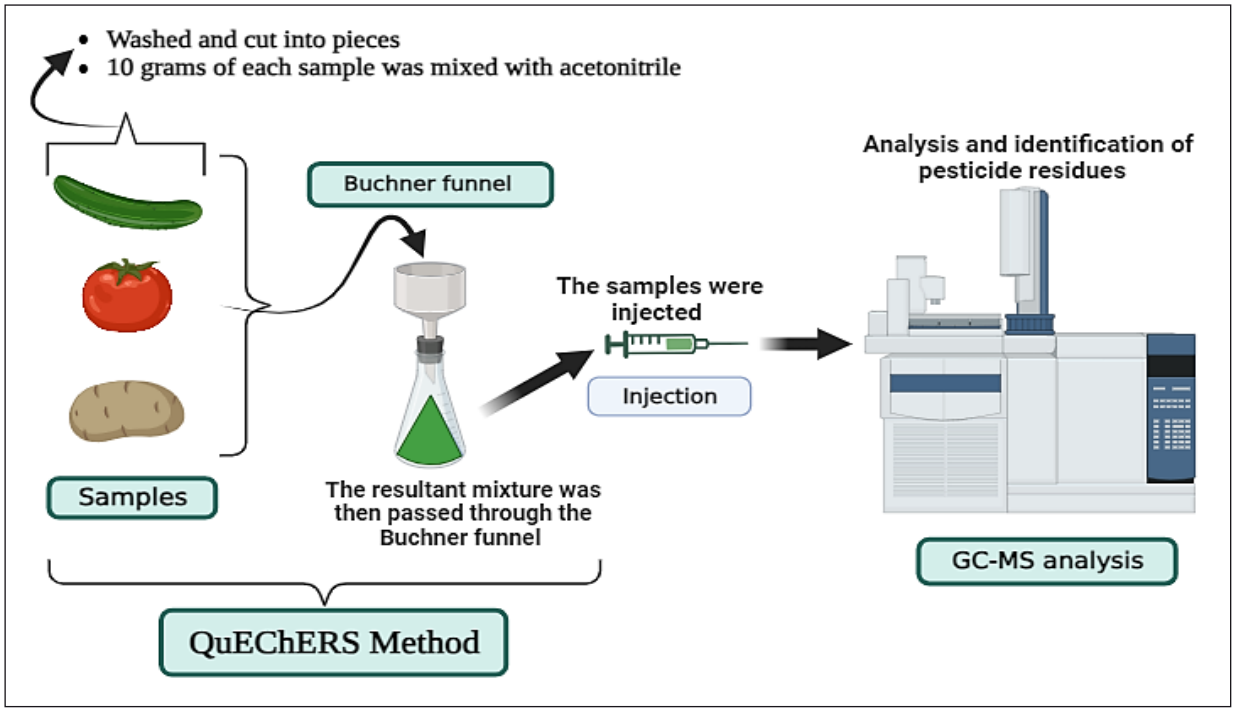

Fig. 2. Schematic of study stages including the sampling, the QuEChERS method, and analysis of pesticides by GC-MS

2.5. GC-MS analysis

For the analysis and identification of pesticide residues in the tomatoes, cucumbers, and potatoes, a gas-chromatography-mass spectrometer (GC-MS) was utilized. The specific instrument used was the Hewlett-Packard 6890, manufactured by Agilent Technology in Santa Clara, California, USA. The GC-MS system was equipped with an HP–5MS 5% phenyl methyl siloxane capillary column measuring 30 m in length, 0.25 mm in diameter, and with a film thickness of 0.25 µm. During the analysis, the samples were injected in a split-less mode, and helium was employed as the carrier gas at a flow rate of 1.0 mL per minute. The injector temperature was set at 250°C, the transfer line temperature at 285°C, the ion source temperature at 280°C, and the quadruple temperature at 150°C. The oven temperature program began at 70°C and was held for 2 minutes, followed by an increase to 150°C at a rate of 25°C per minute. Subsequently, the temperature was further raised to 200°C at a rate of 3°C per minute and maintained for 0 minutes. Finally, the temperature was ramped up from 200 to 280°C at a rate of 8°C per minute and held for 10 minutes. This temperature program resulted in a total run time of 42 minutes, enabling complete separation of all the analyzed compounds.

2.6. Risk assessment

Risk assessment is carried out to investigate effects the effects of exposure to a specified pollutant on human health and define associated carcinogenic and non-carcinogenic risks [21]. Two methods described health risk (HR) assessment [22-24]. the first method uses the health risk index (HI) calculated by dividing the estimated daily intakes (EDI) by their corresponding values of the ADI (mg kg^{-1}) established by WHO/FAO as shown in the following Equation I.

$$HI = \frac{EDI}{ADI} \times 100 \qquad \text{(Eq. I)}$$

Equation II determined the estimated daily intakes (EDI) of the various pesticides in each vegetable species.

$$EDI = \Sigma RLi \times Fi/BW \qquad \text{(Eq. II)}$$

Where: RLi: residue level of the pesticide; Fi: food consumption data; BW: Body weight

The average daily intake of tomato, potato, and cucumber is 118, 61.2, and 5.9 g per day, and the average body weight was considered to be 60 kg for adults. When the chronic health risk index (cHI) is >100; the food involved should be considered as a risk to the consumers, if the index is % <100, this would

indicate that the food involved is considered acceptable. The second method was calculating the pesticide toxicity index for each vegetable (combined risk index), which represents the cumulative health risk. It was determined by calculating its toxicity quotient (TQ) as Equation III.

$$TQ = \frac{C}{MRL} \quad \text{and} \quad PTI = \Sigma TQ \qquad \text{(Eq.III)}$$

C is pesticide residue for individual pesticides (mg kg^{-1}) and MRL is the maximum residue limit (mg kg^{-1}) in each vegetable. A comparison was made with the MRLs to assess the potential risks associated with exposure to pesticide mixtures and individual pesticides and determine the extent of pesticide contamination in each sample. The PTI target, which signifies an acceptable level of risk to human health with no adverse effects, was set to be below 1.0.

3. Results And Discussion

A total of 15 pesticide residues from 10 different groups including organophosphates, carbamates, pyrethroids, neonicotinoids, pyrazoles, etc were detected in tomatoes, cucumbers, and potatoes collected from the main wholesale fruit and vegetable market in Ahvaz city in spring and summer of 2022 (Fig. 3).

Pesticide	Chemical structure	Pesticide	Chemical structure
Diazinon	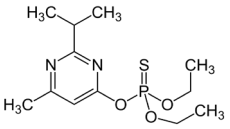	Permethrin	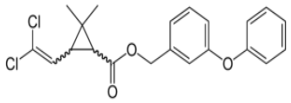
Chlorpyrifos	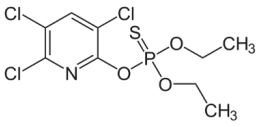	Phosalone	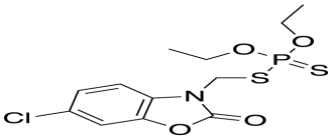
Dichrolovos	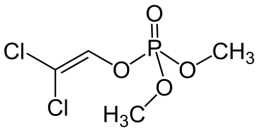	Penconazole	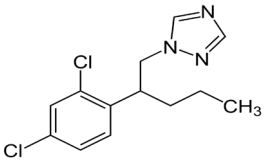
Malathion	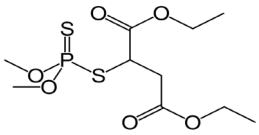	Metalaxyl	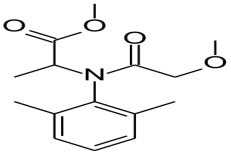
Oxydemethon-methyl	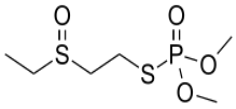	Pendimethalin	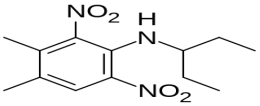
Pirmicarb	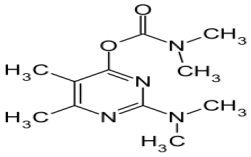	Bromopropylate	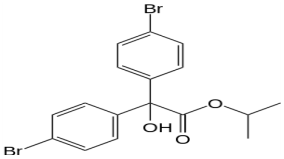
Acetamiprid	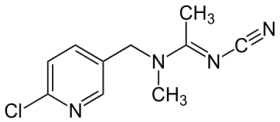	Hexythiazox	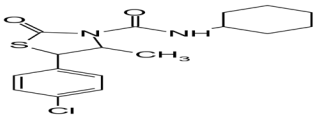
Mancozeb	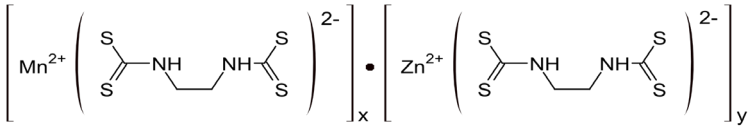		

Fig. 3. Detected pesticides and their chemical structure in the vegetables studied

The most detected pesticides belonged to the organophosphate class. According to WHO classification, various detected pesticides were categorized as moderate to likely no risk in terms of hazardous risk. In all contaminated samples, chlorpyrifos, fuzalon, oxydimeton methyl, pedimethalin, diazinon, and metalaxyl had the highest number of pesticide residues detected with 19, 16, 13, 15, 12 and 11 times (Table 1). Of the total number of analyzed samples (36 samples), 12 samples related to each product, 10 samples (27.8%) did not contain pesticide residues. There were 26 samples (72.2%) with pesticide residues, out of which 13 samples (50%) had residues > MRL and 13 samples (50%) had more than one pesticide residue. Pesticide residues were detected at a frequency of 83.3, 73, and 58.3%, in the cucumber, tomato, and potato samples, respectively. In the contaminated samples of potatoes, tomatoes, and cucumbers, the frequency of samples with pesticide residues >MRL were 57.1, 55.6 and 40%, respectively, and those with more than one pesticide residue in the above products were 57.1, 66.7 and 30%, respectively (Fig. 4).

Table 1. Detected pesticides and their frequencies in the vegetables of the study area.

Pesticide	No. samples	% of samples*	Uses	WHO Classification**	Chemical group
Diazinon	12	46.1	Insecticide	II	Organophosphate
Chlorpyrifos	19	73.1	Insecticide	II	Organophosphate
Dichrolovos	8	30.8	Insecticide	Ib	Organophosphate
Malathion	4	15.4	Insecticide	III	Organophosphate
Phosalone	16	61.5	Insecticide	II	Organophosphate
Oxydemethon-methyl	15	19.2	Insecticide	Ib	Organophosphate
Pirmicarb	3	11.5	Insecticide	II	Carbamate
Acetamiprid	6	23.1	Insecticide	II	Neonicotinoid
Permethrin	3	11.5	Insecticide	II	Pyrethroid
Mancozeb	7	26.9	Fungicide	U	Dithiocarbamate
Penconazole	9	34.9	Fungicide	III	Triazole
Metalaxyl	11	15.4	Fungicide	II	Phenylamide
Pendimethalin	13	50	Herbicide	II	Dinitroaniline
Bromopropylate	10	38.5	Acaricide	II	Benzilate
Hexythiazox	3	11.5	Acaricide	U	Clofentezine

*The frequency of each pesticide: number of samples with each pesticide / total contaminated samples
**WHO Classification: Ia: extremely hazardous, Ib: highly hazardous, II: Moderately hazardous, III, slightly Hazardous, U: Unlikely to present acute hazard in normal use

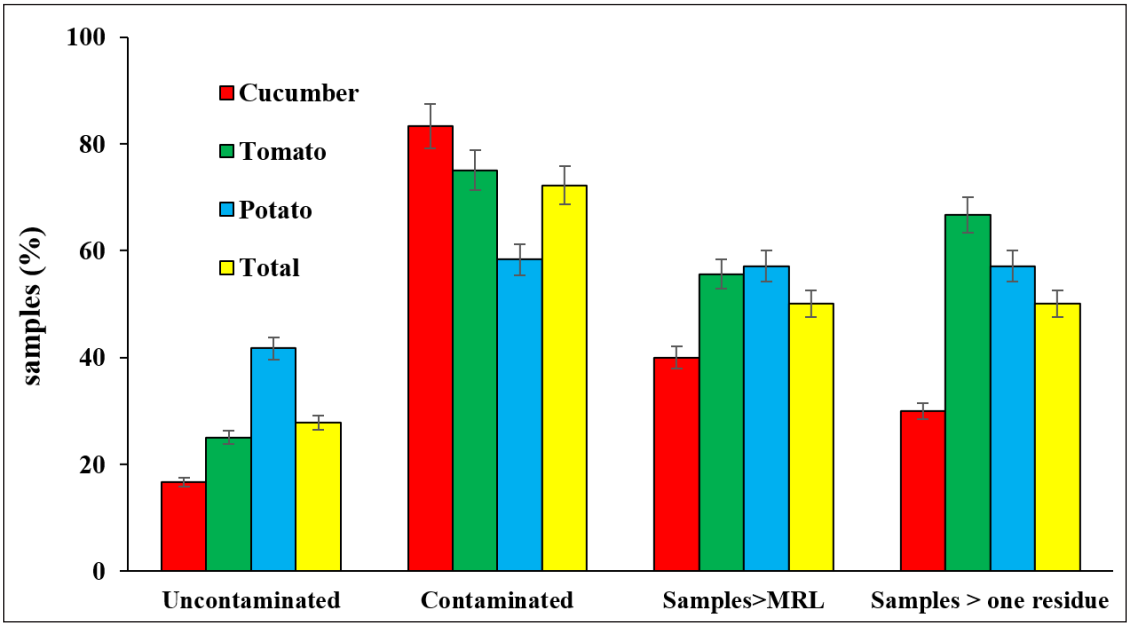

Fig. 4. The total number, of uncontaminated, contaminated, having more than one pesticide of analyzed vegetable samples

Table 2. ADIs, EU MRLs, and National MRLs of detected pesticides in the vegetables of the study area

Pesticides	EU MRL (mg kg^{-1})			National MRL* (mg kg^{-1})			National ADI (mg kg^{-1})
	Cucumber	Tomato	Potato	Cucumber	Tomato	Potato	
Diazinon	0.01	0.01	0.01	0. 1	0.5	0.1	0.005
Chlorpyrifos	0.01	0.01	0.01	0.5	0.1	1	0.01
Dichlorvos	0.01	0.01	0.01	0.2	0.2	0.1	0.004
Malathion	0.02	0.02	0.02	0.2	0.5	005	0.3
Oxydemethon-methyl	0.01	0.01	0.01	0.5	0.05	0.05	0.0003
Pirmicarb	1	0.5	0.5	2	0.5	0.05	0.02
Acetamiprid	0.3	0.3	0.01	0.05	0.05	0.05	0.07
Phosalone	0.01	0.01	0.01	2	0.1	0.1	0.02
Permethrin	0.05	0.05	0.05	0.5	1	0.2	0.05
Mancozeb	2	3	0.3	2	3	0.3	0.03
Penconazole	0.06	0.1	0.01	0.1	0.2	0.05	0.03
Metalaxyl	0.5	0.3	0.02	0.5	0.5	0.5	0.08
Pendimethalin	0.05	0.05	0.05	0.05	0.05	0.1	0.1
Bromopropylate	0.01	0.01	0.01	0.5	0.5	0.5	0.03
Hexythiazox	0.05	0.1	0.01	0.5	0.1	0.7	0.03

*National MRLs were extracted from the website of pesticide Residues of the National Plant Protection Institution (http://mrl.iripp.ir) or Iranian National Standard No. 12581 and 12582.

The standard values of national ADIs, national MRLs, and EU MRLs related to pesticides detected in three products of potato, cucumber, and tomato are shown in Table 2.

The health risk assessment for pesticides whose residual values exceed the MRl values was calculated using native standards and the results are present in Table 3. Among the 15 pesticide residues detected in the examined products, nine pesticides had residual amounts exceeding the MRL in at least one sample including oxydimeton-methyl, chlorpyrifos, diazinon, acetamiprid and metalaxyl in tomatoes; acetamiprid, chlorpyrifos, metalaxyl, and phozalone in cucumbers and four pesticides included dicrovus, oxydimeton- methyl, pendimethalone and piconazole in potatoes. The average pesticide residue detected in each product, the estimated daily intake (EDI), the hazard index (HI) and health risk index (HR), the toxicity index (TQ) of each pesticide, and the cumulative PTI for the mixture of pesticides in the three products were calculated and the results are presented in Table 3. Except for oxydimeton-methyl in tomatoes, all detected pesticides in three vegetables have estimated daily intake values (EDIs) below ADIs, indicating that they do not pose any health risks due to their HI values <below 100. Acetamipride, chlopyriphos, diazinon and metalaxyl had a HI between 0.232 and 23.8%, which was less than 100 in tomato samples, and therefore they did not pose a health risk to humans. The hazard index is 190% for oxydimetone methyl, which means consumption of tomato products that contain residues of this pesticide poses a health risk to the consumer. The hazard index for three pesticides, chlorpyrifos, metalaxyl, and phozalone, in the cucumber samples, ranged between 0.055 and 0.097%, and acetamiprid had the highest hazard index of 60.5%, but all of these values were below the health risk limit. The highest pesticide residue hazard index was 40 and 23 % for oxydimethone- methyl and Dichlorvos in the potato product, respectively (Table 3). The HQ or TQ for a specific pesticide residue is calculated, and the pesticide toxicity index (cumulative risk) is calculated by combining the TQs of different pesticides in each product. A cumulative risk index of pesticide residues in tomatoes, cucumber and potatoes was 15.2, 11.7, and 12.6 and it was higher than the standard value (>1). As a result, long-term consumption of these vegetables containing various pesticide residues may pose a chronic health risk to humans.

Table 3. Average Residue amounts, National MRLs, National ADIs, EDIs, HI, TQ, and PTI of detected pesticides in the vegetables collected from the main wholesale fruit and vegetable market in Ahvaz city, southwest Iran

Crops	Pesticides detected	Freq.	Range (mg kg^{-1})	Average (mg kg^{-1})	National MRL (mg kg^{-1})	National ADI (mg kg^{-1})	EDIs (mg kg^{-1})	HI (%)	HR (Yes/No)	TQ**
Tomato	Oxydemethon-methy	7	0.08-0.56	0.29	0.05	0.0003	0.00057	190	yes	5.8
	Chlorpyrifos	5	0.05- 0.42	0.32	0.1	0.01	0.00063	6.3	No	3.2
	Diazinon	4	0.3-79	0.61	0.5	0.005	0.00119	23.8	No	1.22
	Acetamiparid	5	0.08-0.24	0.19	0.05	0.07	0.00037	0.53	No	3.8
	Metalaxyl	7	0.02-0.67	0.59	0.5	0.5	0.00116	0.232	No	1.18
Pesticide Toxicity Index (PTI)										15.2
Cucumber	Acetamiprid	5	0.29-1.05	0.43	0.05	0.07	0.0423	60.4	No	8.6
	Chlorpyrifos	7	0.16-0.75	0.62	0.5	0.1	0.000061	0.061	No	1.24
	Metalaxyl	3	0.11-0.63	0.59	0.5	0.06	0.000058	0.097	No	0.78
	Phosalone	3	0.07-0.23	0.11	0.1	0.02	0.000011	0.055	No	1.1
Pesticide Toxicity Index (PTI)										11.7
Potato	Dichlorovos	8	0.05-0.19	0.09	0.1	0.0004	0.000092	23	No	0.9
	Oxydemethon-methyl	6	0.02-0.28	0.12	0. 05	0.0003	0.00012	40	No	2.4
	Pendimethalin	4	0.03-0. 8	0.47	0.1	0.1	0.00048	0.48	No	4.7
	Pinconazole	5	0.12-0.31	0.23	0.05	0.03	0.00023	0.767	No	4.6
Pesticide Toxicity Index (PTI)										12.6

***TQ* – toxicity quotients, *ADI* – acceptable daily intake, *EDI* – estimated daily intake, *HI* – hazard index, *HR* – health risk, *MRL* – maximum residue limit.

3.1. Discussion

There has been an increased concern about potential health risks associated with pesticide residues in food, specifically in commonly consumed vegetables such as potatoes, cucumbers, and tomatoes. Acute toxicity symptoms, such as nausea and vomiting, as well as neurological effects, have been observed following high-dose exposures to pesticide residues in food. Several chronic diseases have been linked to long-term pesticide exposure, including cancer, hormone disruption, and reproductive dysfunction [25]. Regulatory authorities in different countries have established MRLs to protect consumers from pesticide residues in food. MRLs are based on comprehensive risk assessments and are set at levels that are considered safe for consumption. These limits vary among countries and are regularly updated to reflect new scientific evidence [26]. Studies have detected pesticide residues in potatoes, cucumbers, and tomatoes, although levels and types of pesticides vary. Organophosphates, carbamates, and pyrethroids are among the pesticides commonly found in these vegetables. The specific risks depend on factors such as agricultural practices, geographical location, and pesticide application methods [27]. In our survey, residues of 15 commonly used pesticides, including insecticides from the organophosphate class, were detected in potatoes, cucumbers, and tomatoes at the main wholesale fruit and vegetable market in Ahvaz city. In the same study, 117 pesticides of organonitrogen, organophosphorus, pyrethroids, triazine, organochlorine, dicarboximides, and strobilurin were detected in some vegetables offered in the main fruit and vegetable market of Tehran in 2014 on 30 samples of cucumbers, tomatoes, cabbage and lettuce by GC-MS method. Out of the 30 samples examined, 53.33% of them were found to contain residues of insecticides. Specifically, the cucumber and tomato samples were found to have residues of endosulfan-I, endosulfan-II, endosulfan-sulfate, chlorpyrifos, and phosalone. However, it is worth noting that the amount of residual pesticides identified in the contaminated samples was significantly lower than the MRLs

recommended by FAO/Codex and the European Union [28]. Our study confirmed the findings of the previous study in terms of the presence of pesticide residues, specifically insecticides, and the detection of chlorpyrifos and phosalone insecticides in tomatoes and cucumbers. However, our study specifically emphasizes that no illegal pesticide residues, particularly from the organochlorine, were detected. In a survey conducted to assess pesticide residue levels in vegetables obtained from major retailers and markets in Dakahlia, Egypt in 2021, it was found that 111 out of 176 samples tested (63.1%) were contaminated with pesticide residues. Among these, 29 samples (16.48%) had residue levels exceeding the MRLs established for safe consumption [22]. Similarly, in our study, out of 36 samples analyzed, 26 samples (72.2%) were found to be contaminated with pesticide residues. Furthermore, 12 samples (36.1%) contained residue levels higher than the MRLs. Notably, both studies detected the presence of chlorpyrifos, acetamiprid, and metalaxyl in tomatoes and cucumbers, while pinconazol and pendimethalin were found in potatoes. There is a significant prevalence of pesticide residues in vegetables obtained from both regions. The detection of certain pesticides across both studies highlights the need for continuous monitoring and regulation to ensure the safety of these food products. Assessment of pesticide residues in commonly used vegetables in Hyderabad, Pakistan in 200 samples of eight vegetables indicated that almost all samples contained pesticides, only 39% contained pesticide residues at or below MRLs, and 61% contained pesticide residues above MRLs [29]. Health risk assessment of pesticide residues involves estimating exposure levels from food consumption and comparing them with toxicological standard values. This process includes evaluating pesticide toxicity, estimating dietary exposure through consumption data, and conducting risk characterizations to determine potential health risks. Uncertainties and variability in data and assumptions are also considered during the assessment [30]. The study included the calculation of individual pesticide HI and Pesticide Toxicity Index (PTI) to assess the health risks associated with the detected pesticide residues in the vegetables. Among the five detected residues, including oxydemethom-methyl, chlorpyrifos, acetamiprid, diazinon, and metalaxyl, the calculated HI ranged from 0.232 to 190. Of particular concern was the highest HI value observed for oxydemethon-methyl, which reached 190 in tomatoes. This indicates a significant health risk for human consumption of tomatoes contaminated with this pesticide residue. Additionally, the study calculated a PTI of 15.2, representing the cumulative toxicity resulting from the detected pesticide residues in the vegetables. This PTI value underscores the overall toxicological impact on human health associated with the presence of these pesticide residues. In the case of cucumbers and potatoes, none of the detected pesticide residues were found to have a hazard risk exceeding 100, indicating that there was no individual pesticide posing a significant health risk. However, the cumulative toxicity of the detected pesticides in cucumbers and potatoes was assessed by calculating the PTI, which yielded values of 11.7 and 12.6. These PTI values confirm the presence of cumulative toxicity resulting from the combined effect of the detected pesticide residues in these vegetables. Our study aligns with the findings of the study in Egypt, which assessed the risk index and cumulative toxicity of pesticide residues in vegetables collected from the main market. In both studies, it was determined that none of the individual pesticides detected in the vegetables except for oxydemethon-methyl in our tomato samples, exceeded a risk index of 100, indicating that they did not pose a significant risk to human health when considered individually. However, the cumulative toxicity (PTI) of the pesticide residues in tomatoes, cucumbers, and potatoes of Egypt was found to be 8.56, 33.92, and 128.44, respectively. These values indicate a high cumulative toxicity resulting from the detected pesticide residues [22]. Our study also observed similar trends in terms of the cumulative toxicity of the pesticide residues in these vegetables, supporting

the findings of the referenced study. These consistent results emphasize the importance of considering the cumulative effects of pesticide residues in assessing their potential impact on human health. Both studies highlight the need for continued monitoring, regulation, and mitigation strategies to ensure the safety of vegetables in the Egyptian market and minimize the cumulative toxicity posed by pesticide residues. Also, many techniques such as gas chromatography with different detectors (FID, MS) based on nanotechnology (CNTs, graphene/graphene oxide, mesoporous silica, MOFs) were used for the removal/separation/extraction/determination of volatile organic materials or nonvolatile organic compounds in water and other matrixes [31-38]. Implementing mitigation strategies can help reduce pesticide residues and associated health risks. Integrated Pest Management (IPM) practices, including biological control, crop rotation, and the use of pest-resistant varieties, can minimize the need for excessive pesticide application. Adhering to Good Agricultural Practices (GAPs), such as proper pesticide handling, application techniques, and observing pre-harvest intervals, is crucial for reducing residues [39]. Consumer awareness plays a vital role in reducing exposure to pesticide residues. Practices such as washing, peeling, and cooking vegetables can further reduce residues. Additionally, choosing organic produce, which prohibits the use of synthetic pesticides, can be an option for individuals concerned about pesticide exposure [40].

4. Conclusion

This survey was the first comprehensive study of the pesticide residues in potatoes, cucumbers, and tomatoes and the health risk assessment of them in Ahvaz city has more recovery for removal of pesticide residues in vegetables (More than 95%). All sample concentrations of pesticide residues in vegetables were determined by GC-MS. Although the health index calculation suggests that only oxydemethon-methyl in tomatoes poses a health risk to humans, the cumulative toxicity index (PTI) values for all three products exceeded the standard (>1). This indicates that there is a potential health risk associated with consuming these products for consumers. Adherence to established MRLs, implementation of mitigation strategies, and consumer awareness can help minimize potential health risks. Continued research, robust monitoring programs, and public education are crucial for ensuring the safety of our food supply and protecting human health in the context of pesticide use in agriculture.

5. Acknowledgment

Mona Sharififard contributed to the conceptualization, data collection, formal analysis, investigation, visualization, and writing the original draft and Afshin Takdastan, Ismaeil Alizadeh Farhad Safdari and Ali Faghihi contributed to the conceptualization, data collection, supervision, resources, writing review and editing. Also, this study was financially by Ahvaz Jundishapur University of Medical Sciences (project No. ETRC-9702) and was approved by the Ethics Committee of Ahvaz Jundishapur University of Medical Sciences (code: IR.AJUMS.REC.1397.173). The authors declare that they have no competing interests.

6. References

[1] J.A. Muñoz, E.F. González, L. Garcıa-Ayuso, A.G. Casado, L. Cuadros-Rodrıguez, A new approach to qualitative analysis of organophosphorus pesticide residues in cucumber using a double gas chromatographic system: GC-pulsed-flame photometry and retention time locking GC–mass spectrometry, Talanta, 60 (2003) 433-447. https://doi.org/10.1016/S0039-9140(03)00108-5.

[2] C. Pan, L. Wang, X. Kong, S. Jiang, C. Qian, Determination of 15 organophosphorus pesticides in cucumber, tomato and pepper samples by capillary gas chromatography with gel permeation chromatographic clean-up, Chin. J. Chromatogr., 20 (2002) 565-568. https://pubmed.ncbi.nlm.nih.gov/12683010/

[3] I. Ferrer, J.F. Garcia-Reyes, M. Mezcua, E.M. Thurman, A.R. Fernández-Alba, Multi-residue

pesticide analysis in fruits and vegetables by liquid chromatography–time-of-flight mass spectrometry, J. Chromatogr. A, 1082 (2005) 81-90. https://doi.org/10.1016/j.chroma.2005.03.040

[4] W. Helferich, C.K. Winter, Food Toxicology, CRC press book, 240 pages, 2000. https://doi.org/10.1201/9781420038316

[5] M. Barriada-Pereira, P. Serôdio, M. González-Castro, J. Nogueira, Determination of organochlorine pesticides in vegetable matrices by stir bar sorptive extraction with liquid desorption and large volume injection-gas chromatography–mass spectrometry towards compliance with European Union directives, J. Chromatogr. A, 1217 (2010) 119-126. https://doi.org/10.1016/j.chroma.2009.10.076

[6] K. Goh, F. Yew, K. Ong, I. Tan, Acute organophosphorus food poisoning caused by contaminated green leafy vegetables, Arch. Environ. Health, 45 (1990) 180-184. https://doi.org/10.1080/00039896.1990.9936713

[7] M.S. Yazgan, A. Tanik, A new approach for calculating the relative risk level of pesticides, Environ. Int., 31 (2005) 687-692. https://doi.org/10.1016/j.envint.2004.12.002

[8] M. Arjomandi, A review: analytical methods for heavy metals determination in environment and human samples, Anal. Methods in Environ. Chem. J. 2 (2019) 97-126. https://doi.org/10.24200/amecj.v2.i03.73

[9] A.Sharma, V. Kumar, B.Shahzad, M. Tanveer, Worldwide pesticide usage and its impacts on ecosystem, SN Appl. Sci., 1 (2019) 1-16. https://doi.org/10.1007/s42452-019-1485-1

[10] F.Norouzi, I, Alizadeh, M. Faraji, Human exposure to pesticides and thyroid cancer: a worldwide systematic review of the literatures, Thyroid Res., 16 (2023) 1-7. https://doi.org/10.1186/s13044-023-00153-9

[11] F. Norouzi, M. Faraji, R. Sadeghi, A. Faghihi-Zarandi, F.S. Boroujeni, Determination and analysis of pesticide residues in fieldgrown and greenhouse-grown tomatoes using liquid chromatography-mass spectrometry, Anal. Methods. Environ. Chem. J., 6 (2023) 100-114. https://doi.org/10.24200/amecj.v6.i01.234

[12] H.D. Burrows, J. Santaballa, S. Steenken, Reaction pathways and mechanisms of photodegradation of pesticides, J. Photochem. Photobiol. B: Biol., 67 (2002) 71-108. https://doi.org/10.1016/S1011-1344(02)00277-4

[13] R.B. Maybury, Codex alimentarius approach to pesticide residue standards, J. AOAC Int., 72 (1989) 538-541. https://doi.org/10.1093/jaoac/72.3.538

[14] M. Hernández Torres, F. Egea González, M. Castro Cano, M. Moreno Frías, J. Martínez Vidal, Residues of methamidofos, malathion, and methiocarb in greenhouse crops, J. Agric. Food Chem., 50 (2002) 1172-1177. https://doi.org/10.1021/jf0108112

[15] C. Torres, Y. Picó, J. Manes, Determination of pesticide residues in fruit and vegetables, J. Chromatogr. A, 754 (1996) 301-331. https://doi.org/10.1016/s0021-9673(96)00407-4

[16] K.L. Bassil, C.Vakil, M. Sanborn, D.C. Cole, J.S. Kaur, K.J. Kerr, Cancer health effects of pesticides: systematic review, Can. Fam. Physician., 53 (2007) 1704-1711. https://www.cfp.ca/content/53/10/1704.long

[17] J.H. Hotchkiss, Pesticide residue controls to ensure food safety, Crit. Rev. Food Sci. Nutr., 31 (1992) 191-203. https://doi.org/10.1080/10408399209527568

[18] N.S. Singh, R. Sharma, T. Parween, P. Patanjali, Pesticide contamination and human health risk factor, Modern age environmental problems and their remediation, Springer publisher, Chapter pages 49-68, 2018. https://doi.org/10.1007/978-3-319-64501-8_3

[19] I. Alizadeh, E. Jahanifard, M. Sharififard, M.E. Azemi, Effects of resident education and self-implementation of integrated pest management strategy for eliminating bed bug infestation in Ahvaz City, Southwestern Iran, J. Arthropod. Borne Dis., 14 (2020) 68. https://doi.org/10.18502/jad.v14i1.2705

[20] M. Sharififard, I. Alizadeh, E. Jahanifard, A. Saki-Malehi, Prevalence and spatial

distribution of bed bug, Cimex lectularius, infestation in the southwest of Iran: GIS approach, J. Arthropod. Borne Dis., 14 (2020) 29. https://doi.org/10.18502/jad.v14i1.2701

[21] A. Mohammadi, M. Faraji, A.A. Ebrahimi, S. Nemati, A. Abdolahnejad, M. Miri, Comparing THMs level in old and new water distribution systems; seasonal variation and probabilistic risk assessment, Ecotoxicol. Environ. Saf., 192 (2020) 110286. https://doi.org/10.1016/j.ecoenv.2020.110286

[22] S.E.M. Shalaby, G.Y. Abdou, I.M. El-Metwally, G. Abou-elella, Health risk assessment of pesticide residues in vegetables collected from Dakahlia, Egypt, J. Plant Prot. Res., (2021) 254-264. https://doi.org/10.24425/jppr.2021.137951

[23] S.A.G. Alla, N.M. Loutfy, A.H. Shendy, M.T. Ahmed, Hazard index, a tool for a long term risk assessment of pesticide residues in some commodities, a pilot study, Regul. Toxicol., 73 (2015) 985-991. https://doi.org/10.1016/j.yrtph.2015.09.016

[24] M. Bhanti, A.Taneja, Contamination of vegetables of different seasons with organophosphorous pesticides and related health risk assessment in northern India, Chemosphere, 69 (2007) 63-68. https://doi.org/10.1016/j.chemosphere.2007.04.071

[25] WHO, Pesticide Residues in Food: Toxicological Evaluations, World Health Organization, 2021. https://www.who.int/publications/i/item/9789240054622

[26] EFSA, European Food Safety Authority, P. Medina-Pastor, G. Triacchini, The 2018 European Union report on pesticide residues in food, EFSA J., 18 (2020) e06057. https://doi.org/10.2903/j.efsa.2020.6057

[27] USFAO, Food and Agriculture Organization of the United Nations, Pesticide residues in food, 2019. http://www.fao.org/3/ca5834en/ca5834en.pdf

[28] EFSA, 2017 European Union report on pesticide residues in food, European Food Safety Authority (EFSA), 2019. https://www.efsa.europa.eu/en/efsajournal/pub/5348

[29] Z. Hadian, M. Azizi, Pesticide residues in vegetables marketed in the main wholesale fruit and vegetable market in Tehran as determined by gas chromatography/mass spectrometry, Iran. J. Nutr. Sci. Food Technol., 1 (2006) 13-20. https://nsft.sbmu.ac.ir/article-1-14-en.html

[30] Y. Latif, S. Sherazi, M. Bhanger, Assessment of pesticide residues in commonly used vegetables in Hyderabad, Pakistan, Ecotoxicol. Environ. Saf., 74 (2011) 2299-2303. https://doi.org/10.1016/j.ecoenv.2011.07.030

[31] M. Asl, H. Shirkhanloo, N. Mansouri, H. S. Mirzahosseini, F. Atabi, Simultaneity comparative evaluation of toluene removal from the air by adsorption and UV semi-degradation-based adsorption procedure, Int. J. Environ. Sci. Technol., 21 (2024) 6677–6694. https://doi.org/10.1007/s13762-024-05503-0

[32] M.M. Asl, H. Shirkhanloo, N. Mansouri, S.A.R.H.S. Mirzahosseini, F. Atabi, Functionalized graphene oxide with bismuth and titanium oxide nanoparticles for efficiently removing formaldehyde from the air by photocatalytic degradation–adsorption process, J. Anal. Test., 7 (2023) 444-458. https://doi.org/10.1007/s41664-023-00272-0

[33] S. Teimoori, H. Shirkhanloo, A.H. Hassani, M. Panahi, N. Mansouri, An immobilization of aminopropyl trimethoxysilane-phenanthrene carbaldehyde on graphene oxide for toluene extraction and separation in water samples, Chemosphere., 316 (2023) 137800. https://doi.org/10.1016/j.chemosphere.2023.13780

[34] S. Teimoori, H. Shirkhanloo, A.H. Hassani, M. Panahi, N. Mansouri, Rapid extraction of BTEX in water and milk samples based on functionalized multi-walled carbon nanotubes by dispersive homogenized-micro-solid phase extraction, Food Chem., 421 (2023) 136229. https://doi.org/10.1016/j.foodchem.2023.136229

[35] S. Teimoori, H. Shirkhanloo, A. Hassani, M. Panahi, N. Mansouri, New extraction of

toluene from water samples based on nano-carbon structure before determination by gas chromatography, Int. J. Environ. Sci. Technol., 20 (2023) 6589-6608. https://doi.org/10.1007/s13762-023-04906-9

[36] J. Rakhtshah, H. Shirkhanloo, N. Esmaeili, A rapid extraction of toxic styrene from water and wastewater samples based on hydroxyethyl methylimidazolium tetrafluoroborate immobilized on MWCNTs by ultra-assisted dispersive cyclic conjugation-micro-solid phase extraction, Microchem. J., 170 (2021) 106759. https://doi.org/10.1016/j.microc.2021.106759

[37] R. Ashouri, H. Shirkhanloo, A. Rashidi, S. Mirzahosseini, N. Mansouri, Dynamic and static removal of benzene from air based on task-specific ionic liquid coated on MWCNTs by sorbent tube-headspace solid-phase extraction procedure, Int. J. Environ. Sci. Technol., 18 (2021) 2377-2390. https://doi.org/10.1007/s13762-020-02995-4

[38] R. Ashouri, S.A. Hajiseyed Mirzahosseini, H. Shirkhanloo, A. Rashidi, N. Mansouri, Synthesis of carbon quantum dots from olive stones for efficient adsorption of benzene from the ambient air, J. Nanostruct., 11 (2021) 480-497. https://doi.org/10.22052/JNS.2021.03.007

[39] US EPA, Pesticide Ecological Risk Assessment, United States Environmental Protection Agency, 2020. https://www.epa.gov/pesticide-science-and-assessing-pesticide-risks/pesticide-ecological-risk-assessment

[40] USDA, good agricultural practices (GAPs), and good handling practices (GHPs), United States Department of Agriculture (USDA), 2021. https://www.ams.usda.gov/grades-standards/gap-ghp

Anal. Methods Environ. Chem. J. 7 (3) (2024) 34-50

AMECJ

Research Article, Issue 3
Analytical Methods in Environmental Chemistry Journal
Journal home page: www.amecj.com/ir

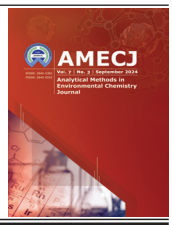

Significant research on meropenem cross-contamination management in a β-Lactam manufacturing unit: A high-performance liquid chromatography approach

Mohabbat Ullah[*, a, b], Obydulla[b, c], and Md. Sohel Rana[a]
[a]*Department of Pharmacy, Jahangirnagar University, Savar, Dhaka, Bangladesh*
[b] *ACME Laboratories Ltd., Dhulivita, Dhamrai, Dhaka, Bangladesh*
[c] *Department of Pharmacy, Daffodil International University*

ARTICLE INFO:
Received 17 May 2024
Revised form 24 Jul 2024
Accepted 30 Aug 2024
Available online 30 Sep 2024

Keywords:
Meropenem,
High-performance liquid chromatography,
Antibiotic resistance,
Cross-contamination,
Drug manufacturing unit,
Microflora

ABSTRACT
Rapid, simple, and sensitive high-performance liquid chromatography with diode-array detection (HPLC-DAD) techniques are described for quantitatively determining meropenem residue from the contact parts of injection filling machines. This involves swab sampling collected after cleaning. The method also addresses the management of meropenem cross-contamination in shared cephalosporin production facilities. Cross-contamination is the product mix-up by which a trace amount of antibiotics can be present in other products that cannot prevent infections but can contribute to initiating antibiotic-resistant pathogens into human microflora. Poor beta-lactam contaminant control can cause residual Meropenem in different dosage forms, resulting in meropenem residue in the human intestinal flora, blood during sepsis, or Environmental wastes. During manufacturing, there should be a validated scientific control with proper monitoring of meropenem contamination. Meropenem residue was determined on the contact parts of production machines using swab sampling collected from surfaces after cleaning. An isocratic chromatographic system used with a mobile phase consisting of acetonitrile: 20% tetrabutylammonium hydroxide adjusted to pH 6.5 ± 0.05 (30:70, v/v) on XTerra RP18 column at a flow rate 1.0 mL min^{-1} with an injection volume, 20 µL and UV (290 nm). HPLC-DAD method developed was found to be linear ($R^2 \geq 0.999$), sensitive, precise (RSD < 2.7%), accurate (recovery between 97% and 109%), and LOD and LOQ were obtained at 0.05 and 0.10 mg $L^{-1,}$ respectively. The area RSD (%) for six replicate injections of LOQ was 7.6. This study validated the Meropenem contaminant controlling procedure for drug manufacturers.

1. Introduction

Meropenem is a parenteral carbapenem that is structurally a B-lactam antibiotic like penicillin and cephalosporin (Fig. 1). It has a broad spectrum Antibiotic with excellent bactericidal activity against clinically significant gram-negative and gram-positive aerobic and anaerobic bacteria [1,2]. Meropenem Antibiotic is manufactured as a β-Lactam group in the same manufacturing unit as other non-penicillin beta-lactam compounds according to cGMP in Bangladesh [3].

*Corresponding Author: Mohabbat Ullah
Email: mohabbatullahhera@gmail.com
https://doi.org/10.24200/amecj.v7.i03.286

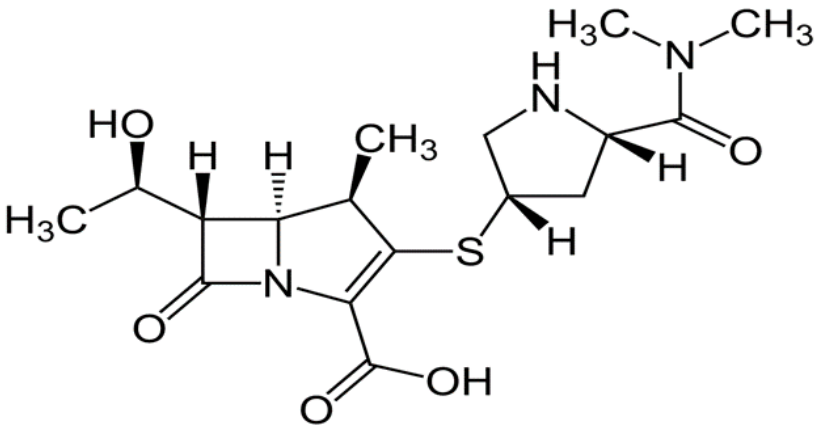

Fig. 1. Structure of Meropenem Trihydrate

Carbapenem, especially Meropenem, is now recognized as the major treatment entity for multi-drug-resistant gram-negative bacteria by WHO, the US CDC, and the ECDC. However, this drug is also becoming resistant among MDR Gram-negative organisms, whereas carbapenem monotherapy may no longer be effective for many patients with severe Gram-negative infections [4]. WHO recommended Carbapenem under the Priority 1 or critical pathogens list for R&D of new antibiotics innovation due to its resistance to several bacteria like Acinetobacter baumannii, Pseudomonas aeruginosa, or Enterobacteriaceae [5]. Meropenem resistance occurs through different mechanisms of action, such as porin-mediated resistance or the overproduction of efflux pumps. Still, Enzyme-mediated resistance to the production of beta-lactamases is, most importantly, the main mechanism by which Bacteria can inactivate carbapenems together with other beta-lactam antibiotics and, therefore, called carbapenemases. This enzyme hydrolyzes almost all beta-lactams [2, 6]. Many sources are found through which bacteria can be resistant, and environmental pollution with residue from carbapenems is one of the main sources of resistant bacteria. Ultimately, all the other pollutions are finally linked to environmental pollution, especially Soil, Water, and Air. Environmental factors, such as lower initial cephalosporin concentration, higher MnO_2 loading, and lower solution pH, promote the oxidative transformation of cephalosporin antibiotics by manganese dioxides [7]. Cephalosporin degradation is accelerated in elevated salt matrices, with chlorine and carbonate radicals involved. High salt-containing hospital wastewater promotes degradation, suggesting thermally activated persulfate as a treatment. However, excessive use of cephalosporin antibiotics in medicine leads to frequent detection in aquatic matrices, posing public health and ecosystem risks [8]. Multiple sources have been identified for this environmental pollution, and the drug manufacturing unit is at the top. Cross-contamination from drug manufacturing exerts a residual amount of Meropenem on other drugs, contributing to this drug's resistance to known pathogens. Meropenem is specially manufactured by injection, and the products whose contamination is likely most significant are those administered by injection [9]. Cross-contamination might cause several organizational risks, like GMP Non-compliance, product recalls, sales loss, or audit failure, which can affect a company's reputation. Besides this, beyond the current concept, this might cause Antibiotic resistance. For example, If Meropenem residue is cross-contaminated with any other dosage forms/products, then it will be available either in the Bloodstream or Intestinal flora where different human pathogens present and the chances of Meropenem-resistant gene or Meropenem-resistant pathogen are purulent [10-15]. When Meropenem products are manufactured combined with other β-Lactms or products, the prevention of cross-contamination becomes one of the major concerns. If residues of Meropenem remain after

cleaning the production equipment, then the product contact surfaces may contaminate the next product manufactured in the same manufacturing equipment. In Bangladesh, around 37 companies are manufacturing the Meropenem injection along with other β-Lactams or products with the same manufacturing machinery [16]. Cleaning validation is the major cGMP tool to control the cross-contamination of pharmaceutical products, and it is performed by considering many factors. The product selection is performed through worse-case determination [9,17], whether Meropenem might be selected. However, considering antibiotic resistance and GMP requirements, pharmaceutical drug manufacturing must have a proper control strategy to manage Meropenem drug residue contamination with other drugs. A literature survey reveals that there are publications on the determination of Meropenem, either alone or in combination with other drugs. These determinations have been carried out using various instruments such as HPLC, UV spectrophotometer, or LC-MS to analyze pharmaceutical dosage forms or human plasma.[18-31]. However, no literature is available on complete control management with residue determination techniques to control the Meropenem residue contamination to the next product manufacturing into a drug manufacturing unit. Several ultra-high performance liquid chromatography with diode-array detection (UHPLC-DAD) methods have been reported for the determination of cephalosporin molecules like cefixime, Cefazoline sodium, ceftazidime, cefotaxime, ceftriaxone, Cephradine dehydrate, Cephapirin sodium, cefepime, Cefuroxime sodium and cephalexin as well as Molecularly imprinted polymers (MIPs) were synthesized for the determination also reported [32], [33], [34]. Only one HPLC method was found to determine the cephalosporin residues on spiked stainless-steel plates and human plasma as a worse-case product for CIP [35]. However, there is still a huge requirement for publication in this area. The analytical technique of choice in this study was high-performance liquid chromatography (HPLC) coupled with a diode array detector (DAD) [36]. This study aims to develop an HPLC method to determine Meropenem in residue levels spiked with different contact parts of the injection production line, including Stainless steel, Teflon, Glass & Silicon, etc. Finally, a complete management procedure is to be established through a validation technique by which it is to be proved that Meropenem residue doesn't contaminate the next manufactured drugs.

2. Experimental

The standard manufacturing process of Meropenem injection starts with sterilizing utensils, Room garments, Flip-off seals, Rubber stoppers, and Product contact parts. The active ingredient of Meropenem for injection is marketed as Meropenem with a mixture of sodium carbonate sterile, and the container is directly transferred to the manufacturing area after weighing in the aseptic filling area and loaded into the hopper of the filling machine. Then, the vials are washed, sterilized, and depyrogenated (at 305^0C with 136mm min^{-1} belt speed). Then, the vials are filled with a vial filling machine and sealed with a vial cap sealing machine. Sealed vials are visually checked and then labeled. Labeled vials are blistered with proper diluents. Finally, the blisters are cartooned for marketing.

A protocol for monitoring Meropenem residue on contact parts before changeover needs to be prepared, through which regular monitoring and management will be performed. The meropenem injection is manufactured by filing the ready-mix API into the vial for injection and market with a diluent-like water for injections (WFI) for intravenous injection. A sample manufacturing flowchart for the meropenem injection filling line is shown in Figure 2.

2.1. Chemicals and reagents

Meropenem (potency: 73.2%) working standard and API obtained from The ACME Laboratories, Dhamrai, Dhaka, Bangladesh. HPLC grade acetonitrile (CAS N.: CAS No.: 75-05-8), tetra butyl ammonium hydroxide 40% (CAS N.: 2052-49-5), and phosphoric acid (CAS N.:7664-38-2) were procured from Sigma Aldrich, Germany. HPLC-grade deionized water was used.

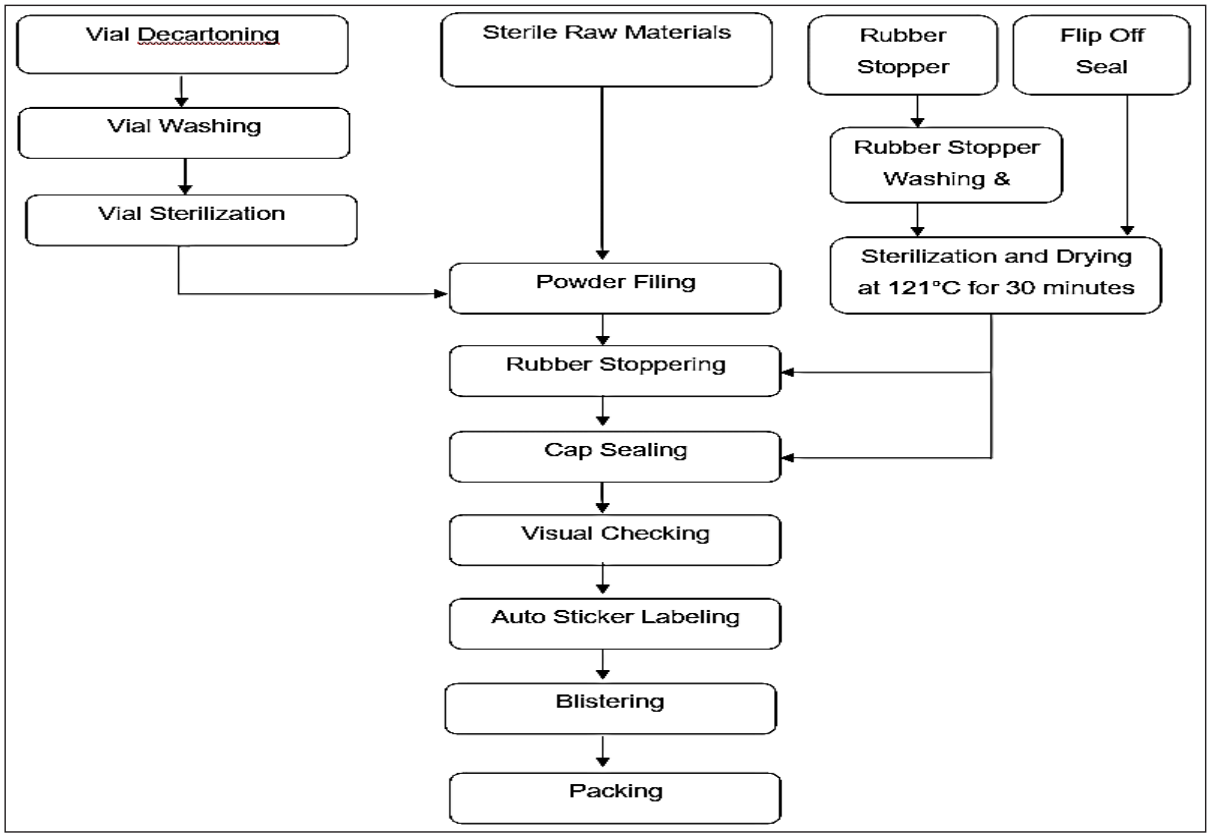

Fig. 2. A sample Manufacturing Flowchart for Meropenem Injection filling line

2.2. Instruments

Waters e2695 HPLC System with 2998 PDA detector (WTR-e2695-2998) includes waters 2695 separations module HPLC system (autosampler, quaternary pump, degasser, and sample heater/ cooler) with waters 2998 photodiode array detector (PDA) (Empower three software), injection volume of 0.1 - 100 µL, the standard of 0.1- 2000 µL, sartorius electronic analytical balance, ultrasonic bath, Mettler Toledo pH meter, and waters XTerra RP18 (4.6 x 250 mm, 5 µm) column was used.

2.3. Mobile Phase & Diluent

Transfer 6.5 mL of Tetra-butyl ammonium hydroxide solution (20%) and dilute with water to obtain 1000 mL solution and mix properly. Adjust the pH of the solution to 6.5 ± 0.05 with phosphoric acid. Dilute 700 mL of this solution with 300 mL acetonitrile and mix the solution. Filter the solution through a 0.22µm membrane filter. This solution has also been used as a diluent to prepare the analytical solutions.

2.4. Wavelength detection

29.7 mg Meropenem sodium carbonate working standard equivalent to 25.0 mg Meropenem was weighed into a 100 mL volumetric flask. 20 mL of mobile phase was added, and the solution was sonicated for 5 minutes until completely dissolved. It made up the volume with the mobile phase and mixed well. Transferred 4 mL of this solution to 100 mL volumetric flask and volume with mobile phase and prepared a solution containing 10 µg/mL concentration of Meropenem. Filtered the solution through a PTFE syringe filter, 0.45 µm, collected the solution in a clean and dry vial, and scanned between 200 and 400 nm with 2998 PDA detector of Waters 2695 HPLC system. The maximum absorbance of each molecule was around 254 nm; thus, the wavelength detection was set at 290 nm.

2.5. Chromatographic conditions

Chromatographic conditions were finalized as ambient column oven temperature with a 290 nm UV detection at a flow rate of 1.0 mL per min at isocratic elution, and the run time was only 6 minutes as the retention time of Meropenem is only 3 minutes. Before injection, the column needs to be equalized with the Mobile phase for 60 minutes. The injection volume was set to 20 µL.

2.6. Pretreatment of swabs & Swab blank solution

Swab Stick (TX714 or TX715, Tex wipe swabs) was used, and the mobile phase was used to swab diluent. The swab sticks were dipped into a sufficient amount of swabbing diluent in a beaker sonicate for 10 minutes, and kept the sticks on a watch glass for drying. A pretreated swab stick was taken into a test tube containing 10 mL of swabbing diluent sonicated for 5 minutes and mixed well to see the blank interference.

2.7. System suitability solution preparation

Weighed accurately and transferred about 29.7 mg of Meropenem with sodium carbonate equivalent to 25.0 mg Meropenem working standard into a 100 mL clean and dried volumetric flask and added 60 mL mobile phase and sonicated about 5 minutes to dissolve, made volume up to 100 mL with mobile phase and mix well. Transfer 4 mL of this solution to a 100 mL volumetric flask and volume with mobile phase. 10.0 µg mL^{-1} solution was prepared through further dilution of this solution with diluent. Filtered the solution through a PTFE syringe filter, 0.45 µm, and collected the solution in a clean and dry vial.

2.8. Selection of Cleaning Level and Cleaning Procedure Identification

Meropenem with sodium carbonate is a salt-form API administered directly after reconstitution. If Meropenem injection is manufactured in the same production line with other β-Lactams/products, then the production of Meropenem injections should be on a Campaign basis. That means the production planning should be done during Meropenem injection manufacturing. Other products will not be manufactured at all into the injection line. So, it will be easy to control the cross-contamination due to manufacturing on a campaign basis. After completion of Meropenem campaign manufacturing, A-type general cleaning needs to be conducted to execute the changeover. Meropenem with sodium carbonate is very soluble in water [37]; thus, cleaning the machine, including contact parts, has been developed with purified water. Finally, the machines and contact parts are rinsed with WFI & Isopropyl alcohol to make them ready by keeping them safe from Microbial contamination.

2.9. Selection of Machine Parts for Meropenem API contacts

After evaluating the contact parts of the Meropenem injection line, it is identified that the injection filling unit has direct contact with the Meropenem API as the API containers are kept on the machine's hopper, and then the automatic filling line starts. Several contact parts of this filling line are available and undergo contact with the Meropenem API, which depends on the brand/model of different manufacturers' injection filling machines. Some common contact parts are the container holder/adapter, stainless steel (S.S) channel, silicon channel, upper hopper, lower hopper made of glass, S. S. powder support, side cover, dosing disc, etc. (Fig. 3). Four types of material of construction for this contact parts have been identified and found as stainless steel, Teflon, glass, and silicon (Fig. 4).

During the sampling exercise, the change parts were visually examined, and a visual inspection was performed before and after the swab sampling. These visual check results were also recorded to validate the cleaning procedure. The sample will be taken from the areas that are most difficult to clean visually. All sampling locations and sample

Fig. 3. A sample powder for injection filling machine from Macofer (Romaco Holding GmbH, sampling Location is shown in Table 1) [38]

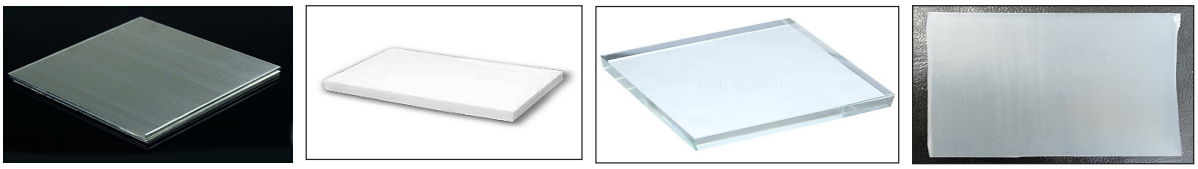

Fig. 4. The contact parts items used for swabbing method validation

Table 1. Sampling location and Sample quantity for residue determination

Equipment Name	Sampling Location		Swab Sample quantity
Vial filling and rubber stoppering machine	A	Container Holder/ Adapter	S-1: Lower side of Adapter S-2: Inner Wall of Adapter
	B	S.S Channel	S-3: Inner wall of S.S Channel S-4:Inner wall of S.S Channel
	C	Silicon Channel	S-5: Inner Side of Silicon Connector S-6: Front Side of Silicon Connector
	D	Upper Hopper	S-7: Inner Wall Corner of Upper Hopper S-8: Inner Middle Side of Upper Hopper S-9: Lower side of Upper Hopper
	E	Lower Hopper (glass)	S-10: Glass of Lower Hopper
	F	S. S Powder support	S-11: Inner side of Lower Hopper
	G	Side Cover	S-12: Glass of Lower Hopper
	H	Dosing disc with Niddle	S-13: Inner side of Dosing Disc S-14: Niddle
Total Samples			14

quantities were determined in Table 1.

2.10. Swabbing Procedure and Preparation for Swabbing Sample

Corresponding to each swab location, one pretreated swab stick with mobile phase as diluent taken containing 10 mL swabbing diluent by dipping and removing the excess swabbing diluent by pressing the wet swab stick head against the walls of the test tube, swabbing the designated cleaned equipment location of size 5×5 cm (25sq.cm) as per the following procedures (Fig. 5). The first side of the swab is swiped horizontally over the designated location, then the swab is flipped over and the second side is swiped vertically downwards over the same surface, dip the swab stick into the diluent, squeeze the swab, and take it out. Now, swab the wet surface area with a dry pretreated swab using the same procedure described above. Immediately after swabbing, transfer the sticks into the test tube containing 10 mL of swabbing diluent. Sonicate the solution for about 5 minutes, squeeze the swab stick, and take it out. Filtered the solution through a PTFE syringe filter, 0.45 µm, and collected the solution in a clean and dry vial.

3. Results and Discussion

3.1. Method validation study

A cost-effective HPLC method has been developed to test the Meropenem residue on the contact parts. The test method has been validated for the analysis of the residue of Meropenem to evaluate the cleaning procedure of the drug product manufacturing equipment. So, the method validation for residue determination of Meropenem has been performed on 5 X 5 cm^2 of 316 stainless steel, Teflon, glass, and silicon. During the validation process, several experiments have been performed to demonstrate that the method used for the residue analysis of Meropenem injection is specific and consistently generates reproducible data. System suitability, specificity, LOD, LOQ, linearity, recovery efficiency/recovery factor, precision, accuracy, stability of the analytical solution and mobile phase, filter evaluation, and robustness have been obtained to confirm the method as validated.

3.2. Validation parameter

3.2.1.Specificity

After evaluating all the materials for the construction of the injection line, we contacted Meropenem and found stainless steel, basically 316 stainless steel, Teflon, Glass, & Silicon. Thus, we collected these items from the same construction material as contact parts of the Injection filling machine and checked the interference of the Diluent used for swabbing diluent. This method can also test the wastewater from the drug manufacturing unit and the Exhaust Air sample. Waste water was checked for specificity by seeing the interference with water, and for the Exhaust Air sample, swabbing from stainless steel was practically done. Thus, the specificity of 316 stainless steel will work for the same. There was no interference peak at the retention time of Meropenem.

3.2.2.Linearity, LOD and LOQ

LOD & LOQ are two of the main parameters that will be determined to ensure the lowest detectability of Meropenem by this method. Thus, to determine the LOD & LOQ, the linearity of the Meropenem

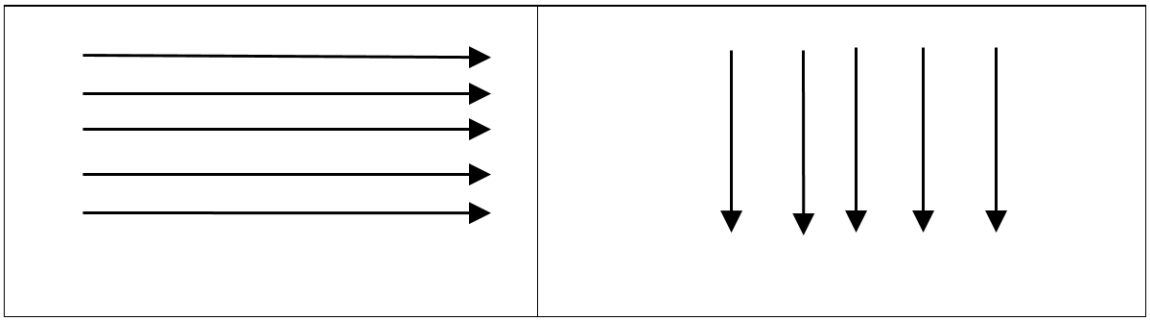

Fig. 5. Swabbing Technique, Total 10 Strokes (5 strokes in each direction)

working standard has been performed individually at concentration levels 0.1 – 15 µg mL^{-1}. The statistical data for linearity has been calculated as per the linear regression line, and the linearity of individual cephalosporin compounds with a correlation coefficient (r) was found to be equal to or more than 1.000. LOD means the lowest detectable amount of a sample solution, which cannot be quantified but can be detected using the analytical procedure. Standard deviation (SD) and slope values (S) were taken to calculate the LOD & LOQ calculated by using the calibration curve with the formula LOD = 3.3 (SD/S) and LOQ = 10 (SD/S).

3.2.3.Determination of recovery efficiency and recovery factor

Evaluation of recovery efficiency is the most critical part of swab recovery. Here, we recovered at LOQ, 50%, 100%, and 150% levels of the nominal concentration of 10 ppm Meropenem. To determine the recovery factor, we used Equation 1 if the mean recovery is below 95%.

$$\textbf{Recovery factor} = \frac{\text{Theoretical result (100 \%)}}{\text{Mean recovery (\%)}}$$

(Eq.1)

3.2.4.Method precision and intermediate precision

Method precision and Intermediate precision were carried out for the swabbing samples injection into two different HPLC systems (Waters and Shimadzu). Prepared the swabbing spiked sample with known concentration at 100% Level (10 mg L^{-1}) of Meropenem onto different contact parts like 316 Stainless steel, Teflon, Glass, & Silicon. The samples were dried, and took swab samples according to the method. Then, the samples were injected, and the peak area was measured. The peak area of Meropenem of six swab sample solutions for different items was calculated and reported along with the standard deviation and RSD% of the peak area of these solutions for Meropenem.

3.2.5.Solution Stability

The stability of the standard solution and swabbing sample solutions from different machine contact parts (316 stainless steel, Teflon, glass, and silicon) has been determined by keeping the samples in an ambient condition and 2-8°C condition.

3.2.6.Filter validation

To demonstrate filter compatibility in standard solution and sample solution by discarding different volumes as well as 2 mL, 4 mL, and 6 mL by using PVDF / PTFE 0.45 µm cartridge filter, swab recovery sample solutions for glass plate, Teflon, SS plate, silicon plate has been considered for filter evaluation study.

3.2.7.Robustness

The robustness has been done with different chromatographic parameter changes like wavelength variation (± 5 nm), Flow rare variation (± 0.1 mL/min), and column oven temperature variation (25°C ± 5°C).

3.2.8.Establishment of acceptance criteria for Meropenem residue

The acceptance criteria of Meropenem residue on each machine contact part (Adapter, S.S Channel, Silicon Channel, Upper Hopper, Lower Hopper, S.S Powder support, side cover, and dosing disc) has been set as No residue will be present / if present, should be less than LOQ level (0.10 mg L^{-1}).

3.3. Discussion

Meropenem residue might cause selective pressure on the pathogens to produce carbapenem, which is difficult to treat and has high mortality rates due to its appearance in multidrug-resistant pathogens such as K. pneumoniae, p. aeruginosa, and Acinetobacter spp. [39]. There are several ways to initiate this contamination. Pharmaceutical drug manufacturing is one of the main sources of this. Meropenem drugs are being manufactured in Bangladesh in the same manufacturing facilities as other beta-lactams/ drugs. Thus, it is a must to ensure the lowest level

of residue contamination with other drugs during the changeover. To facilitate this management technique, Meropenem should be controlled from entry to drug manufacturing to the final dispatch. The management initiated everything from procedural development to the implementation of practices in the drug manufacturing unit. The protocol-based studies represent the total control mechanism of Meropenem residue during manufacturing, and the residue determination method details the capability of this method to identify and quantify the Meropenem residue remaining on contact parts after cleaning. The responsibilities, cleaning procedure, sampling procedure, testing procedure, testing method, acceptance criteria, and reporting have been done according to a protocol-based study. Meropenem residue of machine contact parts can be identified and quantified to a minimum level (0.05 mgL^{-1} LOD) by the developed method with an isocratic mobile phase consisting of TBAH buffer, pH 6.5, and acetonitrile at a ratio of 70:30 with a 250 cm x 4.6 mm, five µ column as the stationary phase at ambient oven temperature and a flow rate of 1.0 mL min^{-1}. The developed method demonstrated no interference with a unique chromatogram for diluent, standard, swabbing diluent, and swab samples with contact parts. The stability of the analytical solution was determined, and the solutions remained stable for up to 24 hours under ambient conditions.

All System Suitability criteria were met as per the requirements. The theoretical plat count for column efficiency was more than 2000 USP, the USP Tailing factor was less than 2.0, and the peak area percentage relative standard deviation (RSD) of six standard solutions was less than 10.0%; the recovery of standard (1) and Standard (2) solution was within 98.0%-102.0%, Overall % RSD of all standard solution (1) and bracketing standard (standard solution1) was within 10.0 %. The solvent interference was checked with a diluent. The retention times of the analyte peak in a spiked sample and the standard are eluted at the same retention times. Therefore, this method was specific. The swabbing diluent/bank and the

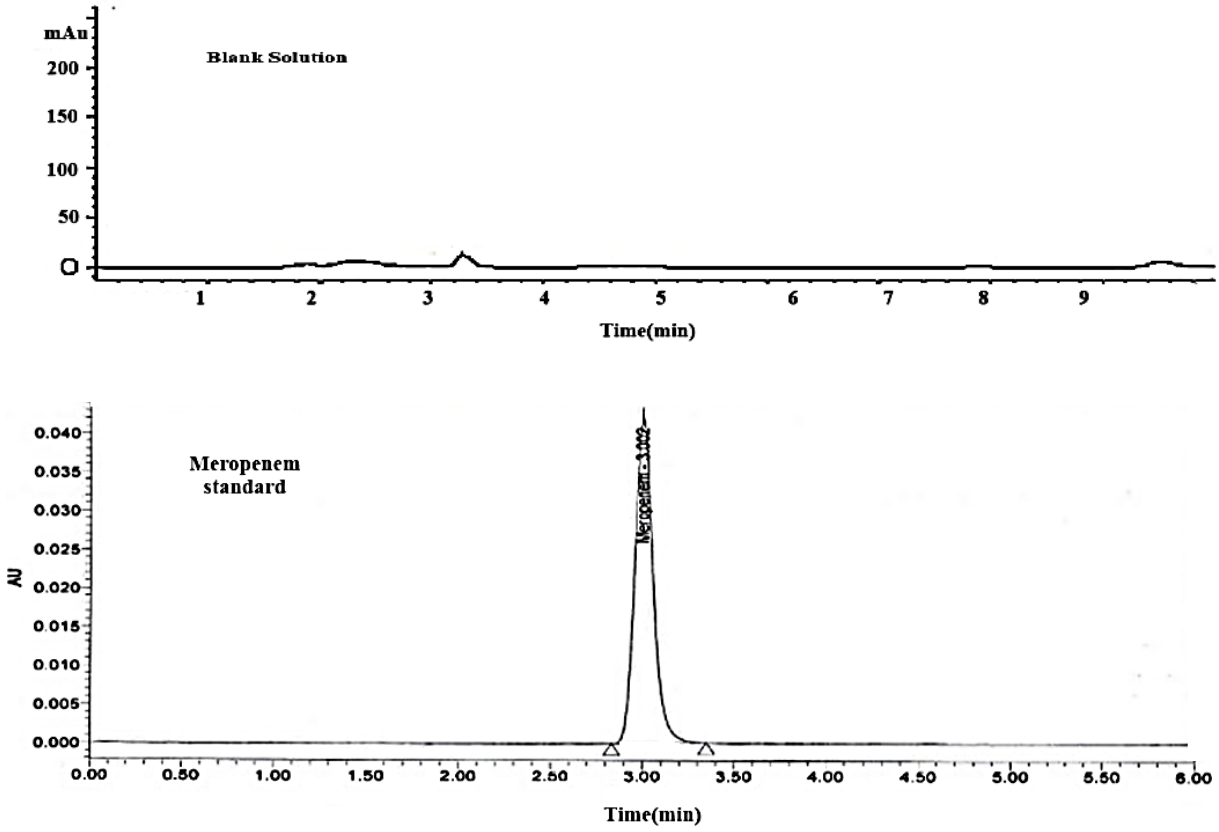

Fig. 6. Chromatogram of swabbing blank and standard

standard chromatogram are shown in Figure 6.

The % recovery for Meropenem was determined for LOQ, 50%, 100%, and 150% levels and found the % recovery within 97.0% to 109.0% that were within the limit, and the recovery factor was determined to be 1.0 as there was no mean recovery for any contact parts of the machine under 95%. The method was found to be precise during method precision and intermediate precision with different analysts and different instruments. The method is linear for the Meropenem compound by giving a correlation coefficient (r) value of 1.000 at concentration levels of 0.1–15.0 µg mL^{-1} for Meropenem. The concentrations of LOD and LOQ based on signal-to-noise ratio (S/N) are 0.05 and 0.1 µg mL^{-1}. LOQ precision was performed by injecting six replicate injections of LOQ solution. Based on the results, the s/n ratio was greater than 10 for LOQ solutions. The area RSD (%) for six replicate injections of LOQ precision was 7.6 for Meropenem. The linearity graph peak responses plotted against peak concentrations of Meropenem evaluated the square of the correlation coefficient (r)

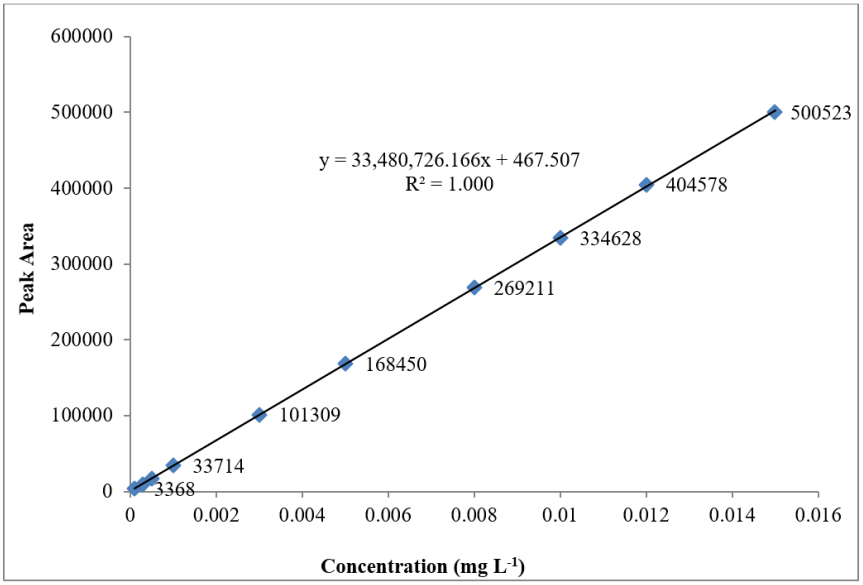

Fig. 7. Linearity curve of Meropenem

Table 2. Analysis of results for LOD and LOQ of Meropenem

Levels	Conc. (µg mL^{-1})	Area	Final LOD	Final LOQ
Level 1	0.1	3368	Based on S/N Ration LOD 0.05 µg mL^{-1}	Based on S/N Ration LOQ 0.1 µg mL^{-1}
Level 2	0.3	10145		
Level 3	0.5	16841		
Level 4	1.0	33714		
Level 5	3.0	101309		
Level 6	5.0	168450		
Level 7	8.0	269211		
Level 8	10.0	334628		
Level 9	12.0	404578		
Level 10	15.0	500523		
Correlation Co-efficient, R		1.000		
STD Response		1243.626		
Y-intercept		467.507		
Slope		33480726.200		
%RSD of LOD and LOQ Precision (6 Injections)			5.1	7.6
S/N Ratio of last injection			12.12	32.54

and found 1.000, Figure 7, Table 2.

After evaluation of data, we found that the system suitability parameters, as cited as Theoretical plates, tailing factor, % RSD of cumulative data, and % Recovery, are within specified limits for original and changed conditions. Thus, the results revealed that the system meets the required system suitability criteria, and the method is robust for wavelength variation and column oven variation but not for flow rate variation (Table 3). The peak area of Meropenem of six swab sample solutions for different items was calculated and reported along with the standard deviation and RSD% of the peak area of these solutions for Meropenem. This shows that the precision of the swabbing method is satisfactory as RSD is not more than 10%, as shown in Tables 4a and b. The spiked sample solutions (n = 6) having RSD (%) were 0.1, 0.16, 0.37, and 0.24 respectively. RSD (%) for preparations (n = 12) of MP and IP spiked samples at specification levels were 2.55, 2.28, 2.38, 2.15, and less than 10.0%. The results show that the method was rugged, as shown in Tables 4a and b. The standard solution and swabbing solution were stable for at least 24 hours at room temperature. So, the solution can be used up to 24 hours. The results revealed that both PTFE and PVDF (0.45 µm) are suitable to use by discarding at least 2 mL for the preparation of sample solution as well as standard solution. The results are summarized in Tables 4a and b.

This method was used to test the validation samples for three (03) consecutive batches after cleaning. The selection of sampling location and sample quantity was based on the direct contact between the Meropenem and the machine, their difficulty in cleaning, and the accumulation of residue or product. This testing will be continued after each Meropenem campaign batch is manufactured according to the procedure. This way, chances of cross-contamination

Table 3. Robustness Data for Meropenem

Parameters	Standard Solution					Sample Solution					Remark
	Theoretical plate	Tailing Factor	Recovery (%)	RSD (%)	RSD (%) with bracketing standard	Result (% content) on SS plate	Result (% content) on Teflon plate	Result (% content) on Silicon plate	Result (% content) on Glass plate	% Difference	
Wavelength Variation (290 nm ± 5 nm)											
Original Condition	4249	1.15	100.9	0.3	0.3	99.9	100.0	99.9	100.2	N/A	N/A
285 nm	4461	1.15	100.3	0.1	0.1	99.2	99.4	99.2	99.6	0.6	Robust
295 nm	4534	1.15	99.9	0.1	0.2	98.8	98.6	99.2	99.4	0.8	
Column Oven (25 ± 50C)											
Original Condition	4249	1.15	100.9	0.3	0.3	99.9	100.0	99.9	100.2	N/A	N/A
20^0C	4181	1.15	99.5	0.2	0.2	98.6	98.6	98.4	98.9	1.3	Robust
30^0C	5145	1.15	98.7	0.1	0.1	97.8	97.9	97.6	98.1	1.1	
Flow Rate (1.0mL ± 0.1mL)											
Original Condition	4249	1.15	100.9	0.3	0.3	99.9	100.0	99.9	100.2	N/A	N/A
0.9	5291	1.16	97.6	0.2	0.2	96.6	96.9	96.9	97.4	2.8	Not Robust
1.1	4641	1.13	97.1	0.2	0.2	95.9	95.7	95.8	96.3	3.9	

Table 4a. Summary of method validation results.

Validation parameters	Acceptance criteria	Results obtained		
System Suitability	NMT 10.0 % from six replicate injection Not more than 2.0 Not less than 2000 98.0%-102.0% NMT 10.0 % No interfering peak	Standard Solution-1	%RSD	0.1
			Tailing Factor	1.21
			Theoretical plate	4533
		Standard Solution- 1& 2	% Recovery	100.7%
		Standard Solution-1& Bracketing Standard	RSD (%) of peak area	0.3%
		Blank & Swabbing Blank Solution	No interfering peak was observed	
Specificity	There should not be any interfering peak in the chromatogram obtained from the diluent and swab stick solution at the retention time corresponding to Meropenem.	No interfering peak was observed in the diluent and swab stick solution.		
		Sample Name	**Analyte Name**	**Retention Time (min.)**
		Standard Solution	Meropenem	3.00
		Swab_SS_Plate	Meropenem	3.01
		Swab_Teflon_Plate	Meropenem	3.00
		Swab_Glass_Plate	Meropenem	3.00
		Swab_Silicon_Plate	Meropenem	2.99
Linearity	The squared correlation coefficient (r^2) should be not less than 0.99.	**Analyte**	**r^2**	
		Meropenem	1.00	
LOQ & LOD determination	Reported value Concentration (mg mL^{-1})	**LOD**	**LOQ**	
		0.000122577	0.000371445	
LOQ precision	For the LOQ solution, the Signal-to-noise ratio should be NLT 10, and RSD (%) for the six replicate responses should be NMT 25%.	**S/N ratio**		**% RSD**
		LOD	**LOQ**	**LOD** **LOQ**
		12.12	36.54	5.1 7.6
Swab Recovery	**LOQ Recovery solution:** The recovery should be between 70.0%-130.0% **50%-150% Recovery solution:** The recovery should be between 80.0%-120.0%	**Recovery**		
		Level	**LOQ**	**50%** **100%** **150%**
		Glass_Plate	109.4	101.7 104.5 100.2
		Teflon_Plate	109.0	101.6 103.6 100.0
		SS_Plate	100.5	101.6 103.6 97.6
		Silicon_Plate	99.5	101.7 103.3 97.3
Filter Evaluation	% Difference between the initial result and after the time interval should be NMT 10.0%.	**Names**	**Area**	**Meropenem** **RSD (%)** **Results (%content)** **% Difference**
		Centrifuged	306191	N/A 99.7 N/A
		PTFE0.45 µm dis. 2 mL	306079	0.14 100.1 0.4
		PTFE0.45 µm dis. 4 mL	306025	0.16 100.1 0.4
		PTFE0.45 µm dis. 6 mL	307196	0.18 100.1 0.4
		PVDF0.45 µm dis. 2 mL	306217	0.09 100.1 0.4
		PVDF0.45 µm dis. 4 mL	306362	0.13 99.9 0.2
		PVDF0.45 µm dis. 6 mL	306191	0.10 100.1 0.4

Table 4b. Continue summary of method validation results.

Validation parameters	Acceptance criteria	Results obtained				
Method Precision (MP) (n = 6)	The Recovery should be between 80.0%-120.0%. RSD of recovery results should not be more than 10.0%.	**Test solution**	**Results (% content)**			
			SS Plate	**Teflon Plate**	**Glass Plate**	**Silicon Plate**
		Sample-1	99.2	98.0	99.1	98.5
		Sample -2	99.0	98.2	98.5	97.8
		Sample -3	99.2	98.3	98.1	98.3
		Sample -4	99.2	98.0	98.2	98.2
		Sample -5	99.1	98.2	98.2	98.1
		Sample -6	99.0	98.4	98.4	98.3
		Mean	**99.1**	**98.2**	**98.4**	**98.2**
		RSD (%)	**0.10**	**0.16**	**0.37**	**0.24**
Intermediate Precision(IP) (n = 6, MP+IP, n = 12)	The Recovery should be between 80.0%-120.0%. RSD of recovery results should not be more than 10.0%.	Sample -1	94.2	93.5	94.2	93.8
		Sample -2	93.6	94.3	93.5	94.2
		Sample -3	94.5	99.3	99.3	97.1
		Sample -4	99.3	94.1	94.3	94.2
		Sample -5	94.2	94.3	99.4	99.1
		Sample -6	99.3	99.2	94.2	94.0
		Mean	**95.9**	**95.8**	**95.8**	**95.4**
		RSD (%)	**2.80**	**2.82**	**2.87**	**2.30**
		Mean (%) (MP+IP, n = 12)	97.48	96.98	97.17	96.80
		Cumulative RSD (%) (MP+IP, n = 12)	2.55	2.28	2.38	2.15
Robustness	Results should be within the specification limit.	**Variations** i. Wavelength variation (290 ± 5 nm) ii. Flow Rate variation (±0.1 mL) iii. Oven Temp.(25 ± 5^{0}C)			The method was found robust for the Wavelength variation & Oven Temp variation.	
Solution Stability	% RSD between the initial result and after the time interval should be NMT 10.0%.	**Swab Samples**	**Meropenem**			
			% Recovery		**Difference (%)**	
			Initial	**24H**		
		Sample SS plate	99.9	97.6	2.3	
		Sample Teflon plate	100.0	97.3	2.7	
		Sample Glass plate	100.2	97.2	3.0	
		Sample Silicon plate	99.9	97.1	2.8	

will be drastically reduced.

The production department has performed the cleaning procedure for the injection filling line. A visual test and a chemical evaluation of the equipment need to be performed after cleaning to demonstrate that Meropenem residue has been removed & cleaned as per the designated cleaning method of the production unit. In many cases, the surface of production equipment will not be made of flat stainless steel. Therefore, the swab must be done as close as practically possible to the validated swab procedure. Besides stainless steel, there are some other materials of construction also involved, like container holder/Adapter, which is made of Teflon, and Silicon channel, which is made of silicon; there is a glass on the lower hopper and side cover. Thus, sampling was done using swab samples according to the analysis method and location (Table 1). The area swabbed area was always 25 cm^2 (5 cm x 5 cm), where it is not possible to swab this size area; swabs were taken from several locations distributed across the equipment product contact surface such that the total area is close to 25 cm^2 (the actual surface area swabbed was calculated and used

for carryover calculations). After establishing the cleaning procedure through this validation, the manufacturing department will clean the machine contact parts according to this established and validated cleaning procedure. After each campaign production of Meropenem injections, the sample will have to be sent to QC for analysis according to the validated analytical method for routine review of the cleaning procedure established to clean the Meropenem residue before changeover to other drug manufacturing as a routine management for prevention of Cross-contamination. If any changes occur in the production machine, such as critical equipment modifications or cleaning procedures, a change control system is in place to ensure that the cleaning process is reassessed at defined intervals and re-validation as necessary.

4. Conclusion

This protocol-based study for the Meropenem residue determination is a must to do by every drug manufacturing unit that manufactures Meropenem drug with other drugs into the same premise. Meropenem cross-contamination is more vital to control than other drugs, whereas this drug is the last resort of antibiotic treatment. To control cross-contamination, residue determination of Machine contact parts is essential to monitor the machine cleaning efficiency during the changeover to other drug manufacturing. A study protocol has been established to control and monitor the cleaning procedure developed for manufacturing Meropenem formulations, especially powder for injections. Besides the cleaning method, the analytical method with swab sampling is a vital tool that needs to be developed and validated to determine the Meropenem residue. In this method, an HPLC method was developed and validated to quantify the Meropenem residue on the machine contact parts selected, such as 316 stainless steel, Teflon, glass, and silicon. The method developed and validated for analyzing swab samples is simple to execute. This HPLC method is very cost-effective as the run time is only 6 minutes with a simple Mobile phase, stationary phase, and chromatographic conditions (recovery of more than 95%). The validation results indicated that the developed HPLC method for determining Meropenem residue is precise, accurate, linear over the test concentration range, rugged, and specific. The isocratic HPLC method to determine Meropenem will not only save cost and time but also it will be a unique method to determine the Meropenem residue from Machine contact parts by swabbing and also the wastes discharged from the manufacturing unit to the environment and because there is only water interference into that samples. Thus, it will be a better option for the analytical & quality control labs to use to control Meropenem cross-contamination in the same manufacturing plant with other drugs manufactured.

5. Abbreviations

HPLC: High-performance liquid chromatography
CIP: Cleaning in process
WHO: World Health Organization
US CDC: United States Centers for Disease Control and Prevention
ECDC: European Center for Disease prevention & control
PDA: Photodiode array detector
CGMP: Current good manufacturing practices
ICH: International Council for Harmonization
RSD: Relative standard Deviation
LOD: Limit of detection
LOQ: Limit of quantification
COT: Column oven temperature
FR: Flow rate
TBAH: Tetra-butyl Ammonium Hydroxide

6. Acknowledgments

The authors are very thankful to the management of ACME Laboratories Ltd., Dhaka, Bangladesh, for supporting this study.

7. References

[1] E. Scholar, Meropenem, xPharm: The comprehensive pharmacology reference, Elsevier publisher book, Pages 1-5, 2007. https://doi.org/10.1016/B978-008055232-

3.62133-6
[2] G. Meletis, Carbapenem resistance: Overview of the problem and future perspectives, Ther. Adv. Infect. Dis., 3 (2016) 15-21. https://doi.org/10.1177%2F2049936115621709
[3] DGDA, Directorate General Of Drug Administration, Allopathic drug database, August 10, 2024. http://dgdagov.info/index.php/registered-products/allopathic
[4] E. Bouza, The role of new carbapenem combinations in treating multidrug-resistant Gram-negative infections, J. Antimicrob. Chemother., 76 (2021) iv38-iv45. https://doi.org/10.1093/jac/dkab353
[5] WHO (World Health Organization), list of bacteria for which new antibiotics are urgently needed, 2024. https://www.who.int/news/item/27-02-2017-who-publishes-list-of-bacteria-for-which-new-antibiotics-are-urgently-needed
[6] A.A. Elshamy, K.M. Aboshanab, A review on bacterial resistance to carbapenems: epidemiology, detection and treatment options, Future Sci. OA, 6 (2020) FSO438. https://doi.org/10.2144%2Ffsoa-2019-0098
[7] M. H. Hsu, T. H. Kuo, W. W. P. Lai, C. H. Huang, C. C. Hsu, Y. E. Chen, A. Y. C. Lin, Effect of environmental factors on the oxidative transformation of cephalosporin antibiotics by manganese dioxides, Environ. Sci. Process Impacts, 21 (2019) 692-700. https://doi.org/10.1039/c8em00562a
[8] Y. Qian, X. Liu, K. Li, P. Gao, J. Chen, Z. Liu, X. Zhou, Y. Zhang, H. Chen, X. Li, G. Xue, Enhanced degradation of cephalosporin antibiotics by matrix components during thermally activated persulfate oxidation process, Chem. Eng. J., 384 (2020) 123332. https://doi.org/10.1016/j.cej.2019.123332
[9] E. Mathia, Pharmaceutical product cross-contamination: industrial and clinical pharmacy practice, Dar Es Salaam Med. Stud. J., 19 (2012) 17-19. http://dx.doi.org/10.4314/dmsj.v19i2.5
[10] E. Peterson, P. Kaur, Antibiotic resistance mechanisms in bacteria: relationships between resistance determinants of antibiotic producers, environmental bacteria, and clinical pathogens, Front. Microbiol., 9 (2018) 2928. https://doi.org/10.3389/fmicb.2018.02928
[11] J.A. Gilbert, J.K. Jansson, R. Knight, The earth microbiome project: successes and aspirations, BMC Biol., 12 (2014) 1-4. https://doi.org/10.1186/s12915-014-0069-1
[12] H. Sørum, M. Sunde, Resistance to antibiotics in the normal flora of animals, Vet. Res., 32 (2001) 227-241. https://hal.science/hal-00902706/document
[13] J. Sun, The microbiome in health and disease, academic press, first ed., 171 (2020). https://shop.elsevier.com/books/the-microbiome-in-health-and-disease/sun/978-0-12-820000-1#full-description
[14] C. Casals-Pascual, A. Vergara, J. Vila, Intestinal microbiota and antibiotic resistance: Perspectives and solutions, Hum. Microbiome J., 9 (2018) 11-15. https://doi.org/10.1016/j.humic.2018.05.002
[15] S.B. Levy, Factors impacting on the problem of antibiotic resistance, J. Antimicrob. Chemother., 49 (2002) 25-30. https://doi.org/10.1016/j.humic.2018.05.002
[16] Medex, Available brands of Meropenem Trihydrate, 2024. https://medex.com.bd/generics/731/meropenem-trihydrate/brand-names
[17] A. Raj, Cleaning validation in pharmaceutical industries, J. Atom. Mol., 4 (2014) 779. https://dx.doi.org/10.33289/IJRPC.10.2.2020.10(39)
[18] A.S. Mendez, M. Steppe, E.E. Schapoval, Validation of HPLC and UV spectrophotometric methods for determining meropenem in pharmaceutical dosage form, J. Pharm. Biomed. Anal., 33 (2003) 947-954. https://doi.org/10.1016/s0731-7085(03)00366-2
[19] K. Kameda, K. Ikawa, K. Ikeda, N. Morikawa, A. Nakashima, H. Ohge, T. Sueda, HPLC method for measuring meropenem and biapenem concentrations in human peritoneal

fluid and bile: application to comparative pharmacokinetic investigations, J. Chromatogr. Sci., 48 (2010) 406-411. https://doi.org/10.1093/chromsci/48.5.406

[20] M.A. Al–Meshal, M.A. Ramadan, K.M. Lotfi, A.M. Shibl, Determination of meropenem in plasma by high–performance liquid chromatography and a microbiological method, J. Clin. Pharm. Ther., 20 (1995) 159-163. https://doi.org/10.1111/j.1365-2710.1995.tb00642.x

[21] X. Ren, J. Ye, X. Chen, F. Wang, G. Liu, J. Wang, Development of a novel HPLC method for the analysis of impurities in meropenem and identification of unknown impurities by 2D LC-IT-TOF MS, Chromatographia, 84 (2021) 937-947. https://doi.org/10.1007/s10337-021-04081-4

[22] B. Balaswami, P.V. Ramana, B.S. Rao, P. Sanjeeva, A new simple RP-HPLC method for simultaneous estimation of meropenem and vaborbactam in tablet dosage form, Asian J. Res. Chem., 11 (2018) 111-116. https://doi.org/10.5958/0974-4150.2018.00023.8

[23] C. Jamieson, M.C. Allwood, D. Stonkute, A. Wallace, A.S. Wilkinson, T. Hills, Investigation of meropenem stability after reconstitution: the influence of buffering and challenges to meet the NHS yellow cover document compliance for continuous infusions in an outpatient setting, Eur. J. Hosp. Pharm., 27 (2020) e53-e57. https://doi.org/10.1136/ejhpharm-2018-001699

[24] V.P. Dhokiya, J.B. Dave, Stability and analysis of meropenem and B-Lactamase inhibitors in injectable preparations, World J. Pharm. Res., 7 (2017) 1029-1048. https://wjpr.s3.ap-south-1.amazonaws.com/article_issue/1516169774.pdf

[25] S. Fawaz, S. Barton, L. Whitney, J. Swinden, S. Nabhani-Gebara, Stability of meropenem after reconstitution for administration by prolonged infusion, Hosp. Pharm., 54 (2019) 190-196. https://doi.org/10.1177/0018578718779009

[26] V. Negi, V. Chander, R. Singh, B. Sharma, P. Singh, K. Upadhaya, Method development and validation of meropenem in pharmaceutical dosage form by RP-HPLC, Indian J. Chem. Technol., 24 (2017) 441-446. http://op.niscair.res.in/index.php/IJCT/article/view/12989/1335

[27] A.K. Kammoun, A. Khedr, A.N. Khayyat, M.A. Hegazy, Ultra-performance liquid chromatography-tandem mass spectrometric method for quantitation of the recently food and drug administration approved combination of vaborbactam and meropenem in human plasma, R. Soc. Open Sci., 7 (2020) 200635. https://doi.org/10.1098/rsos.200635

[28] L.V. Rao, G. Ramu, M.S. Kumar, C. Rambabu, Reverse phase HPLC and visible spectrophotometric methods for the determination of meropenem in pure and pharmaceutical dosage form, Int. J. PharmTech. Res., 4 (2012) 957-962. https://www.sphinxsai.com/2012/july_sept12/Pharm/pdfpharm/PT=08(957-962)JS%2012.pdf

[29] B. Narola, A.S. Singh, M. Mitra, P.R. Santhakumar, T.G. Chandrashekhar, A validated reverse phase HPLC method for the determination of disodium EDTA in meropenem drug substance with UV-detection using precolumn derivatization technique, Anal. Chem. Insights, 6 (2011) ACI-S5953. https://doi.org/10.4137/ACI.S5953

[30] P. Zalewski, J. Cielecka-Piontek, M. Paczkowska, Development and validation of stability-indicating HPLC method for simultaneous determination of meropenem and potassium clavulanate, Acta Pol. Pharm., 71 (2014) 255-60. https://ptfarm.pl/pub/File/Acta_Poloniae/2014/2/255.pdf

[31] M. A. Al–Meshal, M. A. Ramadan, K. M. Lotfi, A. M. Shibl, Determination of meropenem in plasma by high–performance liquid chromatography and a microbiological method, J. Clin. Pharm. Ther., 20 (1995) 159-163. https://doi.org/10.1111/j.1365-2710.1995.tb00642.x

[32] A.N. Baeza-Fonte, I. Garcés-Lobo, M.D. Luaces-Alberto, L.M. Gonçalves, M.D. Sotomayor, A.C. Valdés-González, Determination of cephalosporins by UHPLC-DAD using molecularly imprinted polymers, J. Chromatogr. Sci., 56 (2018) 187-193. https://doi.org/10.1093/chromsci/bmx099

[33] A. Abdollahi, A. Bavili-Tabrizi, Determination of some cephalosporins in pharmaceutical formulations by a simple and sensitive spectrofluorimetric method, Pharm. Sci., 22 (2016) 28-34. https://doi.org/10.15171/PS.2016.06

[34] M. A. Omar, O. H. Abdelmageed, T. Z. Attia, Kinetic spectrophotometric determination of certain cephalosporins in pharmaceutical formulations, Int. J. Anal. Chem., 2009 (2009) 596379. https://doi.org/10.1155% 2F2009 % 2F596379

[35] M.E. Hassouna, M.A. Mohamed, Efficient HPLC method for determination of cephalosporin residues on spiked stainless-steel plates and human plasma: application of a worst-case product for Cosa® CIP, Int. J. Environ. Anal. Chem., 100 (2020) 82-98. https://doi.org/10.1080/03067319.2019.1631301

[36] W. Setyaningsih, A. Rohman, M. Palma, Development and validation of HPLC-DAD method for simultaneous determination of seven food additives and caffeine in powdered drinks, Foods, 9 (2020) 1119. https://doi.org/10.3390/foods9081119

[37] USP (United States Pharmacopeia), Meropenem for Injection, USP43-NF38, 2798, 2020. https://doi.org/10.31003/USPNF_M49436_05_01

[38] Romaco Group, Macofar, Micro series for powder filling, 2024. https://www.romaco.com/products/product-details/micro-series, August 10, 2024

[39] A.M. Queenan, K. Bush, Carbapenemases: the versatile β-lactamases, Clin. Microbiol. Rev., 20 (2007) 440-458. https://doi.org/10.1128/CMR.00001-07

Anal. Methods Environ. Chem. J. 7 (3) (2024) 51-82

AMECJ

Research Article, Issue 3
Analytical Methods in Environmental Chemistry Journal
Journal home page: www.amecj.com/ir

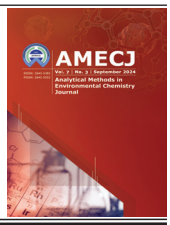

A review in analytical methods: Removal and extraction of pollutants in different matrixes by nanotechnology

Mohammad Reza Rezaei Kahkha[a], Ali Faghihi Zarandi[b,*], Hasti Daraei[c,d], Alireza Nasiri[d], Somayyeh Karami-Mohajeri[e], Maryam Faraji[c,d], Hamideh Asadollahzade[f], Fatemeh alsadat Bahador[b], and Anahita Hejazi[b]

[a] *PhD in Analytical Chemistry Department of Environmental Health Engineering, Zabol University of Medical Sciences, Zabol, Iran*
[b] *Department of Occupational Health Engineering and Safety at Work, Faculty of Public Health, Kerman University of Medical Sciences, Kerman, Iran*
[c] *Department of Environmental Health Engineering, Faculty of Public Health, Kerman University of Medical Sciences, Kerman, Iran*
[d] *Environmental Health Engineering Research Center, Kerman University of Medical Sciences, Kerman, Iran*
[e] *Department of Toxicology and Pharmacology, Faculty of Pharmacy, Kerman University of Medical Sciences, Kerman, Iran*
[f] *Department of Chemistry, Faculty of Science, Kerman branch, Islamic Azad University, Kerman, Iran, P. O. Box 7635131167, Kerman, Iran*

ARTICLE INFO:

Received 14 Apr 2024
Revised form 12 Jun 2024
Accepted 16 Aug 2024
Available online 30 Sep 2024

Keywords:
Removal,
Pollutants,
Nanotechnology,
Adsorbents,
Analytical methods,

ABSTRACT

The field of nanotechnology has demonstrated remarkable potential in effectively addressing environmental issues through remediation, particularly in extracting and removing pollutants from water, air, and human samples. The unique properties of nanomaterials, such as their high surface area (HSA) to volume ratio, size, and optical and magnetic behavior, make them well-suited for various applications in pollution control in different matrixes. Nanotechnology-based adsorbents are utilized in multiple fields such as water wastewater treatment, air purification filters, photocatalysis, environmental monitoring, electrochemical sensors, industrial, human sample analysis, and bioanalysis. Nanoadsorbents such as carbon nanotubes (CNTs), graphene (G), metal oxide nanoparticles(MONPs), metal-organic frameworks (MOFs), nanocomposites, magnetic nanoparticles, and silica-based nanomaterials are materials at the nanoscale that can remove pollutants by solvent extraction, membrane separation, photocatalysis, sorption, filtration, adsorption, precipitation, ion exchange, bioremediation, phytoremediation, coagulation, flocculation, and chemical oxidation/reduction technique. These nanomaterials are designed to have high surface areas and unique properties that effectively absorb various contaminants. The choice of nano adsorbent depends on the specific pollutants targeted, the environmental conditions, the physicochemical characteristics of the pollutant, and the desired application. Ongoing research is exploring new nanomaterials and optimizing existing ones to improve efficiency and address potential environmental and safety concerns. In summary, nanotechnology holds great potential for extracting and removing pollutants in water, air, soil, and human samples, using innovative methods for environmental protection and public health.

1. Introduction

Environmental pollution results from human activities introducing harmful substances into the environment, causing negative impacts on the environment and ecology. An instance of this is wastewater discharge into surface water sources such as tanks and rivers, a form of water pollution. Pollutants are substances or agents introduced into the environment that cause harm or discomfort to living organisms. These pollutants can be classified into various categories based on their origin, physical state, and environmental impact.

*Corresponding Author: Ali Faghihi Zarandi
Email: alifaghihi60@yahoo.com
https://doi.org/10.24200/amecj.v7.i03.1004

One of the important types of pollutants are VOCs, BTEX, and organic materials. Volatile Organic Compounds (VOCs) and organic materials can serve as pollutants in water and air and pose potential health risks to humans [1-3]. Industrial processes and indoor sources such as manufacturing, painting, printing, chemical production, building materials, and household products can release VOCs into the air [1,2]. Also, vehicle emissions include the combustion of fossil fuels, which releases VOCs and other organic compounds. VOCs can react with other atmospheric pollutants, contributing to ground-level ozone and smog formation. High exposure to VOCs may cause respiratory irritation, headaches, and potential long-term health effects [4,5]. Factories and manufacturing facilities may release VOCs and other organic pollutants into soil and water bodies. Pesticides, fertilizers, and herbicides can introduce organic compounds into water systems. Stormwater can carry pollutants from roads, parking lots, and urban areas into water bodies. VOCs can contaminate drinking water sources and affect the aquatic ecosystem [6,7]. Organic pollutants may accumulate in aquatic organisms, leading to biomagnification in the food chain. Consumption of contaminated water may result in health issues, including gastrointestinal and neurological effects. Inhalation of VOCs, ingesting contaminated food and water, and direct skin contact with contaminated materials cause respiratory problems in rats [8]. According to the serious health effects of VOCs, analyzing biological samples (blood, urine) to assess human exposure to chemical pollutants and monitoring air and water quality is needed to further evaluate risk assessment and consequent control and mitigation by regulation of governments and environmental agencies. Therefore, controlling or reducing the emission of pollutants is achieved by establishing and implementing environmental regulations and standards [9]. The enforcement of regulations on industrial emissions, vehicle standards, and water quality to limit VOC/BTEX and organic material pollution is required. Technological solutions, including implementing air and water treatment technologies, could effectively remove or reduce VOCs and organic pollutants. Regular monitoring and assessment are crucial to understanding the extent of contamination and implementing effective mitigation strategies. Adsorption using activated carbon (AC), multi-walled carbon nanotubes (MWCNTs), carbon quantum dots (CQDs), and graphene/graphene oxide (G and GO) is a common technique for trapping BTEX from the air [10-13]. Biofiltration uses microorganisms to break down VOCs into less harmful byproducts. Biofilters are often filled with organic materials or microorganisms that promote biodegradation. Photocatalytic materials, such as titanium dioxide, can be used to break down VOCs under the influence of UV light [14-16]. Ozone (O_3) can oxidize and decompose VOCs, and O3 generators can treat air in industrial settings [17]. Microorganisms, such as bacteria and fungi, can biodegrade organic pollutants in water. Membrane technologies can selectively remove VOCs from water, including reverse osmosis and nanofiltration [18]. Advanced Oxidation Processes (AOPs), such as UV/H_2O_2 and UV/O3, generate highly reactive species that can oxidize and break down VOCs in water [14-16]. Human metabolic processes can naturally transform and eliminate certain VOCs [19]. Medical interventions, such as chelation therapy or specific medications, may be employed in acute exposure to certain VOCs. The effectiveness of different treatment methods depends on the specific VOCs involved, their concentrations, and the environmental or physiological context. Ongoing research focuses on improving existing technologies, exploring new materials, and developing innovative approaches to enhance VOC removal in the air or heavy metal from water samples [20-23]. Heavy metals (Pb, Hg, Cd, Cr, As, etc) can be mentioned among other dangerous environmental pollutants. The impact of heavy metals on water, air, and human health and the role

of nanotechnology in their removal are important considerations. Nanotechnology holds promise for efficient and targeted removal of metals in water samples [24-28]. Acknowledging the potential risks associated with nanomaterials and ensuring responsible and sustainable implementation in environmental remediation is crucial. Regular monitoring, research, and advancements in nanotechnology will contribute to developing effective and safe strategies for heavy metal removal. Heavy metals can contaminate drinking water sources and harm aquatic ecosystems. Ingesting water contaminated with heavy metals can lead to gastrointestinal issues, cancer, and long-term health problems [29-32]. Human exposure to heavy metals, elements with high atomic weights known as heavy metals (Pb, Hg, Cd, Cr, and As), are also ongoing toxicological scenarios [23]. The impact of heavy metals on the quality of water and air, human health, and the role of nanotechnology in their removal are important considerations [23]. Biomagnification leads to the buildup of heavy metals in aquatic organisms, leading to increased concentrations in the food chain [33]. Heavy metals may contribute to particulate matter and affect air quality. Inhalation of heavy metals such as mercury, manganese, chromium, lead, cadmium, and vanadium can lead to respiratory and health problems Such as lung damage, cardiovascular effects, and cancer. Certain heavy metals can accumulate in the kidneys and liver, causing organ damage [34]. Lead and mercury exposure can impact the nervous system, leading to developmental issues in children. Engineered nanoparticles, such as nanoscale zero-valent iron, are removed from heavy metals through adsorption, precipitation, or reduction processes [35]. Nanotechnology-based filtration systems with nanoscale pores can selectively remove heavy metal ions from water. Nanomaterials with functionalized surfaces can enhance their affinity for specific heavy metals [25-27]. Nanomaterials like titanium dioxide nanoparticles can be employed in photocatalytic processes to degrade BTEX in air [14-16]. The potential toxicity of nanomaterials themselves is a concern and requires careful evaluation. The transport of nanoparticles in the environment needs consideration to prevent unintended consequences. Regulations and standards for using nanomaterials in water and air treatment must be established to ensure safety. Radioactive pollution in water and air refers to the release and presence of radioactive substances that can contaminate these environmental mediums [36,37]. The sources of radioactive pollutants include nuclear power plants, industrial facilities, medical institutions, and incidents such as nuclear accidents. The impact of radioactive pollution can be severe due to the potential health hazards associated with exposure to ionizing radiation. Radioactive substances can accumulate in aquatic organisms, leading to potential biomagnification in the food chain. Ingesting water contaminated with radioactive substances can lead to internal exposure and Increased risk of cancer, genetic mutations, and other long-term health effects. Radioactive particles released into the air can disperse large distances, affecting local and distant populations. Many radioactive isotopes have long half-lives, leading to persistent contamination. Radioactive metals can contaminate water and air through various pathways, leading to environmental and health concerns. These radioactive elements in water and air can result from natural sources, industrial activities, nuclear accidents, or improper disposal of nuclear waste [38,39]. Microplastics, small plastic particles less than 5 mm in size, can act as carriers for various pollutants, including heavy metals and VOCs. Microplastics are isolated from the sample matrix using filtration, density separation, or solvent extraction methods. Identification of microplastics is often done using microscopy techniques. Digestion breaks down the plastic matrix and releases any heavy metals associated with microplastics [40,41]. Heavy metal analysis is typically performed using techniques such as Inductively Coupled Plasma Mass Spectrometry (ICP-MS) or Atomic Absorption Spectroscopy (AAS). ICP-MS was

widely used for its sensitivity and ability to analyze multiple elements simultaneously. AAS is used as a specific method for individual metals. Solvent extraction methods, such as Soxhlet extraction or sonication, are employed to release VOCs from Microplastics. Gas chromatography-mass spectrometry (GC-MS) is a widely used technique for analyzing VOCs in water/air samples [14-16]. After extraction, the collected VOCs can be separated and identified using GC-MS. Solid phase microextraction (SPME) is an alternative technique for directly extracting VOCs from the microplastic sample. Determining heavy metals and VOCs in water, air, and human samples typically involves a combination of sample collection, preparation, and analytical techniques [14-16]. Inductively Coupled Plasma Optical Emission Spectroscopy (ICP-OES) is used for multi-element analysis. Gas Chromatography-Mass Spectrometry (GC-MS) is highly effective for separating and identifying VOCs in water/air samples [42]. Gas Chromatography with Flame Ionization Detection (GC-FID) is suitable for organic complex samples [14-16].

The issue of pollution control is brought to the forefront by environmental pollution. Various technologies are utilized to minimize the release of pollutants into the environment through air pollution control, wastewater treatment, solid-waste management, hazardous waste management, and recycling. For instance, catalytic converters, filtration, nanotechnology processes, etc., ensure that pollutants are treated before being discharged into environment matrixes. Each technology is vital in a comprehensive strategy to reduce environmental pollution. The review study aims to evaluate and present applied and new analytical methods used for extracting and removing pollutants such as heavy metals, VOCs, and organic compounds based on nanoadsorbent in different matrixes by nanotechnology coupled to the analyzer.

2. Pollutants Analysis by Nanotechnology

Nanotechnology has been used in analytical chemistry for different fields, such as water and wastewater treatment, air Purification, human analysis [23], and treatment and environmental monitoring [43-45]. In summary, nanotechnology holds great potential for the extraction and removal of pollutants such as mercury in water [46], air [10-13], and human samples [23], offering innovative solutions for environmental protection and public health.

2.1. Water and Air Purification

Due to their small pore size and high surface area, nanomaterials can effectively remove many pollutants, including heavy metals, VOCs, BTEX, and bacteria. Materials, such as ionic liquids and filters, help to separate nanomaterials from the liquid phase [22, 20, 47, 48]. With the small pore size and high surface area, these materials can efficiently remove contaminants, including heavy metals, VOCs, BTEX, and bacteria [21,48]. Also, nanoparticles like iron oxide and titanium dioxide have been used to remove heavy metals and organic materials from water (adsorption). They can be functionalized to remove the pollutants [15,16,21]. Moreover, nanomaterial-based filters such as nanofibers and nanoparticles are integrated into air filters to enhance their efficiency in capturing particulate matter, allergens, and pollutants. Nanostructured materials provide a larger surface area for adsorption and filtration. In addition, Nanomaterials, such as titanium dioxide nanoparticles, exhibit photocatalytic properties. When exposed to light, they can break down pollutants like VOCs into less harmful substances [15,16].

2.2. Human and Animal Sample Analysis and Treatment

Nanotechnology based on biosensors, nanostructures, and nanomedicine can remove pollutants from the human body. Nanotechnology is used to develop highly sensitive biosensors for detecting contaminants in human samples [25, 48-53]. These biosensors can identify specific biomarkers associated with pollutant exposure, providing early detection and diagnosis of related

health issues. Also, nano adsorbents, ionic liquids, and ligands can be used for heavy metal extraction in human and fish samples [54-57]. Nanoparticles such as functionalized SBA-15 can remove heavy metals from the different matrices [58-60].

2.3. Environmental Monitoring

Nanoparticles and nanostructures can monitor the movement of environmental pollutants and remove them [61-63]. This helps in understanding the pathways and sources of pollution, leading to better pollution management strategies. Despite the numerous advantages, using nanotechnology in environmental applications raises concerns about the potential toxicity of specific nanomaterials and their long-term environmental impact. Therefore, ongoing research focuses on developing safe and sustainable nanomaterials for environmental remediation.

2.4. Nanoadsorbents

Nanoadsorbents such as metallic nanoparticles (CdS NPs), G, GO, AC, amine-functionalized bimodal mesoporous silica nanoparticles (NH2-UVM7), and carbon nanotubes (CNTs) are materials at the nanoscale that can adsorb or attach pollutants, in their environment [24, 27, 64-68]. These nanomaterials are designed to have high surface areas and unique properties that make them effective in adsorbing various contaminants. The choice of nanoadsorbent depends on the specific pollutants targeted, the environmental conditions, and the desired application. Ongoing research is exploring new nanomaterials and optimizing existing ones to improve efficiency and address potential environmental and safety concerns. The following section lists various types of nanoabsorbents.

2.4.1.Carbon Nanotubes (CNTs)

The CNTs have tube structures of carbon atoms with HSA and high adsorption capacity. There are different types of carbon nanotubes based on their structure, namely Single-Walled Carbon Nanotubes (SWCNTs) and MWCNTs. The critical difference lies in the number of layers of carbon atoms that make up the tube structure. CNTs such as MWCNTs and SWCNTs can absorb heavy metals, organic pollutants, and gases. They may be functionalized with metal oxides, organic compounds, and ionic liquids or coated with other nanoparticles. The versatile properties of CNTs make them attractive for various applications across different industries, including electronics, materials science, energy, and medicine. However, challenges related to production scalability, purification, and cost still need to be addressed for widespread commercial adoption. Ongoing research continues to explore new applications and improve the manufacturing processes of CNTs. SWCNTs exhibit unique electronic properties, with either metallic or semiconducting behavior, depending on the specific rolling angle and chirality [23, 42]. Due to their biocompatibility, they have different applications in electronics (transistors, sensors), energy storage, drug delivery, and imaging. MWCNTs have multiple layers of graphene concentrically arranged to form a tube with excellent mechanical and thermal properties and can exhibit metallic or semiconducting behavior. MWCNTs reinforce materials, such as polymers and composites, enhancing their mechanical strength [44, 45]. MWCNTs, similar to SWCNTs, are explored for applications in supercapacitors and batteries and can be used as a catalyst and biosensor support due to their high surface area (SA). There are several methods for synthesizing carbon nanotubes (CNTs), and the choice of method depends on the desired properties, application, and production scale (Fig.1). These methods are: A) Chemical Vapor Deposition (CVD) involves the catalytic decomposition of hydrocarbons at elevated temperatures. By the CVD method, a substrate with a catalyst (usually iron, nickel, or cobalt nanoparticles) is exposed to a hydrocarbon gas (such as methane or ethylene) at high temperatures (typically 600-1000°C). B) Arc discharge is an effective method for producing MWCNTs (MWCNTs) on a relatively large scale. A high-current electric arc is generated between two graphite electrodes in an inert atmosphere. Carbon

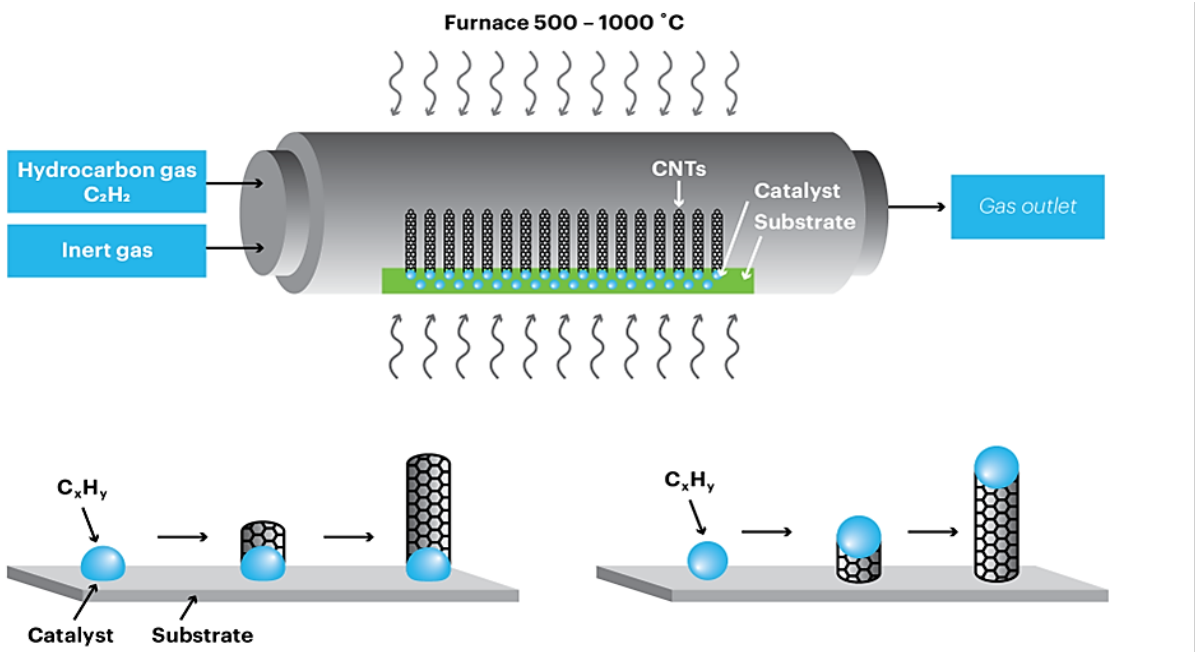

Fig.1. The standard chemical vapor deposition (CVD) method for synthesizing carbon nanotubes

is vaporized from one electrode and condenses to form nanotubes on the other electrode. This method can produce a significant quantity of CNTs, but the process tends to yield a mixture of SWCNTs and MWCNTs. C) Laser ablation, a high-power laser beam, is used to ablate a carbon target in the presence of a reactive gas. Laser ablation can produce high-quality SWCNTs with fewer impurities. Other methods, such as the Chemical Reduction of Carbon Sources, High-Pressure Carbon Monoxide (HiPCO) Method, and Template-Assisted Growth, were used for CNT synthesis [23, 42,44, 45].

2.4.2.Graphene and Graphene Oxide(G/GO):

Graphene oxide is known for its high surface area, offering numerous active sites for chemical reactions and a strong attraction to organic and inorganic pollutants. Its versatility in removing many substances, including pharmaceuticals, personal care products, and endocrine-disrupting chemicals, makes it a valuable tool in water treatment. Additionally, graphene oxide can be tailored to target specific contaminants, enhancing its effectiveness. Its cost-effectiveness, abundance, stability under harsh conditions, and efficiency in water treatment systems make it a promising solution for addressing emerging contaminants. Single layers of carbon atoms are designed as hexagonal lattices based on HSA, good electrical conductivity, and strong adsorption capabilities [10]. G and GO were used to remove heavy metals, organic pollutants, and dyes from water. Graphene synthesis by various methods: mechanical exfoliation (Scotch Tape Method) involves using adhesive tape to peel off layers of graphene from a highly ordered pyrolytic graphite (HOPG) crystal; CVD is a popular method for large-scale graphene synthesis, liquid-phase exfoliation involves exfoliating graphene from graphite in a liquid medium, and in chemical reduction of GO. The GO can be reduced to rGO, near pristine graphene [14,16]. Graphene oxide is often used as an intermediate precursor for graphene production. It is synthesized through the oxidation of graphite (Fig.2). The Hummers' and the Brodie methods are two common approaches. G and graphene oxide have similar applications to CNTs. Functional groups on GO enhance their interactions with target molecules, making them useful in sensors. These applications demonstrate the versatility of graphene and graphene oxide in various fields, and ongoing research continues to explore new possibilities and improve production methods [64,68].

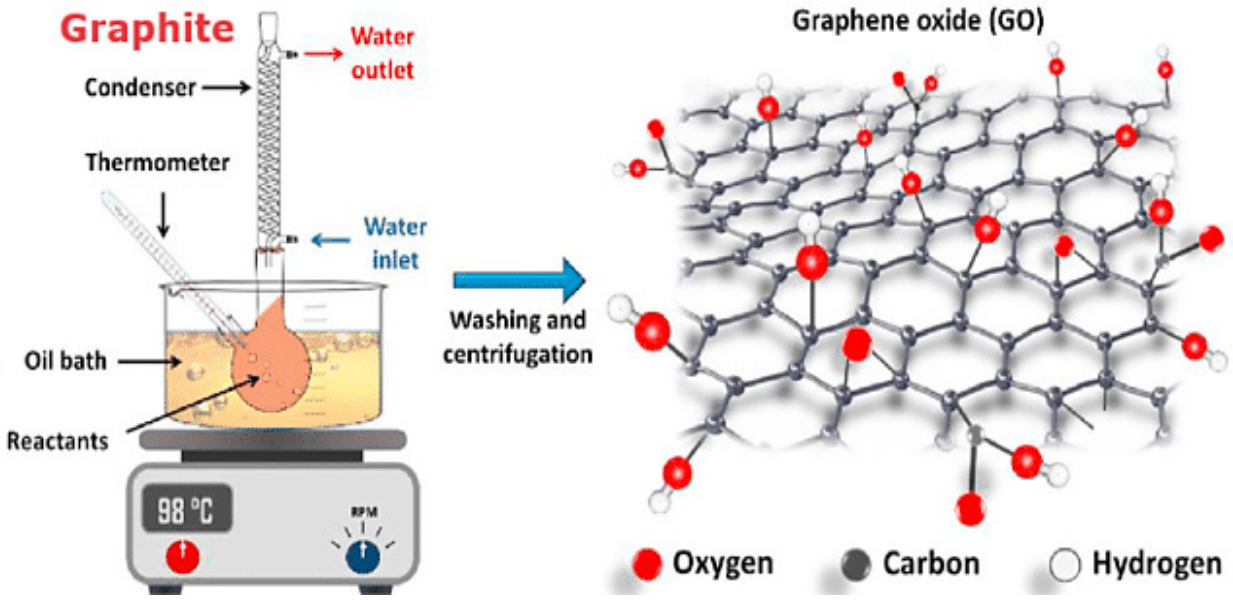

Fig.2. Synthesized GO based on reactants in an oil bath in a condenser by the oxidation of graphite [14.15]

2.4.3.Metal Oxide Nanoparticles

Metal oxide nanoparticles (MONPs) are metal precursors and are utilized in various fields such as physics, chemistry, and material sciences. These nanoparticles can form various oxide compounds with diverse structural geometries and electronic properties, exhibiting insulators, semiconductors, or metal characteristics. MONPs possess unique optoelectrical features due to their localized surface plasmon resonance characteristics, particularly in noble metals like Ag, Au, and Cu. The synthesis of metal nanoparticles, including their size and shape, is crucial in modern materials research. Metal nanoparticles, especially gold nanoparticles, are commonly used in SEM analysis to enhance electronic conductivity and produce high-quality images. Nanosized metal oxides, such as manganese, iron, titanium oxides, and others, have high removal capacity and selectivity for heavy metals, making them promising adsorbents. The effectiveness of MONPs in antibacterial activities and dye removal from wastewater depends on factors like morphology, size, and aggregation, emphasizing the importance of synthesis techniques focusing on these aspects. MONPs such as titanium dioxide (TiO_2), bismuth oxide (Bi_2O_3), and iron oxide (Fe_2O_3, Fe_3O_4) were used for the removal of pollutants in various matrixes. The properties of metal oxide nanoparticles are photocatalytic activity, high surface area, and magnetic properties for iron/copper oxide. This material removes pollutants through photocatalytic degradation, extraction, and adsorption [14-16].

2.4.4.Clay-Based Nanomaterials

Clay-based nanomaterials such as Montmorillonite and kaolinite have high surface area, porosity, and ion exchange capacity. Clay-based nanomaterials are used for adsorption of heavy metals, organic pollutants, and dyes [69-71].

2.4.5. Metal-Organic Frameworks (MOFs), Nanocomposites and Biopolymer

MOFs are porous materials with metal ions that can connect to organic linkers. MOFs have a high surface area, tunable structure, and large pore volume used for the adsorption of gases and the removal of organic pollutants and heavy metals. Nanocomposites are a category of nanomaterials in which nano-sized components are incorporated into a ceramic, metal, or polymer matrix, leading to the emergence of novel characteristics. These materials are engineered to demonstrate properties that surpass, and in some

cases significantly surpass, the combined capabilities of their elements. These nanomaterials offer enhanced oxidation resistance, high efficiency, and energy-saving benefits. Nanocomposites combine nanomaterials with polymers or other materials with Synergistic effects, improved stability, and enhanced adsorption properties for removing various pollutants in water and air. Biopolymer-based nanomaterials such as chitosan nanoparticles and cellulose nanocrystals were adsorbed by heavy metals and aromatic compounds. Biopolymer-based nanomaterials have unique properties that are biodegradable, renewable, and modified for specific adsorption [72-74].

2.4.6. Silica-Based Nanomaterials and Nano-Zero Valent Iron (nZVI)

Silica nanoparticles with high surface area, tunable surface chemistry, and stability were used to adsorb heavy metals, organic pollutants, and dyes. Silica-based nanoparticles (SNPs) have biomedical applications such as nanocarriers and biomodulators. SNPs, or silica nanoparticles, can be used as carriers for delivering therapeutics [27,58,59,64]. Scientists have worked on modifying their physical properties, such as particle size, shape, and structure, to improve their effectiveness. However, due to the inert nature of the silica framework, conventional SNPs are typically limited to being used as carriers for targeted delivery and controlled release. Nano-Zero Valent Iron (nZVI), based on reductive capability and a high surface area, was used to remove heavy metals and degrade chlorinated compounds [35]. Figure 3 shows three synthetic ways for mesoporous silica nanoparticles.

2.4.7. Magnetic Nanoparticles and Bimetallic Nanoparticles

Magnetite, formed from a combination of Fe(II) and Fe(III) salts through co-precipitation in alkaline conditions, possesses distinctive superparamagnetic properties and absorption capabilities. Its utilization not only enables the absorption and elimination of pollutants but also allows for its modification as a reusable heterogeneous catalyst for converting

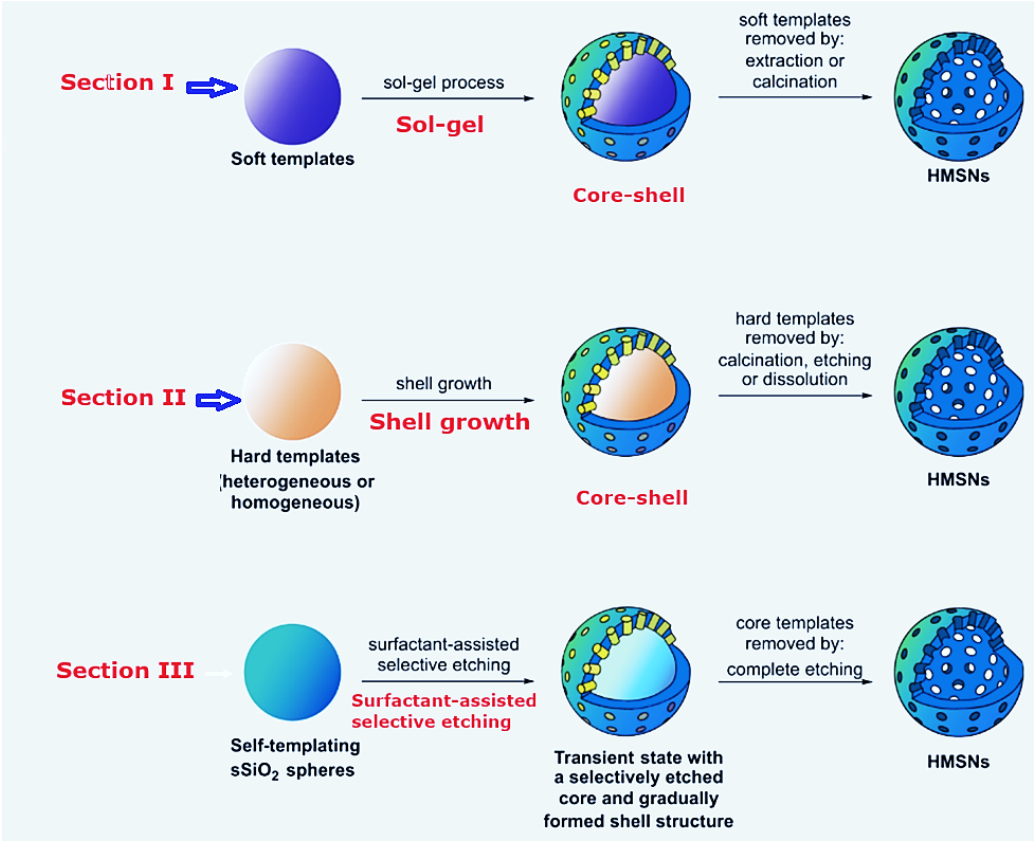

Fig. 3. Section I is the soft-templating method, Section II is the hard-templating method, and Section III shows the process of self-templating fabrication of HMSNs [64]

contaminants into valuable by-products. Magnetic nanomaterials have extensive applications in water treatment due to their easy separability, reusability, non-toxic nature, and controllable size and shape. Magnetite nanoparticles are crucial in various fields, such as magnetics, electronics, biomedical sciences, and sensor technology. These nanoparticles serve as effective adsorbents in water treatment, facilitating easy separation through high magnetism. Functionalized magnetite composites are commonly employed for metal separation and water purification, offering improved outcomes and cost efficiency. Composite nanoparticles reduce the required dosage and enhance the efficiency of functionalized particles. Magnetite (Fe3O4) nanoparticles based on magnetic properties for easy separation and high surface area were used for targeted removal of contaminants with an external magnetic field [36,44,54,61]. Bimetallic nanoparticles, such as palladium-silver nanoparticles, based on the synergistic effects of two different metals, can effectively remove chlorinated hydrocarbons.

3. Methods for extraction and removal of pollutants by nanotechnology

Extraction and removal techniques for pollutants from different sources (including water, air, soil, and biological samples) encompass a variety of methods [26,28,75,76,77]. Nanotechnology-based nanoadsorbent was used for the extraction/removal of pollutants in different matrixes [78-82]. Recently, researchers have presented some common extraction and removal methods, including both traditional and nanotechnology. Filtration involves the physical separation of solid particles from a liquid or gas using a porous membrane such as nano filters or membranes, CNTs [23, 42,44, 45], nanographene (NG)[64,68], NGO[14,16], Metal-organic frameworks: MOFs [72-74], Mesoporous silica nanoparticles: MSNs) with nanoscale pores (< 100 nm) [27, 58-60] for enhanced filtration efficiency. Adsorption is the adherence of molecules or particles to the surface of a solid or liquid material. The adsorption process may be followed by nanotechnology based on nanoadsorbents, such as CNTs (MWCNTs and SWCNTs) [42,44], NG-silica [64], NGO [68], metal oxide nanoparticles (MO-NPs), functionalized carbon structure (ionic liquid-CNTs, Fe_3O_4-GO) to enhance adsorption capacity [36,44,54,61]. Researchers reported the Unified Bioaccessibility Method (UBM) and NiCo2O4@ ZnCo2O4 nanomaterial to help determine pollutants [83-86]. The formation of solid particles from dissolved substances in a liquid phase causes precipitation and removal of pollutants. Some nanoparticles, such as zinc oxide (ZnO), Fe3O4, or MO-NPs, are used to induce or catalyze precipitation reactions to increase removal efficiency. In this removal, the pH is critical for precipitation such as Zn $(OH)_2$. Ion Exchange causes the replacement of ions in a solution with other ions. The ion-exchange properties of nanostructures are used to target the removal of specific ions in solution at optimized pH. On the other hand, coagulation and flocculation of aggregate particles are created by adding reagents to the solution by nano adsorbents. By bioremediation, microorganisms or their metabolic products are used to break down or transform pollutants. Also, Plants are used to absorb, accumulate, or transform contaminants by phytoremediation and incorporation of nanoparticles to enhance plant uptake and remediation efficiency. In addition, the oxidizing or reducing agents cause the breakdown of pollutants by chemical oxidation/reduction with nanocatalysts, such as zero-valent iron nanoparticles (ZVINPs), for enhanced oxidation or reduction reactions [35]. Occasionally, light (UV, Vis) and a catalyst act as photocatalysis to initiate chemical reactions that decompose pollutants (Titanium dioxide nanoparticles TiO_2, Bi_2O_3 enhanced degradation of pollutants) [14-16]. Sorption is a process of adsorption and absorption of contaminants onto a solid material. In extraction-based solvents, the solvents or extraction agents are used to separate pollutants from a matrix by designing nanocarriers to extract or encapsulate contaminants efficiently. Also, membranes with specific pore sizes are used to separate components

based on size or other properties. The different methods and nano adsorbents can be employed individually or in combination, depending on the pollutants and the characteristics of the matrix. Nanotechnology provides innovative solutions to enhance the effectiveness of these techniques and address challenges associated with traditional methods. Pollutants are substances of the environment that cause harm or discomfort to living organisms. These pollutants can be classified into various categories based on their origin, physical state, and environmental impact. Some common types of pollutants are classified as air, soil, water pollutants (heavy metals), radioactive pollution, microplastics, greenhouse gases, and VOCs. For air pollutants, particulate matter (PM), such as fine particles and droplets, is suspended in the air, including dust [76], soot, and aerosols. Nitrogen oxides (NOx), SO2, CO, and O3 are also air pollutants. Water pollutants include heavy metals (lead, mercury, and cadmium) [26-28, 46], nutrients, pathogens (bacteria, viruses, and parasites), and chemical contaminants (Pesticides, herbicides, pharmaceuticals, industrial chemicals, and other synthetic compounds). Heavy Metals, pesticides and herbicides (chemicals used in agriculture to control pests and weeds), and industrial wastes are soil pollutions. Radioactive substances are elements or isotopes that emit radiation, often produced as byproducts of nuclear processes or present in certain minerals. Microplastics are tiny plastic particles (less than 5 mm) that can accumulate in water and soil [40,41]. Greenhouse gases such as CO_2, CH4, and N2O are another source of air pollution. VOCs (VOCs) can evaporate into the air, and other organic materials, such as methyl orange or blue pollution, can be analyzed in water and biological matrixes [71,69]. The impact of pollutants on the environment and human health varies, and efforts are made to monitor, regulate, and reduce their emissions through environmental management and conservation practices. Nanotechnology methods have been developed for the extraction/ removal, and adsorption of pollutants from different sources such as water, air, agriculture, and human samples. Hosseini et al. proposed a new method that utilizes a nanomagnetic composite material called Fe3O4@4-PhMT-GO, which is modified with graphene oxide (Fig.4).

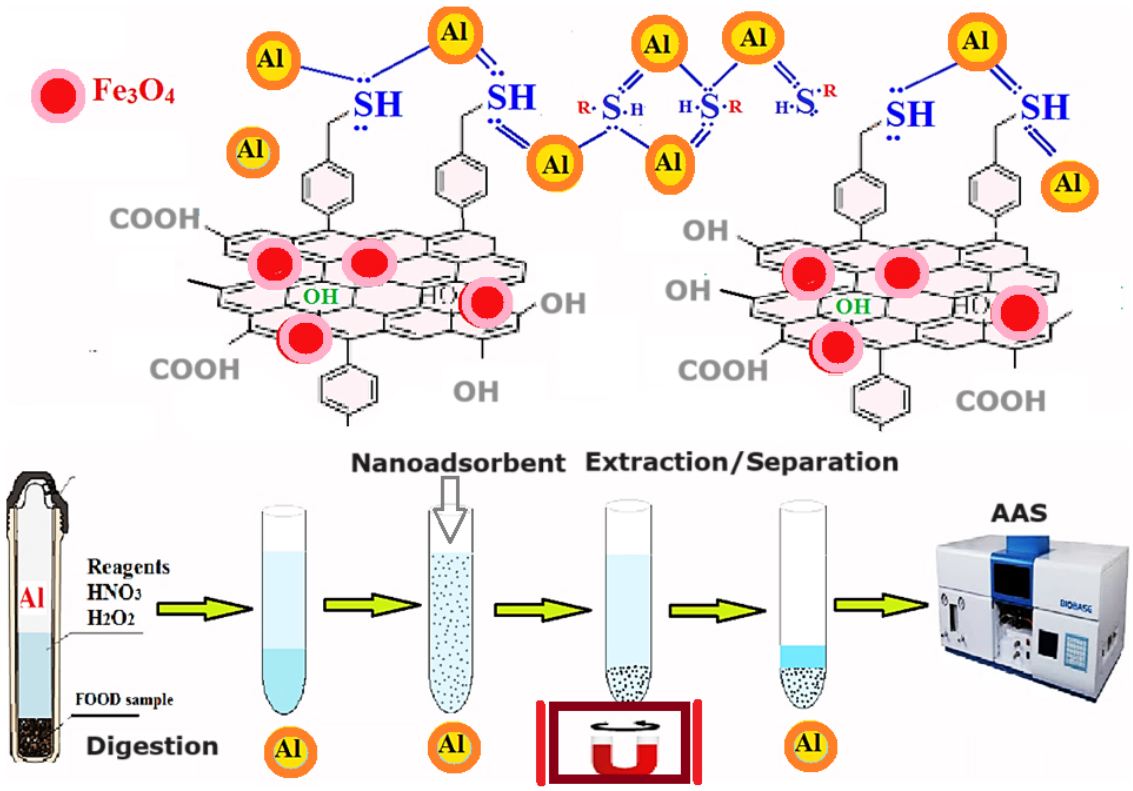

Fig.4. Determination of aluminum (Al) from wastewater, food, and vegetable samples by the Fe3O4@4-PhMT-GO adsorbent [87]

This method is used for the extraction of aluminum (Al) from wastewater, food, and vegetable samples. The extraction process is carried out by a microwave system coupled to magnetic micro SPE. The result showed the working and linear ranges between 0.005 to 5 and 1.6 mg L^{-1}, respectively; the LOD and an enrichment factor were obtained at 1.5 µg L^{-1} and 50, respectively (RSD= %2.5). The organic, inorganic, and total aluminum were achieved in water samples through the MDM-µ-SPE procedure. [87]. Faghihi et al. used ionic liquids on glassy balls (ILs/GBs) to remove toluene from the air. Toluene vapor was absorbed on 0.2 g of ionic liquids at room temperature and desorbed from the adsorbent at 110 °C before being determined by GC-FID. The removal of toluene [Ph3P-(CH2)3-SO3H] [TOS] was obtained at more than 95%, and the adsorption mechanism of toluene was dependent on π–π interaction between toluene and ionic liquids.

The ILs-GBs with chemical adsorption between tri-phenyl / imidazolium/ pyridinium and toluene vapor have been ascribed to π–π /n–π EDA interaction as compared to ILs without aliphatic chains [20, 88]. Golbabaei et al. used a new procedure for the speciation of Hg in human samples, which was ionic liquid-liquid extraction with CV-AAS. By procedure, 1 mL of Ammonium pyrrolidin-dithiocarbamat (1%, APDC) solution was mixed with 10 mL of human blood (pH 7) with 0.2 g of IL. Mercury was complexed as Hg-APDC in IL. Total Hg was determined after the blood sample was put in the microwave [89]. In another study, cadmium in blood samples was extracted/separated with magnetic -N-thiol-functionalized graphene oxide (M-NT-GO) by USA-DM-µ-SPE before measured by ET-AAS. The linear range, LOD, and PF were achieved at 0.03–1.5 µg L^{-1}, 0.01 µg $L^{-1,}$ and less than 5%, respectively (MRSD<2 %). The adsorption capacities of M-NT-GO were 185.3 mg g^{-1} for cadmium. They used 20 mg of the M-NT-GO at pH 6 [90]. Karamzadeh et al. reported a new adsorbent CysSB/MetSB@MWCNTs for Ni/Co determination in human samples by ultrasound-assisted coupled to dispersive ionic liquid-suspension SPME. The adsorbent was suspended in IL and added to the blood samples. Co/Ni (II) extracted by IL-CysSB @MWCNTs in a conical tube and determined by ET-AAS. The LOD and EF of MWCNTs adsorbent were achieved (30 ng L^{-1}; 20 ng L^{-1}) and 50 for Ni and Co ions, respectively. The adsorption capacity for Ni and Co was 226.7 and 193.3 mg g^{-1}, respectively [91]. Esmaeili et al. showed that MWCNTs@ [Apmim] [PF_6] adsorbent could be specified the mercury (Hg^{2+}, O-Hg) in water samples (pH 8.5) by UAS-D-SPE before determined by CV-AAS. The linear range and LOD for inorganic/organic mercury were 20–3500 ng L^{-1} and 5-6 ng L^{-1}, respectively (RSD<2%). The capacity absorption of MWCNTs@ [Apmim][PF_6] for Hg(II) ions was achieved at 186.2 mg g^{-1} [92]. Also, Esmaeili et al. used the TSIL functionalized on MWCNTs for styrene extraction in water samples by cyclic conjugation-micro-solid phase extraction procedure (CC-µSPE). The linear range (LR) and LOD were 0.001–6.5 mg L^{-1} and 260 ng L^{-1}, respectively (RSD%=1.45). The absorption capacities of MWCNTs@[Hemim][BF_4] was 183.2 mg g^{-1} [93]. Mousavi et al. presented a magnetic carbon nanotube-nickel hybrid (MNi-CNT) for extracting four tyrosine kinase inhibitors (imatinib, sunitinib, erlotinib,and nilotinib).Thelimits of quantification for imatinib, sunitinib, erlotinib, and nilotinib were obtained at 0.7, 1.7, 0.6, and 1.0 µg L^{-1}, respectively(RSD<4.5%) [94]. Faghihi et al. used the B_2O_3-NG/NGO adsorbent for removing xylene from the air by UV radiation-catalectic degradation-adsorption procedure (UV-PCDA)/ GC-MS. The capacity adsorption of BONPs-NG/NGO achieved 223 mg g^{-1} [14] (Fig. 5). Also, Faghihi et al. used ionic liquids to remove toluene vapor from the air [20]. Marek Trojanowicz reported that the flow methods used in the analysis are based on nanotechnology. Nanotechnology affects analytical instrumentation and methods [95].

Rakhtshah et al used 2,3-dimercapto-1-propanol functionalized on MWCNTs for lead speciation in different matrixes by dispersive ionic liquid-

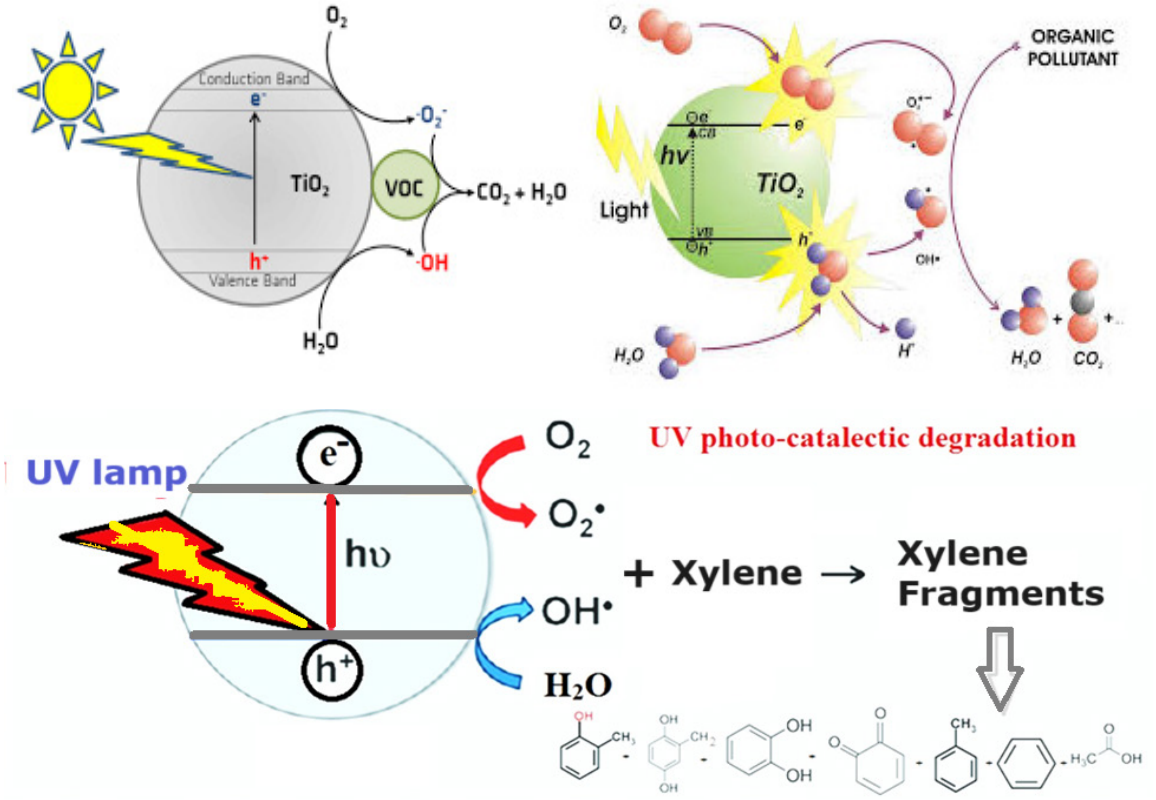

Fig.5. UV photo-catalectic degradation for removal of xylene and BTEX from the air [14]

suspension SPE. They showed that the linear range and adsorption capacity were reported at 9.5–480 μg L^{-1} and 191.6 mg g^{-1}, respectively (RSD < 5%) [96]. Mirzahosseini et al analyzed the heavy metals (vanadium, cobalt, nickel, arsenic, and mercury) in water, soil, and vegetables by GIS. They used GIS to display the distribution of heavy metals at various locations. [97]. Soylak et al can determine the concentrations of the different elements in the children's cosmetic products in Turkey.

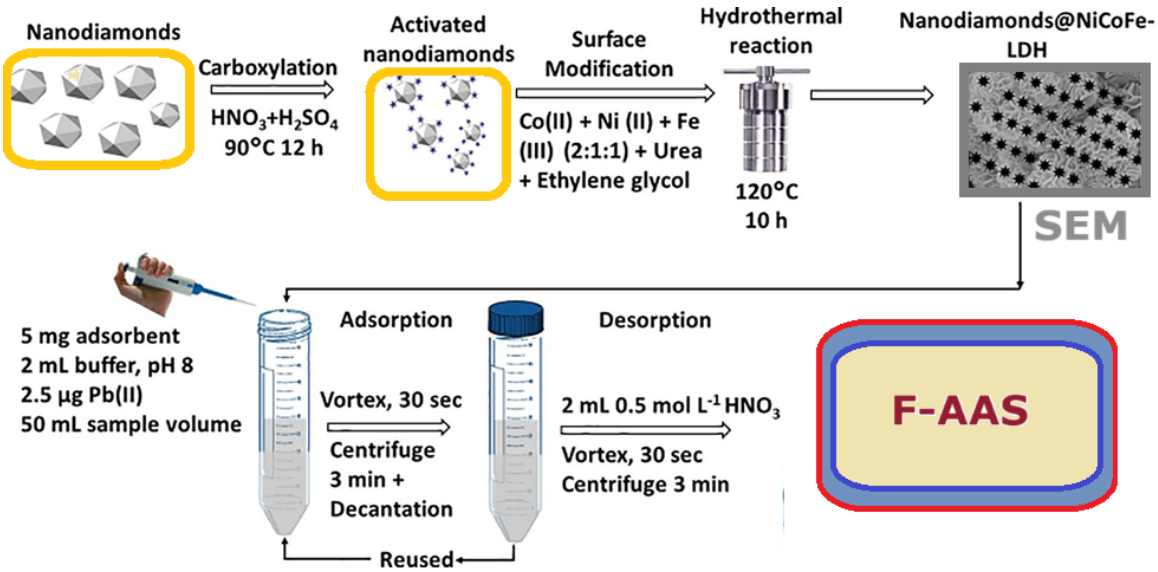

Fig.6. The nanodiamonds@NiCoFe-LDH for separation of lead based on SPME before determination by F-AAS [78,99]

The ICP-MS technique was used to analyze the children's cosmetic products after processing with the microwave digestion system.[98]. Due to Figure 6, Soylak et al. used a new SPME based on nanodiamonds@NiCoFe-LDH for extraction of Pb(II) before determination by F-AAS[78, 99]. The LOD was obtained as 0.62 ng mL^{-1}. Also, Soylak et al. studied MCOFs as an adsorbent in the magnetic SPE method in environmental analysis for pesticides, VOCs, drugs, heavy metal ions, and other environmental contaminants (Fig.7) [100]. Mustafa Tuzen et al. demonstrated a fast hydrophobic deep eutectic solvent (HDES) coupled DLLME for analyzing benzoic acid in food samples using UV-vis spectrophotometry. The LOD of 12 µg L^{-1} and linear range of 40–1000 µg L^{-1} were obtained [80]. Also, they used copolymer-gadolinium oxide nanoparticles (Gd_2O_3) for the extraction of total arsenic [81]. The enrichment factor and LOD for arsenic were obtained at 128 and 0.02 µg L^{-1}, respectively. In addition, many methods were recently presented for the extraction/ separation/removal of VOCs, BTEX, dyes, drugs, amino acids, and aerosol pollution in water and air samples [12,16, 21, 69, 93, 101-110]. Zhang et al. showed the adsorption of heavy metals by modified biochar in water samples [111]. Golbabaei et al. used micro-columns of amin-mesoporous silica nanoparticles (MSN) to remove and specify chromium in water samples[112]. Eskandari et al reported a DLLME method with ionic liquids for determination/ speciation of chromium in human samples and also, and they reported a cloud point assisted based-DLLME by isopropyl 2-[(isopropoxycarbothiolyl) disulfanyl [56,113]. Mousavi et al used acetylcysteine for chromium speciation in human samples by D-LLME [114]. A review of the determination of famotidine drug using the chemiluminescence method presented by Al-Samarrai [115]. Advanced analysis in green analytical chemistry studied by Alsayadi et al. [116]. According to Jaber Ibrahim, Ultra trace elements in the human blood of radiography workers were evaluated by GF-AAS [117]. Rouhollahi and Osanloo used nanotechnology (AgNPS) for mercury removal from the air [118-120]. Golbabaei et al.

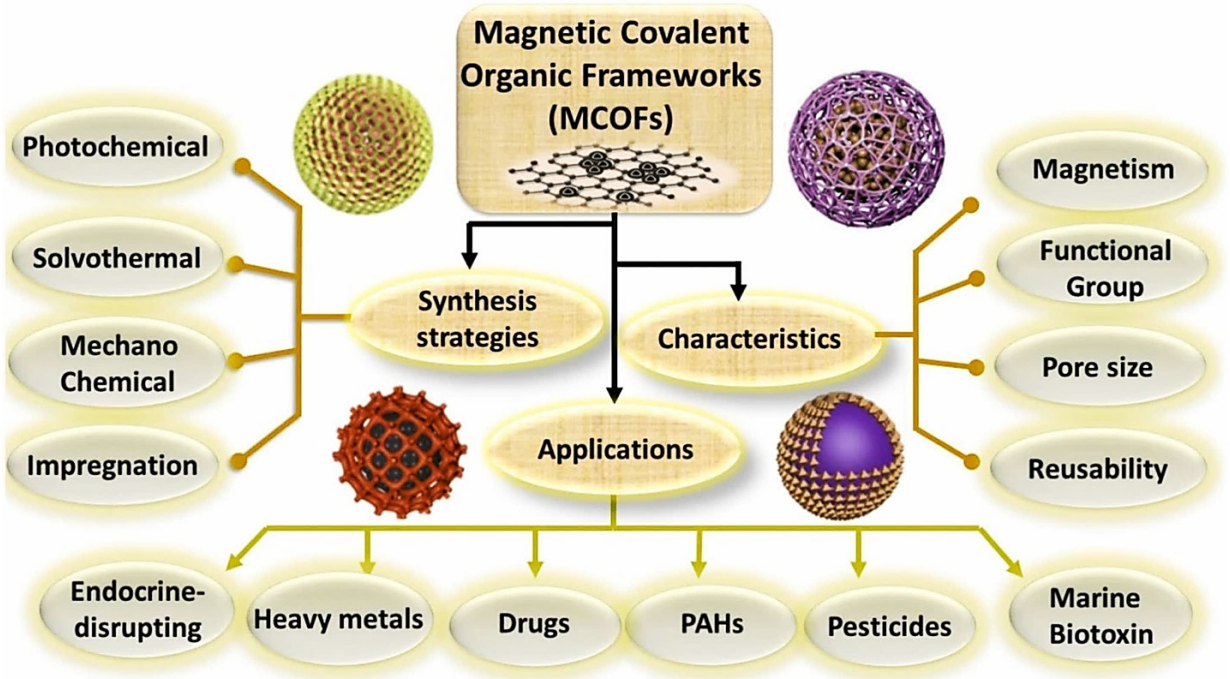

Fig.7. Magnetic covalent organic frameworks (MCOFs) as an adsorbent in the magnetic SPE method in environmental analysis for pesticides, VOCs, drugs, and heavy metal ions [100]

used nano-palladium embedded in MSN for mercury removal from air [121]. Also, Many adsorbents such as bismuth oxide (Bi_2O_3) nanoparticles, Cu-doped ZnO nanotubes, hydrogel-based spin-column, amine-functionalized-MSN, IL-modified nano-graphene, functionalized MWCNTs, and Ni-Fe modified $Cu(OH)_2$ needle were used for extraction/removal/determination pollutant in different matrixes by analytical techniques[122-128]. In addition, various analytical methods were used for the evaluation of neurobehavioral symptoms for Mn and Hg exposure, heavy metal determination in multiple sclerosis patients, and heavy metal concentration in environmental samples and human workers [129-132]. In all analytical techniques to remove pollutants based on nanotechnology, the physical and chemical properties, basic chemistry, and metal complexation are important factors that must be considered and studied [133-136].

The high oxidation of iron complexes plays a critical role in catalytic processes and analytical chemistry or the removal of pollutants. Martin Keilwerth et al used high-valent Fe(VI) nitride as a reactive, super-oxidized, heptavalent Fe(VII) nitride [137] which is shown in Figure 8.

In another study, UV/O_3 is used for the degradation of VOCs and the removal efficiency of toluene [138] (Fig.9). The removal of Cu^{2+}, Ni^{2+}, and Zn^{2+} in water by the ZnO-modified date pits (MDP) was studied. The adsorption capacity for Cu^{2+}, Ni^{2+}, and Zn^{2+} based on MDP were achieved at 82.4, 71.9, and 66.3 mg g^{-1}, respectively [139]. Also, the heavy metals (Fe^{3+}, Mn^{2+}, and Ni^{2+}) were removed from the Lanthanides solution by graphene oxide-citrate (GO-C) adsorbent. The Langmuir model yielded the best adsorption isotherm. The adsorption capacity for Fe^{3+}, Mn^{2+}, and Ni^{2+} was achieved at 530, 223, and 174 mg g^{-1} [140].

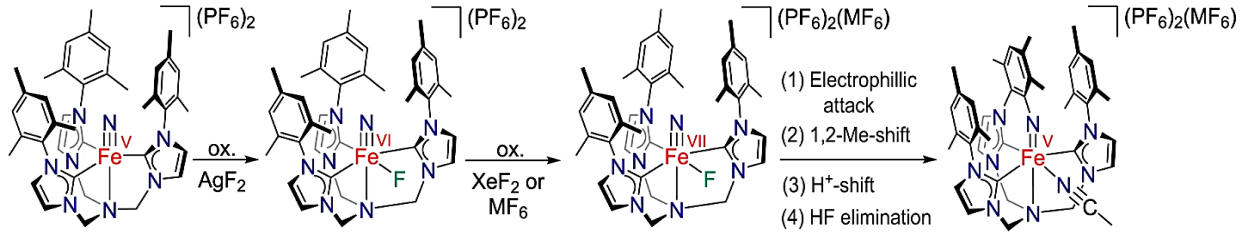

Fig.8. Oxidation of the Fe(VI) nitride to Fe(VII) nitride (MF6 with M = Mo, Re), therefore, rearranges intramolecularly and causes a high-valent, unusual Fe(V) imide[137].

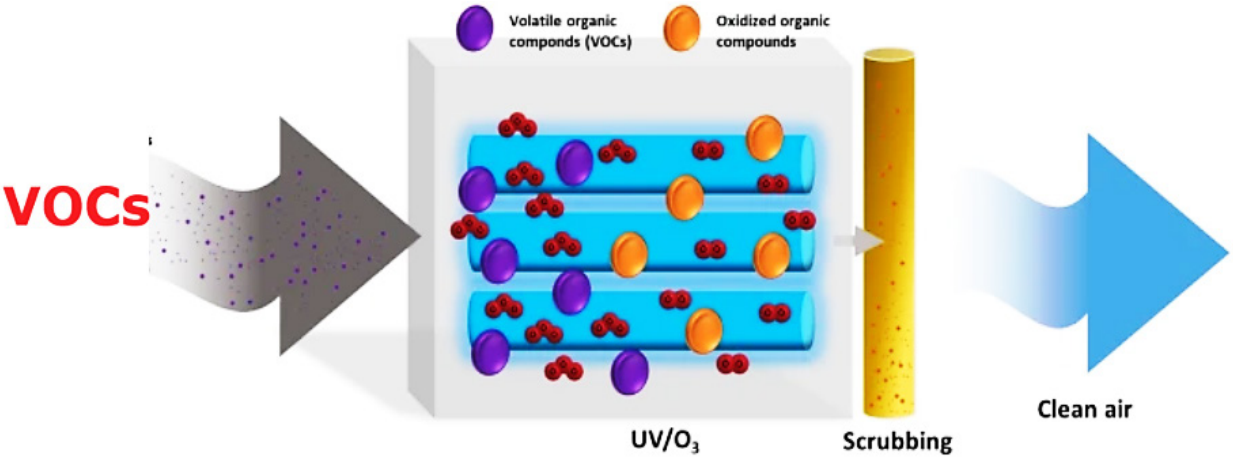

Fig.9. The UV-assisted ozonation (UV/O_3) is used for the degradation of VOCs [140]

Vinicius Diniz et al. reported that the organic contaminant (caffeine) could be adsorbed by the porous sulfur polymers (PSPs) [141]. Due to the procedure, 100 mg of the PSPs was added to caffeine solutions and stirred (300 rpm). At various times, samples were passed through a filter, and the caffeine concentrations were measured using a UV–vis spectrometer at 273 nm (Fig.10). Also, formaldehyde and methyl tert-butyl ether in environmental and human samples were analyzed by headspace coupled to gas chromatography-mass spectrometry (HS-GC-MS) [142].

4. Comparing different adsorbents for the removal of pollutants

To remove VOCs and BTEX from different matrixes such as air and water samples kinds of adsorbents such as nano-graphene modified by ionic liquid, Polyethylene glycol 200 (PEG200) and ionic liquids (ILs), Nano-activated carbons (NACs), IL:[BMIM][PF6], bismuth oxide-fullerene nanoparticles (B_2O_3NPs), ionic liquids were pasted on micro glass balls, copper oxide, Functionally magnetic multi-walled nanotubes (MWCNTs), Fe_3O_4 nanoparticles in zeolitic imidazolate frameworks, hierarchical mordenite framework inverted (MFI) type nano zeolite including Si-MFI, Pd/CeO_2 nanoparticles, Na-P1 zeolite, Platinized titanium dioxide, MnOx/TiO_2/AC, Alkylation-modified pistachio shell-based biochar, B_2O_3NPs-NG/NGO, Modified MIL-101(Cr) using any modulator, Butyl-3-methyl imidazolium hexafluorophosphate, Al-MFI, Zeolite, Spinel-type Mesoporous $ZnFe_2O_4$ Nanoparticles, N@S-TiO_2 Nanotubes, M-IANC, mesoporous carbon–ZrO_2 nanocomposite, hollow Co/N doped carbon frameworks, NiAl/Fe-Al Nanoparticles, 1-benzyl imidazole pasted on TiO_2@NGO Nanostructure, and C_6H_5- [NH_2HIM] [PF_6] @MWCNTs were compared together in Table 1 and different absorption capacities and recovery were obtained [88,11,14,15, 20, 21,106, 143-162]. Also, different methods for determination heavy metald was compared as Table 2.

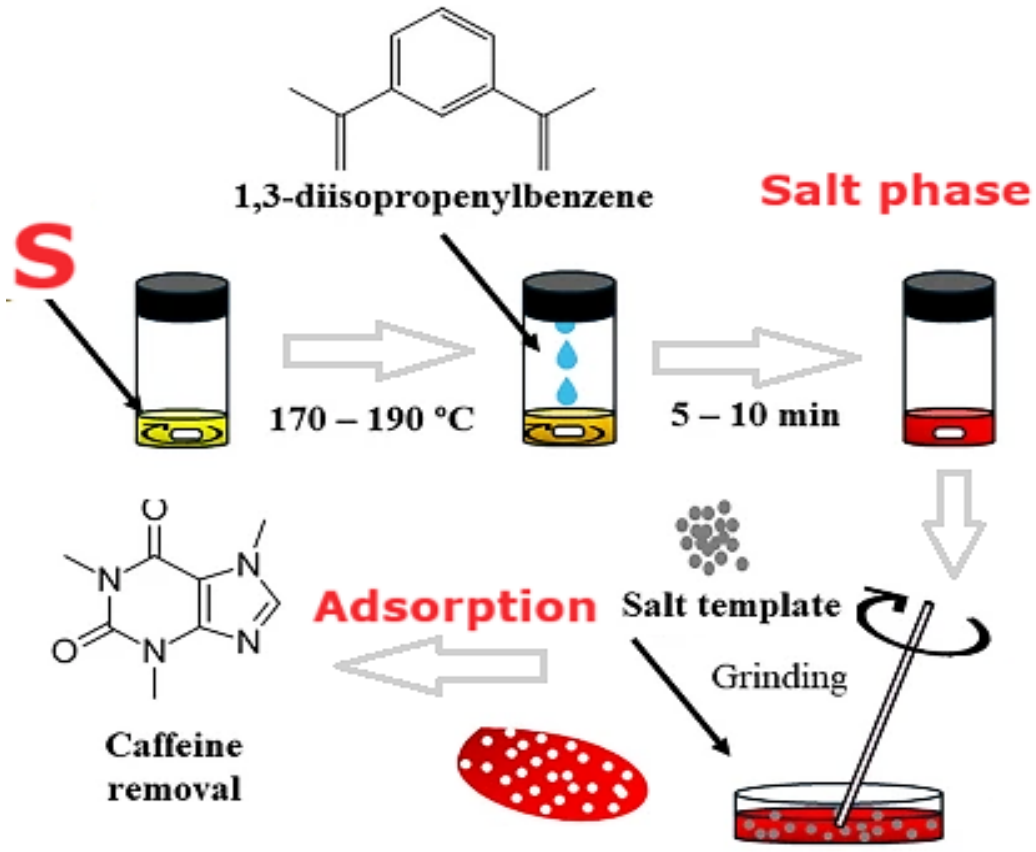

Fig.10. The v removal based on the porous sulphur polymers (PSPs) before determination by UV–vis spectrometer [141]

Table 1. Comparing different adsorbents for VOC/BTEX removal from the air and water by various methods

ollutant	Sorbents	Techniques	Sample	Recovery (%) / AC	Ref.
Toluene	Nano-graphene modified by ionic liquid (NG-IL)	Adsorption	Air	90-95% 126 mg g^{-1}	[88]
Benzene	PEG200- Ionic liquid	Absorption	Water	R:85.4 T R:87.2% B 114.97 mg g^{-1}	[143]
Xylene	Nano-activated carbons (NACs)	Adsorption/GC-FID	Air	116.8-205.2 mg g^{-1} 76.55%	[11]
Toluene	[BMIM][PF6]	Absorption	Milk	5.16 mg g^{-1} 82.85%	[144]
Toluene	bismuth oxide-fullerene nanoparticles	UV-photocatalytic oxidation method (UV-PCOM /GC-FID	Air	212 mg g^{-1} and more than 95%	[21]
Toluene	ionic liquids were pasted on micro glass balls	Adsorption	Air	218.4 mg g^{-1} More than 90%	[20]
Toluene benzene	CuO-NPs	Extraction	Water	Benzene: 100.24 mg g^{-1} Toluene: 111.31 mg g^{-1} R: 92.5%	[145]
BTEX	Functionally magnetic multi-walled nanotubes (MWCNTs)	Adsorption	water	Toluene = 63.34 mg g^{-1} EB = 249.44 mg g^{-1} Xylene = 227.05 mg g^{-1}	[146]
Toluene benzene	Fe3O4 nanoparticles in zeolitic imidazolate frameworks	Adsorption GC-FID	Water	Toluene: 133.1 mg g^{-1} Benzene: 137.3 mg g^{-1} R Benzene: 94.4% R Toluene: 93.1%	[147]
Toluene	MFI (Si-MFI, Al-MFI, Ti-MFI)	Adsorption	Gas	58 mg g−1	[148]
Toluene	0.5%(Pd/CeO_2) Nanoparticles	Adsorption	Air	R Toluene: 90 %	[149]
BTEX	Na-P1 zeolite ($Na_6Al_6Si_6O_{32}$. $12H_2O$)	Adsorption GC-FID	Water	Benzene:0.032 mg g^{-1} Toluene: 0.050 mg g^{-1} AC o-X: 0.147 mg g^{-1} AC p-X: 0.129 mg g^{-1}	[150]
VOCs	Platinized titanium dioxide	Photocatalytic Degradation	Air	Toluene: 68.2% Benzene: 46.5% Xylene: 95.9%	[151]
Toluene	MnOx/TiO_2/AC	MDELs photo-degradation	Gas	94%	[152]
BTEX	AMPSB	Absorption	water	Toluene: 169.9 mg g^{-1} Ethyl acetate: 96.77 mg g^{-1}	[153]

Xylene	BONPs-NG/NGO	UV-PCDA	Air	134.6 -223 mg g^{-1} 38.8 % and 98.7 %	[14]
BTEX	Modified MIL-101(Cr) using any modulator	Adsorption	Gas	90.14 %	[154]
Toluene	Al-MFI	Adsorption	Wet gas	58 mg g^{-1}	[155]
Toluene	Zeolite	Absorption	Water	AC: 95 mg g-1 R= 92.6	[156]
Toluene	Spinel-type Mesoporous $ZnFe_2O_4$ Nanoparticles	Photocatalytic Degradation	Gas	R Toluene: 60 %	[157]
VOCs	N@S-TiO_2 Nanotubes	Photocatalytic Degradation	Gas	94%	[158]
Toluene, Benzene	M-IANC	Adsorption	Ambient	Benzene: 18.22 mg g^{-1} Toluene:82.1 mg g^{-1}	[159]
BTEX	MC- $ZrO_{2:}$	Headspace Mode-Solid-Phase Microextraction/ GC-FID	Water	R: 93% R^2> 0.996	[160]
Toluene	Hollow Co/N co-doped carbon frameworks	Photocatalytic Degradation	Gas	Toluene: 78.2%	[161]
Toluene	NiAl/Fe-Al Nanoparticles	Hybrid Plasma-Catalysis	Vapor	Toluene 96%	[162]
Toluene	BIM-TiO_2@NGO Nanostructure	Adsorption/ Semi degradation/Desorption process	Air	99% 234.5 mg g^{-1}	[15]
BTEX	Phe and [NH_2HIM] [PF_6] @ MWCNTs	Absorption/Extraction	Water Milk	AC Benzene: 286.6 mg g-1 AC EB: 248.5 mg g-1 AC Toluene: 234.6 mg g-1 AC xylene: 195.6 mg g-1 R> 95%	[106]

AC: Absorption capacity, **R**: Recovery, **SA**: Surface area, **BTX**: Benzene, Toluene, Xylene
MWCNTs: magnetic multi-walled carbon nanotube
MFI: Mordenite Framework Inverted
Si-MFI: Hierarchical Mordenite Framework Inverted (MFI) type nano zeolite including Si-MFI
BIM:1-benzyl imidazole
PCD: Photocatalytic destruction
UV-PCDA: UV photo-catalectic degradation-adsorption procedure
MnOx/TiO2/AC: Catalyst prepared by the solvent-deficient method
MWCNT: Magnetic multi-walled carbon nanotube
AC: Activated carbon
PEG200-ILs: Polyethylene glycol 200 (PEG200) and ionic liquids (ILs)
complex absorbents composed of [EMIM][Cl], [BMIM][Cl],[HMIM][Cl], [BMIM][BF4], [BMIM][PF6], [BMIM][NTF2], and PEG200
[Bmim][PF6]: Butyl-3-methyl imidazolium hexafluorophosphate
MC- ZrO2: mesoporous carbon–ZrO2 nanocomposite
AMPSB: Alkylation-modified pistachio shell-based biochar
BTX: Benzene, Toluene, Xylene

Table 2. Comparing the different procedure for analysis heavy metals in water and food samples

Method Extraction	Adsorbent	Technique	Matrix	Metal	*LOD	*PF/ EF	*LR	RSD%	Ref.
MDMSPE/ SFODME	M - $ZnFe_2O_4$ NT	ET-AAS	Tap water	Mn (II), Mn (VII)	<0.1	200	----	4.8	[163]
DIL-S-μSPE	MWCNTs@DMP	F-AAS	water,	Pb (II)	3.2	10.4	9.5–480	5.0	[96]
USA-DILT-μ-SPE	N-acetylcysteine on chloro-functionalized MWCNTs	F AAS	Water/ Food	Mn (VII)	0.18	96.8	0.6–38.7	4.6	[164]
SPME	PSCOVC	F AAS	water	Mn, Zn	0.2,7.9	145	0.15–250	2.1-3.4	[165]
SPE	Graphene oxide		Water	Pb	2.1	102.5	7–260	4.1	[68]
SPE	graphene	F-AAS	Water	Pb	0.61	50	10-600	3.25	[166]
Co-precipitation	------	F AAS	Water/ Food	Mn (II), Mn (VII)	0.75	50	0.1-3.0	<7.0	[167]
US-D-μ-SPE	NH_2-UVM-7	AT-F AAS	Water	Mn (II), Mn (VII)	------	102.3, 98.8	0.5-48.7	2.3, 2.8	[168]
USA-D-μSPE	Graphene- Clinoptilolite Hybrid	ETAAS	Water	Cd- Pb	0.07	20	0.24-10.3	3.4	[169]
USA-CP-MSPE	Amine functionalized silica aerogel	ETAAS	Water	Pb	0.01	102	0.04–1.4	3.25	[170]
MDM- μ-SPE	Fe_3O_4@4-PhMT-GO	ET-AAS	Water/ Food	Al (III)	0.012	48.8	0.05–2.5	2.8	[87]
DES-LPME	HPhImNaph	F AAS	Water	Mn (II)	0.52	92.9	3-100	2.7	[171]
IL- DLLME/ SFS	IL-Oxine	SF	Water	A l(III)	0.05	100	0.06–15	1.7	[172]
SPE	XAD-1180-PV	AAS	Water	Al(III)	0.021	-----	5-10	4.32	[173]

*__EF/PF__: Enrichment factor/ preconcentration factor, __LOD:__ Limit of detection, μgL^{-1}, __LR:__ Linear Range, μgL^{-1}
__PSCOVC__: Poly(styrene)-co-2-vinylpyridine copolymer
__AT-FAAS__: Atom trapping-flame atomic absorption spectrometry
__SF__: spectrofluorometry
__MSM__: Multivariate statistical methods.
__HPhImNaph:__ 3-[[(2-hydroxyphenyl) imino]methyl]-2-naphthalenol
__DES-LPME__: Deep eutectic solvent-based liquid phase microextraction
__DLLME__: Dispersive liquid-liquid microextraction
__PAN:__ 1-(2-Pyridylazo)-2-naphthol
__NGO-PTT__: Graphene oxide (GO) packed column and 1-Phenyl-3-(2-phenylmethyl) thiourea (PPT)
__SPE__: Solid phase extraction (SPE)
__ESM__: Eggshell membrane
__DMSPE__: Dispersive micro solid-phase extraction
__MDMSPE__: Magnetic dispersive micro-solid phase extraction
__SFODME__: solidified floating organic drop microextraction
__M -$ZnFe_2O_4$ NT__: Magnetic $ZnFe_2O_4$ nanotubes
__ET-AAS__: graphite furnace atomic absorption spectrometer
__USA-CP-MSPE__: Ultrasound-assisted cloud point-micro solid phase extraction

5. Conclusions

The application of nanotechnology for removing and extracting pollutants from various matrices helps simple, efficient methods for determining, separating, and preconcentrating pollutants. Due to the statistical results, the nanomaterials such as MWCNTs, SWCNTs, NG/NGO, AC, MSN, and MOFs had more efficiency in removing pollutants in different environmental samples. The previous research showed that ionic liquids (ILs) and TSILs can separate nanoparticles and nano adsorbents from liquid phased with high recovery. Also, ILs passed on nanosorbents could absorb VOCs and heavy metals from air, water, and human biological samples, respectively. By harnessing the unique properties of nanoparticles, such as high surface area and reactivity, significant advancements have been made in enhancing pollutant removal efficiencies (more than 95%) and minimizing environmental impacts. Using nanoadsorbent highlights nanotechnology's versatility in removing heavy metals or VOCs from air, water, soil, or human samples. Statistical results in analytical methods such as LOD, LOQ, linear range, absorption capacity, RSD%, enrichment factor, and recovery (%) reveal compelling evidence of the effectiveness of nanomaterials in achieving pollutant removal targets, thereby contributing to sustainable environmental management strategies.

6. Acknowledgments

The authors are very thankful to the management of the Analytical Chemistry Department of Environmental Health Engineering, Zabol, Iran, and the Department of Chemistry, Faculty of Science, Kerman branch, Islamic Azad University for supporting this study.

7. References

[1] ATSDR, Toxicological profile for benzene, Department of Health and Human Services, Agency for Toxic Substances and Disease Registry, USA, 2007. https://www.atsdr.cdc.gov/toxprofiles/tp3.pdf

[2] Sh. Teimoori, S. A. Mirzahossein, Removing toluene from atmospheric air by nano activated carbon adsorbent, J. Nat. Environ., 72 (2019) 45-58. https://doi.org/10.22059/jne.2019.257086.1515

[3] A. Bolden, C. Kwiatkowski, T. Colborn, New look at BTEX: are ambient levels problematic, Environ. Sci. Technol., 49 (2015) 5261-5276. https://doi.org/10.1021/es505316f

[4] U. B. Nurmatov, N. Tagiyeva, S. Semple, G. Devereux, A. Sheikh, Volatile organic compounds and risk of asthma and allergy: a systematic review, Eur. Respir. Rev., 24 (2015) 92-101. https://doi.org/10.1183/09059180.00000714

[5] C. N. Maesano, D. Caillaud, H. Youssouf, S. Banerjee, J. P. Homme, C. Audi, K. Horo, Y. Toloba, O. Ramousse, A. I. Maesano, Indoor exposure to particulate matter and VOCs in dwellings and workplaces and respiratory health in French farmers, Multidiscip. Respir. Med., 14 (2019) 14-33. https://doi.org/10.1186/s40248-019-0194-3

[6] P. Zeitz Ruckart, F. J Bove, M. Maslia, Exposure to VOCs in drinking water and specific birth defects and childhood cancers, U.S. Marine Corps Base Camp Lejeune, Environ. Health, 12 (2013) 104. https://doi.org/10.1186/1476-069X-12-104

[7] ATSDR, interaction profile for benzene, toluene, ethylbenzene, and xylenes (BTEX), U.S. Department of Health and Human Services, Public Health Service, Agency for Toxic Substances and Disease Registry, Atlanta, GA. 2004. https://www.atsdr.cdc.gov/interactionprofiles/ip-btex/ip05.pdf

[8] J. Huff, Absence of carcinogenic activity in Fischer rats and B6C3F1 mice following 103-week inhalation exposure to toluene, Int. J. Occup. Environ. Health, 9 (2003) 46-138. https://doi.org/ 10.1179/oeh.2003.9.2.138

[9] D. M. Chambers, D. O. McElprang, M. G. Waterhouse, B. C. Blount, An improved approach for accurate quantitation of benzene, toluene, ethylbenzene, xylene,

and styrene in blood, Anal. Chem., 78 (2006) 5375-5383. https://doi.org/10.1021/ac060341g

[10] A. Tabrizi, F. Golbabaei, M. Jafarizaveh, R. Yarahmadi, Evaluation of the adsorption capacity of nano-graphene and nano-graphene oxide for xylene removal from air and their comparison with the standard adsorbent of activated carbon to introduce the optimized one, J. Health Saf. Work, 6 (2016) 25-34. https://journals.tums.ac.ir/jhsw/article-1-5415-en.html

[11] M. Jafarizaveh, F. Golbabaei, A. Tabrizi, K. Azam, M. Ghasemkhani, Nobel method for xylene removal from the air on nano activated carbon adsorbent compared to NIOSH approved carbon adsorbent, J. Health Saf. Work, 6 (2016) 23-30. https://jhsw.tums.ac.ir/browse.php?a_id=5374&sid=1&slc_lang=en

[12] R. Ashouri, N. Mansouri, Dynamic and static removal of benzene from air based on task-specific ionic liquid coated on MWCNTs by sorbent tube-headspace solid-phase extraction procedure, Int. J. Environ. Sci. Technol., 18 (2021) 2377-2390. https://doi.org/10.1007/s13762-020-02995-4

[13] R. Ashouri, S. A. Hajiseyed Mirzahosseini, N. Mansouri, Synthesis of Carbon Quantum Dots from Olive Stones for Efficient Adsorption of Benzene from the Ambient Air, J. Nanostruct., 11 (2021) 480-497. https://doi.org/10.22052/JNS.2021.03.007

[14] A. Faghihi-Zarandi, J. Rakhtshah, B. B. Yarahmadi, A rapid removal of xylene vapor from environmental air based on bismuth oxide coupled to heterogeneous graphene/graphene oxide by UV photo-catalectic degradation-adsorption procedure, J. Environ. Chem. Eng., 8 (2020) 104193. https://doi.org/10.1016/j.jece.2020.104193

[15] M. Mohammadi Asl, N. Mansouri, S. A. R. Haji Seyed Mirzahosseini, F. Atabi, Simultaneity comparative evaluation of toluene removal from the air by adsorption and UV semi-degradation-based adsorption procedure, Int. J. Environ. Sci. Technol., 21 (2024) 6677-6694. https://doi.org/10.1007/s13762-024-05503-0

[16] M. M. Asl, F. Atabi, Functionalized graphene oxide with bismuth and titanium oxide nanoparticles for efficiently removing formaldehyde from the air by photocatalytic degradation–adsorption process, J. Anal. Test., 7 (2023) 444-458. https://doi.org/10.1007/s41664-023-00272-0

[17] M. S. Waring, J. R. Wells, Volatile organic compound conversion by ozone, hydroxyl radicals, and nitrate radicals in residential indoor air: Magnitudes and impacts of oxidant sources, Atmos. Environ., 106 (2015) 382-391. https://doi.org/10.1016/j.atmosenv.2014.06.062

[18] H. N. Altalyan, B. Jones, J. Bradd, L. D. Nghiem, Y. M. Alyazichi, Removal of volatile organic compounds (VOCs) from groundwater by reverse osmosis and nanofiltration, J. Water Proc. Eng., 9 (2016) 9-21. https://doi.org/10.1016/j.jwpe.2015.11.010

[19] Y. Wang, H. Song, L. Li, J. Ma, F. Yu, Generation characteristics and spreading risk of VOCs released from a biological fermentation pharmaceutical factory, Environ. Sci.: Processes Impacts, 25 (2023) 507-518. https://doi.org/10.1039/D2EM00378C

[20] A. Faghihi-Zarandi, H. Shirkhanloo, C. Jamshidzadeh, A new method for removal of hazardous toluene vapor from air based on ionic liquid-phase adsorbent, Int. J. Environ. Sci. Technol., 16 (2019) 2797-2808. https://doi.org/10.1007/s13762-018-1975-5

[21] C. Jamshidzadeh, A new analytical method based on bismuth oxide-fullerene nanoparticles and photocatalytic oxidation technique for toluene removal from workplace air, Anal. Methods Environ. Chem. J., 2 (2019) 73-86. https://doi.

org/10.24200/amecj.v2.i01.55

[22] F. Golbabaei, M. Seyedsomea, A. Ghahri, H. Hassani, Assessment of welders exposure to carcinogen metals from manual metal arc welding in gas transmission pipelines, Iran, Iran. J. Public Health, 41 (2012) 61-70. https://www.ncbi.nlm.nih.gov/pmc/articles/PMC3469034/pdf/ijph-41-61.pdf

[23] A. F. Zarandi, An immobilization of 2-(Aminomethyl) thiazole on MWCNTs used for rapid extraction of manganese ions in hepatic patients, J. Pharm. Biomed. Anal., 240 (2024) 115941. https://doi.org/10.1016/j.jpba.2023.115941

[24] A. Khaligh, H. Z. Mousavi, Speciation and determination of inorganic arsenic species in water and biological samples by ultrasound assisted-dispersive-micro-solid phase extraction on carboxylated nanoporous graphene coupled with flow injection-hydride generation atomic absorption spectrometry, RSC Adv., 5 (2015) 93347-93359. https://doi.org/10.1039/C5RA17229B

[25] A. Rouhollahi, H. Z. Mousavi, Ultra-trace arsenic determination in urine and whole blood samples by flow injection-hydride generation atomic absorption spectrometry after preconcentration and speciation based on dispersive liquid-liquid microextraction, Bull. Korean Chem., 32 (2011) 3923-3927. http://dx.doi.org/10.5012/bkcs.2011.32.10.1

[26] A. Rouhollahi, H. Z. Mousavi, Preconcentration and Determination of Trace Amount of Nickel in Water and Biological Samples by Dispersive Liquid-Liquid Microextraction J. Chin. Chem. Soc., 57 (2010) 1035-1041. https://doi.org/10.1002/jccs.201000144

[27] A. Rashidi, A. Vahid, Arsenic speciation based on amine-functionalized bimodal mesoporous silica nanoparticles by ultrasound assisted-dispersive solid-liquid multiple phase microextraction, Microchem. J., 130 (2017) 137-146. https://doi.org/10.1016/j.microc.2016.08.013

[28] H. Shirkhanloo, ZH. Mousavi, A. Rouhollahi, Preconcentration and determination of heavy metals in water, sediment and biological samples, J. Serb. Chem. Soc., 76 (2011) 1583-1595. https://doi.org/10.2298/JSC101024139S

[29] A. A. Miran Beigi, On-line pre-concentration and separation of Iinorganic arsenic based on nano platinum-multiwall carbon nanotubes, J. Nanoanal., 1 (2014) 52-57. https://doi.org/10.22034/jna.2014.02.001

[30] M. Jaishankar, B. B. Mathew, M. S. Shah, K. R. S. Gowda, Biosorption of few heavy metal ions using agricultural wastes, J. Environ. Pollut. Human Health, 2 (2014) 1-6. https://doi.org/ 10.12691/jephh-2-1-1

[31] L. Järup, Hazards of heavy metal contamination, Br. Med. Bull., 68 (2003) 167-182. https://doi.org/10.1093/bmb/ldg032

[32] R. Khlifi, A. Hamza-Chaffai, Head and neck cancer due to heavy metal exposure via tobacco smoking and professional exposure: a review, Toxicol. Appl. Pharmacol., 248 (2010) 71-88. https://doi.org/10.1016/j.taap.2010.08.003

[33] L. Zhang, Z. Shi, Z. Jiang, J. Zhang, F. Wang, X. Huang, Distribution and bioaccumulation of heavy metals in marine organisms in east and west Guangdong coastal regions, South China, Mar. Pollut. Bull., 101 (2015) 930–937. https://doi.org/10.1016/j.marpolbul.2015.10.041

[34] S. J. Stohs, D. Bagchi, Oxidative mechanisms in the toxicity of metal ions, Free Radicals Biol. Med., 18 (1995) 321-336. https://doi.org/10.1016/0891-5849(94)00159-H

[35] M. M. Tarekegn, A. M. Hiruy, A. H. Dekebo, Nano zero-valent iron (nZVI) particles for the removal of heavy metals (Cd^{2+}, Cu^{2+} and Pb^{2+}) from aqueous solutions, RSC Adv., 11 (2021) 18539-18551. https://doi.org/10.1039/D1RA01427G

[36] E. Zolfonoun, Solid phase extraction, and determination of indium using multiwalled

carbon nanotubes modified with magnetic nanoparticles, Anal. Methods Environ. Chem. J., 1 (2018) 5-10. https://doi.org/10.24200/amecj.v1.i01.14

[37] E. Zolfonoun, S. M. R. Pakzad, M. Salahinejad, Determination of 137Ba isotope abundances in water samples by inductively coupled plasma-optical emission spectrometry combined with least-squares support vector machine regression, Anal. Bioanal. Chem. Res., 3 (2016) 65-72. https://doi.org/10.22036/ABCR.2016.14143

[38] I. G. Canu, O. Laurent, N. Pires, D. Laurier, I. Dublineau, Health effects of naturally radioactive water ingestion: The need for enhanced studies, Environ. Health Perspect., 119 (2021) 1676 – 1680. https://doi.org/10.1289/ehp.1003224

[39] E. Zolfonoun, Dispersive liquid-liquid microextraction technique combined with UV–Vis spectrophotometry for determination of zirconium in aqueous samples, Anal. Methods Environ. Chem. J., 3 (2020) 25-31. https://doi.org/10.24200/amecj.v3.i03.107

[40] V. A. Wirnkor, E. C. Ebere, V. E. Ngozi, The importance of microplastic pollution studies in water and soil of Nigeria ecosystems, Anal. Methods Environ. Chem. J., 2 (2019) 89-96. https://doi.org/10.24200/amecj.v2.i03.69

[41] E. C. Ebere, V. E. Ngozi, Microplastics, an emerging concern: A review of analytical techniques for detecting and quantifying microplatics, Anal. Methods Environ. Chem. J., 2 (2019) 13-30. https://doi.org/10.24200/amecj.v2.i2.57

[42] M. B. H. Abadi, H. Shirkhanloo, J. Rakhtshah, Air pollution control: The evaluation of TerphApm@ MWCNTs as a novel heterogeneous sorbent for benzene removal from air by solid phase gas extraction, Arabian J. Chem., 13 (2020) 1741-1751. https://doi.org/10.1016/j.arabjc.2018.01.011

[43] M. Soylak, A. N. Çoban, H. E. H. Ahmed, Micro solid phase extraction of lead and cadmium using functionalized nanodiamonds@ $CuAl_2O_4$@ HKUST-1 nanocomposite for FAAS analysis in food and water samples, Food Chem., 442 (2024) 138426. https://doi.org/10.1016/j.foodchem.2024.138426

[44] N. Kizil, D. Erbilgin, E. Basaran, M. L. Yola, E. Yilmaz, S. Marouch, M. Soylak, Determination of rhodamine B in cosmetics, candy, water, and plastic by a novel multiwalled carbon nanotube (MWCNT)@ Zinc oxide@Magnetite nanocomposite for magnetic solid-phase extraction (MSPE) with spectrophotometric detection, Anal. Lett., 57 (2024) 1182-1196. https://doi.org/10.1080/00032719.2023.2243353

[45] H. E. H. Ahmed, M. Soylak, A MWCNTs@ CuAl2O4@SiO2 nanocomposite for the speciation of Cr(III), Cr(VI), and total chromium prior to high-resolution continuum source flame atomic absorption spectrometric determination, Water, Air, Soil Pollut., 235 (2024) 217. https://doi.org/10.1007/s11270-024-07020-9

[46] H. Zavvar Mousavi, A. Asghari, H. Shirkhanloo, Determination of Hg in water and wastewater samples by CV-AAS following on-line preconcentration with silver trap, J. Anal. Chem., 65 (2010) 935-939. https://doi.org/10.1134/S106193481009008X

[47] A. Rouhollahi, Determination of mercury concentration in the air of dental clinics and the urines of their personnel with cold vapor atomic absorption spectrometry, Iran. J. Toxicol., 2 (47) 287-291. http://ijt.arakmu.ac.ir/article-1-66-en.html

[48] H. Hassani, F. Golbabaei, A. Ghahri, M. Hosseini, H. Shirkhanloo, B. Dinari, D. Eskandari, M. Fallahi, Occupational exposure to manganese-containing welding fumes and pulmonary function indices among natural gas transmission pipeline welders, J. Occup. Health, 54 (2012) 316-322. https://doi.org/10.1539/joh.11-0269-FS

[49] M. Aliomrani, M.A. Sahraian, Blood concentrations of cadmium and lead in multiple sclerosis patients from Iran, Iran. J. Pharm. Res., 15 (2016) 825-833. https://doi.org/10.22037/ijpr.2016.1941

[50] X. Wu, Wei Jia, Multilayer annotation strategy annoSePS: Disentangling the intricate structure of selenium-containing polysaccharides based on preferential fragmentation patterns, Anal. Chem., 2024. https://doi.org/10.1021/acs.analchem.4c01576

[51] H. Shirkhanloo, H. Z. Mousavi, Cadmium determination in human biological samples based on trioctylmethyl ammonium thiosalicylate as a task-specific ionic liquid by dispersive liquid-liquid microextraction method, J. Mol. Liq., 218 (2016) 478-483. https://doi.org/10.1016/j.molliq.2016.02.035

[52] M. Aliomrani, M. A. Sahraian, M. Sharifzadeh, M. R. Khoshayand, M. H. Ghahremani, Correlation between heavy metal exposure and GSTM1 polymorphism in Iranian multiple sclerosis patients, Neurol. Sci., 38 (2017) 1271–1278. https://doi.org/10.1007/s10072-017-2934-5

[53] Z. Karamzadeh, A novel biostructure sorbent based on CysSB/MetSB@MWCNTs for separation of nickel and cobalt in biological samples by ultrasound assisted-dispersive ionic liquid- suspension solid phase microextraction, J. Pharm. Biomed. Anal., 172 (2019) 285-294. https://doi.org/10.1016/j.jpba.2019.05.003

[54] H. Z. Mousavi, Ultrasound-assisted dispersive micro solid-phase extraction of four tyrosine kinase inhibitors from serum and cerebrospinal fluid by using magnetic nanoparticles coated with nickel-doped silica as an adsorbent, Microchim. Acta, 183 (2016) 2779-2789. https://doi.org/10.1007/s00604-016-1927-z

[55] H. Shirkhanloo, A. Khaligh, H. Z. Mousavi, M. M. Eskandari, A. A. Miran-Beigi, Ultra-trace arsenic and mercury speciation and determination in blood samples by ionic liquid-based dispersive liquid-liquid microextraction combined with flow injection-hydride generation/cold vapor atomic absorption spectroscopy, Chem. Pap., 69 (2015) 779-790. https://doi.org/10.1515/chempap-2015-0086

[56] M. M. Eskandari, Cloud point assisted dispersive ionic liquid-liquid microextraction for chromium speciation in human blood samples based on isopropyl 2-[(isopropoxycarbothiolyl) disulfanyl] ethane thioate, Anal. Chem. Res., 10 (2016) 18-27. https://doi.org/10.1016/j.ancr.2016.10.002

[57] S. Tokalioglu, Z. Gonulalan, E. Simsek, N. E. Onmaz, E. Yılmaz, Bioaccumulation of heavy metals in freshwater fish species retailed in Kayseri Region: Potential public health hazard of toxic metal, Bozok Veterinary Sci., 4 (2023) 27-36. https://doi.org/10.58833/bozokvetsci.1290269

[58] Y. Qi, Y. Song, C. Liu, S. Qi, H. Wang, J. Cao, Q. Zhao, Highly efficient heavy-metal-ion removal from shellfish processing liquid with low protein and polysaccharide loss by hybrid mesoporous silica diol-APDC-SBA15, J. Ocean Univ. China, 22 (2023) 221–228. https://doi.org/10.1007/s11802-023-5195-3

[59] Y. Zhang, X. Cao, J. Sun, G. Wu, J. Wang, D. Zhang, Synthesis of pyridyl Schiff base functionalized SBA-15 mesoporous silica for the removal of Cu(II) and Pb(II) from aqueous solution, J. Sol-Gel Sci. Technol., 4 (2020) 658-670. https://doi.org/10.1007/s10971-019-05205-x

[60] Y. Qi, J. Wei, H. Wang, Y. Zhang, J. Xu, X. Qian, Y. Guan, Improved selection of LMW over HMW proteins from human plasma by mesoporous silica particles with external modification, Talanta, 80 (2010) 703-709. https://doi.org/10.1016/j.talanta.2009.07.050

[61] Q. Salamat, M. Soylak, Novel magnetic

deep eutectic solvent/Zn-MOF composite for extraction of Carmoisine from water and food samples, J. Food Compos. Anal., 128 (2024) 105997. https://doi.org/10.1016/j.jfca.2024.105997

[62] J. Ali, M. Tuzen, W. B. Jatoi, X. Feng, G. Sun, T. A. Saleh, A review of sequential extraction methods for fractionation analysis of toxic metals in solid environmental matrices, TrAC, Trends Anal. Chem., 173 (2024) 117639. https://doi.org/10.1016/j.trac.2024.117639

[63] R. Ullah, M. Tuzen, B. Hazer, H. Wahba, T. A. Saleh, Synthesis of poly (3-hydroxy butyrate)-g-poly (ricinoleic acid)-Ag nanocomposite for adsorption of methyl blue with multivariate optimization, J. Mol. Liq., 399 (2024) 124369. https://doi.org/10.1016/j.molliq.2024.124369

[64] M. Ghazaghi, H. Z. Mousavi, A. M. Rashidi, H. Shirkhanloo, R. Rahighi, Graphene-silica hybrid in efficient preconcentration of heavy metal ions via novel single-step method of moderate centrifugation-assisted dispersive micro solid phase extraction, Talanta, 150 (2016) 476-484. https://doi.org/10.1016/j.talanta.2015.12.074

[65] S. J. Schmidt, W. Dou, S. A. Sydlik, Regeneratable graphene-based water filters for heavy metal removal at home, ACS EST Water, 3 (2023) 2179–2185. https://doi.org/10.1021/acsestwater.3c00010

[66] H. Şahin, S. Ciraci, Chlorine adsorption on graphene: Chlorographene, J. Phys. Chem. C, 116 (2012) 24075– 24083. https://doi.org/10.1021/jp307006c

[67] M. Musielak, A. Gagor, B. Zawisza, E. Talik, R. Sitko, Graphene oxide/carbon nanotube membranes for highly efficient removal of metal ions from water, ACS Appl. Mater. Interfaces, 11(2019) 28582– 28590. https://doi.org/10.1021/acsami.9b11214

[68] H. Shirkhanloo, A. Khaligh, H. Z. Mousavi, A. Rashidi, Graphene oxide-packed micro-column solid-phase extraction combined with flame atomic absorption spectrometry for determination of lead (II) and nickel (II) in water samples, Int. J. Environ. Anal. Chem., 95 (2015) 16-32. https://doi.org/10.1080/03067319.2014.983437

[69] A. Ibrahim, H. A. W. Dwesh, A. R. Y. Al-Sawad, Adsorption of methylene blue dye onto bentonite clay: Characterization, adsorption isotherms, and thermodynamics study by using UV-Vis technique, Anal. Chem., 6 (2023) 5-18. https://doi.org/10.24200/amecj.v6.i03.243

[70] S. Bahah, Analytical study on lead elimination by anionic clays: Characterization, adsorption kinetics, isotherm, thermodynamic, mechanism and adsorption, Anal. Methods Environ. Chem. J., 6 (2023) 67-88. https://doi.org/10.24200/amecj.v6.i03.248

[71] S. Javan, M. R. Rezaei Kahkha, F. Moghaddam, M. Faghihi-Zarandi, A. Hejazi, Photocatalytic degradation of methyl orange using Cerium doped zinc oxide nanoparticles supported bentonite clay, Anal. Methods Environ. Chem. J., 5 (2022) 87-95. https://doi.org/10.24200/amecj.v5.i04.216

[72] N. Motakef kazemi, Zinc-based metal-organic framework for nickel adsorption in water and wastewater samples by ultrasound assisted-dispersive-micro solid phase extraction coupled to electrothermal atomic absorption spectrometry, Anal. Methods Environ. Chem. J., 3 (2020) 5-16. https://doi.org/10.24200/amecj.v3.i04.123

[73] M. O. Odar, Adsorption and determination of Lead in water and human urine samples based on Zn_2 $(BDC)_2$(DABCO)MOF as polycaprolactone nanocomposite by suspension micro solid phase extraction coupled to UV–VIS spectroscopy, Anal. Methods Environ. Chem. J., 4 (2021) 5-20. https://doi.org/10.24200/amecj.v4.i03.145

[74] N. Motakef Kazemi, A novel sorbent based on metal-organic framework for mercury

separation from human serum samples by ultrasound-assisted- ionic liquid-solid phase microextraction, Anal. Methods Environ. Chem. J., 2 (2019) 67-78. https://doi.org/10.24200/amecj.v2.i03.68

[75] Y. Chen, H. R Chen, J. L Shi, Construction of homogenous/heterogeneous hollow mesoporous silica nanostructures by silica-etching chemistry: Principals, synthesis, and applications, Acc. Chem. Res., 47 (2014) 125–137. https://doi.org/10.1021/ar400091e

[76] F. Golbabaei, A. Ebrahimi, A. Koohpaei, A. Faghihi-Zarandi, Single-Walled Carbon Nanotubes (SWCNTs), as a Novel Sorbent for Determination of Mercury in Air, Glob J Health Sci., 8 (2016) 273-280. https://doi.org/10.5539/gjhs.v8n7p273

[77] N. Manousi, D. A. Giannakoudakis, E. Rosenberg, G. A. Zachariadis, Extraction of metal ions with metal-organic frameworks, Molecules, 24 (2019) 4605. https://doi.org/10.3390/molecules24244605

[78] M. B. Arain, H. E. H. Ahmed, M. Soylak, Functionalized nanodiamonds with NiCoFe layered double hydroxides used as a novel adsorbent in dispersive solid-phase microextraction for Pb (II) determination in juice samples, Microchem. J., 199 (2024) 109922. https://doi.org/10.1016/j.microc.2024.109922

[79] H. E. H. Ahmed, Z. P. Gumus, M. Soylak, Determination of atrazine in food, water, and synthetic urine by activated carbon cloth (ACC) micro-solid-phase extraction (μSPE) with high-performance liquid chromatography-diode array detection (HPLC-DAD), Anal. Lett., 57 (2024) 681-693. https://doi.org/10.1080/00032719.2023.2221754

[80] N. Altunay, M. F. Lanjwani, H. U. Haq, M. Tuzen, A. Elik, Sensitive method for determination of benzoic acid in beverages and food samples using air–assisted hydrophobic deep eutectic solvent-based dispersive liquid-liquid microextraction, Sustainable Chem. Pharm., 38 (2024) 101464. https://doi.org/10.1016/j.scp.2024.101464

[81] J. Ali, M. Tuzen, W. B. Jatoi, B. Hazer, A novel block copolymer containing gadolinium oxide nanoparticles in ultrasound assisted-dispersive solid-phase microextraction of total arsenic in human foodstuffs: A multivariate optimization methodology, Food Chem., 437 (2024) 137908. https://doi.org/10.1016/j.foodchem.2023.137908

[82] Ş. Tokalıoğlu, S. Shahir, Y. Yılmaz, Ş. Patat, Selective and fast magnetic dispersive solid phase micro-extraction of copper and lead in water and vegetables after synthesis of magnetic mesoporous carbon, Talanta, 266 (2024) 125002. https://doi.org/10.1016/j.talanta.2023.125002

[83] Ş. Tokalıoğlu, B. B. Banata, Bioaccessibility of fifteen elements from dried fruits by the BARGE (Bioaccessibility Research Group of Europe) unified bioaccessibility method (UBM) and multivariate statistical analysis, Anal. Lett., 57 (2024) 1-20. https://doi.org/10.1080/00032719.2023.2242536

[84] Ş. Tokalıoğlu, S. Shahir, E. T. Akgül, B. F. Şenkal, Dispersive solid-phase microextraction of lead in waters and edible lettuce and dill extracts in the unified bioaccessibility method (UBM) Saliva Solution, Biol. Trace Elem. Res., (2023) 1-10. https://doi.org/10.1007/s12011-023-04001-7

[85] Ş. Tokalıoğlu, S. T. H. Moghaddam, Y. Yılmaz, Ş. Patat, NiCo2O4@ZnCo2O4 nanomaterial for selective and fast dispersive solid phase micro-extraction of manganese and lead in water, tea and cinnamon samples followed by FAAS determination, Microchem. J., 195 (2024) 109515. https://doi.org/10.1016/j.microc.2023.109515

[86] S. Ray, R. Vashishth, From water to plate: Reviewing the bioaccumulation of heavy metals in fish and unraveling human health risks in the food chain, Emerg. Contam., 10

(2024)100358. https://doi.org/10.1016/j.emcon.2024.100358

[87] M. K. Abbasabadi, F. Hosseini, Nanographene oxide modified phenyl methanethiol nanomagnetic composite for rapid separation of aluminum in wastewaters, foods, and vegetable samples by microwave dispersive, Food Chem., 347 (2021) 129042. https://doi.org/10.1016/j.foodchem.2021.129042

[88] M. Osanloo, O. Q. Dadras, Nobel method for toluene removal from air based on ionic liquid modified nanographene, Int. J. Occup. Hyg., 6 (2014) 1-5. https://ijoh.tums.ac.ir/index.php/ijoh/indexing

[89] F. Golbabaei, H. Hassani, F. Eftekhar, M. J. Kian, Occupational Exposure to Mercury: Air Exposure Assessment and Biological Monitoring based on Dispersive Ionic Liquid-Liquid Microextraction, Iran. J. Public Health, 43 (2014) 793–799. https://www.ncbi.nlm.nih.gov/pmc/journals/1793/

[90] M. K. Abbasabadi, Speciation of cadmium in human blood samples based on Fe_3O_4-supported naphthalene-1-thiol- functionalized graphene oxide nanocomposite by ultrasound-assisted dispersive magnetic micro solid phase extraction, J. Pharm. Biomed. Anal., 189 (2020)113455. https://doi.org/10.1016/j.jpba.2020.113455

[91] G. Alvial-Hein, H. Mahandra, Separation and recovery of cobalt and nickel from end of life products via solvent extraction technique: A review, J. Clean. Prod., 297 (2021) 126592. https://doi.org/10.1016/j.jclepro.2021.126592

[92] N. Esmaeili, J. Rakhtshah, Ultrasound assisted-dispersive-modification solid-phase extraction using task-specific ionic liquid immobilized on multiwall carbon nanotubes for speciation and determination mercury in water samples, Microchem. J., 154 (2020) 104632. https://doi.org/10.1016/j.microc.2020.104632

[93] J. Rakhtshah, H. Shirkhanloo, N. Esmaeil, A rapid extraction of toxic styrene from water and wastewater samples based on hydroxyethyl methylimidazolium tetrafluoroborate immobilized on MWCNTs by ultra-assisted dispersive cyclic conjugation-micro-solid phase extraction Author links open overlay panel, Microchem. J., 170 (2021) 106759. https://doi.org/10.1016/j.microc.2021.106759

[94] M. Ghazaghi, H. Zavvar Mousavi, A. Rashidi, Stirring-controlled solidified floating solid-liquid drop microextraction as a new solid phase-enhanced liquid-phase microextraction method by exploiting magnetic carbon nanotube-nickel hybrid, Anal. Chim. Acta, 951 (2017) 78-88. https://doi.org/10.1016/j.aca.2016.11.034

[95] M. Trojanowicz, Impact of nanotechnology on progress of flow methods in chemical analysis: A review, Anal. Chim. Acta, 1276 (2023) 341643. https://doi.org/10.1016/j.aca.2023.341643

[96] N. Esmaeili, J. Rakhtshah, E. Kolvari, A. Rashidi, H. Shirkhanloo, Rapid Speciation of Lead in Human Blood and Urine Samples Based on MWCNTs@DMP by Dispersive Ionic Liquid-Suspension-Micro-Solid Phase Extraction, Biol. Trace Elem. Res., 199 (2021) 2496–2507. https://doi.org/10.1007/s12011-020-02382-7

[97] S. A. H. Mirzahosseini, S. A. Moussavi-Najarkola, H. Farahani, the evaluation and determination of heavy metals pollution in edible vegetables, water and soil in the south of Tehran province by GIS, Arch. Environ. Prot., 41 (2015) 63-72. https://doi.org/10.1515/aep-2015-0020

[98] S. Kopru, M. Soylak, Inductively coupled plasma-mass spectrometry (ICP-MS) detection of trace metal contents of children cosmetics, Opt. Quantum Electron., 56 (2024) 399. https://doi.org/10.1007/s11082-023-06166-w

[99] L. Jafari Foruzin, Z. Rezvani, Ultrasonication

construction of the nano-petal NiCoFe-layered double hydroxide: An excellent water oxidation electrocatalyst, Ultrason. Sonochem., 64 (2020) 104919. https://doi.org/10.1016/j.ultsonch.2019.104919

[100] Q. Salamat, M. Soylak, Magnetic covalent organic frameworks-based adsorbents in solid phase extraction of trace analytes in environmental samples, Trends Environ. Anal. Chem., 41 (2024) e00222. https://doi.org/10.1016/j.teac.2023.e00222

[101] M. Arjomandi, H. Shirkhanloo, A review: analytical methods for heavy metals determination in environment and human samples, Anal. Methods Environ. Chem. J., 2 (2019) 97-126. https://doi.org/10.24200/amecj.v2.i03.73

[102] A. F. Zarandi, P. Paydar, A novel method based on functionalized bimodal mesoporous silica nanoparticles for efficient removal of lead aerosols pollution from air by solid-liquid gas-phase extraction, J. Environ. Health Sci. Eng., 18 (2020) 177–188. https://doi.org/10.1007/s40201-020-00450-7

[103] S. Khodadoust, N. Cham Kouri, Preconcentration of Sn (II) using the methylene blue on the activated carbon and its determination by spectrophotometry method, Spectrochim, Acta A Mol. Biomol., 123 (2014) 85-88. https://doi.org/10.1016/j.saa.2013.12.058

[104] S. Teimoori, A. H. Hassani, M. Panahi, N. Mansouri, An immobilization of aminopropyl trimethoxysilane-phenanthrene carbaldehyde on graphene oxide for toluene extraction and separation in water samples, Chemosphere, 316 (2023) 137800. https://doi.org/10.1016/j.chemosphere.2023.137800

[105] E. Zolfonoun, Spectrofluorometric determination of L-tryptophan after preconcentration using MWCNTs, Anal. Methods Environ. Chem. J., 2 (2019) 43-48. https://doi.org/10.24200/amecj.v2.i01.43

[106] S. Teimoori, A. H. Hassani, M. Panahi, N. Mansouri, Rapid extraction of BTEX in water and milk samples based on functionalized MWCNTs by dispersive homogenized-micro-solid phase extraction, Food Chem., 421 (2023) 136229. https://doi.org/10.1016/j.foodchem.2023.136229

[107] S. Khodadoust, T. Nasiriani, F. Zeraatpisheh, Preparation of a magnetic molecularly imprinted polymer for the selective adsorption of chlordiazepoxide and its determination by central composite design optimized HPLC, New J. Chem., 42 (2018) 14444-14452. https://doi.org/10.1039/C8NJ02643B

[108] S. Teimoori, A. H. Hassani, New extraction of toluene from water samples based on nano-carbon structure before determination by gas chromatography, Int. J. Environ. Sci. Technol., 20 (2023) 6589–6608. https://doi.org/10.1007/s13762-023-04906-9

[109] K. I. Alabid, H. N. Nasser, H. K. Maleh, Reduction of graphene oxide by new chemical and green methods, J. Ultrafine Grained Nanostruct. Mater., 55 (2022) 172-185. https://doi.org/10.22059/jufgnsm.2022.02.09

[110] A. Choudhary, A. Kadawasara, S. S Poonia, P. kumar, V. K. Janu, Pyrolytic preparation of active carbons from peanut shell biomass for adsorptive elimination of fluoride from groundwater of Shekhawati region, Orient. J. Chem., 38 (2022) 1338-1350. http://dx.doi.org/10.13005/ojc/380602

[111] A. Zhang, X. Li, J. Xing, G. Xu, Adsorption of potentially toxic elements in water by modified biochar: A review, J. Environ. Chem. Eng., 8 (2020) 104196. https://doi.org/10.1016/j.jece.2020.104196

[112] F. Golbabaei, Z. Sadeghi, A. Vahid, A. Rashidi, On-line micro column preconcentration system based on amino bimodal mesoporous silica nanoparticles as a novel adsorbent for removal and speciation of chromium (III, VI) in environmental samples, J. Environ. Health Sic. Eng., 13 (2015) 1-12. https://doi.org/10.1186/

s40201-015-0205-z
[113] M. M. Eskandari, B. Kalantari, Dispersive liquid-liquid microextraction based on task-specific ionic liquids for determination and speciation of chromium in human blood, J. Anal. Chem., 70 (2015) 1448-1455. https://doi.org/10.1134/S1061934815120072
[114] H. Shirkhanloo, M. Ghazaghi, H. Z. Mousavi, Chromium speciation in human blood samples based on acetylcysteine by dispersive liquid-liquid biomicroextraction and in-vitro evaluation of acetylcysteine/cysteine, J. Pharm. Biomed. Anal., 118 (2016) 1-8. http://dx.doi.org/10.1016/j.jpba.2015.10.018
[115] S. Y. Al-Samarrai, Analytical method: Determination of famotidine drug using chemiluminescence method, Anal. Methods Environ. Chem. J., 7 (1) (2024) 65-75. https://doi.org/10.24200/amecj.v7.i01.320
[116] D. Kumari, Y. Alsayadib, N. A. Sharma, A review: Exploratory analysis of recent advancement in green analytical chemistry application, Anal. Methods Environ. Chem. J., 7 (2024) 86-114. https://doi.org/10.24200/amecj.v7.i01.279
[117] A. Jaber Ibrahim a, Determination and evaluation of trace elements in the blood of radiography workers using graphite furnace atomic absorption spectrometry, Anal. Methods Environ. Chem. J., 7 (2024) 76-85. https://doi.org/10.24200/amecj.v6.i04.321
[118] M. Osanloo, H. Hassani, Validation of a new and cost-effective method for mercury vapor removal based on silver nanoparticles coating on micro glassy balls, Atmos, Pollut. Res., 8 (2017) 359-365. https://doi.org/10.1016/j.apr.2016.10.004
[119] S. Swami, N. Sharma, A. Saini, A review: Captivating nanosensors for mercury detection: a promising approach for monitoring of toxic mercury in environmental samples, RSC Adv., 14 (2024) 18907-18941. https://doi.org/10.1039/D4RA02787F
[120] M. Osanloo, O. Qorban Dadrass, Using silver nanoparticles for sampling of toxic mercury vapors from industrial air sample, J. Health Safe. Work, 4 (2014) 21-30. http://jhsw.tums.ac.ir/article-1-5119-en.html
[121] F. Golbabaei, A. Vahid, A. Faghihi Zarandi, A novel nano-palladium embedded on the mesoporous silica nanoparticles for mercury vapor removal from air by the gas field separation consolidation process, Appl. Nanosci., 12 (2022) 1667-1682. https://doi.org/10.1007/s13204-022-02366-0
[122] M. Safari, S. M. Amini, M. Rashidi, Novel semisolid design based on bismuth oxide (Bi_2O_3) nanoparticles for radiation protection, Nanomed. Res. J., 2 (2017) 230-238. http://doi.org/10.22034/nmrj.2017.04.004.
[123] S. D. Ahranjani, A lead analysis based on amine-functionalized bimodal mesoporous silica nanoparticles in human biological samples by ultrasound assisted-ionic liquid trap-micro solid phase extraction, J. Pharm. Biomed. Anal., 157 (2018) 1-9. https://doi.org/10.1016/j.jpba.2018.05.004
[124] S. Davari, F. Hosseini, H. Shirkhanloo, Dispersive solid-phase microextraction based on aminefunctionalized bimodal mesoporous silica nanoparticles for separation and determination of calcium ions in chronic kidney disease, Anal. Methods Environ. Chem. J., 1 (2018) 57-66. https://doi.org/10.24200/amecj.v1.i01.37
[125] K. Merchant, M. D. Mobarake, Ultrasound-assisted solid-liquid trap phase extraction based on functionalized multi-wall carbon nNanotubes for preconcentration and separation of nickel in petrochemical waste water, J. Anal. Chem., 74 (2019) 865-876. https://doi.org/10.1134/S1061934819090090
[126] T. Mollaei, A. Rouhollahi, Improvement of photoelectrochemical water splitting performance by electrochemical synthesis of Cu-doped ZnO nanotubes decorated with silver nanoparticles, Anal. Bioanal. Electrochem., 15 (2023) 1001-1017. https://doi.org/10.22034/ABEC.2023.709116

[127] M. Manouchehri, Sh. Seidi, M. Taghi Naseri, A. Rouhollahi, Trace determination of antifungal drugs in biological fluids through a developed approach of hydrogel-based spin-column micro-solid-phase extraction followed by LC-MS/MS analysis, J. Sep. Sci., 45 (2022) 594-601. https://doi.org/10.1002/jssc.202100560

[128] A. Barabi, S. Seidi, A. Rouhollahi, M. Manouchehri, M. Shanehsaz, F. Rasouli, Electrochemically synthesized NiFe layered double hydroxide modified Cu(OH)2 needle-shaped nanoarrays: A novel sorbent for thin-film solid-phase microextraction of antifungal drugs, Anal. Chim. Acta, 1131 (2020) 90-101. https://doi.org/10.1016/j.aca.2020.07.053

[129] R. Arora, Adsorption of Heavy Metals–A Review, Mater. Today: Proc., 18 (2019) 4745-4750. https: // doi.org/ 10.1016/j.matpr.2019.07.462

[130] M. Bagheri Hosseinabadi, N. Khanjani, M.D. Mobarake, Neuropsychological effects of long-term occupational exposure to mercury among chloralkali workers, Work, 66 (2020) 491-498. https://doi.org/10.3233/WOR-203194

[131] B. Paknejad, Is there any relevance between serum heavy metal concentration and BBB leakage in multiple sclerosis patients?, Biol. Trace Elem. Res., 190 (2019) 289-294. https://doi.org/10.1007/s12011-018-1553-1

[132] A. Rouhollahi, Speciation and determination of trace amount of inorganic arsenic in water, environmental and biological samples, J. Chin. Chem. Soc., 58 (2011) 623-628. https://doi.org/10.1002/jccs.201190097

[133] E. Boschmann, Physical and chemical properties, J. Chem. Educ., 64 (1987) 891. https://doi.org/10.1021/ed064p891.1

[134] R. Gupta, H. Chauhan, Chapter 9 - Chemical and physical properties of nanoparticles and hybrid materials, Sustainable Nanotechnology for Environmental Remediation, Micro Nano Technol., (2022) 199-220. https://doi.org/10.1016/B978-0-12-824547-7.00024-2

[135] B. Dolgin, V. Bulatov, H. Hadar-Abuhatzira, Inhomogeneous complexation of trace metals in water with organic nano-complexants, Opt. Mater., 34 (2011) 391-398. https://doi.org/10.1016/j.optmat.2011.05.022

[136] E. Boschmann, G. A. Nypaver, J. P. Majors, S. M. Ealy, M. V. Horn, Synthesis and characterization of (-)-Sparteine metal salt complexes, J. Coord. Chem., 7 (2006) 141-147. https://doi.org/10.1080/00958977808073053

[137] M. Keilwerth, W. Mao, M. Malischewski, The synthesis and characterization of an iron (VII) nitrido complex, Nat. Chem., 16 (2024) 514–520. https://doi.org/10.1038/s41557-023-01418-4

[138] G. Oliva, J. R. Comia Jr, V. Senatore, T. Zarra, F. Ballestreros, V. Belgiorno, V. Naddeo, Degradation of gaseous VOCs by a novel UV-ozone technology, Sci. Rep., 12 (2022) 11112. https://doi.org/10.1038/s41598-022-14191-0

[139] K. K. Hummadi, L. Zhu, S. He, Bio-adsorption of heavy metals from aqueous solution using the ZnO-modified date pits, Sci. Rep., 13 (2023) 22779. https://doi.org/10.1038/s41598-023-50278-y

[140] E. M. Abu Elgoud, A. I. Abd-Elhamid, Sh. Emam, H. F. Aly, Selective removal of some heavy metals from Lanthanide solution by graphene oxide functionalized with sodium citrate, Sci. Rep., 12 (2022) 13755. https://doi.org/10.1038/s41598-022-17949-8

[141] V. Diniz, J. C. Bear, S. Rath, C. R. Crick, Porous sulfur polymers for effective aqueous-phase organic contaminant removal, Sci. Rep., 14 (2024) 8144. https://doi.org/10.1038/s41598-024-57856-8

[142] A. A. M. Beigi, M. Shamsipur, Biochemistry Method: Simultaneous determination of formaldehyde and methyl tert-buthyl ether in environmental and human biological matrices using static headspace gas

chromatography-mass spectrometry, Anal. Method Environ. Chem. J., 2 (2019) 33-42. https://doi.org/10.24200/amecj.v2.i01.40

[143] W. Zhang, J. Luo, T. Sun, F. Yu, C. Li, The absorption performance of ionic liquids–PEG200 complex absorbent for VOCs, Energies, 14 (2021) 3592. https://doi.org/10.3390/en14123592

[144] X. Ma, W. Wang, C. Sun, J. Sun, Comprehensive evaluation of ionic liquid [Bmim][PF6] for absorbing toluene and acetone, Environ. Pollut., 285 (2021) 117675. https://doi.org/10.1016/j.envpol.2021.117675

[145] L. Mohammadi, Adsorptive Removal of benzene and toluene from aqueous environments by cupric oxide nanoparticles: Kinetics and isotherm studies, J. Chem., 2017 (2017) 2069519. https://doi.org/10.1155/2017/2069519

[146] F. Yu, J. Ma, Magnetic iron oxide nanoparticles functionalized multi-walled carbon nanotubes for toluene, ethylbenzene and xylene removal from aqueous solution, Chemosphere, 146 (2016) 162-172. https://doi.org/10.1016/j.chemosphere.2015.12.018

[147] G. Z. Kyzas, G. McKay, T. J. Al-Musawi, S. Salehi, D. Balarak, Removal of benzene and toluene from synthetic wastewater by adsorption onto magnetic zeolitic imidazole framework nanocomposites, Nanomater., 12 (2022) 3049. https://doi.org/10.3390/nano12173049

[148] A. Bahadori, Removal of organic dye compounds in water and wastewater samples based on covalent organic frameworks-titanium dioxide before analysis by UV-VIS spectroscopy, Anal. Method Environ. Chem. J., 4 (2021) 58-67. https://doi.org/10.24200/amecj.v4.i01.131

[149] D. P. Ebecker, Total oxidation of propane with a nano-RuO_2/TiO_2 catalyst, Appl. Catal. A, 481 (2014) 11-18. https://doi.org/10.1016/j.apcata.2014.04.043

[150] l. Bandura, D. Kołodyńska, W. Franus, Adsorption of BTX from aqueous solutions by Na-P1 zeolite obtained from fly ash, Process, Saf. Environ. Prot., 109 (2017) 214-223. https://doi.org/10.1016/j.psep.2017.03.036

[151] J. Zhang, K. Vikrant, K. H. Kim, F. Dong, Photocatalytic destruction of volatile aromatic compounds by platinized titanium dioxide in relation to the relative effect of the number of methyl groups on the benzene ring, Sci. Total Environ., 822 (2022) 153605. https://doi.org/10.1016/j.scitotenv.2022.153605

[152] Q. Feng, B. Liu, J. Ji, K. Li, B. Zhang, H. Huang, Enhanced photo-degradation of gaseous toluene over MnOx/TiO2/activated carbon under a novel microwave discharge electrodeless lamps system, Appl. Surf. Sci., 547 (2021) 148955. https://doi.org/10.1016/j.apsusc.2021.148955

[153] T. Cheng, J. Li, X. Ma, L. Zhou, H. Wu, L. Yang, Alkylation modified pistachio shell-based biochar to promote the adsorption of VOCs in high humidity environment, Environ. Pollut., 295 (2022) 118714. https://doi.org/10.1016/j.envpol.2021.118714.

[154] M. Shafiei, M. S. Alivand, A. Rashidi, A. Samimi, D. Mohebbi-Kalhori, Synthesis and adsorption performance of a modified micro-mesoporous MIL-101 (Cr) for VOCs removal at ambient conditions, J. Chem. Eng., 341 (2018) 164-174. https://doi.org/10.1016/j.cej.2018.02.027

[155] S. Huang, W. Deng, L. Zhang, D. Yang, Q. Gao, Z. Tian, T. Ishihara, Adsorptive properties in toluene removal over hierarchical zeolites, Micropor. Mesopor. Mater., 302 (2020) 110204. https://doi.org/10.1016/j.micromeso.2020.110204

[156] Y. Lv, J. Sun, G. Yu, W. Wang, Z. Song, X. Zhao, Y. Mao, Hydrophobic design of adsorbent for VOC removal in humid environment and quick regeneration by microwave, Micropor. Mesopor. Mater., 294

(2020) 109869. https://doi.org/10.1016/j.micromeso.2019.109869

[157] H. Mehrizadeh, A. Niaei, H. H.Tseng, D. Salari, A. Khataee, Synthesis of $ZnFe_2O_4$ nanoparticles for photocatalytic removal of toluene from gas phase in the annular reactor, J. Photochem. Photobiol. A J., 332 (2017) 188-195. https://doi.org/10.1016/j.jphotochem.2016.08.028

[158] D. Van Thuan, N. T. Hanh, N. H. T. Vy, T. T. M. Hang, H. Van Ha, T. D. Pham, Synthesis of N and S Co-doped TiO_2 nanotubes for advanced photocatalytic degradation of VOCs in gas phase, Top Catal., 63 (2020) 1077-1085. https://doi.org/10.1007/s11244-020-01347-3

[159] N. H. M. H. Tehrani, M. S. Alivand, A. Rashidi, K. R. Shamskar, M. Samipoorgiri, M. D. Esrafili, M. Shafiei-Alavijeh, Preparation and characterization of a new waste-derived mesoporous carbon structure for ultrahigh adsorption of benzene and toluene at ambient conditions, J. Hazard. Mater., 384 (2020) 121317. https://doi.org/10.1016/j.jhazmat.2019.121317

[160] M. Saraji, N. Mehrafza, Mesoporous carbon–zirconium oxide nanocomposite derived from the carbonized metal-organic framework: A coating for solid-phase microextraction, J. Chromatogr. A, 1460 (2016) 33-39. https://doi.org/10.1016/j.chroma.2016.07.036

[161] X. Li, J. Li, Y. Shi, M. Zhang, S. Fan, Z. Yin, X. Li, Rational design of cobalt and nitrogen co-doped carbon hollow frameworks for efficient photocatalytic degradation of gaseous toluene, J. Colloid Interface Sci., 528 (2018) 45-52. https://doi.org/10.1016/j.jcis.2018.05.067

[162] L. Liu, Q. Wang, S. Ahmad, X. Yang, M. Ji, Y. Sun, Steam reforming of toluene as model biomass tar to H2-rich syngas in a DBD plasma-catalytic system, J. Energy Inst., 91 (2018) 927-939. https://doi.org/10.1016/j.joei.2017.09.003

[163] S. Chen, J. Yan, Y. Liu, C. Wang, D. Lu, Determination of Mn(II) and Mn(VII) in beverage samples using magnetic dispersive micro-solid phase extraction coupled with solidified floating organic drop microextraction followed by graphite furnace atomic absorption spectrometry, Food Chem., 359 (2021) 129958. https://doi.org/10.1016/j.foodchem.2021.129958

[164] J. Rakhtshah, H. Shirkhanloo, M. Dehghani Mobarake, Simultaneously speciation and determination of manganese (II) and (VII) ions in water, food, and vegetable samples based on immobilization of N-acetylcysteine on multi-walled carbon nanotubes, Food Chem., 389 (2022) 133124. https://doi.org/10.1016/j.food chem.2022.133124

[165] M. Tuzen, A. Elik, B. Hazer, S. Şimşek, N. Altunay, Poly(styrene)-co-2-vinylpyridine copolymer as a novel solid-phase adsorbent for determination of manganese and zinc in foods and vegetables by FAAS, Food Chem., 333 (2020) 127504. https://doi.org/10.1016/j.foodchem.2020.127504

[166] Y. Wang, S. Gao, X. Zang, J. Li, J. Ma, Graphene-based solid-phase extraction combined with flame atomic absorption spectrometry for a sensitive determination of trace amounts of lead in environmental water and vegetable samples, Anal. Chim. Acta, 716 (2012) 112-118. https://doi.org/10.1016/j.aca.2011.12.007

[167] M. Tuzena, M. Soylak, Speciation of Mn(II), Mn(VII) and total manganese in water and food samples by coprecipitation–atomic absorption spectrometry combination Demirhan Citaka, J. Hazard. Mater., 173 (2010) 773–777. https://doi.org/10.1016/j.jhazmat.2009.09.004

[168] H. Shirkhanloo, A. Khaligh, H. Zavvar Mousavi, A. M. Rashidi, Ultrasound assisted-dispersive-micro-solid phase extraction based on bulky amino bimodal mesoporous silica nanoparticles for speciation of trace manganese (II)/(VII)

ions in water samples, Microchem. J., 124 (2016) 637–645. https://doi.org/10.1016/j.microc.2015.10.008

[169] M. Ghazaghi, A. M. Rashidi, Ultrasound-assisted dispersive solid phase extraction of cadmium (II) and lead (II) using a hybrid nanoadsorbent composed of graphene and the zeolite clinoptilolite, Microchim. Acta, 182 (2015) 1263-1272. https://doi.org/10.1007/s00604-015-1446-3

[170] M. Falahnejad, H. Z. Mousavi, A. Rashidi, Preconcentration and separation of ultra-trace amounts of lead using ultrasound-assisted cloud point-micro solid phase extraction based on amine functionalized silica aerogel nanoadsorbent, Microchem. J., 125 (2016) 236-241. https://doi.org/10.1016/j.microc.2015.11.026

[171] B. Tışlı, T. Unutkan Gösterişli, B. Tuğba Zaman, E. Gülhan Bakırdere, S. Bakırdere, Determination of manganese in coffee and wastewater using deep eutectic solvent based extraction and flame atomic absorption spectrometry, Anal. Lett., 54 (2020) 1-11. https://doi.org/10.1080/00032719.2020.1789871

[172] H. Abdolmohammad-Zadeh, G. H. Sadeghi, Combination of ionic liquid-based dispersive liquid–liquid micro-extraction with stopped-flow spectrofluorometry for the pre-concentration and determination of aluminum in natural waters, fruit juice and food samples, Talanta, 81 (2010) 778-85. https://doi.org/10.1016/j.talanta.2010.01.012

[173] I. Narin, M. Tuzen, M. Soylak, Aluminium determination in environmental samples by graphite furnace atomic absorption spectrometry after solid phase extraction on Amberlite XAD-1180/pyrocatechol violet chelating resin, Talanta, 63 (2004) 411-8. https://doi.org/10.1016/j.talanta.2003.11.005

Anal. Methods Environ. Chem. J. 7 (3) (2024) 83-98

AMECJ

Research Article, Issue 3
Analytical Methods in Environmental Chemistry Journal
Journal home page: www.amecj.com/ir

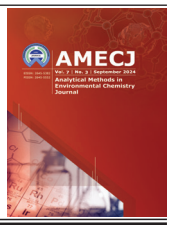

A novel approach to simultaneously determine elements in seawater using total reflection X-ray fluorescence spectroscopy

Aleksandr Kozhevnikov[*,a], Dmitry Lakhmanov[a], Emil Pobliahin[a], Evgenia Zholobova[a], and Alexey Malkov[a]
[a]*Core Facility Center, Arktika, Northern (Arctic) Federal University, 163002 Arkhangelsk, Russia*

ARTICLE INFO:
Received 19 May 2024
Revised form 20 Jul 2024
Accepted 18 Aug 2024
Available online 30 Sep 2024

Keywords:
Trace elements,
Total reflection X-ray fluorescence spectroscopy,
Diethyldithiocarbamate,
Seawater,
Extraction and back-extraction,
Arctic pollution

ABSTRACT
We have applied the modern total reflection X-ray fluorescence spectroscopy (TXRF) method to simultaneously determine the number of elements in seawater. However, seawater contains a large number of salts, so it negatively affects the detection limit of elements and requires a preliminary separation procedure based on liquid-liquid microextraction (LLE) with diethyldithiocarbamate ($NaS_2CN(C2H5)_2$) as a chelating agent, and tetrachloromethane as an extractant. We have studied the effect of pH on the separation of elements and proposed an additional stage of sample preparation and mercury stabilization in solution using sodium diethyldithiocarbamate. The calibration curves for 12 elements (V, Cr, Fe, Co, Ni, Cu, Zn, Se, Cd, Hg, Pb, Bi) were obtained. The detection limit of trace elements for Hg, Pb, Zn, Cr, and Cd was achieved from 0.1 to 7 g L^{-1}. The preconcentration factors for selenium (Se) and zinc (Zn) were obtained at 4.25 and 25.1, respectively (recovery more than 95%). This approach has been successfully applied to estimate the content of elements in the seawater of the Arctic region, demonstrating its practical applicability. Metals such as Fe, Zn, Pb, Ni, Cu, Cr, and V were found in seawater samples with RSD below 5%. We found that the concentrations of Cu, Ni, Zn, and Pb correlate with each other and do not correlate with the content of Fe, Cr, and V. The study found that the concentrations of trace elements in seawater are below their maximum permissible concentrations.

1. Introduction

Seawater contains many elements, including those that migrate there due to anthropogenic activity. Information about the distribution of these elements is important for geochemistry and ecology. The first publications on metal distribution in seawater were released in the 1950s of the last centuries, and this topic is still relevant [1]. For example, in 2021, about 200 articles on this topic were published [2, 3]. The studies carried out in hard-to-reach places of our planet, such as the Arctic seas, are especially interesting [4]. The trace elements (heavy metals) content in seawater is relatively low and usually does not exceed 100 µg L^{-1}. The content of elements depends on many factors, such as depth, currents, etc. For example, in the East Sea (Japan Sea), the Mn concentrations in the surface layer (0–50 m) ranged from 0.1 to 0.4 µg L^{-1}, and the Co concentrations ranged from 2.5 to 7.0 ng L^{-1}. The Cu concentrations were higher in the surface layer, from 0.09 to 0.22 µg L^{-1}.

*Corresponding Author: Aleksandr Kozhevnikov
Email: akozhevnikov@mail.ru
https://doi.org/10.24200/amecj.v7.i03.318

The concentrations of Cd and Ni were 9–31 ng L^{-1} and 0.11–0.20 μg L^{-1}, respectively [5]. Compared to the background values, the increase in trace element concentrations may indicate anthropogenic pollution. Seawater pollution has a direct negative impact on marine organisms and the ecosystem in general [6]. Trace elements are distinguished by their high toxicity to living organisms in relatively low concentrations and their ability to bioaccumulate and bio-magnify. Almost all heavy metals are involved in biological processes and are part of many enzymes. The most toxic metals include mercury, cadmium, and lead [7]. The most significant threat is the pollution of water by mercury. Mercury has specific properties, such as affinity for sulfur-containing compounds, the ability to form stable methylated compounds, and reducing to metal from these compounds. These factors determine the high migration mobility of mercury in the biosphere and its volatility and toxicity to most living organisms. The interaction of inorganic mercury compounds with benthic microorganisms produces water-soluble, high-toxic organomercury compounds, including methylmercury. Mercury and methylmercury are also found in Laptev Sea surface sediments [8]. Aluminum, arsenic, cadmium, chromium, copper, lead, nickel, and silver are toxic metals that migrate into the marine environment via natural processes and anthropogenic impacts [9]. The determination of all these elements in seawater has its difficulties. On the one hand, the concentrations of metals found in water are deficient. On the other hand, seawater contains many salts, and various organic substances in the water. As a result, the analytical methods are to meet such requirements as high sensitivity (low detection limit) and high selectivity. During the monitoring studies, methods of analysis that allow simultaneous measurement of the content of several heavy metals in the sample are preferable. The atomic absorption spectroscopy method is traditionally used to determine heavy metals in seawater (cold vapor method for determining mercury and electrothermal atomization method for other metals). The methods of atomic emission spectroscopy and mass spectrometry with inductively coupled plasma are also widely used [10]. ICP MS method has the best characteristics and allows achieving detection limits for most heavy metals at 0.01 μg L^{-1} [11]. However, the problem of eliminating matrix effects in analyzing seawater using these methods remains unresolved. The high salts in the sample lead to contamination of the internal communications of the devices and the need for frequent maintenance of the equipment to avoid its quick failure. In addition, the cost of analysis is high because of the complexity of the equipment and the use of a significant amount of expensive consumables (high-purity argon, graphite cuvettes, etc.). The total reflection X-ray fluorescence spectroscopy (TXRF) method might be an alternative to the abovementioned methods [12]. The TXRF method is based on the analysis of the fluorescence spectrum of a sample, usually liquid, that is deposited on a flat substrate (sample holder). The method allows multi-element analysis, also characterized by high selectivity and a wide dynamic range (5...6 orders of magnitude). An essential advantage of the method is the equipment's low power consumption and compactness, so it is possible to analyze the samples in a mobile laboratory near the sampling site [13]. The expensive consumables are not necessary for the analysis. These advantages make it promising to use the TXRF to determine the content of trace elements in natural waters and seawater. Direct analysis of seawater by the TXRF method allows for the determination of the content of elements in concentrations of not less than 0.1 mg L^{-1}, but such sensitivity does not meet the requirements for microelement analysis [14]. Preliminary separation of seawater makes it possible to eliminate the salt matrix and increase the concentration of analytes to determine trace amounts of elements. Such methods as adsorption, electrochemical precipitation, solid-phase extraction, and chromatographic separation of chelate complexes are used for separation and preconcentration [15–22]. We used microextraction preconcentration in the form of diethyldithiocarbamate complexes to determine Ni, Co, Cu, Cd, and Pb. At the first stage of extraction preconcentration, metal complexes are extracted from

water into tetrachloromethane; at the second stage (back-extraction), they are destroyed, and the metals pass into nitric acid [23]. Diethyldithiocarbamate can bond with various metals, and this property has been used in analytical chemistry for a long time [24]. This work aims to improve the methodology of determining heavy metals, including mercury, in seawater using the TXRF method and its application to assess the distribution of some aspects in the Arctic seas. To achieve this purpose, we need to determine the conditions of mercury complexation in seawater samples and to study the pH influence on the separation of mercury ions and other elements during sample preparation. Also, we should calibrate elements in seawater and test the proposed approach on actual seawater samples. Finally, we need to assess the content of elements and the correlation of their concentrations in the waters of the Arctic seas.

2. Material and methods

2.1. The object of the study

We used surface water samples from the Kara, Laptev, and East Siberian Sea as the research objects. The samples were obtained during the 2020 expedition on the vessel (Akademik Mstislav Keldysh; AMK 86) during the work on the International Program for the Study of the Siberian Shelf (ISSS). The samples were filtered and preserved by acidification with nitric acid to pH 1-2 immediately after sampling. The program Arc Gis © 10.4.1 for desktop was used for visualization.

2.2. Equipment and reagents

We used a total reflection X-ray fluorescence spectrometer S2 Picofox (Bruker, Germany) in a modification with a high-efficiency module and automatic sample loading to determine the content of heavy metals. The source of exciting radiation was an X-ray tube with a Mo anode equipped with a multilayer Ni/C monochromator (energy 17.5 keV). The maximum power of the X-ray tube was 37 W (50 kV, 750 μA). The detector is a Si drift detector (area of 30 mm^2) with thermoelectric cooling. The maximum counting rate is over 100000 pulses per second, and the energy resolution is <150 eV on the Mn Kα line. sodium N, N-diethyldithiocarbamate (Na-DEDTC) (CAS Number:20624-25-3), and HNO_3 (CAS Number: 7697-37-2) purchased from Sigma, Germany. Tetrachloromethane (Sigma, CAS Number: 56-23-5) was used as a reagent.

2.3. Preparation of solutions

Pre-purified 1% solution of sodium N, N-diethyldithiocarbamate (Na-DEDTC), and the acetate buffer solution with a pH of 3.2-6.3 were used to obtain metal complexes. Diethyldithiocarbamate solution was purified by threefold extraction (25 mL solution with 2.5 mL tetrachloromethane) [10]. The buffer solution was prepared by dissolving ammonium acetate (PA ACS, Panreac) in deionized water and adding glacial acetic acid to a defined pH. pH control was carried out by the pH meter (Econix-Expert 001; Russia) with a combined glass electrode. Solutions with pH 6.3; 5.9; 5.4; 5.0; 4.8; 4.4; 4.3; 4.0; 3.6; 3.2 and an ionic strength 4 mol L^{-1} were obtained. We added 1 mL of 1% dithiocarbamate solution to 100 mL of buffer and extracted it three times with 5 mL of tetrachloromethane for purification. Standard solutions were prepared using the state standard reference samples of metals, and diluting aliquots were selected using micropipettes in volumetric flasks with deionized water. The Simplicity UV water purification system obtained deionized water with an 18.2 M /cm resistance (Millipore, France). For stability, standard solutions were acidified with HNO_3 purists, spectroscopy, grade, and refined by sub-boiling distillation at the DST-1000 system (Savillex, USA). Calibration solutions contained NaCl (35 g L^{-1}) and the specified amounts of metals for seawater modeling. The initial NaCl solution with a concentration of 70 g L^{-1} was previously purified using the same method as the buffer solution. We used Ga solution for ICP (Panreac, Reference standards acc. NIST SRM 3119a) with a concentration of 1.000 ± 0.002 g L^{-1} as an internal standard to establish the precise concentration of calibration solutions. Tetrachloromethane "for spectroscopy" grade was used to extract metal complexes without additional purification.

2.4. Sample preparation

Extraction was performed in polypropylene microcentrifuge test tubes with a volume of 1.5 mL. In the two test tubes, 1200 µL of samples were mixed with 100 µL of acetate buffer and 50 µL of sodium diethyldithiocarbamate solution. 100 µL of tetrachloromethane was added into the test tube, and extraction was carried out for 5 minutes by shaking on the IKA MS3 digital vortex at the frequency of 1500 rpm. We separated the resulting emulsion by centrifugation for 2 minutes on the IKA mini G centrifuge. 80 µL of the lower organic layer (extract) was taken from each test tube and transferred to the 0.2 mL microcentrifuge test tube; 5 µL of HNO_3 was added and shaken again for 5 min. At that point, metal complexes disintegrate and pass into nitric acid (re-extraction). After adding 45 µL of deionized water and stirring, the sample was centrifuged again. Then 25 µL of the re-extract (the top layer in the test tube) was transferred to another test tube of the same volume and mixed with 25 µL of manganese solution (500 µg L^{-1}, internal standard) and 4 µL of sodium diethyldithiocarbamate (mercury stabilizer). 10 µL of the resulting solution was placed in quartz glass sample holders by micropipette and dried on a heating panel with a surface temperature of 65 ± 1 ° C for 300 ± 5 seconds or in a vacuum desiccator for 20 minutes. Thus, the sample preparation included the following stages, shown in the diagram (Fig. 1). At stage 1 of the process (extraction), the concentration of elements should increase 12 times. At stage 2 of the process (re-extraction), the concentration of elements should increase by 3.2 times. Thus, the overall theoretical preconcentration factor should be 38.4. We performed from 4 to 6 parallel measurements for each solution. The blank sample (deionized water that has passed all stages of sample preparation, including acidification) was analyzed ten times.

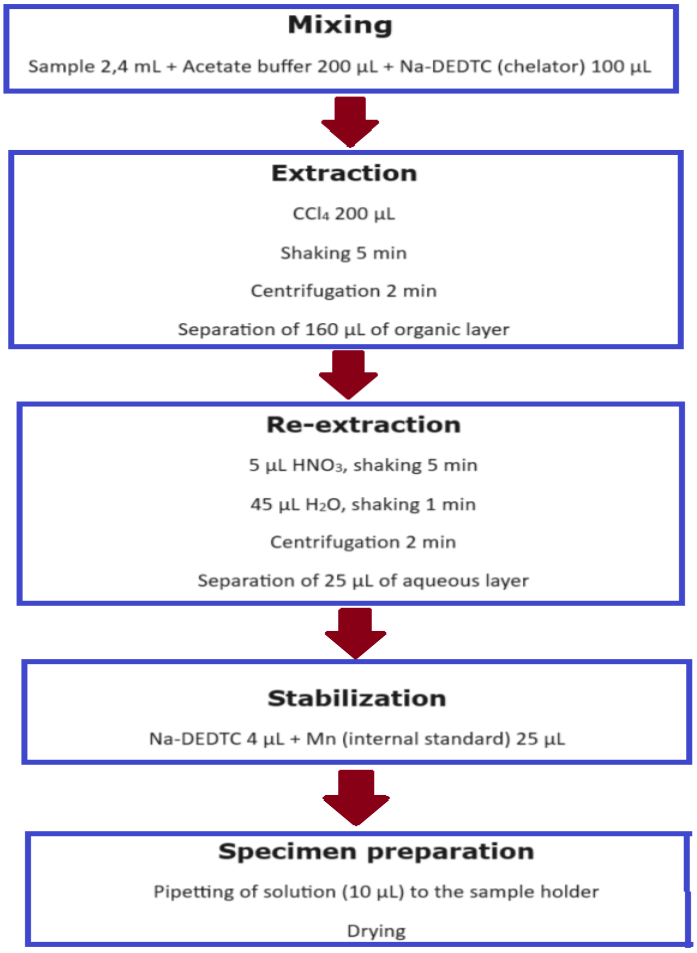

Fig. 1. Scheme of sample preparation

2.5. Determination of metal concentrations.

The TXRF spectra were registered using a Mo Kα (17.5 keV) X-ray source, working at 50 kV and 600 μA with an acquisition time of 1200s. Then, the resulting spectrum was automatically processed with the spectrometer software (Spectra 7, Bruker) using the Profile Bayes (regular fit) deconvolution mode. Element concentrations in the prepared sample were calculated using the internal standard method. The blank sample analysis result was subtracted from the obtained value. We calculated the metal concentrations in the initial sample according to the calibration and the dependence of the metal concentration in the re-extraction on its measured concentration in the initial solution. Twelve solutions of metals with different concentrations were used to carry out the calibration. We added NaCl to the calibration solutions to model the composition of seawater; its final concentration was 35 g L^{-1}. Using the Grubbs criterion [25], we excluded anomalous results from the obtained data and calculated the average value.

3. Results and discussion

3.1. Mercury stabilization in solution

We used extraction of heavy metal complexes with organic solvents to separate them from seawater with subsequent determination by various methods. Mercury, along with other heavy metals, can react with dithiocarbamates. We used sodium diethyldithiocarbamate (Na-DEDTC) as a complexing agent. Determining metals by the TXRF method directly in the extract is difficult because of the uneven distribution of the sample on the sample holder and the necessity to inject the internal standard into the organic phase. These difficulties can be eliminated by including the stage of re-extraction - the destruction of complexes under the action of acid and the transfer of metals into the aqueous layer. However, during back-extraction, mercury passes into a mobile form and can be lost while the sample is drying on the sample holder. Thus, stabilization of mercury compounds in the re-extraction is required, so we used a repeated addition of a complexing agent for this purpose. The method of drying the aliquot of the sample pipetted to the sample holder may also affect the result of the mercury determination. Drying can occur in a vacuum desiccator or on a temperature-controlled heating surface. We used 65 °C. We experimentally determined the sample drying method and the required volume of Na-DEDTC for subsequent analysis. For this purpose, we analyzed a standard mercury solution with a 500 μg L^{-1} concentration. The concentration of added Na-DEDTC varied from 0.03 to 0.10 %. The results are presented in Table 1. Without using Na-DEDTC, regardless of the drying method, we observed an almost complete loss of mercury, which was unacceptable during the analysis. The table shows that the best results are obtained if sodium diethyldithiocarbamate with a concentration of 0.07 % is used, regardless of the drying method. The measured mercury concentration during drying in a vacuum desiccator is slightly lower than when the sample holder is heated to 65 ° C due to the more extended contact of the sample with acid during vacuum drying (20 min and 5 min, respectively). Thus, we have proposed the original approach to eliminating the problem of mercury losses. For this purpose, sodium diethyldithiocarbamate must be added to the re-extract after the destruction of the complexes with nitric acid to hold mercury in the sample.

Table 1. Measured concentrations of mercury ions depending on the drying method and stabilizer (Na-DEDTC) concentration

Na-DEDTC concentration	Vacuum drying		Drying at 65°C	
	Concentration (μg L^{-1})	Recovery (%)	Concentration (μg L^{-1})	Recovery (%)
0	13	2.6	15	3.0
0.03	339	67.8	464	92.8
0.05	361	72.2	458	91.6
0.07	413	82.6	488	97.6
0.10	389	77.8	489	97.8

3.2. The pH effect on the extraction of the metal

The pH of the solution affects the completeness of elements bonding into chelate complexes and has its optimal value for each metal. In the case of group separation of metals, the best pH will be the one that allows extracting the most significant number of elements. We treated a standard solution containing 13 elements using buffer solutions with a pH in the range of 3.2 to 6.3 at the first stage. Metal concentrations in re-extract were determined in reference to the gallium standard solution and added at the last analysis stage. We did not take into account the content of elements in the blank sample in this experiment. Table 2 and Figure 2 show the results of two independent measurements for each pH value. According to the presented data, we can conclude that in the studied pH range, the concentration in the re-extract, in comparison with the initial solution, increases for all studied elements except manganese and arsenic. At the same time, the degree of extraction of various metals at fixed pH is different and is always significantly lower than 100%. Non-quantitative extraction of elements from the sample leads to the necessity of determining the concentration of each element according to the calibration. Our task was determining the pH that would provide the most complete extraction of mercury ions from the solution. Figure 2 shows the dependence of mercury concentration in the re-extraction on the pH. Mercury ions are most effectively extracted from the standard solution at a pH equal to 5.0. At pH = 5.0, in addition to mercury, other elements such as V, Cr (VI), Fe, Co, Ni, Cu, Zn, Se, Cd, Pb, and Bi were effectively concentrated.

Table 2. Element concentrations (μg L^{-1}) in re-extract at different pH of the buffer solution

pH	V	Cr	Mn	Fe	Co	Ni	Cu	Zn	As	Cd	Hg	Pb	Bi
6.3	283	98	40	365	281	299	258	567	10.4	304	49	378	297
	294	97	38	366	287	304	268	581	7.7	296	54	381	306
5.9	432	131	27	521	425	446	393	763	8.7	465	84	579	472
	431	139	28	527	435	448	393	766	6.1	445	108	585	469
5.4	386	128	8.4	518	414	438	384	772	11.8	308	178	557	471
	390	137	9.5	541	428	441	387	776	12.1	363	126	567	466
5.0	500	167	3.5	766	627	683	571	1116	15.9	608	181	832	644
	481	168	4.0	760	612	672	552	1091	12.5	572	136	795	626
4.8	378	159	2.3	735	623	673	515	943	5.5	477	170	865	629
	376	154	4.7	741	614	671	511	931	7.2	453	135	854	624
4.4	309	176	0.0	750	620	678	566	676	6.9	763	158	939	636
	338	135	6.6	823	652	717	601	719	3.3	659	141	1011	681
4.3	198	158	0.0	651	497	578	463	361	7.3	710	91	929	515
	212	159	0.0	657	511	592	481	382	6.9	645	104	973	551
4.0	99	106	0.0	451	364	466	367	62	6.7	200	66	758	351
	92	104	0.0	443	361	454	356	59	7.4	254	67	753	356
3.6	83	65	1.9	373	237	317	248	30	7.1	24	42	848	274
	76	64	2.0	374	229	309	242	27	5.6	22	39	833	270
3.2	77	56	2.5	118	274	358	547	49	3.5	0.0	124	3.4	707
	70	59	2.5	133	281	371	559	50	3.0	0.0	150	4.0	730

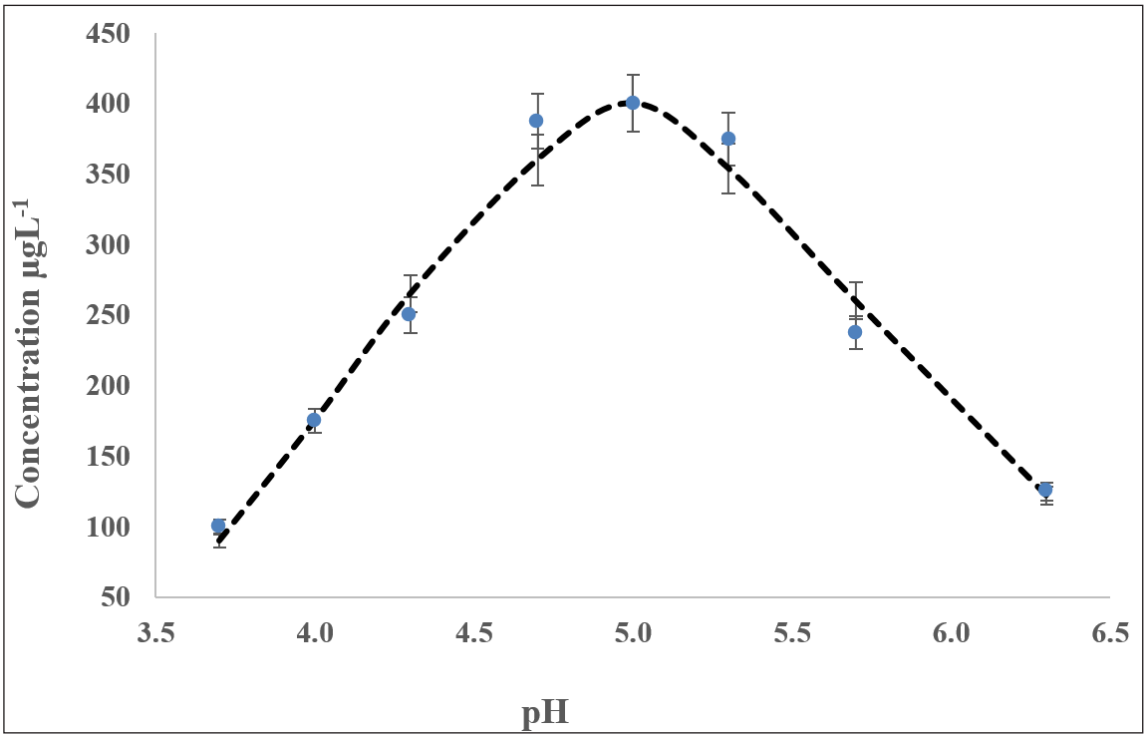

Fig. 2. Dependence of mercury concentration on the pH of buffer solution.

3.3. Calibrations obtaining

We obtained calibrations for 12 different elements, taking into account the influence of seawater's salt matrix. Given the low concentrations of elements in seawater, calibration data is necessary to determine accurately their concentrations. The concentrations are low because the object of study is seawater from the Arctic region, which is little subject to anthropogenic influence. We analyzed multi-element standard solutions with various concentrations to obtain calibrations for each metal. The concentration range was from 1 to 400 µg L^{-1} for mercury and approximately 2 to 1000 µg L^{-1} for lead, and other elements [26]. While performing the analysis, we used previously selected pH and stabilizer concentration (Na-DEDTC). We performed six parallel measurements for each calibration solution per the abovementioned procedure. We used 12 multi-element calibration solutions; 8 of them had approximately equal concentrations of all elements, covering the entire range of concentrations under study. In addition, for each element, we used two solutions with low concentration (10 µg L^{-1}) at the average concentration of the remaining elements (100 µg L^{-1}) and two solutions with high concentration (1000 µg L^{-1}) at the average concentration of the remaining elements (100 µg L^{-1}). We chose the lowest value based on the possibility of directly determining the concentration of these elements using a spectrometer. The solubility of chelate complexes in tetrachloromethane limits the maximum concentration. We previously measured the exact concentration of calibration solutions obtained by mixing mono-element standards (State standard reference samples of metals) in reference to the standard gallium solution. Figure 3 represents the example of the X-ray fluorescence spectrum of one of the standard solutions. We considered the calibrations obtained for all elements as linear, described by the equation $y=ax+b$. Parameter a is the enrichment factor. The deviation of parameter b from zero observed for some elements is explained by calibration inaccuracy. We also calculated the correlation coefficient R^2, and its values are more than 0.8, indicating the obtained equations' correctness (Table 3). Table 3 also shows the maximum permissible concentrations for the elements under study [27]. The lower detection limit was calculated based on the standard deviation

of the background signal under the element line, according to Equation 1.

$$LOD_i = \frac{3 \cdot \sigma_{Bg\,i}^{rel} \cdot C_{IS}}{S_{IS}^{rel} \cdot K_i} \quad \text{(Eq.1)}$$

LOD_i: lower limit of detection of element i, µg L^{-1}

$\sigma_{Bg\,i}^{rel}$: The standard deviation of the relative background intensity under the analytical line of element i.

C_{IS} : Internal standard concentration (500 µg L-1 Mn).

S_{IS}^{rel} : The sensitivity coefficient of element i is normalized by the sensitivity coefficient of the internal standard.

K_i : Enrichment factor of element i.

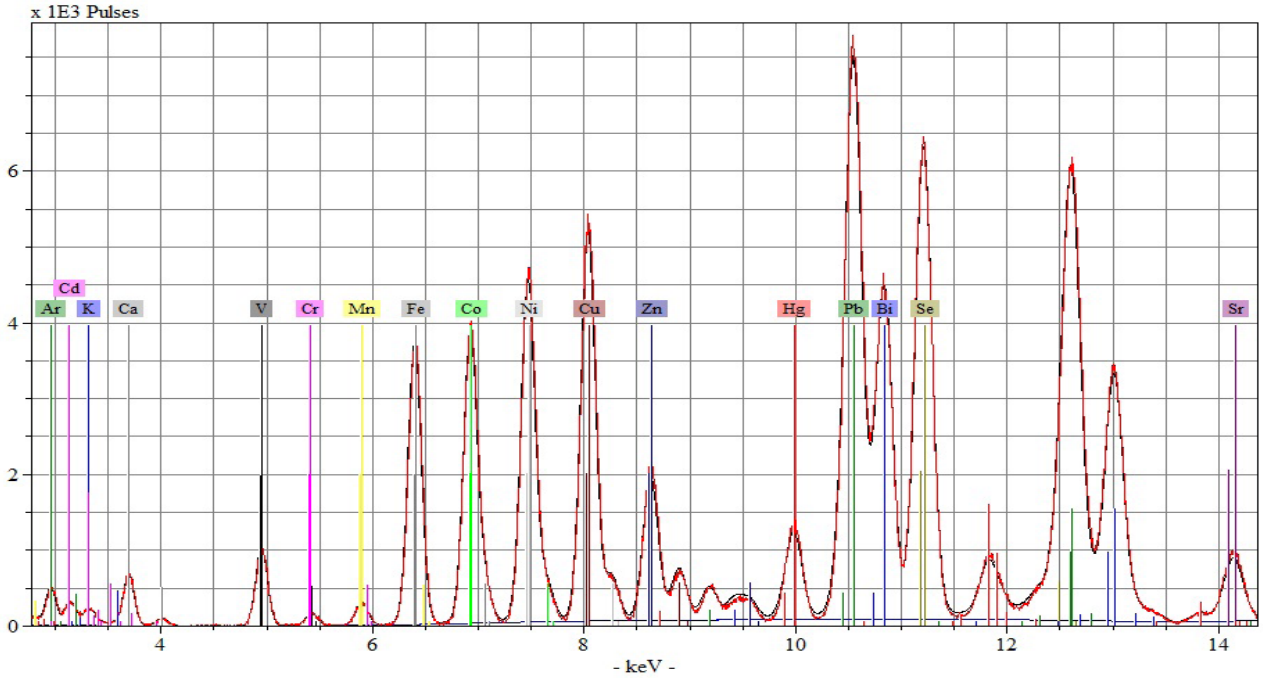

Fig. 3. X-ray fluorescence spectrum of the standard solution with a concentration of 500 µg L^{-1}; internal standards: 500 µg L^{-1} Mn and 500 µg L^{-1} Sr.

Table 3. The concentration range and parameters of calibrations of elements are determined

Element	Conc. range (µg L^{-1})	a	b	R^2	LOD (µg L^{-1})	MPC (µg L^{-1})
V	2.0-1000	5.25	0.16	0.89	1.0	1
Cr (VI)	1.5-1100	14.12	-0.99	0.99	0.1	20
Fe	15.0-1100	10.42	1.24	0.83	0.7	50
Co	2.0-1050	10.13	0.77	0.85	0.6	5
Ni	2.0-1100	10.57	0.54	0.81	0.4	10
Cu	2.0-1000	12.67	0.21	0.84	0.3	5
Zn	1.5-1100	25.10	-4.87	0.96	0.1	50
Se	1.5-1100	4.27	-2.89	0.99	0.6	1.6
Cd	1.5-1050	18.53	0.50	0.99	7.0	10
Hg	1.0-400	11.81	0.94	0.80	0.1	0.1
Pb	2.5-1200	19.68	1.12	0.93	0.1	10
Bi	2.0-1000	10.77	-0.50	0.86	0.3	100

a: Slope of linear calibration (observed enrichment factor);
b: Intercept of linear calibration;
MPC: Maximum permissible concentration of the element

Figures 4a (for Pb, Zn, Cd, Cr), 4b (for V, Fe, Co, Se), and 4c (for Ni, Cu, Hg, Bi) show the calibration for all elements and lead. Table 3 represents the parameters of metal calibrations. The technique was validated using the "add-found" method. The seawater sample was analyzed, mixed with a standard metal solution, and analyzed again. The obtained results are shown in Table 4.

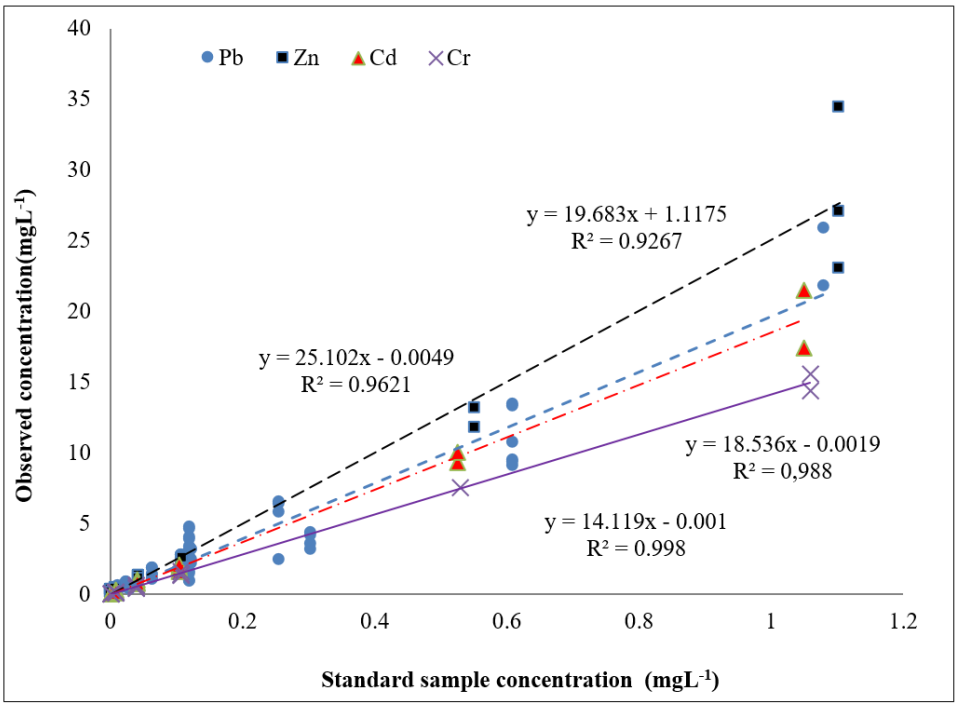

Fig. 4a. Calibration for different elements (Pb, Zn, Cd, Cr)

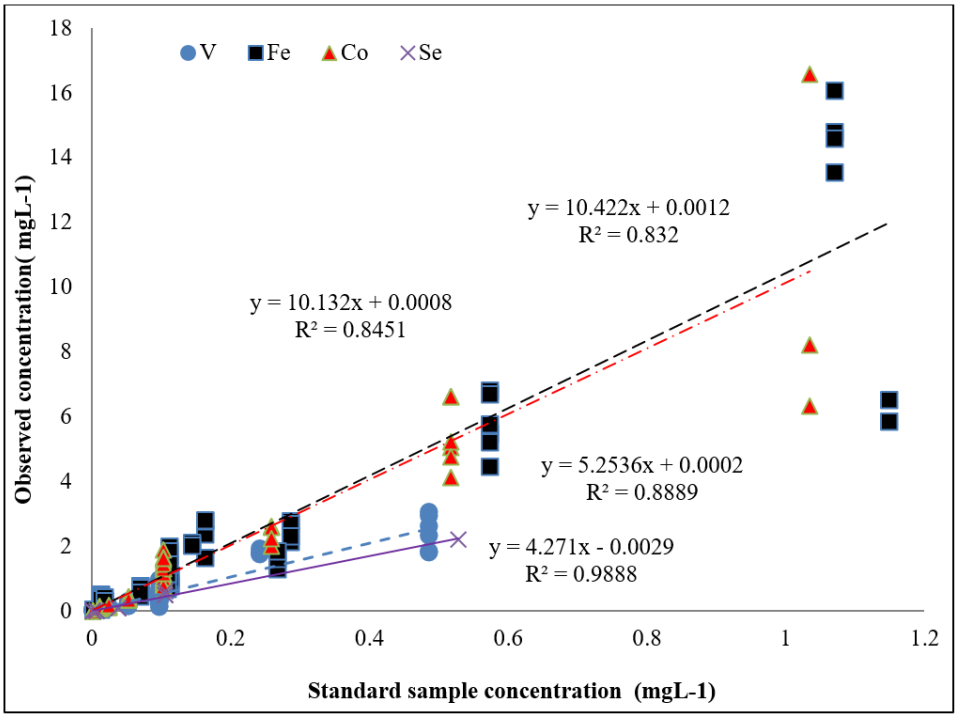

Fig. 4b. Calibration for different elements (V, Fe, Co, Se)

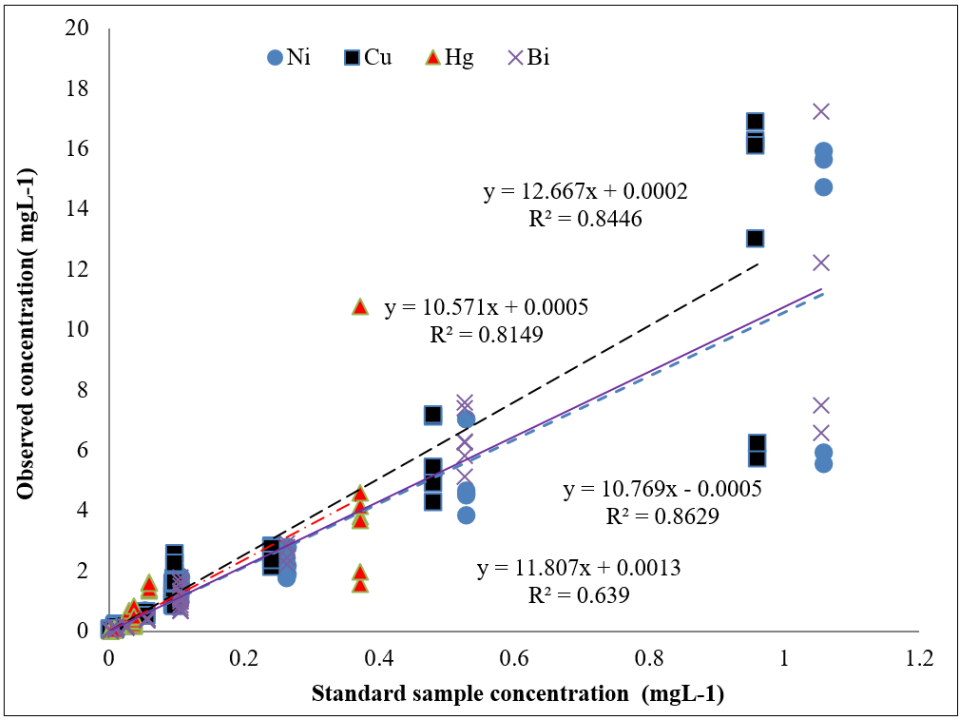

Fig. 4c. Calibration for different elements (Ni, Cu, Hg, Bi)

Table 4. Results of method validation for metal determination by procedure

Element	Add Standard (µg L^{-1})	Found sample (µg L^{-1})	Found standard (µg L^{-1})	Recovery (%)
V	----	4.60	----	----
	2.50	6.71	2.11	85
Cr (VI)	----	0.11	----	----
	0.20	0.32	0.22	105
Fe	----	8.2	----	----
	20.0	29.0	20.8	104
Co	----	----	----	----
Ni	----	2.82	----	----
	5.0	7.22	4.4	88
Cu	----	33.4	----	----
	100.0	129.4	95.9	96
Zn	----	29.8	----	----
	100.0	115.8	86.0	86
Se	----	----	----	----
Cd	----	----	----	----
Hg	----	----	----	----
Pb	----	4.99	----	----
	10.0	14.50	48.1	95
Bi	----	----	----	----

3.4. Investigation of the content of elements in samples of seawater of the Arctic region

We used this approach to determine the element's content in Arctic seawater. For this purpose, 39 samples of seawater were obtained during the expedition work on the research vessel "Academik Mstislav Keldysh" AMK-86 in 2020 as part of an international marine expedition. The International Siberian Shelf Study (ISSS) Program is a Russian-Swedish-led international collaboration. Seawater samples were taken in different seas with different salinity and trace element content. The obtained results are presented in Table 5.

Table 5. The results of the determination of elements in the seawater of the Arctic region*

C (μg L^{-1})	V	Cr (VI)	Fe	Ni	Cu	Zn	Pb
Sw20_1	3.86	----	5.80	3.88	18.04	11.42	1.33
Sw20_2	4.42	----	17.91	5.42	13.33	18.79	1.62
Sw20_3	4.09	----	17.50	13.55	208.11	98.13	8.77
Sw20_4	4.60	0.11	8.20	2.82	33.44	29.81	4.99
Sw20_5	2.28	----	65.50	9.37	55.08	247.72	67.86
Sw20_6	1.96	0.58	13.11	2.09	11.88	11.71	0.64
Sw20_7	3.16	----	11.52	3.57	43.00	38.50	3.34
Sw20_8	2.74	----	37.22	1.43	3.97	5.60	0.39
Sw20_9	1.83	0.31	41.81	1.10	1.84	3.36	0.28
Sw20_10	3.34	0.19	4.80	0.59	0.69	1.85	1.36
Sw20_11	3.64	0.03	5.40	0.69	0.84	8.41	0.33
Sw20_12	3.39	0.24	10.00	1.38	2.37	16.81	0.92
Sw20_13	2.17	0.30	15.40	0.77	1.61	2.13	0.17
Sw20_14	2.43	0.11	7.30	1.29	0.93	7.97	0.26
Sw20_15	2.34	-	29.40	0.62	1.57	9.71	0.33
Sw20_16	2.07	0.21	8.00	0.85	0.94	2.31	0.55
Sw20_17	2.25	----	19.80	1.31	1.25	2.00	0.09
Sw20_18	1.92	----	7.40	1.15	2.26	7.99	0.55
Sw20_19	1.73	0.12	22.20	1.01	1.08	2.91	0.39
Sw20_20	1.54	----	92.20	1.05	0.77	13.46	0.09
Sw20_21	3.02	1.17	709.50	1.99	3.96	10.38	0.38
Sw20_22	1.04	0.38	298.30	1.11	1.40	5.63	0.17
Sw20_23	1.15	0.17	7.60	1.30	2.72	1.18	0.21
Sw20_24	0.26	0.10	131.80	0.55	3.41	17.57	0.20
Sw20_25	1.00	----	45.60	1.05	1.13	6.54	----
Sw20_26	2.36	0.13	11.90	1.36	1.03	2.36	0.20
Sw20_27	2.33	0.57	239.10	1.34	1.50	3.56	0.31
Sw20_28	2.95	0.16	64.80	0.65	1.16	1.77	0.61
Sw20_29	2.62	0.40	32.20	1.31	1.30	0.33	----
Sw20_30	1.75	----	31.10	1.27	0.89	1.70	0.17
Sw20_31	1.31	----	88.00	0.84	1.20	2.22	0.04
Sw20_32	2.32	0.23	123.70	0.95	1.13	5.12	----
Sw20_33	3.74	0.40	27.90	0.83	1.19	6.50	0.26
Sw20_34	3.02	0.41	----	1.37	1.46	13.39	0.18
Sw20_35	3.02	0.09	53.30	0.78	0.72	10.51	----
Sw20_36	5.09	0.04	0.20	0.37	1.80	27.02	0.14
Sw20_37	4.19	0.34	28.90	0.37	1.43	4.20	0.14
Sw20_38	2.52	0.10	36.20	0.58	2.21	10.00	0.35
Sw20_39	1.79	----	61.00	0.47	0.65	3.27	0.29

- below the limit of quantitative detection

*Co, Se, Cd, Hg, and Bi not detected

The approach allowed us to determine the content of the following elements: V, Cr(VI), Fe, Ni, Cu, Zn, Pb, Co, Se, Cd, Hg, Bi. The advantage of the proposed approach is the simultaneous determination of 12 elements, including mercury, with a simple separation procedure to eliminate the interfering influence of the salt matrix. During the study, we used the previously established parameters of sample preparation and determination of elements by calibrations. We used a blank sample (deionized water that has passed all stages of sample preparation, including acidification) to consider the presence of element impurities in the used reagents. In addition to determining trace elements in the samples, we determined the dissolved oxygen and pH of the seawater at the moment of sampling in the vast majority of cases. The Data visualization is in Figure 5. Based on the data visualization, we can conclude that the content of the studied elements in seawater is low, and most are below the detection limit. We have revealed no dependence of the element's concentration in seawater on currents or river runoff. The average concentrations (μg L^{-1}) for V, Cr (VI), Fe, Ni, Cu, Zn, and Pb are 40.0, 2.87, 843, 13.6, 18.8, 98.5, and 2.64, respectively. However, the average concentration value is not used correctly because of the abnormally high values of metals at specific points. It is more accurate to use the median values of concentrations, which were 2.39, 0.21, 28.9, 1.11, 1.46, 6.54, 0.33 μg L^{-1} for V, Cr (VI), Fe, Ni, Cu, Zn, Pb, respectively. We also conducted a correlation analysis (Table 6) of the element content. We observed correlations for pairs of elements: Cr—Fe, Ni—Cu; Ni—Zn; Ni—Pb; Zn—Cu; Zn—Pb; Pb—Cu. We also found the correlation between dissolved oxygen and pH, as well as correlations between V—pb and Ni—O_2. The concentration of vanadium does not correlate with the concentrations of other found elements. Iron correlates only with chromium and with no other elements. Similarly, chromium correlates only with iron. The content of copper, zinc, nickel, and lead correlates with each other. Thus, vanadium, iron, and the group (Cu, Ni, Zn, Pb) come from different sources. A group of elements (Cu, Ni, Zn, Pb) have similar geochemical characteristics and probably come from the same source. The presented methodology allows us to estimate the levels of seawater pollution in reference to environmental standards. The study found that the concentrations of trace elements in seawater are below the MPC.

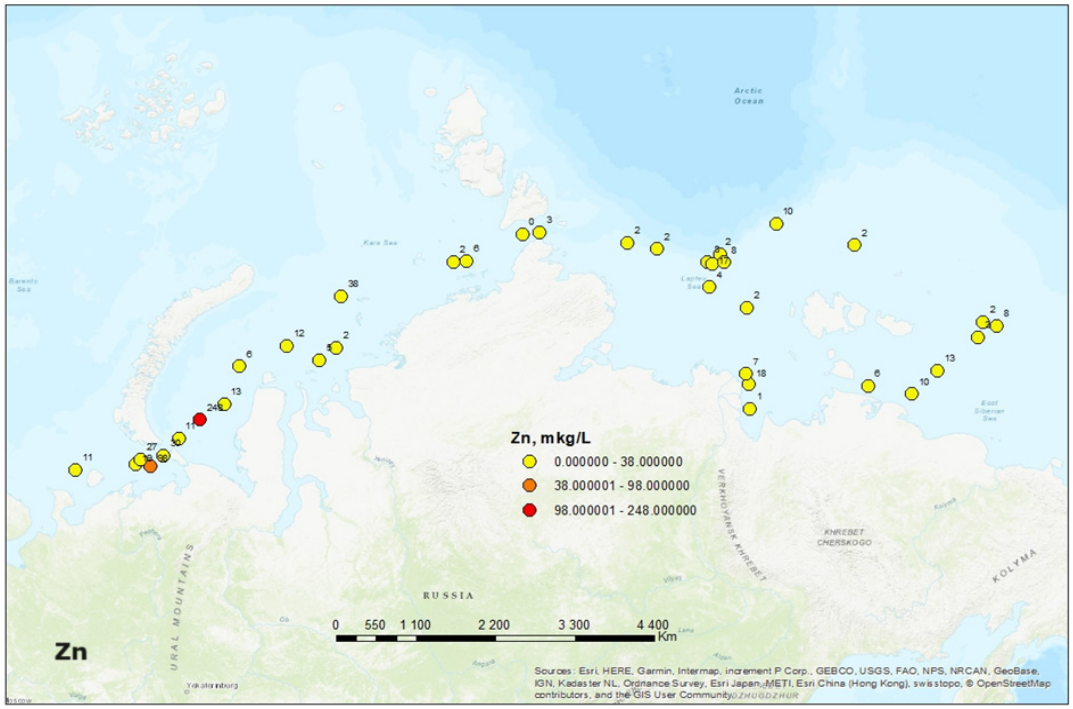

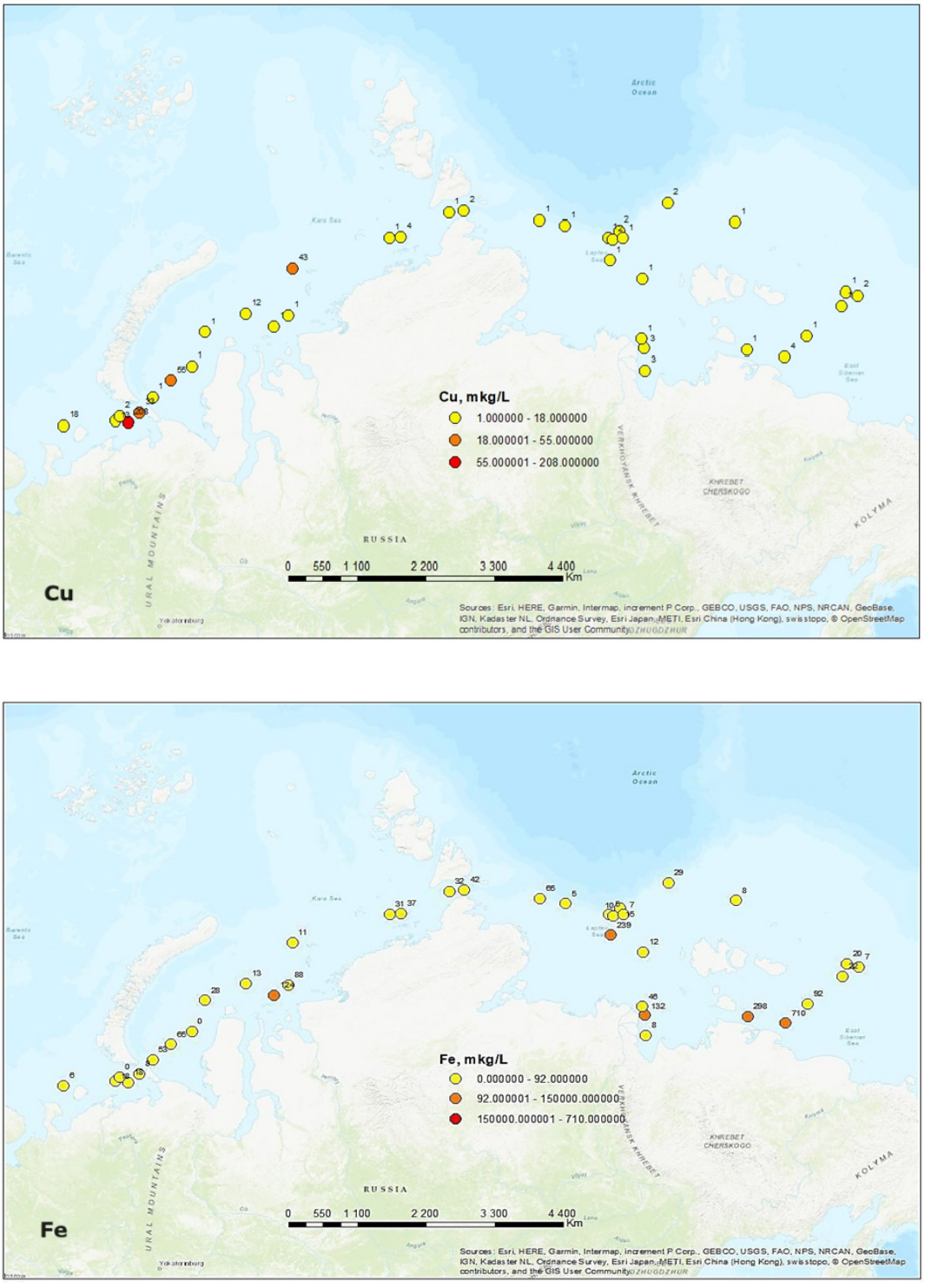

Fig. 5. The distribution of Fe, Cu, and Zn in the seawater of the Arctic seas

Table 6. Pearson correlations between elements, dissolved oxygen, and pH

	V	Cr	Fe	Ni	Cu	Zn	Pb	pH	O_2
V	1								
Cr	0.061	1							
Fe	0.028	0.772**	1						
Ni	0.393*	0.152	0.033	1					
Cu	0.415*	0.173	0.083	0.931**	1				
Zn	0.150	0.180	0.014	0.781**	0.553**	1			
Pb	0.065	0.151	0.013	0.612**	0.328	0.963**	1		
pH	0.639**	0.202	0.291	0.367	0.288	0.255	0.219	1	
O_2	0.354	0.013	0.035	0.565**	0.458*	0.417*	0.355	0.635**	1

*. The correlation is significant at the 0.05 level (two-tailed).

4. Conclusion

We found that during sample preparation for mercury bonding in seawater, an additive of sodium diethyldithiocarbamate with a concentration of 0.07 % is required after re-extraction. The optimal pH for the most complete extraction of mercury ions is equal to 5. We also obtained individual calibrations for 12 trace elements. Concentration ranges and lower limits of detection have been determined. We have determined the concentrations of elements in the seawater of the Arctic Seas and calculated the median values of concentrations. The presented methodology allows us to estimate the levels of seawater pollution in reference to environmental standards. The study found that the concentrations of trace elements in seawater are below the MPC. We found correlations between the content of certain elements, pH, and dissolved oxygen content.

5. Acknowledgements

This research was performed using instrumentation at the Core Facility Center "Arktika" of the Northern (Arctic) Federal University. It was supported by the Ministry of Science and Higher Education of the Russian Federation (state assignment project No. 0793-2020-0007). The authors have no relevant financial or non-financial interests to disclose.

6. References

[1] K.B. Krauskopf, Factors controlling the concentrations of thirteen rare metals in sea-water, Geochim. Cosmochim. Acta, 9 (1956) 1-32. https://doi.org/10.1016/0016-7037(56)90055-2

[2] S. Piarulli, B.H. Hansen, T. Ciesielski, A.L. Zocher, A. Malzahn, P.A. Olsvik, J. Farkas, Sources, distribution and effects of rare earth elements in the marine environment: Current knowledge and research gaps, Environ. Pollut., 291 (2021) 118230. https://doi.org/10.1016/j.envpol.2021.118230

[3] V. Sattarova, K. Aksentov, A. Alatortsev, R. Shakirov, M. Ivanov, A. Legkodimov, Distribution and contamination assessment of trace metals in surface sediments of the South China Sea, Vietnam, Marine Pollut. Bull., 173 (2021) 113045. https://doi.org/10.1016/j.marpolbul.2021.113045

[4] V. Sattarova, K. Aksentov, A. Astakhov, X. Shi, L. Hu, A. Alatortsev, E. Yaroshchuk, Trace metals in surface sediments from the Laptev and East Siberian Seas: Levels, enrichment, contamination assessment, and sources, Marine Pollut. Bull., 173 (2021) 112997. https://doi.org/10.1016/j.marpolbul.2021.112998

[5] H. Seo, G. Kim, T. Kim, I. Kim, K. Ra, H. Jeong, Trace elements (Fe, Mn, Co, Cu, Cd, and Ni) in the East Sea (Japan Sea): Distributions, boundary inputs, and scavenging processes, Marine Chem., 239 (2022) 104070. https://doi.org/10.1016/j.marchem.2021.104070

[6] A. Botté, C. Seguin, J. Nahrgang, M. Zaidi, J. Guery, V. Leignel, Lead in the marine

environment: concentrations and effects on invertebrates, Ecotoxicol., 31 (2022) 194-207. https://doi.org/10.1007/s10646-021-02504-4

[7] A.R. de Matos, M.C. da Silva Faria, B.M. Freire, R.M. Pereira, B.L. Batista, J.L. Rodrigues, Determination of 14 trace elements in blood, serum and urine after environmental disaster in the Doce River basin: Relationship between mining waste and metal concentration in the population, J. Trace Elem. Med. Biol., 70 (2022) 126920. https://doi.org/10.1016/j.jtemb.2021.126920

[8] V. Liem-Nguyen, B. Wild, O. Gustafsson, I. Semiletov, O. Dudarev, S. Jonsson, Spatial patterns and distributional controls of total and methylated mercury of the Lena River in the Laptev Sea sediments, Marine Chem., 238 (2022) 104052. https://doi.org/10.1016/j.marchem.2021.104052

[9] P. de Almeida Rodrigues, R.G. Ferrari, L.S. Kato, R.A. Hauser-Davis, C.A. Conte-Junior, A systematic review on metal dynamics and marine toxicity risk assessment using crustaceans as bioindicators, Biol. Trace Elem. Res., 200 (2022) 881-903. https://doi.org/10.1007/s12011-021-02685-3

[10] K. Grasshoff, K. Kremling, M. Ehrhardt, Methods of seawater analysis, 3rd. ed., Weinheim; New York; Chiester; Brisbane; Singapore; Toronto: Wiley-VCH, 602 pages, 2007. https://doi.org/10.1002/9783527613984

[11] S.F.J. Vegueria, J.M. Godoy, R. Calixto de Campos, R.A. Goncalves, Trace element determination in seawater by ICP-MS using online, offline and bath procedures of preconcentration and matrix elimination, Microchem. J., 106 (2013) 121-128. https://doi.org/10.1016/j.microc.2012.05.032

[12] A. Von Bohlen, R. Klockenkämper, Total-reflection X-ray fluorescence analysis and related methods, Wiley, New York, 2015. https://doi.org/10.1002/9781118985953

[13] M. Mages, S. Woelfl, M.J. Óvári, The use of a portable total reflection X-ray fluorescence spectrometer for field investigation, Spectrochim. Acta B, 58 (2003) 2129-2138. https://doi.org/10.1016/S0584-8547(03)00197-6

[14] V.B. Yadav, S.K. Jha, Status of trace and toxic elements pollution in creek ecosystem using TXRF method, J. Radioanal. Nucl. Chem., 295 (2013) 1759-1762. https://doi.org/10.1007/s10967-012-2095-1

[15] I.N.I. Aretaki, N.G. Kallithrakas-Kontos, Total reflection X-ray fluorescence selenium analysis after reduction and quartz reflector adsorption, J. Anal. Atom. Spect., 24 (2009) 979-982. https://doi.org/10.1039/b900962k.

[16] H. Shirkhanloo, M.K. Abbasabadi, F. Hosseini, A.F. Zarandi, Nanographene oxide modified phenyl methanethiolnanomagnetic composite for rapid separation of aluminum in wastewaters, foods, and vegetable samples by microwave dispersive magnetic micro solid-phase extraction, Food Chem., 347 (2021) 129042. https://doi.org/10.1016/j.foodchem.2021.129042

[17] A. Faghihi-Zarandi, H. Shirkhanloo, C. Jamshidzadeh, A new method for removal of hazardous toluene vapor from air based on ionic liquid-phase adsorbent, Int. J. Environ. Sci. Technol., 16 (2019) 2797–2808. https://doi.org/10.1007/s13762-018-1975-5

[18] J. Rakhtshah, H. Shirkhanloo, M.D. Mobarake, Simultaneously speciation and determination of manganese (II) and (VII) ions in water, food, and vegetable samples based on immobilization of N-acetylcysteine on multi-walled carbon nanotubes, Food Chem., 389 (2022) 133124. https://doi.org/10.1016/j.foodchem.2022.133124

[19] N. Esmaeili, J. Rakhtshah, E. Kolvari, H. Shirkhanloo, Ultrasound assisted-dispersive-modification solid-phase extraction using task-specific ionic liquid immobilized on multiwall carbon nanotubes for speciation and determination mercury in water samples, Microchem. J., 154 (2020) 104632. https://doi.org/10.1016/j.microc.2020.104632

[20] A. Ritschel, P. Wobrauschek, E. Chinea, F. Grass, C. Fabjan, An electrochemical enrichment procedure for the determination of heavy metals by total-reflection X-ray fluorescence spectroscopy, Spectrochim. Acta B, 54 (1999) 1449-1454. https://doi.org/10.1016/S0584-8547(99)00070-1

[21] B. Staniszewski, P. Freimann, A solid phase extraction procedure for the simultaneous determination of total inorganic arsenic and trace metals in seawater: Sample preparation for total-reflection X-ray fluorescence, Spectrochim. Acta B, 63 (2008) 1333-1337. https://doi.org/ 10.1016/j.sab.2008.08.018

[22] P. Freimann, D. Schmidt, Application of total reflection X-ray fluorescence analysis for the determination of trace metals in the North Sea, Spectrochim. Acta B, 44 (1989) 505-510. https://doi.org/10.1016/0584-8547(89)80057-6

[23] A.V. Malkov, A.Y. Kozhevnikov, D.S. Kosyakov, A.E. Kosheleva, Determination of Ni, Co, and Cu in seawater by total external reflection X-ray fluorescence spectrometry, J. Anal. Chem., 72 (2017) 608-616. https://doi.org/10.1134/S1061934817060107

[24] T. Kuroha, S. Shibuya, Determination of trace metals by fluorescent x-ray spectrometry with solvent extraction thin film method, Bunseki Kagaku, 17 (1968) 801-805. https://doi.org/10.2116/bunsekikagaku.17.801

[25] V.A. Dementiev, V.A. Statistical Methods in Analytical Chemistry. In: V.P. Kolotov, N.S. Bezaeva, (eds) Advances in Geochemistry, Analytical Chemistry, and Planetary Sciences. Springer, 2023. https://doi.org/10.1007/978-3-031-09883-3_37

[26] MM Eskandari, Cloud point assisted dispersive ionic liquid-liquid microextraction for chromium speciation in human blood samples based on isopropyl 2-[(isopropoxycarbothiolyl) disulfanyl ethane thioate, Anal. Chem. Res., 10 (2016) 18-27. https://doi.org/10.1016/j.ancr.2016.10.002

[27] Maximum Permissible Concentrations (MPC) of Chemical Substances in the Water of Water Objects for Household and Drinking and Cultural and Household Water Use, GN 2.1.5.1315-03, 2003. http://www.dioxin.ru/doc/gn2.1.5.1315-03.htm [in Russian]

Anal. Methods Environ. Chem. J. 7 (3) (2024) 99-112

AMECJ

Research Article, Issue 3
Analytical Methods in Environmental Chemistry Journal
Journal home page: www.amecj.com/ir

Simultaneous transmittance and fluorescence excitation-emission matrix spectroscopy coupled to multivariate analysis for the determination of Galaxolide in surface water samples

Thomas Ingwani[a], Nhamo Chaukura[b,*], Bhekie B. Mamba[a], Thabo T.I. Nkambule[a], and Adam M. Gilmore[a,c]

[a]*Institute for Nanotechnology and Water Sustainability, College of Engineering, Science and Technology, University of South Africa, Johannesburg,1709, South Africa*

[b]*Department of Physical and Earth Sciences, Sol Plaatje University, Kimberley, 8300, South Africa*

[c]*Horiba Instruments Incorporated, Piscataway, New Jersey, 08854, USA.*

ARTICLE INFO:

Received 26 May 2024
Revised form 30 Jul 2024
Accepted 27 Aug 2024
Available online 29 Sep 2024

Keywords:
Fluorescence excitation-emission matrices spectroscopy,
Absorbance-transmittance spectroscopy,
Galaxolide,
Surface water,
Multivariate analysis,
Analytical method

ABSTRACT

Recently, emerging micropollutants have gained significant attention from researchers and the general public due to their expanding distribution in the environment and mostly unknown effects on human and environmental health. To detect and quantify Galaxolide (HHCB) in surface water, we used simultaneous absorbance-transmittance and fluorescence excitation-emission matrices (A-TEEM) spectroscopy in conjunction with partial least squares (PLS) and parallel factor (PARAFAC) analyses. The fluorescence spectra of surface water samples laced with HHCB standard solutions were obtained using an A-TEEM spectrometer. The PARAFAC analysis of the fluorescence spectra revealed four fluorescent organic matter components; among them, the HHCB spiked into the samples. Regression analysis of the measured versus predicted concentrations showed a high correlation coefficient of calibration (0.966), high Pearson r value (0.999), good root mean square of prediction error divided by the standard deviation (1.715), and a low ratio of range error (14.286). The results of the A-TEEM-PLS technique under optimized and validated conditions were as follows: a low limit of detection (LLOD:4.01×10^{-8} M), a reasonably wide working range (WWR: 1.16 × 10^{-8} - 1.16 ×10^{-6} M), a narrow mean relative standard deviation (MRSD: 0.198 %), and a high recovery (R: 101%). These findings demonstrate the importance of using the straightforward and effective A-TEEM-PLS method to detect and monitor this ubiquitous environmental material in aquatic systems.

1. Introduction

Galaxolide, hexahydro-4,6,6,7,8, hexamethyl cyclopenta[g]benzopyran (HHCB), is a synthetic polycyclic musk that is used as a fragrance component in an assortment of personal care products, including cosmetics, perfumes, shampoos, detergents, lotions, fabric softeners, and cleaning agents (Fig.1). Because of its extensive usage in personal care products, HHCB is commonly found in aquatic systems [1,2]. The chemical structure of HHCB renders it recalcitrant to hydrolysis under environmental conditions; hence, it will persist in aquatic systems. Given that HHCB is toxic to marine life and humans, studies into its prevalence, toxicity, characterization, and treatment have recently attracted considerable attention [3,4]. Human exposure pathways include

*Corresponding Author: Nhamo Chaukura
Email: nhamo.chaukura@spu.ac.za
https://doi.org/10.24200/amecj.v7.i03.322

the skin, lungs, and gastrointestinal tract. Due to the capacity to interfere with hormonal function in humans [5,6], HHCB has been assigned a moderate risk to human health. Many ailments related to metabolism, behavior, reproduction, and development are linked to hormone disruption. Consequently, the U.S. Environmental Protection Agency (EPA) classified HHCB as a high-priority substance [7,8]. Therefore, extracting, characterizing, and removing HHCB from environmental water sources is crucial. Therefore, simple, reasonably priced techniques are crucial for identifying HHCB in aquatic settings. The occurrence of HHCB has been reported in various aquatics systems worldwide. For example, surface waters in Canada, Sweden, the USA, Korea, China, and Austria have high HHCB concentrations of as high as 1.017×10^{-7} M [9-11]. In South Africa, water samples from Gauteng, the North West, and Mpumalanga Provinces had high HHCB concentrations (1.361×10^{-5} M) [12,6]. With the aid of a light beam, electrons of certain compounds are excited and, upon relaxation, release light in the process of fluorescence [13,14]. Fluorometry, or fluorescence spectroscopy, is an instrumental method of analyzing the light emitted. For HHCB determination, an aqueous solution containing HHCB is scanned on a simultaneous absorbance-transmittance and excitation-emission matrices (A-TEEM) spectrometer. By concurrently acquiring the three-dimensional (3-D) excitation-emission matrices and the absorbance spectra, the effects of inner filters are removed, allowing for accurate interpretation of the data [15] and minimization of variations resulting from sample conditions or geometry [16]. The fluorescence spectral data are then interpreted using chemometric algorithms, for example, partial least squares (PLS), extreme gradient boosting (XGB), artificial neural networks, and parallel factor (PARAFAC) analyses. The versatility of the A-TEEM method, in conjunction with multi-way analysis, allows the examination of various organic materials. Hence, this method presents a water quality monitoring tool that is quick, nearly real-time, sensitive, user-friendly, cost-effective, reagent-free, and extraction-free [17]. A-TEEM spectroscopy has been used in several analyses, including the characterization of aromatic petroleum hydrocarbons or oils, polycyclic aromatic hydrocarbons [18], dyes [19], monitoring micropollutants [17] membrane integrity [20], and monitoring extracellular polymeric materials [21]. Multivariate analysis provides a more thorough analysis of the data by examining every potential independent variable and how they might relate to each other. This, consequently, assists in making decisions about procedures, forecasting future results, and fixing errors. The cause-and-effect relationships between variables can be determined, and large data sets can be analyzed. The main analytical techniques for the analysis of HHCB include high-performance liquid chromatography (HPLC) and gas chromatography in tandem with mass spectrometry (GC/MS) [22-24]. This is after sample treatment using solid-phase microextraction [24] and photolytic breakdown [25]. Some of the benefits of GC/MS over alternative techniques include high separation efficiency, identification of isomers, instrument accessibility, reproducibility, sensitivity, robustness, low cost, and ease of use [26-28]. Herein, A-TEEM-PARAFAC and A-TEEM-PLS techniques for identifying and quantifying HHCB in surface water samples, respectively, at trace levels were developed, optimized, and validated for analyzing surface water samples laced with HHCB following some International Conference on Harmonization [29], United States Pharmacopeia [30], and American Society for Testing and Materials [31], recommendations and meeting requirements for acceptance. The EEM data acquired using the A-TEEM were analyzed using optimized three-way PARAFAC and PLS models. The qualitative analysis model for HHCB and fluorophores in surface water was established using PARAFAC modeling. Then, the categorization of fluorophores in HHCB-spiked surface water was performed based on previous studies. The model for quantitative analysis of HHCB was developed by applying PLS modeling, and then the concentration of HHCB in the validation sets was determined. Excellent and relevant statistical results were obtained to quantify HHCB in surface water.

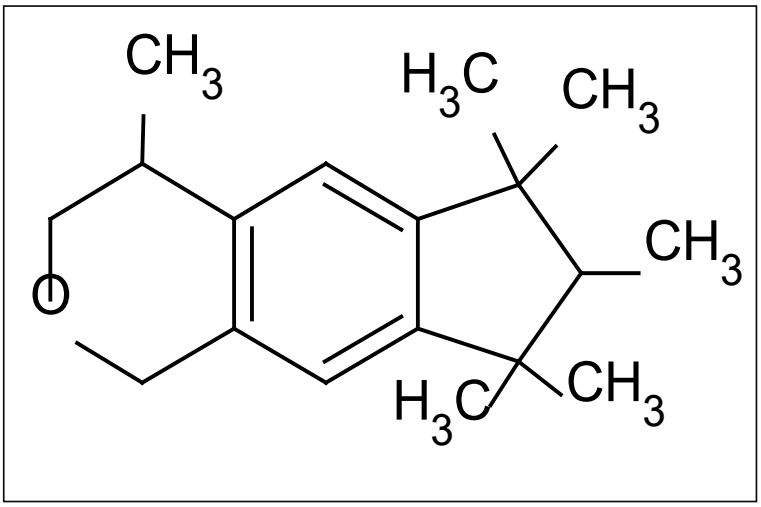

Fig. 1. Galaxolide chemical structure

2. Experimental

2.1. Materials and reagents

Analytical grade (AG) of methanol (CAS Number: 67-56-1) and HHCB (CAS Number: 1222-05-5) with a purity grade of 99%, and 0.45 micron glass microfiber (GMF) filters were purchased from Sigma-Aldrich® (Johannesburg, South Africa). Deionized water was produced using an Elix Integral 10 filter for water from Merck Millipore (South Africa).

2.2. Sampling

The Florida stream in Johannesburg, Gauteng, South Africa (26.1739° S, 27.8971° E) was the source of grab water samples taken on January 31, 2023, in one liter of clean amber glass bottles [32]. The samples were then kept at 4°C before being spiked with HHCB, and their fluorescence characteristics were examined. Subsequently, the samples were allowed to warm to room temperature, filtered through 0.45 micron GMF filters, and spiked with known concentrations of HHCB.

2.3. Preparation of a stock solution and an intermediate standard solution

A 100 mL volumetric flask containing 0.102 g of 99% pure HHCB was weighed using a Mettler Toledo analytical balance (Greifensee, Switzerland). This was dissolved in methanol and then topped to the mark to produce a 3.87×10^{-3} M stock solution. In a 100 mL volumetric flask, 0.1 mL of the stock solution was diluted to the mark with AG methanol to give a 3.87×10^{-6} M intermediate standard solution.

2.4. General procedure

2.4.1. Titration method for calibration

Aliquots of filtered surface water samples and intermediate HHCB standard solutions were placed in the same quartz cuvette to obtain 100 calibration standards with concentrations within the 1.16×10^{-8} to 1.16×10^{-6} M range and 20 validation samples with HHCB concentrations within the 5.8 10^{-8} to 1.16×10^{-6} M range. On completion, the cuvette had a total volume of 4000 µL. After that, the cuvette was vigorously shaken to homogenize the sample. To rule out the possibility of methanol altering the solution's refractive index or creating a luminous background, less than 2% of the final methanol concentration in the cuvette was maintained [33].

2.4.2. Instrumental and software

Absorbance spectra and EEM data were collected from surface water samples that had been spiked with HHCB-standard solutions and samples that had not, using the Aqualog® spectrometer (HORIBA Yobin Yvon model UV-800C, New Jersey, USA). The instrument was set at a fixed optical slit width of 5 nm, emission wavelengths between 245.21 and 827.32 nm separated by 8 pixels (4.66 nm),

and excitation wavelengths between 200 and 800 nm separated by 5 nm. Data from the EEM were gathered using the sample queue technique, and the EEM spectra were used as fluorescent signatures.

2.4.3. PARAFAC modeling

The 120 EEM dataset was modeled using PARAFAC via Eigenvector Solo software (version 8.7). Inner filter effects, primary and secondary Raman scatter, and artifactual first- and second-order Rayleigh scatter were all corrected using customized spectrometer software functions [34]. For EEM filtering, the first-order Rayleigh filter was set to 16 nm and the second-order Rayleigh filter to 32 nm. The default Raman shift of 3382 cm^{-1} and a filter half-width of 16 nm were used to eliminate Raman scattering. The Ex/Em 350/396.5 nm 2D-spectrum of a sealed water-Raman cuvette was measured and used to normalize the corrected EEM into Raman units. The bandwidth was adjusted to avoid fluorescence peaks crossing over or getting too close to the Rayleigh or Raman scatter. A PARAFAC model must be fitted with the correct number of components for the chemical interpretation to be valid. Models with one to five components were validated using split-half analysis, spectral loadings, the core consistency diagnostic, and the percent captured variance.

2.4.4. PLS modeling

A calibration model was built using 100 EEM spectra from the calibration set, and a validation model was tested using 20 EEM spectra. This allowed for the analysis of the concentration of HHCB validation samples. Eigenvector Solo software suite version 8.6 was used to perform the PLS analysis program for model building and validation. PLS modeling compared the variables in the EEM data to variables in the HHCB concentration. When using the Solo software suite, the PLS workflow has three primary phases: (1) *EEM data importation*: Mean-centering is used to preprocess the data after they have been imported. Beginning with the one with the most minor partial correlation with the EEM data variable, each HHCB concentration variable is gradually removed from the equation. The process is terminated when none of the equation's variables satisfies the elimination requirements. In this work, latent variables (LVs) were chosen; (2) *EEM data splitting*: A total of 120 EEM data points were manually divided into two datasets: a validation dataset (20 data points) and a calibration dataset (100 data points); and (3) *Iterations*: Cross-validation is repeated until the lowest root mean square error for cross-validation (RMSECV) and highest R^2 values are obtained. A preprocessing step was not performed on the spectral (X-block) calibration dataset. After mean-centering and autoscaling [35], the concentration calibration (Y-block) data were preprocessed. The calibration, cross-validation, and prediction correlation coefficients were used to assess the efficacy of the regression model. Based on the parameters of the generated error matrix, the data were classified using the strict ($p > 0.5$) and most likely rules of the total number of positive identifications. The quality of the model was assessed by evaluating several PLS model performance parameters derived from PLS analyses of the EEM data from surface water samples spiked with HHCB standard solutions at concentrations ranging from 1.16×10^{-8} to 1.16×10^{-6} M. The parameters included the number of LVs, the slope of the calibration curve, the correlation coefficients for calibration (R^2 Cal), cross-validation (R^2 CV), and prediction (R^2 Pred), bias in the calibration and prediction processes, and root mean square errors for calibration (RMSEC), prediction (RMSEP), and RMSECV.

2.5. Validation of spiked samples

Origin version 8.6 was used to regress further the data obtained from the PLS analysis of the validation samples. A regular residual versus the HHCB concentration plot and a predicted and measured HHCB concentration plot were generated. The regression parameters were generated using the predicted and measured HHCB concentration plot, and they were then combined with other goodness-of-fit parameters to create a linear regression report. The regression parameters included slope, standard

error of the slope, intercept, and adj. R^2, Pearson r value, residual sum of squares, and intercept standard error. Plotting the regular residual against the HHCB concentration provides the residual distribution. The statistical parameters for the degrees of freedom, sum of squares, mean squares, F-value, and Prob > F or p-value were obtained in an ANOVA table. The F value was used to determine the statistical significance of the analysis at p-value (Prob > F). The relationship between the predicted and measured HHCB concentration variables was determined by calculating the p-value (Prob > F value), which was used to evaluate the null hypothesis, which claims that there is no relationship between any of the measured or predicted HHCB concentrations [36].

2.5.1.Limits of quantitation and detection

Based on the slope and intercept of the calibration curve as well as the intercept standard error, the limits of detection (LOD) and limits of quantitation (LOQ) of HHCB were calculated and showed in Equations 1 and Equations 2, respectively [33]. Table 1 of the report on linear regression analysis contains the appropriate linear regression parameters used to compute the LOD and LOQ.

$$LOD = 3 \times \frac{Standard\ error\ of\ intercept + Intercept}{Slope\ of\ calibration\ curve} \quad \text{(Eq.1)}$$

$$LOQ = 10 \times \frac{Standard\ error\ of\ intercept + Intercept}{Slope\ of\ calibration\ curve} \quad \text{(Eq.2)}$$

2.5.2.Method recovery

Three concentrations of HHCB standards were spiked into blank surface water samples. These were (1) close to the highest possible quantitation (high), (2) close to the middle of the calibration range (medium), and (3) close to the quantification point (low). After that, the fluorescence spectra of the samples were obtained to evaluate the validity of the recovery method. The calibration spectra were acquired similarly to the spectra of the validation samples to provide accurate results. The percentage recovery (Equation 3) was computed at three HHCB concentrations (1.16×10^{-8}, 3.503×10^{-7}, and 1.16×10^{-6} M) [37]:

$$\%Recovery = \frac{obtained\ result}{expected\ result} \times 100 \quad \text{(Eq.3)}$$

Previous studies show that the recommended range for the mean recovery is between 70% and 120% [38]. Based on the outcomes, compliance with these recommendations was evaluated. The concentrations of HHCB in three surface water samples spiked with HHCB standard solutions at concentrations of 1.16 10^{-8}, 3.503 10^{-7}, and 1.16 10^{-6} M were measured four times each using the A-TEEM-PLS technique. The relative standard deviation (%RSD) was calculated as Equation 4 [39]. The %RSD must be at least 2% as the acceptance criterion [40].

$$\%RSD = \frac{standard\ deviation}{mean} \times 100 \quad \text{(Eq.4)}$$

3. Results and discussion

3.1. Fingerprint of the excitation-emission matrix of HHCB

We compared the two-dimensional (2-D) fluorescence spectra of two surface water samples one spiked with HHCB and the other not spiked with HHCB (Fig. 2). Figure 2a shows the EEM of fluorescent organic matter in a neat (baseline or blank) surface water sample. In the neat surface water sample, it was discovered that the fluorophores showed wavelengths of 230–425 nm for excitation and 325–600 nm for emission, suggesting the presence of humic substances [RS 41, RS42]. Figure 2b shows the molecular fingerprint of the EEM of HHCB in a surface water sample that was spiked with 8.13×10^{-8} M of HHCB. This figure shows that the wavelengths at which HHCB was found to excite and emit were ~275 and ~296 nm, respectively.

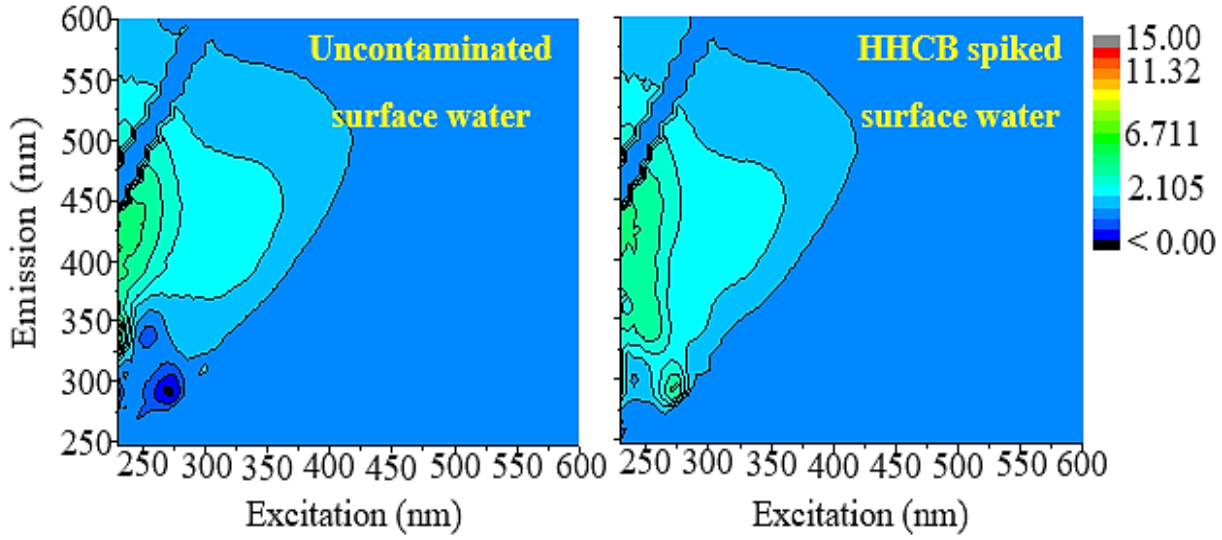

Fig. 2. The 2-D EEMs of two samples of surface water: **(a)** one that is unspiked (DOC = 1.73 ppm) and **(b)** HHCB (1.74×10^{-7} molL^{-1}) spiked in surface water

3.2. PARAFAC modeling and validation

Four components were the ideal number because the explained variance, split-half similarity evaluation, core consistency, spectral loadings, and component identification were balanced. Figure 3 shows the 2-D contour maps of EEMs for the four fluorophores identified in surface water samples spiked with HHCB, as determined by PARAFAC. The categorization of the PARAFAC components shown in this figure was performed after a review of the literature. Component #1, which had maximum wavelengths of ~270 and ~300 nm, respectively, for excitation and emission, represented HHCB (Fig. 3a). This component's Ex/Em wavelength pair almost agreed with those used for fluorescence detection of HHCB in a previous study [25]. The second, third, and fourth components represented organic substances that resembled tryptophan (Fig. 3c) [RS43], fulvic acid (Fig. 3e), and humic acid (Fig. 3g) [RS44] with maximum excitation and emission wavelengths of, respectively, ~ 390 and 450 nm [RS45], 240 to 320 nm and ~ 450 nm, and ~ 390 and 450 nm [RS46]. Furthermore, the spectral loading plots for emission and excitation wavelengths produced by PARAFAC modeling of the EEM data are shown in Figures 3b, 3d, 3f, and 3h. These plots correspond with the wavelengths at which the 2-D contour plots of the emission and excitation of the four components are depicted.

3.3. PLS modeling and validation

Figure 4 displays the fluorescence spectra for 120 HHCB-spiked samples of surface water (Figure 4a) [RS47]., as well as the evolution of the RMSECV, represented by a blue line, and the fundamental RMSEC, represented by a green line, depending on the number of latent LVs used to construct the PLS HHCB prediction model (Figure 4b). Upon analyzing the peaks visually, a single area exhibiting a maximum emission wavelength of ~296 nm was identified and is shown in Figure 4a. A minimum of 5 LVs is shown (Figure 4b) [RS48].

Plots of samples and scores were created to locate and ostensibly eliminate outliers (Fig. 5) [RS49]. The measured and predicted HHCB concentrations using the 120 EEM spectra show a strong correlation, with a high R^2 Cal value of 0.966 in Figure 5a. The plot of scores on LV2 and LV1 indicated six outliers (Fig. 5b). There were a significant number of outliers on the plot that were outside the 95% confidence intervals (blue dashed lines), according to the Q residuals reduced versus the T^2 statistic of the Hotelling plot (Fig. 5c). Four observations with high leverage in the middle and left of the plot shown in Figure S2d were noted. All outliers were eliminated because they can skew statistical analyses [RS50].

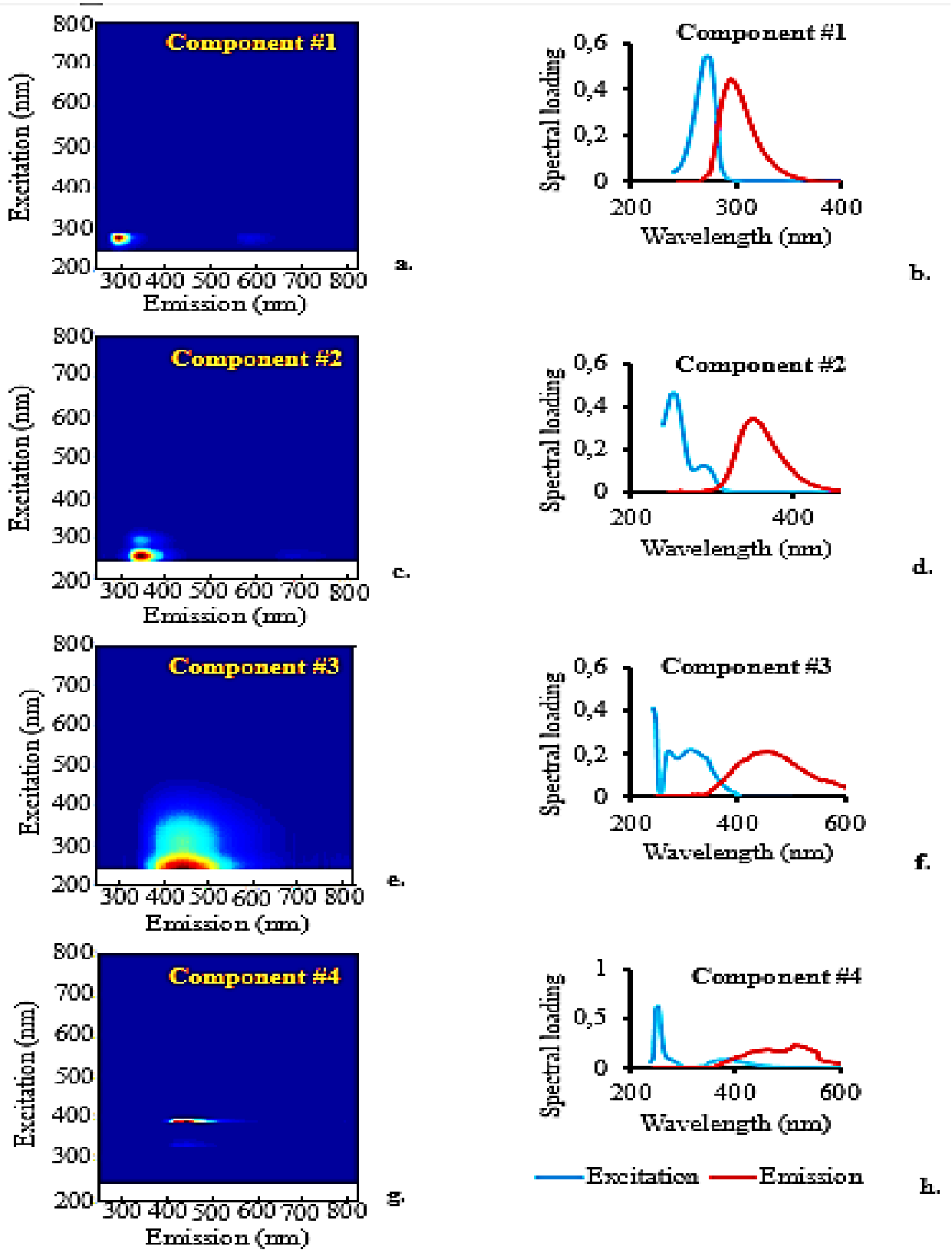

Fig. 3. Four-constituent PARAFAC model: 2-D EEM maps and spectral loadings for excitation and emission of the four constituents of the HHCB-spiked surface water spectral dataset. Components #1, #2, #3, and #4 represent, HHCB, organic material resembling tryptophan acid, organic material resembling fulvic acid, and organic material resembling humic acid.

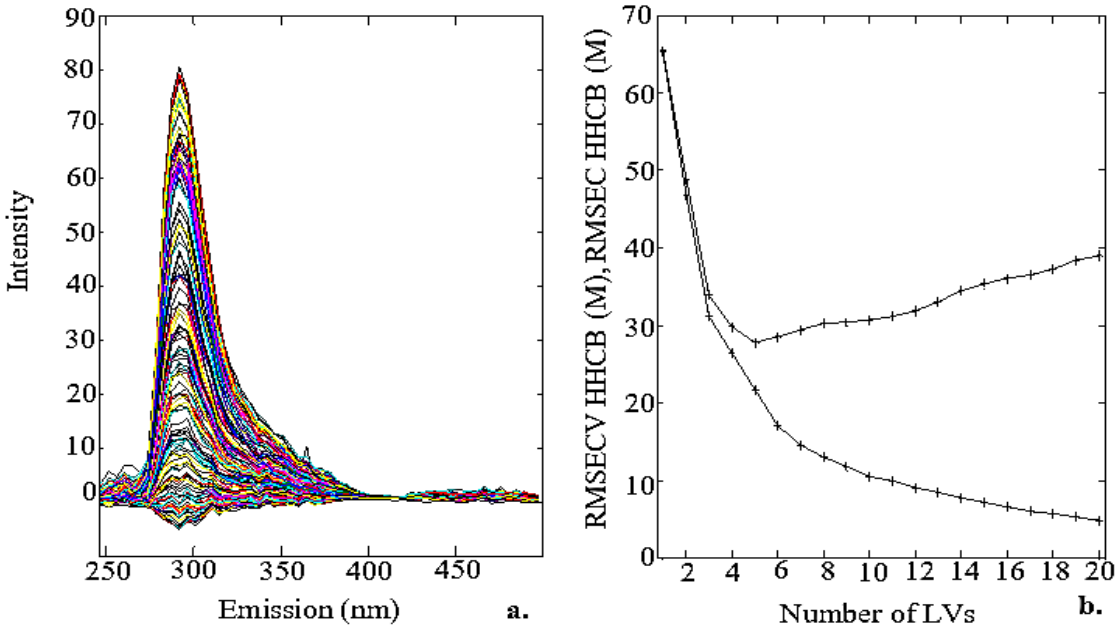

Figure 4 (a) Emission spectra for 120 surface water samples that were spiked with HHCB standard solutions at concentrations between 1.16×10^{-8} and 1.16×10^{-6} M.
(b) Development of the RMSECV (blue line) and the basic RMSEC (green line) per the number of LVs used to build the PLS HHCB prediction model. A minimum of 5 LVs is shown.

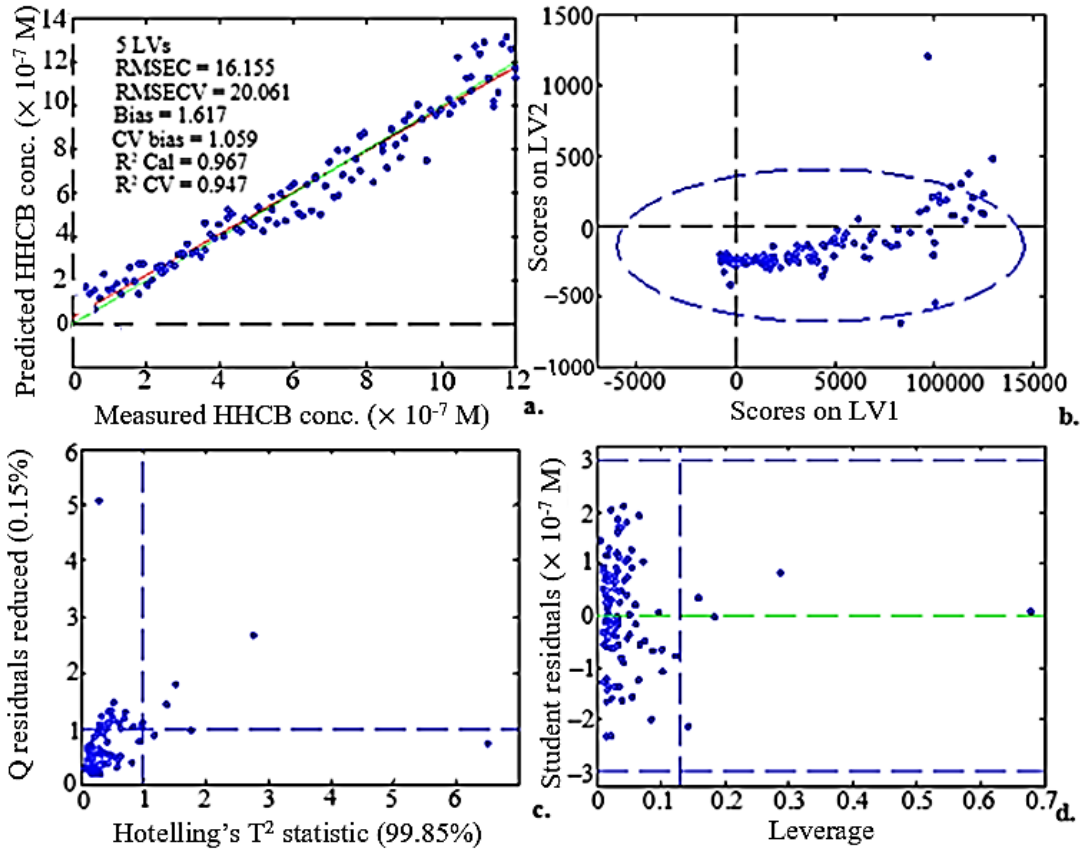

Fig. 5. Plots of **(a)** predicted versus measured HHCB concentration (M), **(b)** scores on LV2 versus scores on LV1, **(c)** Q residuals reduced versus Hotelling's T^2 statistic, and **(d)** studentized residuals HHCB (M) versus leverage for the HHCB concentration range (1.16×10^{-8} and 1.16×10^{-6} M)

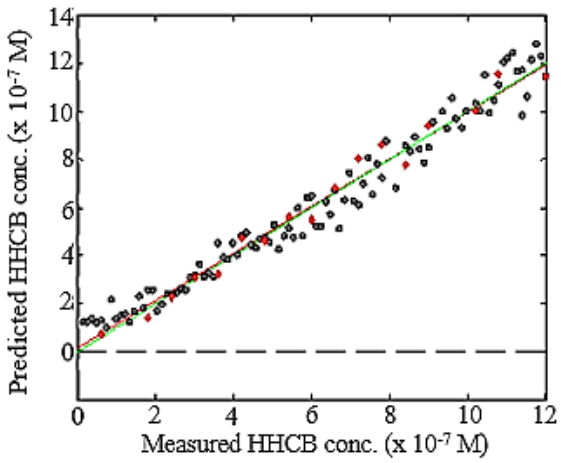

Table 1. The linear regression analysis report for the analysis of HHCB (From Origin V8.6)

Parameter	Value
Number of LVs	5
% Variance captured	95.42
RMSECV (M)	8.058 × 10-8
RMSEC (M)	6.3 × 10-8
RMSEP (M)	5.613 × 10-8
R2 (Cal, CV)	0.966, 0.944
R2 Pred	0.976
RPD (RMSECV, RMSEP)	1.715, 1.187
Slope of calibration curve	1.00
Prediction Bias	–0.623
Calibration Bias	1.554
CV Bias	1.036

Fig. 6. A graph of the measured HHCB concentration (M) against the predicted one for a validation dataset consisting of 18 data points (shown as red diamonds) and a calibration dataset composed of 100 data points (shown as black dots) along with the performance metrics of the PLS model for the examination of HHCB-spiked surface water are shown. LVs is an abbreviation of latent variables, RMSEC means calibration root mean square error, RMSECV means cross-validation accuracy root mean square error, RMSEP means root mean square error of prediction, R^2 (Cal, CV) means calibration and cross-validation accuracy correlation coefficients, R^2 Pred stands for the prediction accuracy correlation coefficient, and CV bias is bias brought on by the coefficient of variation.

Figure 6 shows the calibration and validation of HHCB concentration curves after dividing 120 HHCB EEM spectra into two sets of data: a validation set of 20 data points (red diamonds) and a calibration set of 100 data points (black dots). According to the performance parameters, all validation samples for the PLS model demonstrated accuracy and dependability. There was a value of 6.3 × 10-8 M in the calibration set, and 8.058 × 10-8 M was found in the validation set for the RMSECV. These results implied excellent robustness and predictive accuracy of the PLS model [51].

3.4. Spike sample validation results

The measured versus predicted HHCB concentration plot shows 95% confidence and prediction intervals (Fig. 7a). It is necessary to compute the confidence interval for each potential value of the independent variable. Figure 7b shows the regular residual versus the HHCB concentration plot. The linear regression model successfully predicted the data, as demonstrated by the regular residuals of ±7.74 × 10^{-8} M and the randomly distributed points on the residual plot along the horizontal axis [52].

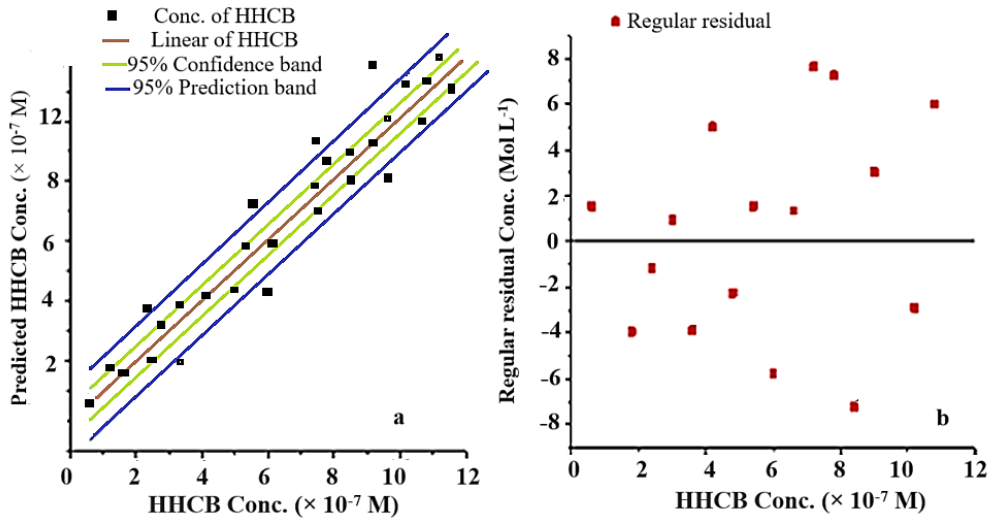

Fig. 7. **(a)** The linear fit of the data from the HHCB validation.
(b) The HHCB regular residuals against the HHBC concentration graph Mol L^{-1}

3.5. Statistical evaluation

The linear regression parameters are shown in Table 2. The small residual sum of squares in the linear regression analysis of HHCB concentrations suggests that the PLS model adequately fits the data [RS53]. The small intercept standard error value for the HHCB regression analyses (Table 2) proved that the analytical approach was valid [RS54]. The predicted HHCB concentration could account for 98.0% of the variation in the measured HHCB concentration, according to the linear fit with R^2 = 0.98.

Furthermore, a highly significant F value of 775.325 [RS55] indicates that the model correctly predicted the HHCB concentration. The Prob > F (p-value) of $5.551E^{-15}$ (Table 2) showed significant goodness of fit between the model and data, further supporting the significance of the analytical method from a statistical standpoint [RS56]. The p-value, which was less than 0.05, meant that the null hypothesis according to which there should be no relationship between any of the predicted HHCB concentrations and the measured HHCB concentrations was not accepted [RS57].

3.6. Detection and quantitation thresholds

The lowest concentration of HHCB in surface water that the suggested method could reliably detect was 5.9×10^{-8} M, and the lowest concentration of HHCB that the technique could quantify while still maintaining the required levels of precision, accuracy, and uncertainty was 1.97×10^{-7} M.

3.7. Recovery of the proposed technique

As per the UNODC [RS58] and BioPharma international [RS59] guidelines, Table 4 presents the percentage recoveries of the method at the three concentration levels. The average recovery results, which came in at 101.12% of the predicted value, demonstrated the method's accuracy.

Table 2. The linear regression analysis report for the analysis of HHCB (From Origin V8.6)

Parameter	Value
Residual sum of squares	2352.03
R-Square (COD)	0.98
Adj. R-Squared	0.979
Pearson's r value	0.99
Intercept	1.288
Standard error of the intercept	6.464
Slope	1.086
Standard error of the slope	0.019

Table 3. ANOVA table for linearity of the HHCB regression model

ANOVA	Mean Squares	Sum of Squares	Prob > F	F Value	Degrees of Freedom
Model	-------	113974.198	$5.551E^{-15}$	775.325	0
Error	147.002	2352.03	-------	-------	16
Total	-------	116326.228	-------	-------	16

Table 4. Percentages of HHCB recovered from surface water samples spiked at three distinct concentration levels

Measured HHCB conc. (mol L^{-1})	Predicted HHCB conc. (mol L^{-1})	Recovery (%)
$1.161\ 10^{-8}$	$1.17\ 10^{-8}$	100.78
$3.503\ 10^{-7}$	$3.572\ 10^{-7}$	101.97
$1.161\ 10^{-6}$	$1.168\ 10^{-6}$	100.6

3.8. Relative standard deviation

HHCB concentrations typically had low % RSD during replicate measurement concentration. The fact that these RSD values are less than the acceptance threshold of 2.0% indicates the procedure for determining the HHCB concentration was accurate and consistent [40 and RS60]. The %RSD values of 0.195, 0.149, and 0.249 at HHCB concentrations of 1.106×10^{-8}, 3.513×10^{-7}, and 1.106×10^{-6} M, respectively, showed the effectiveness of the A-TEEM-PLS approach for HHCB analysis in surface water.

4. Conclusion

Using the fluorescence EEM data along with the PLS and PARAFAC chemometric modeling, it was possible to identify and measure HHCB in surface-level water. The fluorescence EEM data from surface water laced with HHCB allowed the two chemometric models to produce much more focused information. The HHCB could be detected by acquiring the fluorescence EEM contour plots and PARAFAC modeling of these. The maximum excitation and emission wavelengths for HHCB in surface water were ~ 270 and 296 nm, respectively. PLS modeling of fluorescence EEMs with detection and quantification limits in the lower parts per billion range can be used to predict HHCB concentrations in water. The following parameters defined the optimized and validated A-TEEM-PLS technique: working range (1.16×10^{-8} to 1.16×10^{-6} M) recovery (101%), mean relative standard deviation (0.198%), LOD (4.01×10^{-8} M), and LOQ (1.203×10^{-7} M). Using extraction- and reagent-free methods for fluorescence measurement of water contaminated with HHCB has allowed the development of a simple-to-use, cost-effective, sensitive, and rapid approach to measuring HHCB at minute amounts in water samples. Only surface water filtration is required. Thus, environmental monitoring can be conducted regularly using the suggested methodology, especially in areas where HHCB is more pronounced.

5. Acknowledgements

We are grateful to Dr. W. Moyo for the assistance in operating the Aqualog® spectrometer and Mr. S. Mhlongo for general assistance. This work was funded by the Institute for Nanotechnology and Water Sustainability at the University of South Africa. All writers have no competing interests, either monetary-related or not.

6. References

[1] H. P. Hutter, P. Wallner, W. Hartl, M. Uhl, G. Lorbeer, R. Gminski, V. Mersch-Sundermann, M. Kundi, Higher blood concentrations of synthetic musks in women above fifty years than in younger women, Int. J. Hyg. Environ. Health, 213 (2010) 124–130. https://doi.org/10.1016/j.ijheh.2009.12.002

[2] S. Teimoori, A. H. Hassani, M. Panahi, N. Mansouri, Rapid extraction of BTEX in water and milk samples based on functionalized multi-walled carbon nanotubes by dispersive homogenized-micro-solid phase extraction, Food Chem., 421 (2023) 136229. https://doi.org/10.1016/j.foodchem.2023.136229

[3] K. Vimalkumar, N. P. Nikhil, E. Arun, M. Mayilsamy, R. Babu-Rajendran, Synthetic musks in surface water and fish from the rivers in India: Seasonal distribution and toxicological risk assessment, J. Hazard. Mater., 414 (2021) 1–10. https://doi.org/10.1016/j.jhazmat.2021.125558

[4] J. H. Hong, J. Y. Lee, H. J. Ha, J. H. Lee, S. R. Oh, Y. M. Lee, M. Y. Lee, K. D. Zoh, Occurrence and sources of synthetic musk fragrances in the sewage treatment plants and the Han River, Korea, Water, 13 (2021) 1–14. https://doi.org/10.3390/w13040392

[5] D. B. Simmons, V. L. Marlatt, V. L. Trudeau, J. P. Sherry, C. D. Metcalfe, Interaction of Galaxolide with the human and trout estrogen receptor-α, Sci. Total Environ., 408 (2010) 6158–64. https://doi.org/10.1016/j.scitotenv.2010.09.027

[6] S. Teimoori, An immobilization of aminopropyl trimethoxysilane-phenanthrene carbaldehyde on graphene oxide for toluene extraction and separation in water samples, Chemosphere, 316 (2023) 137800. https://doi.org/10.1016/j.chemosphere.2023.137800

[7] EPA, Final Scope of the Risk Evaluation for 1, 3, 4, 6, 7, 8 - Hexahydro - 4, 6, 6, 7, 8, 8 - Hexamethylcyclopenta [γ] - 2 - Benzopyran. Office of Chemical Safety and Environmental Protection Agency Pollution Prevention, Washington, DC, (2020). https://www.epa.gov/assessing - and - managing - chemicals-under-tsca/risk - evaluation - 134678 - hexahydro - 466788

[8] J. Rakhtshah, A rapid extraction of toxic styrene from water and wastewater samples based on hydroxyethyl methylimidazolium tetrafluoroborate immobilized on MWCNTs by ultra-assisted dispersive cyclic conjugation-micro-solid phase extraction, Microchem. J., 170 (2021) 106759. https://doi.org/10.1016/j.microc.2021.106759

[9] K. M. Blum, P. L. Andersson, L. Ahrens, K. Wiberg, P. Haglund, Persistence, mobility and bioavailability of emerging organic contaminants discharged from sewage treatment plants, Sci. Total Environ., 612 (2018) 1532–1542. https://doi.org/10.1016/j.scitotenv.2017.09.006

[10] F. Wong, M. Robson, L. Melymuk, C. Shunthirasingham, N. Alexandrou, M. Shoeib, E. Luk, P. Helm, L. Diamond Miriam, H. Hung, Urban sources of synthetic musk compounds to the environment, Environ. Sci.: Process. Impacts, 21 (2019) 74–88. https://doi.org/10.1039/C8EM00341F

[11] M. Clara, O. Gans, G. Windhofer, U. Krenn, W. Hartl, K. Braun, S. Scharf, C. Scheffknecht, Occurrence of polycyclic musks in wastewater and receiving water bodies and fate during wastewater treatment, Chemosphere, 82 (2011) 1116–1123. https://doi.org/10.1016/j.chemosphere.2010.11.041

[12] E. M. Wanda, B. B. Mamba, T. A. Msagati, Hydrochemical modelling of water quality in terms of emerging micropollutants in Mpumalanga, Gauteng and North West Provinces, Phys. Chem. Earth. Parts A/B/C, 100 (2017) 143–57. https://doi.org/10.1016/j.pce.2016.12.004

[13] H. Itagaki, Fluorescence spectroscopy, Experimental Methods in Polymer Science, Academic Press, San Diego, CA, pages155-260, 2000. https://doi.org/10.1016/B978-0-08-050612-8.50009-X

[14] R. Ashouri, Dynamic and static removal of benzene from air based on task-specific ionic liquid coated on MWCNTs by sorbent tube-headspace solid-phase extraction procedure, Int. J. Environ. Sci. Technol., 18 (2021) 2377-2390. https://doi.org/10.1007/s13762-020-02995-4

[15] D. N. Kothawala, K. R. Murphy, C. A. Stedmon, G. A. Weyhenmeyer, L. J. Tranvik, Inner filter correction of dissolved organic matter fluorescence, Limnol. Oceanogr.: Meth., 11 (2013) 616–630. https://doi.org/10.4319/lom.2013.11.616

[16] A. Quatela, A. M. Gilmore, K. E. Gall, M. Sandros, K. Csatorday, A. Siemiarczuk, B. B. Yang, L. Camenen, A-TEEM, a new molecular fingerprinting technique: Simultaneous absorbance-transmission and fluorescence excitation-emission matrix method, Methods Appl. Fluoresc., 6 (2018) p.027002. https://doi.org/10.1088/2050-6120/aaa818

[17] M. Park, S. A. Snyder, Sample handling and data processing for fluorescent excitation-emission matrix (EEM) of dissolved organic matter (DOM), Chemosphere, 193 (2018) 530–537. https://doi.org/10.1016/j.chemosphere.2017.11.069

[18] A. K. Driskill, J. Alvey, A. D. Dotson, P. L. Tomco, Monitoring polycyclic aromatic hydrocarbon (PAH) attenuation in Arctic waters using fluorescence spectroscopy, Cold Reg. Sci. Technol., 145 (2018) 76–85. https://doi.org/10.1016/j.coldregions.2017.09.014

[19] M. A. Pendergraft, D. J. Grimes, S. N. Giddings, F. Feddersen, C. M. Beall, C. Lee, M. V. Santander, K. A. Prather, Airborne transmission pathway for coastal water pollution, PeerJ, 9 (2021) 1–19. https://doi.org/10.7717/peerj.11358

[20] S. Sharma, A. Bhattacharya, Drinking water contamination and treatment techniques, Appl. Water Sci., 7 (2017) 1043–1067. https://doi.

org/10.1007/s13201-016-0455-7

[21] O.Y.A. Costa, J. M. Raaijmakers, E. E. Kuramae, Microbial extracellular polymeric substances: Ecological function and impact on soil aggregation, Front. Microbiol., 9 (2018) 1–14. https://doi.org/10.3389/fmicb.2018.01636

[22] S. Herrera López, M. D. Hernando, M. J. Gómez, J. Santiago-Morales, R. Rosal, A. R. Fernández-Alba, Investigation of Galaxolide degradation products generated under oxidative and irradiation processes by liquid chromatography/hybrid quadrupole time-of-flight mass spectrometry and comprehensive two-dimensional gas chromatography/time-of-flight mass spectrometry, Rapid Commun., 27 (2013) 1237–1250. https://doi.org/10.1002/rcm.6575

[23] M. Celeiro, J. P. Lamas, M. Vila, C. Garcia-Jares, V. Homem, N. Ratola, T. Dagnac, M. Llompart, Determination of multiclass personal care products in continental waters by solid-phase microextraction followed by gas chromatography-tandem mass spectrometry, J. Chromatogr. A, 1607 (2019) 460398. https://doi.org/10.1016/j.chroma.2019.460398

[24] B. D. Su, C. Z. Min, C. D. Hui, The Determination of Galaxolide in water samples with SPME coupled with GC-MS, Adv. Mater. Res., 183 (2011) 184–187. https://doi.org/10.4028/www.scientific.net/AMR.183-185.184

[25] A. Sokol, A. Ratkiewicz, I. Tomaszewska, J. Karpinska, Kinetics and mechanistic studies of photochemical and oxidative stability of galaxolide, Water, 13 (2021) 1813. https://doi.org/10.3390/w13131813

[26] J. C. Lindon, G. E. Tranter, D. Koppenaal, Encyclopedia of spectroscopy and spectrometry, Academic Press, (2016). https://www.amazon.ca/-/fr/John-C-Lindon/dp/0128032243

[27] J. Rakhtshah, H. Shirkhanloo, N. A. Esmaeili, Rapid extraction of toxic styrene from water and wastewater samples based on hydroxyethyl methylimidazolium tetrafluoroborate immobilized on MWCNTs by ultra-assisted dispersive cyclic conjugation-micro-solid phase extraction, Microchem. J., 170 (2021) 106759. https://doi.org/10.1016/j.microc.2021.106759

[28] S. Teimoori, A.H. Hassani, New extraction of toluene from water samples based on nano-carbon structure before determination by gas chromatography, Int. J. Environ. Sci. Technol., 20 (2023) 6589–6608. https://doi.org/10.1007/s13762-023-04906-9

[29] B. Darpo, T. Nebout, P. T. Sager, Clinical evaluation of QT/QTc prolongation and proarrhythmic potential for nonantiarrhythmic drugs: The international conference on harmonization of technical requirements for registration of pharmaceuticals for human use E14 guideline, J. Clin. Pharmacol., 46 (2006) 498–507. https://doi.org/10.1177/0091270006286436

[30] USP 30 The United States Pharmacopeia 30th ed. (United States Pharmacopeial Convention: Rockville, 2007. https://www.usp.org/

[31] ASTM Standard Practice for Validation of Empirically Derived Multivariate Calibrations Methods, Document E2617–17, West Conshohocken, USA, 2018. https://standards.globalspec.com/std/4384102/astm-e2617-17

[32] V. Diwan, C. Stålsby Lundborg, A. J. Tamhankar, Seasonal and temporal variation in release of antibiotics in hospital wastewater: estimation using continuous and grab sampling, PLOS One, 8 (2013) e68715. https://doi.org/10.1371/journal.pone.0068715

[33] A. M. Gilmore, L. Chen, Optical early warning detection of aromatic hydrocarbons in drinking water sources with absorbance, transmission and fluorescence excitation-emission mapping (A-TEEM) instrument technology, In Next-Generation Spectroscopic Technologies XII, SPIE publisher, 10983 (2019) 45–52. https://doi.

org/10.1117/12.2522498

[34] S. M. Clegg, E. Sklute, M. D. Dyar, J. E. Barefield, R. C. Wiens, Multivariate analysis of remote laser-induced breakdown spectroscopy spectra using partial least squares, principal component analysis, and related techniques, Spectrochim. Acta B At. Spectrosc., 64 (2009) 79–88. https://doi.org/10.1016/j.sab.2008.10.045

[35] E. R. Ziegel, Handbook of Chemometrics and Qualimetrics, Part B, Technometrics, 42 (2000) 218-219. https://doi.org/10.1080/00401706.2000.10486023

[36] N. Altman, M. Krzywinski, P values and the search for significance, Nat. Methods, 14 (2017) 3–4. https://doi.org/10.1038/nmeth.4120

[37] D. Steiner, R. Krska, A. Malachová, I. Taschl, M. Sulyok, Evaluation of matrix effects and extraction efficiencies of LC–MS/MS methods as the essential part for proper validation of multiclass contaminants in complex feed, J. Agric. Food Chem., 68 (2020) 3868–3880. https://doi.org/10.1021/acs.jafc.9b07706

[38] A. Fajgelj, A. Ambrus, Guidelines for single-laboratory validation of analytical methods for trace-level concentrations of organic chemicals, In Principles and practices of method validation, pages179–252, 2000. https://doi.org/10.1039/9781847551757-00179

[39] S. Singh, N. Sharma, N. Kanojia, G. Kaur, S. Arora, Development and validation of UV-spectrophotometer method for analysis of fluvastatin sodium in polyethylene glycol 6000 and polyvinyl pyrollidone K-30 solid dispersions, Plant Arch., 20 (2020) 3365–3371. https://www.plantarchives.org/

[40] T. N. Rao, Validation of analytical methods, Calibration and validation of analytical methods- A sampling of current approaches, book publisher: Intech Open, 25 (2018) 131–41. http://dx.doi.org/10.5772/intechopen.72087

Anal. Methods Environ. Chem. J. 7 (3) (2024) 113-126

AMECJ

Research Article, Issue 3
Analytical Methods in Environmental Chemistry Journal
Journal home page: www.amecj.com/ir

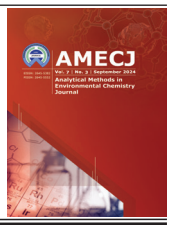

An efficient method for removing toluidine blue and malachite green from industrial wastewater using limestone as an adsorbent surface

Firas Fadhel Ali[a], Riyadh Mohammed Jihad[a,*], Nibras Basim Mohammed[a], Eman Husam Mohamed[a], and Sumood Al-Hadithy[b]

[a]*University of Anbar, College of Education for Women, Department of Chemistry*
[b]*University of Anbar, College of Basic Education, Haditha*

ARTICLE INFO:

Received 2 Jun 2024
Revised form 6 Aug 2024
Accepted 30 Aug 2024
Available online 30 Sep 2024

Keywords:
Removal,
Adsorbent,
Toluidine blue dye,
Malachite green dye,
UV-Vis spectrophotometers,
Thermodynamic

ABSTRACT

This study used an applied method to remove toluidine blue (TB) and malachite green dye (MG) via limestone residue as an adsorbent. The results showed that the TB and MG dyes were removed at a weight (4.0 g and 2.5 g) of limestone residue, pH (10 and 7), temperature (298 ^{o}K and 303 ^{o}K), and removal rate (98.07% and 99.65%) based on an equilibrium time 40 min with a granular size of 300 µm, respectively. The recovery, RSD (%), and absorption capacity (AC) for TB and MG were obtained at (98.8, 1.4, 1.98 mg g^{-1}) and (96.1, 0.89%, 0.55 mg g^{-1}), respectively, by UV-Vis spectrophotometers. The adsorption isotherms of the dyes and their applicability were studied using the Lankmeyer and Freundlich equations. The results also obtained showed that the application of the adsorption process to the Tamkin, Freundlich, and Lankmeyer equation through the values of the correlation coefficient (R^2), where the values for TB dye were (0.96, 0.81, 0.043) and for MG dye (0.9526, 0.7193, 0.819), respectively. Due to the thermodynamic studies, the positive ΔG^{o} values for toluidine blue dye (8.986, 9.293, 10.17, 10.12) and negative ΔH^{o} for malachite green dye (7.756, 8.015, 8.288, 8.614) were achieved at temperatures (293, 303, 313, 323^{o}K), respectively. So, ΔG^{o} values indicate that the adsorption processes were non-spontaneous and showed TB dye with positive ΔH^{o} values is endothermic, and MG with negative ΔH^{o} indicates exothermic. The positive entropy values indicate increased randomness when there is contact between the adsorbent surface and the dye solution.

1. Introduction

Throughout industry growth and development, water is susceptible to pollution, as humans employ chemicals in most aspects of their lives. Pollution directly impacts human health, and the types of pollutants include organic compounds and heavy metals [1]. Organic pollutants, commonly detected in water systems, can be considered dangerous [2-4]. Most of the dyes produced are used in several complementary industries, and their release into bodies of water seriously impacts the aquatic environment [5,6]. The presence of dyes in the aquatic environment calls for great concern because most of these dyes are harmful to human and aquatic life [7]. Many dyes are widely used in various industries, such as fabrics, leather, medicines, etc. The consumption of large quantities of dyes in textile industries has produced a large

*Corresponding Author: Riyadh Mohammed Jihad
Email: edw.riyadhihad@uoanbar.edu.iq
https://doi.org/10.24200/amecj.v7.i03.323

amount of waste in the environment [8]. Malachite green (MG) is one of the most widely used dyes for coloring cloth, wool, leather, cotton, etc., and is also used as an antimicrobial and antifungal agent [9]. The presence of malachite green pigment in water causes kidney and liver damage and heart failure, reduces the fertility rate, and is carcinogenic [10]. Another dye is toluidine blue, which is free from organic pollutants and is widely used to dye textiles such as cotton, cellulose, wood, and silk [8]. This dye causes harmful effects on humans and the environment due to its solubility in water. It causes carcinogenesis and chronic toxicity, mainly to the central nervous system [11]. Liquid waste from the textile industry is dangerously colored [12]. Many chemical and physical processes remove these dyes from water [13]. The most crucial method is adsorption, and it is considered one of the best techniques used not only in water treatment but can also be used to treat crude oil due to its ease of use, low cost, and high efficiency [14]. Adsorption is the process of adhesion or gathering of a liquid or gaseous adsorbent (Adsorbate) on the surface of a material. Solid substance: Adsorbent [15] is the process of physical or chemical bonding of several molecules with active sites on the surface of a solid material [16]. This process leads to forming a layer or several layers of molecules or atoms accumulated and densely concentrated on the surface of the solid [17]. The degree of adsorption depends on the relationship between the nature and size of the adsorbent and its surface area. Adsorption is also defined as the transfer of dissolved pollutants (adsorbent) from aqueous solutions to the surface of a solid material (adsorbent surface) [18]. In this research, limestone was used after grinding it to different sizes as an adsorbent surface to remove malachite green and toluidine blue dyes from water and purify them. The tests were conducted in the Hit laboratory, and the factors affecting adsorption efficiency, including adsorbent surface weight, contact time, adsorbent surface granular size, acidity function, and temperature, were studied.

2. Experimental

2.1. Preparation of the adsorbent

Limestone was collected from the waste of sculpture factories in Hit, Anbar, Iraq. It was dried at 105 °C, then ground with a grinder and sieved to obtain three particle sizes (150, 250, 300 mm) [14]. Limestone contains 80% or more calcium or magnesium carbonate, including marble, chalk, oolite, and marl. limestone composition has high Ca^{2+}, argillaceous (clayey), SiO_2, conglomerate, Mg^{2+}, dolomite, and other limestones. Limestone is extracted from mines. Due to its chemical composition and optical granulometry, it is calcinated at about 900 °C in lime kilns to produce quicklime and is hydrated to slaking. Then, the slaked lime slowly reacts with carbon dioxide to form calcium carbonate (limestone), as shown in Equation 1.

$$CaCO_3 \rightarrow CaO + CO_2$$
$$CaO + H_2O \rightarrow Ca(OH)_2$$
$$Ca(OH)_2 + CO_2 \rightarrow CaCO_3 + H_2O$$

(Eq.1)

2.2. Materials used

The standard solution of toluidine blue (CAS number: 92-31-9, BDH company) and malachite green (CAS number: 569-64-2, BDH Company) was prepared at a concentration of (100 mg L^{-1}) by dissolving (0.05 g) of each dye separately in (500 mL) of distilled water. A series of standard solutions for the two dyes were prepared from the leading solution at concentrations (0.1-10 mg L^{-1}) to conduct the standard calibration curve. Before mixing the adsorbent, the pH of each solution was adjusted to the required value using 0.1N sodium hydroxide or 0.1N hydrochloric acid.

2.3. Adsorption Procedure

An adsorption experiment was conducted using toluidine blue dye, where the effect of contact time was studied by mixing a specific weight of limestone with (100 mL) at a concentration of (25 mg L^{-1}) of toluidine dye in a conical flask (Scheme 1). The flask was shaken for different periods (20, 40, 60,

80, 100, and 120 min). The filtrate was separated from the precipitate using a centrifuge, and the concentration of each solution was measured after adsorption using a UV-Vis spectrophotometer. The effect of the acid function was also studied at pH of 2, 4, 6, 8, 9, and 10 in different temperatures (298, 273, 313, 323 K). Adsorption experiments were also conducted using various concentrations of dye (5, 25, 45, 65, 85, and 95 mg L^{-1}). The effect of the adsorbent weight was studied using different limestone weights (0.5, 1, 1.5, 2.5, 3, 3.5, and 4 g). An adsorption experiment was also conducted using malachite green dye as an adsorbent; a specific weight of limestone was mixed with (100 mL) at a concentration of (50 mg L^{-1}) of malachite green dye in a conical flask. The flask was shaken for different periods (20, 40, 60, 80, 100, 120 min). The filtrate was separated from the precipitate using a centrifuge, and the concentration of each solution was measured after adsorption using an atomic absorption device. The adsorption experiment was also conducted at pH = (2, 4, 6, 8, 9, and 10) and different temperatures (298, 273, 313, and 323°K). Adsorption experiments were also conducted using different concentrations of dye (5, 25, 45, 65, 85, and 95 mg L^{-1}). The influence of the size of the particle on the adsorbent surface was also studied using various sizes of the particle (150, 250, 300 µm), and the effect of the weight of the adsorbent was studied using different weights of limestone (0.5, 1, 1.5, 2.5, and 3.0 g). After the adsorption procedure, the concentration was measured using a UV-Vis spectrophotometer, and the adsorption capacity was calculated through Equation 2 and 1.

$$Q_e = \frac{(C_0 - C_e)V_L}{Wt} \quad \text{(Eq.2)}$$

Qe: The adsorption capacity (mg g^{-1})
VL: Total volume of dye solution (Liter)
C0: Initial concentration of dye solution (mg L^{-1})
Ce: The equilibrium concentration of the dye solution (mg L^{-1})
Wt: weight of the adsorbent surface (g)

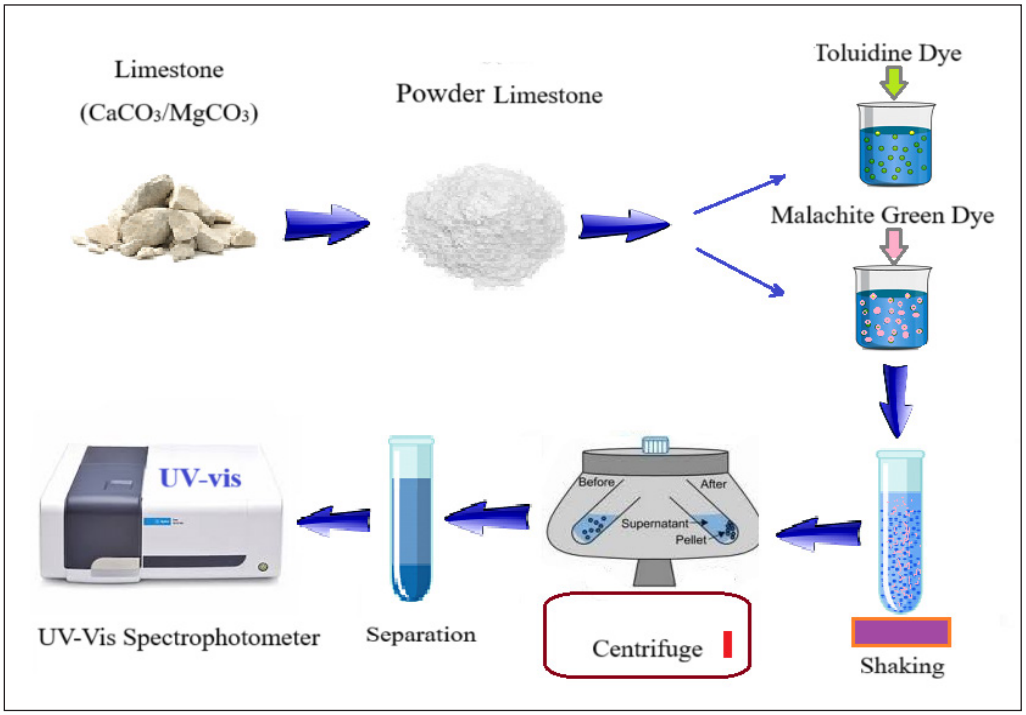

Scheme 1. Adsorption procedure for removal of MG and TB in water sample by limestone

3. Results and Discussion

This study aims to use limestone as an adsorbent to remove toluidine blue and malachite green (MG) from aqueous solutions. The current study aimed to examine the factors affecting their adsorption efficiency, as well as to study the adsorption isotherms and their applicability to the Langmuir, Freundlich, and Tamkin equations.

3.1. Characterization of limestone

The FE-SEM image of the limestone in Figure 1 shows a rough and highly porous surface that explains the high adsorption of toluidine blue and malachite green from their aqueous solutions. The XRD image of limestone in Figure 2 shows that calcite is the dominant mineral in limestone [20]. Figure 3 shows the FTIR spectrum of the limestone sample. It shows the characteristic bands of calcite at 1,397, 875, and 712 cm^{-1} [21].

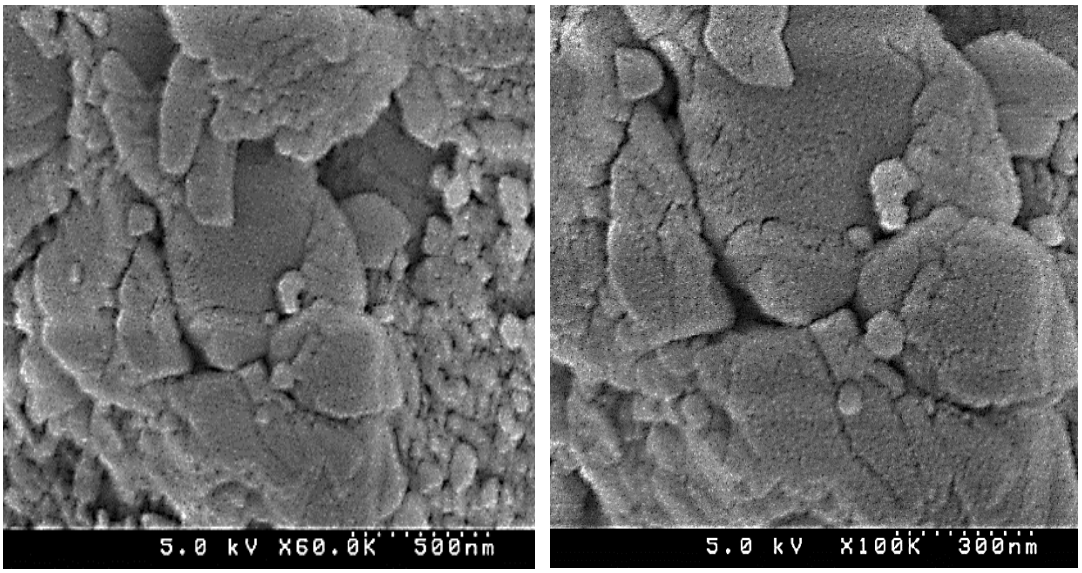

Fig. 1. SEM image of limestone

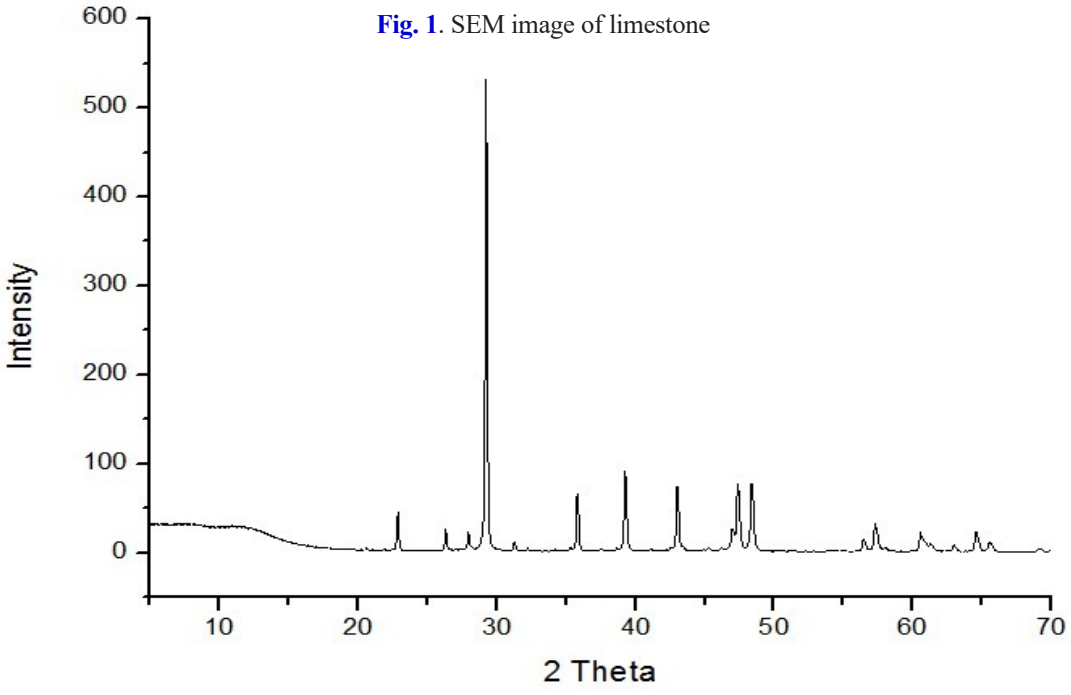

Fig. 2. XRD image of limestone

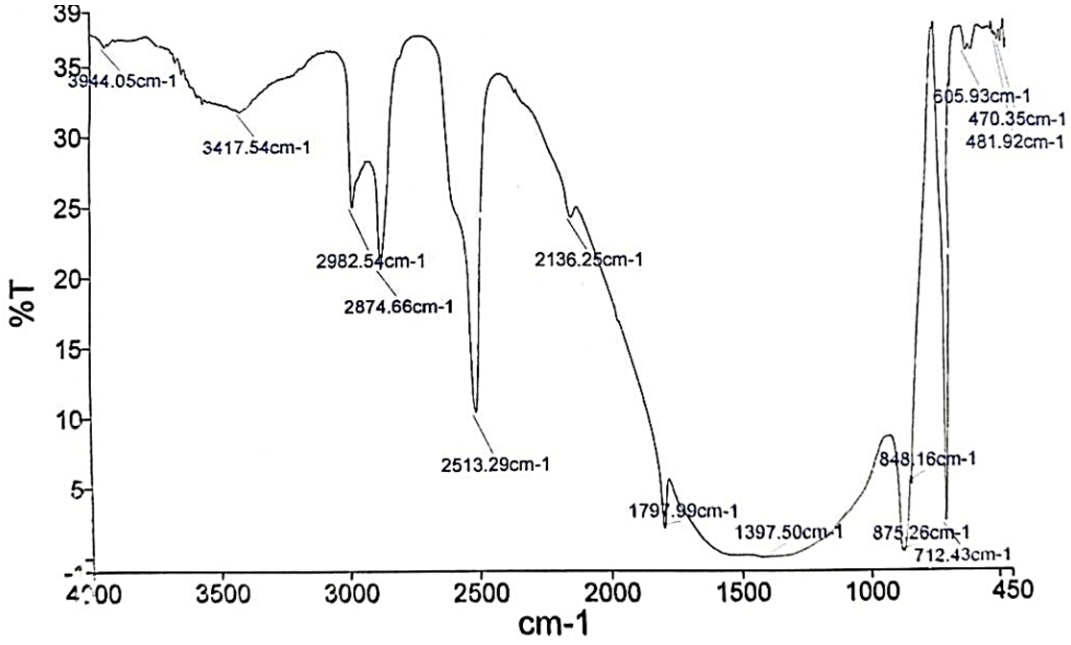

Fig. 3. FTIR spectrum of bulk limestone sample.

3.2. Effect of the adsorbent amount (limestone)

The effect of the adsorbent amount on removing toluidine blue dye was studied, and the results showed that the highest adsorption percentage was (89.08%) when using an amount of 4.0 g of limestone, as shown in Figure 4. As for the effect of the adsorbent surface on removing the malachite green dye, the results showed that the highest adsorption rate (99.30) was recorded when using an amount of 2.5 grams of limestone. This is ascribed to the availability of a larger surface area with increasing locations of active sites prepared for adsorption, and thus, the removal rate increases [22]. Stability is explained by the balance between the adsorbate (malachite green) and the adsorbent (limestone) [23], as shown in Figure 4.

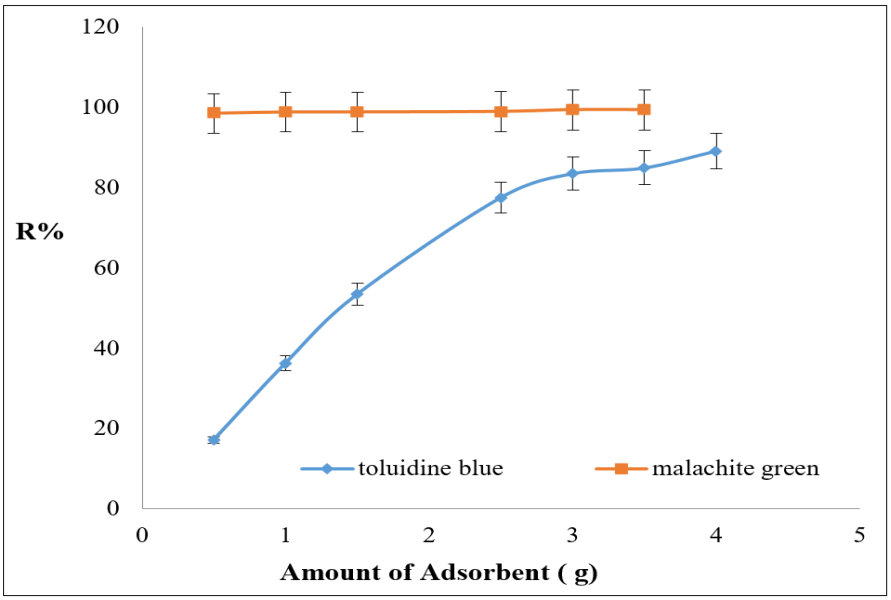

Fig. 4. The effect of limestone amounts on dye removal.

3.3. Effect of contact time

The effect of contact time between the adsorbent surface (limestone) and the adsorbent material (toluidine dye) was studied using a weight of (4.0 g) of the adsorbent surface and a fixed concentration (25 mg L^{-1}) of the dye at a temperature of (20°C) and (pH = 7). Using different periods (20-40-60-80-100-120min), it was observed that the highest adsorption percentage (90.96%) was at 40min, as shown in Figure 5. The effect of the equilibrium time between the adsorbent surface (limestone) and the MG dye was also studied using a weight of 2.5 g of the adsorbent surface and a fixed concentration (50 mg L^{-1}) of the dye and at different times (20-40-60-80-100-120 min). The outcomes have shown that 40 minutes is the best equilibrium time for MG dye, giving the best removal rate (99.46%). It was also reported that there was an increase in time and a decreased removal rate. This is due to the saturation of the active sites of the adsorbent surface [24], as shown in Figure 5.

3.4. Adsorbent surface grain size effect

The effect of changing adsorbent surface grain size on the adsorption process of toluidine blue dye and malachite green dye was studied using different granule sizes (150-250-300 µm). Among the results obtained was that the highest removal percentage was reported at the grain size of 300 µm for the two dyes, (95.6%) of toluidine blue dye with a removal rate reaching (99.48%) when using malachite green dye as shown in Figure 6.

3.5. The effect of pH

The removal of toluidine blue dye from the surface of limestone was studied with different pH functions (2-4-6-8-9-10) using a fixed concentration of 25 mg L^{-1}, a weight of 4.0 g, and an equilibrium time of 40 minutes. Based on the results provided in Figure 7, it was shown that the function of pH = 10 gave the best dye removal percentage (99.9%). The removal of MG dye on the surface of limestone was also studied at different pH levels (2-4-6-7-8-9) using a fixed concentration (50 mg L^{-1}), a weight of 2.5 g, and an equilibrium time of 40 min. The results obtained are offered in Figure 7. It was found that the neutral pH = 7 gave the best removal percentage of MG dye (99.48%). pH = 9 was excluded to study its effect on removing the MG dye because the color of the dye disappears in this medium before the adsorption process starts.

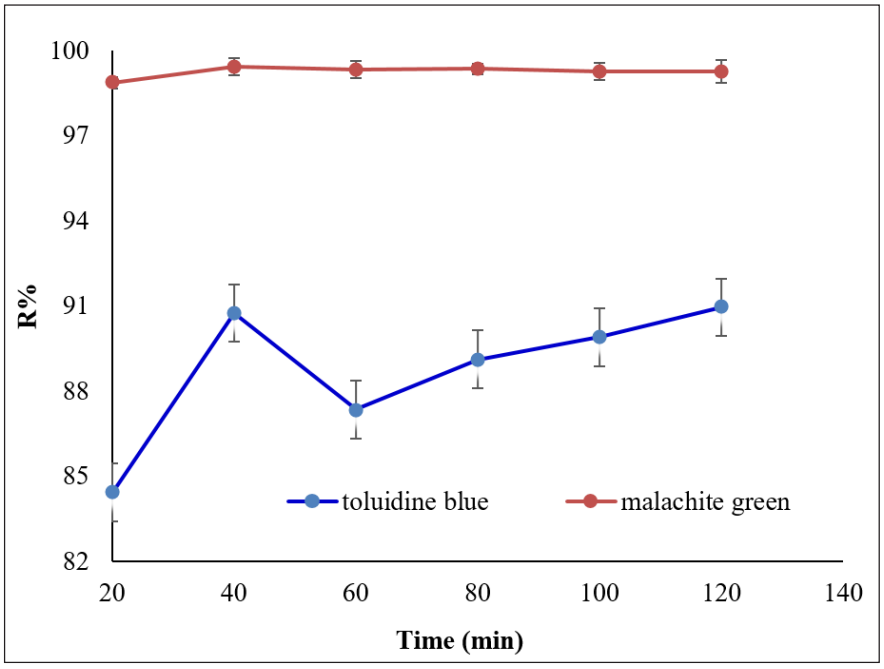

Fig. 5. The effect of time on the removal of dyes

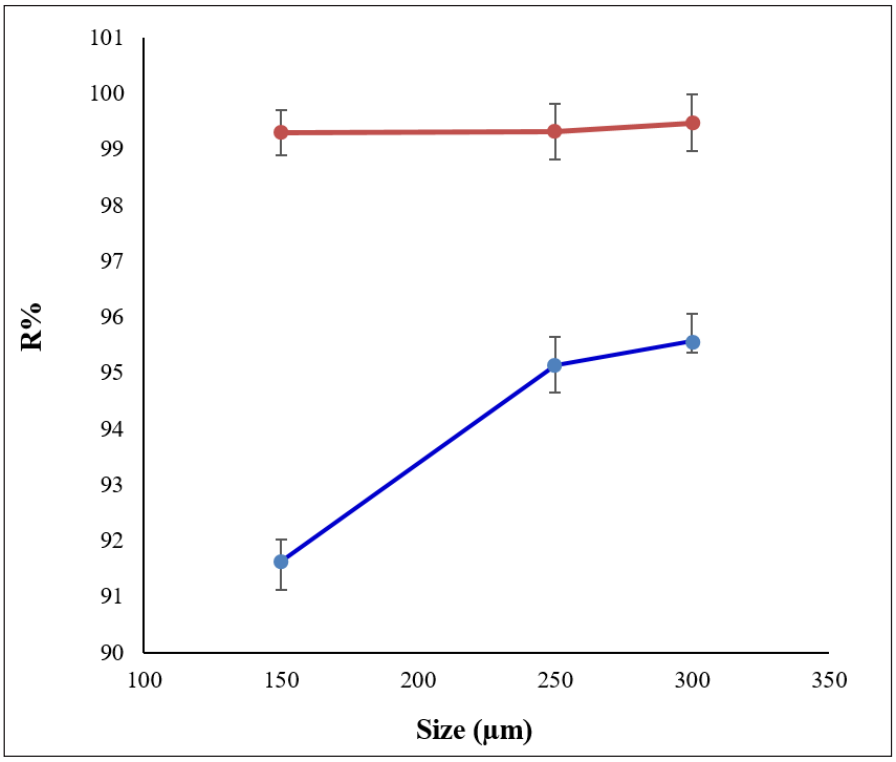

Fig. 6. The effect of the adsorbent particle size on the dye removal (TB blue and MG red)

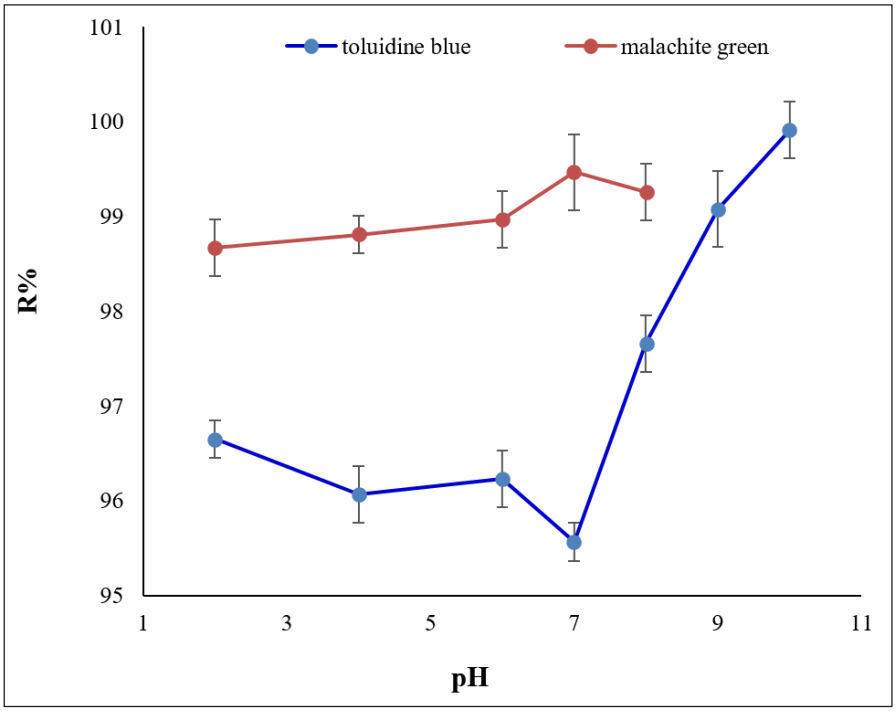

Fig. 7. The effect of pH on the removal of dyes

3.6. Effect of temperature

The effect of temperature on the removal of toluidine blue dye was studied, and the results show that the optimum temperature for adsorption was 293°K with a removal rate of 98.07%. Temperature decreased but started to increase at a temperature of 323°K. As shown in Figure 8, the effect of temperature on removing malachite green (MG)

dye was also studied. The results showed that the optimum temperature for adsorption was 303°K, with a removal rate of (99.65%). The temperature then began to decrease. It was found that increasing the temperature led to a decrease in the adsorption rate because increasing temperature led to an increase in the kinetic energy of the molecules adsorbed on the surface, which in turn led to the possibility of their separation from the adsorbent surface and their return to the solution [25,26]. As shown in Figure 8.

3.7. Adsorbent (dye) concentration effect

The effect of the concentrations of the dyes (toluidine blue and malachite green) on the adsorption rate was studied, and the results showed that the adsorption rate increased due to the increase in the dye concentration, as shown in Figure 9.

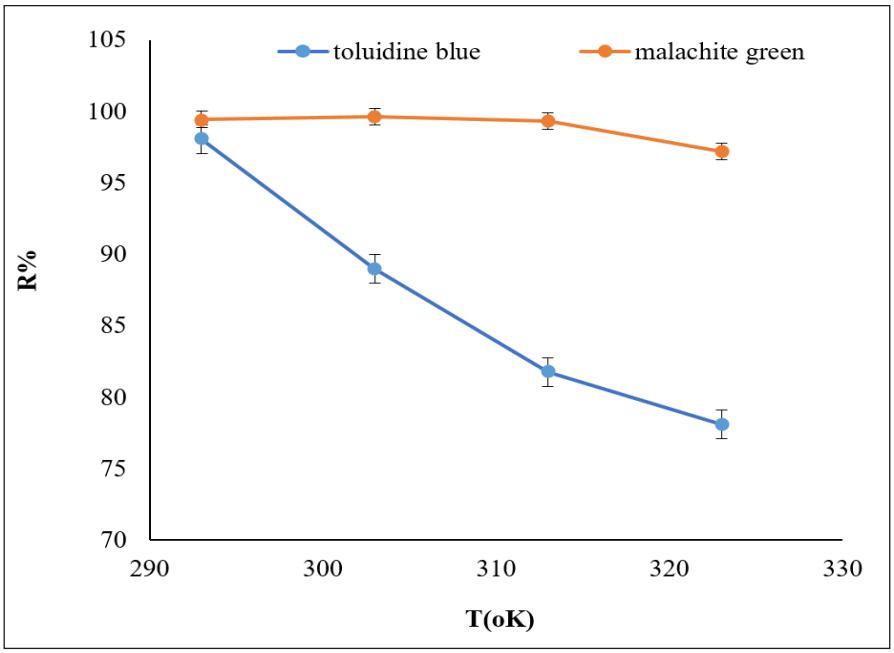

Fig. 8. The effect of temperature on the removal of dyes

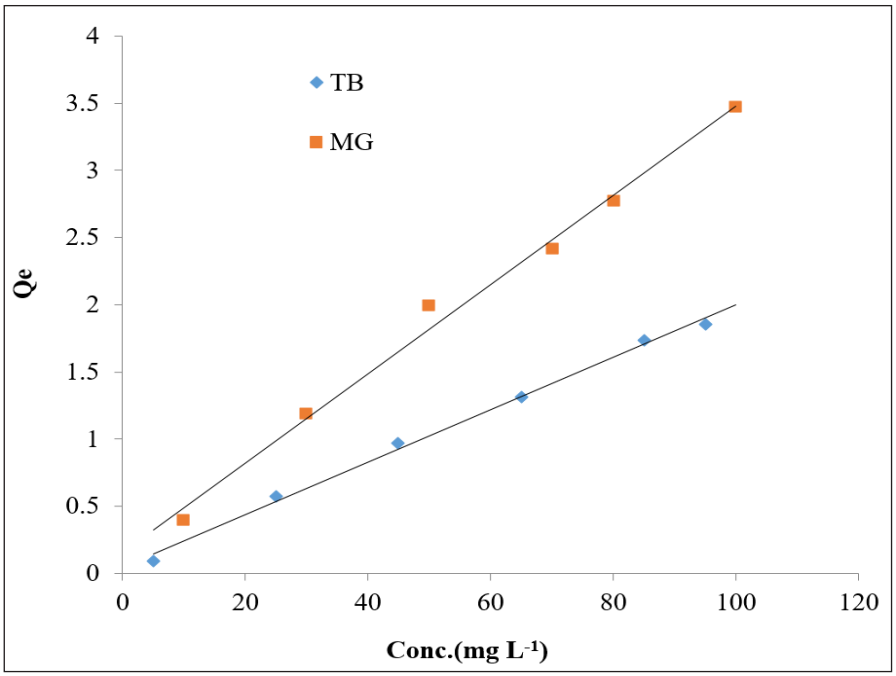

Fig. 9. The effect of initial concentration on the removal of dyes

3.8. Calculating thermodynamic functions

The thermodynamic functions (ΔH^o, ΔG^o, ΔS^o) for the adsorption processes of toluidine blue and malachite green dyes were calculated via van't Hoff equation by plotting the values of (LnK) versus (1/T), where the slope represents the value of ΔHo/R. As for the intersection, it means (ΔS^o/R), and the values of (ΔG^o) were calculated. Below are the Equations (3-5) used for calculating thermodynamic functions (ΔG^o, K, Ln K) [27]. K is the adsorption equilibrium constant and is calculated through Equation 4.

$$\Delta G^{\circ} = RT\ LnK \qquad \text{(Eq.3)}$$

$$K_{eq} = \frac{X_{eq}}{a - X_{eq}} \qquad \text{(Eq.4)}$$

$$LnK = \frac{\Delta S^{\circ}}{R} - \frac{\Delta H^{\circ}}{RT} \qquad \text{(Eq.5)}$$

R = General gas constant (8.314 J K^{-1} $mole^{-1}$)
T = Absolute temperature.
Keq = Equilibrium constant.
a = Initial concentration
Xeq = Amount of adsorbed substance at equilibrium
a-xeq = Concentration of the unadsorbed substance at equilibrium

Based on Table 1 for the adsorption process of toluidine blue dye, it is clear through the positive ΔG^o values that the reaction occurred non-spontaneously, that the reaction was endothermic through the positive ΔH^o value, and that the positive entropy value indicated an increase in randomness, at the contact between the adsorbent surface and the solution. Table 2 shows, through the positive ΔG^o values, that the reaction continued to be non-spontaneously for the process of adsorption of the malachite green dye (MG) and that the reaction produced heat through the negative ΔH^o value and the negative entropy value indicated a decrease in randomness when there is in contact between the adsorbent surface and the solution [28].

3.9. Adsorption isotherms

The adsorption isotherm was studied to determine the applicability of the adsorption process with the Langmuir and Freundlich equations. The study was conducted at a temperature of 293 K, an equilibrium time of 40 minutes, and a particle size of 300 µm in a neutral aqueous medium using different concentrations (5, 25, 45, 65, 85, 95 mg L^{-1}). When using toluidine blue dye, the concentrations (10, 30, 50, 70, 80, 100 mg L^{-1}) when using malachite green dye (MG). As shown in Tables 3 and 4. Also, the adsorption isotherm was shown in Figures 14-16, respectively. Table 5 shows a comparison of different adsorbents for the removal of MG and TB.

Table 1. The values of the thermodynamic functions for the adsorption process of TB dye on the limestone surface.

C_o (mg L^{-1})	T(^{o}K)	K_{eq}	ΔH^o KJ $mole^{-1}$	ΔS^o KJ (mol K)$^{-1}$	ΔG^o KJ $mole^{-1}$
25	293	0.025	1.677	0.000079	8.986
	303	0.025			9.293
	313	0.020			10.17
	323	0.023			10.12

Table 2. The values of the thermodynamic functions for the adsorption process of MG dye on the limestone surface

C_o (mg L^{-1})	T(^{o}K)	K_{eq}	ΔH^o KJ $mole^{-1}$	ΔS^o KJ (mol K)$^{-1}$	ΔG^o KJ $mole^{-1}$
50	293	0.041	-0.620	-0.028	7.756
	303	0.042			8.015
	313	0.041			8.288
	323	0.040			8.614

Table 3. Experimental constants for both the Freundlich and Langmuir model and their values when using toluidine blue dye

T(°K)	Freundlich Constants			Langmuir Constants			Temkin Constants		
293	R^2	n	K_f	R^2	Q_o	K_L	R^2	B	A
	0.805	1.124	0.045	0.957	9.709	0.0017	0.043	0.587	4.528

Table 4. Experimental constants for both the Freundlich and Langmuir model and their values when using MG dye

T(°K)	Freundlich Constants			Langmuir Constants			Temkin Constants		
293	R^2	n	K_f	R^2	Q_o	K_L	R^2	B	A
	0.7193	3.3647	73.62	0.9524	3.106	1.528	0.819	0.4437	67.20

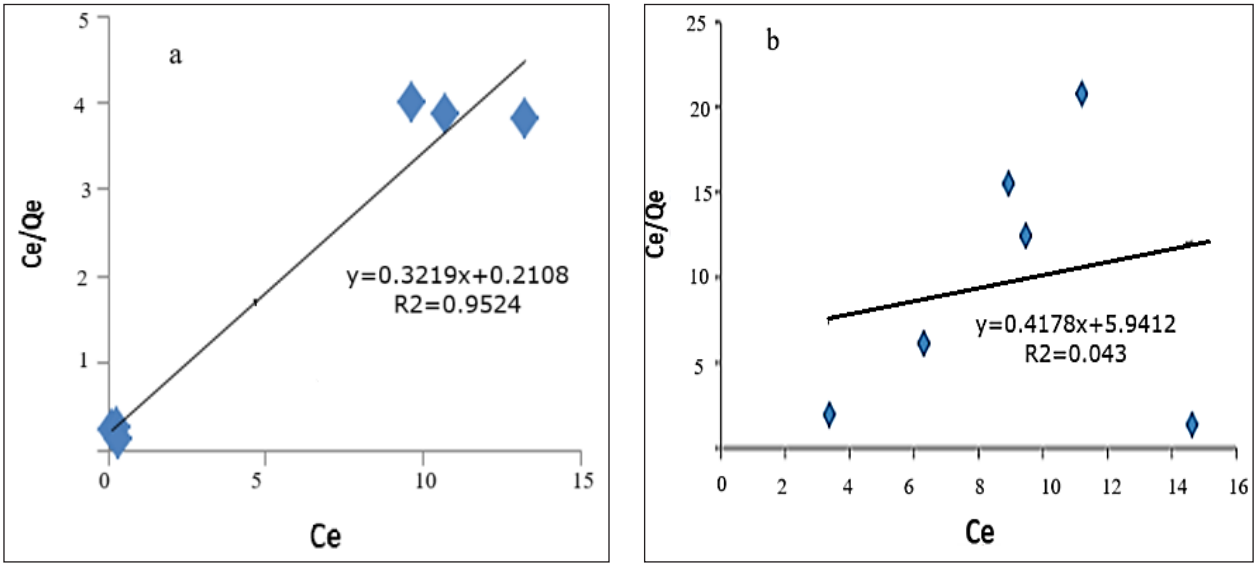

Fig. 14. The linear relationship of the Langmuir isotherm for adsorption a) MG b) TB

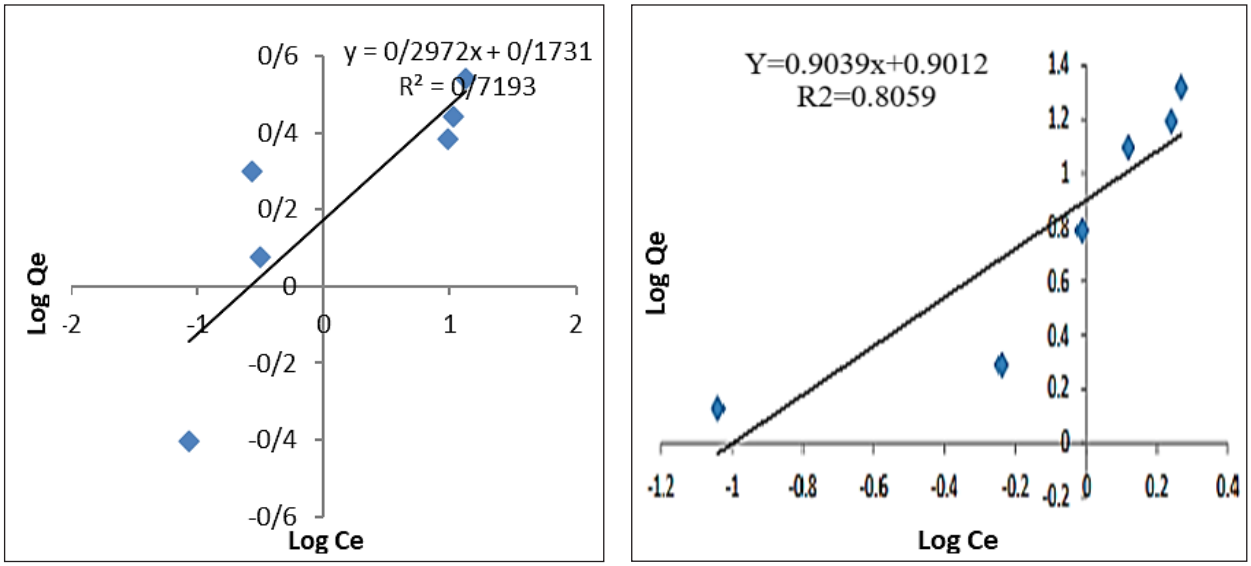

Fig. 15. The linear relationship of the Freundlich isotherm (MG, left) and (TB, right) dye adsorption

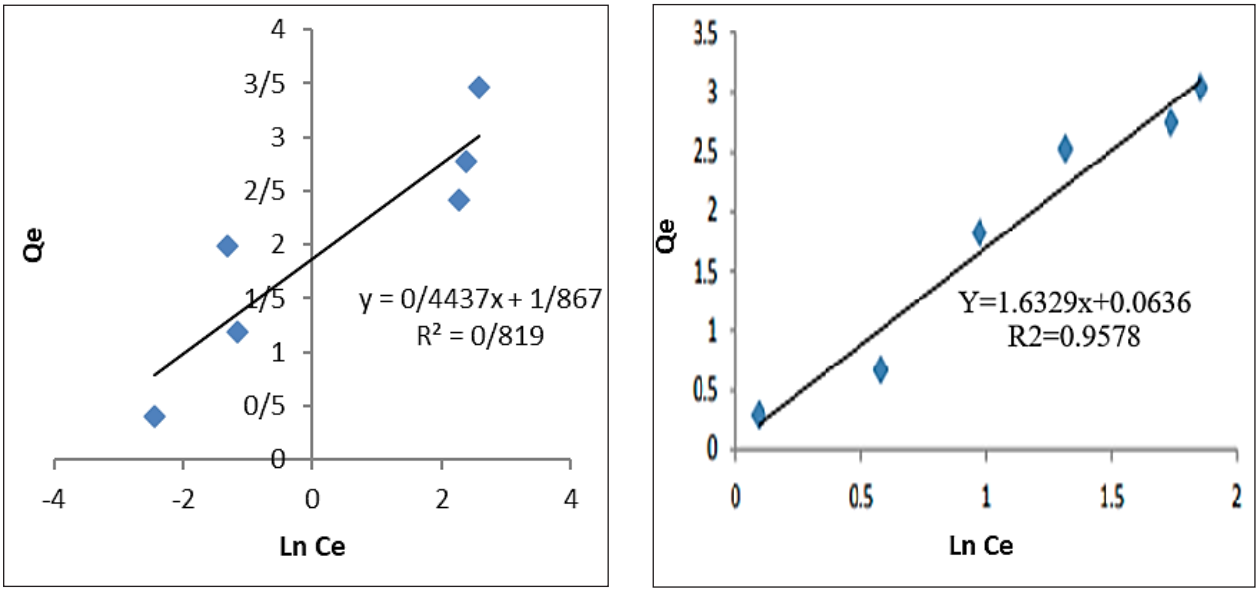

Fig. 16. The linear isotherm relationship enables adsorption for MG(Left) and TB (Right)

Table 5. The removal efficiency (RE%) of various adsorbents for the removal of MG and TB from aqueous solutions

Adsorbents	RE for MG	RE for TB	References
Remnants of tea leaf	---	96 %	29
Walnut shells	99.5 %	---	30
Chitosan-zinc oxide	98.5 %	---	31
Activated carbon (Rumex abyssinicus)	95.2 %	---	32
MgO nano-composite	92 %	---	33
TiO_2 nano-composite	---	99.6 %	34
Gum Arabic / acrylamide hydrogel	---	60 %	35
This work	99.65 %	98.07 %	---

4. Conclusion

The results showed limestone's high efficiency in removing malachite green dye and toluidine blue dye from aqueous solutions. This method is environmentally friendly and characterized by ease and low cost due to the availability of adsorbent surfaces in large quantities. The removal efficiency of malachite green dye was 99.65% at 2.5 g, pH=7, an equilibrium time of 40min, a particle size of 300 µm, and a temperature of 303°K. In addition, the removal effeciency for 4 g of toluidine blue dye was obtained at 98.07% (pH=10). Also, the equilibrium time of 40 minutes, a granular size of 300 µm, and a temperature of 298°k were obtained for TB dye. The recovery, RSD%, and absorption capacity of limestone for toluidine blue for malachite green were obtained at (98.8, 1.4%, and 1.98 mg g^{-1}) and (96.1, 0.89%, and 0.55 mg g^{-1}), respectively.

5. Acknowledgements

This research was obtained by the College of Education for Women, Department of Chemistry Northern, University of Anbar.

5. References

[1] R.M. Jihad, Determination of some heavy metals in selected cosmetic products sold at Iraqi markets, System. Rev. Pharm., 11 (2020) 1632-1635. https://www.sysrevpharm.org

[2] S. Teinmoori, H. Shirkhanloo, A.H. Hassani, M. Panahi, N. Mansouri, An immobilization of aminopropyl trimethoxysilane-phenanthrene carbaldehyde on graphene oxide for toluene extraction and separation in water samples, Chemosphere, 316 (2013) 137800. https://doi.org/10.1016/j.chemosphere.2023.137800

[3] S. Teinmoori, A.H. Hassani, M. Panahi, N. Mansouri, Rapid extraction of BTEX in water and milk samples based on functionalized multi-walled carbon nanotubes by dispersive homogenized-micro-solid phase extraction, Food Chem., 421 (2023)136229. https://doi.org/10.1016/j.foodchem.2023.136229

[4] S. Teinmoori, M. Panahi, N. Mansouri, New toluene extraction from water samples based on nano-carbon structure before determination by gas chromatography, Int. J. Environ. Sci. Technol., 20 (2023) 6589–6608. https://doi.org/10.1007/s13762-023-04906-9

[5] R. Ashouri, H. Shirkhanloo, A.M. Rashidi, A. Mirzahosseini, N. Mansouri, Dynamic and static removal of benzene from air based on task-specific ionic liquid coated on MWCNTs by sorbent tube-headspace solid-phase extraction procedure, Int. J. Environ. Sci. Technol., 18 (2021) 2377-2390. https://doi.org/10.1007/s13762-020-02995-4

[6] J. Rakhtshah, N. Esmaeili, A rapid extraction of toxic styrene from water and wastewater samples based on hydroxyethyl methylimidazolium tetrafluoroborate immobilized on MWCNTs by ultra-assisted dispersive cyclic conjugation-micro-solid phase extraction, Microchem. J., 170 (2021) 106759. https://doi.org/10.1016/j.microc.2021.106759

[7] A.K. Alsukaibi, Various approaches for the detoxification of toxic dyes in wastewater, Process., 10 (2022) 1968. https://doi.org/10.3390/pr10101968

[8] M. Berradi, R. Hsissou, M. Khudhair, M. Assouag, O. Cherkaoui, A. El Bachiri, A. El Harfi, Textile finishing dyes and their impact on aquatic environs, Heliyon, 5 (2019) e02711. https://doi.org/10.1016/j.heliyon.2019.e02711

[9] N.P. Raval, P.U. Shah, N.K. Shah, Malachite green a cationic dye and its removal from aqueous solution by adsorption, Appl. Water Sci., 7 (2017) 3407-3445. https://doi.org/10.1007/s13201-016-0512-2

[10] S. Srivastava, R. Sinha, D. Roy, Toxicological effects of malachite green, Aquat. Toxicol., 66 (2004) 319-329. https://doi.org/10.1016/j.aquatox.2003.09.008

[11] H. Tsade Kara, S.T. Anshebo, F.K. Sabir, G. Adam Workineh, Removal of methylene blue dye from wastewater using periodiated modified nanocellulose, Int. J. Chem. Eng., 2021 (2021) 965452. https://doi.org/10.1155/2021/9965452

[12] L. Vutskits, A. Briner, P. Klauser, E. Gascon, A.G. Dayer, J.Z. Kiss, D.R. Morel, Adverse effects of methylene blue on the central nervous system, J. Am. Soc. Anesthesiol., 108 (2008) 684-692. https://doi.org/10.1097/ALN.0b013e3181684be4

[13] I.A. Al-Jarjary, Study the factors affecting the adsorption of same azo dyes complexes and calculations of the thermodynamic functions, MSc Thesis, Mosul University, 2005. https://sciences.uodiyala.edu.iq

[14] R.S. Al-Khalisy, A.M.A. Al-Haidary, A.H. Al-Dujaili, Aqueous phase adsorption of cephalexin onto bentonite and activated carbon, Sep. Sci. Technol., 45 (2010) 1286-1294. https://doi.org/10.1080/01496391003689017

[15] C. Bellmann, Surface modification by adsorption of polymers and surfactants, Polymer Surfaces and Interfaces: Characterization, Modification and Applications, Springer, Berlin, Heidelberg, pages 235-259, 2008. https://doi.org/10.1007/978-3-540-73865-7_12

[16] G.M. Al-Senani, F.F. Al-Fawzan, Study on adsorption of Cu and Ba from aqueous solutions using nanoparticles of Origanum (OR) and Lavandula (LV), Bioinorg. Chem. Appl., 2018 (2018) 936178. https://doi.org/10.1155/2018/3936178

[17] D. Farrington, Experimental Physical Chemistry, Mcgraw Hill Book Company Inc., 7th edition, 1970. https://www.amazon.ca/Experimental-Physical-Chemistry-Farrington-Daniels/dp/0070153396

[18] M.N. Rashed, Adsorption technique for the removal of organic pollutants from water and wastewater, Organic pollutants-monitoring, risk and treatment, Intech Open Publisher, 7 (2013) 167-194. https://doi.org/10.5772/54048

[19] J.A. Naser, F.A. Al-ani, I.M. Radhi, T.A. Himdan, Kinetic study of Malachite green dye adsorption on poly aniline-formaldehyde/chitosan composite, IOP Conf. Ser.: Mater. Sci. Eng., 928 (2020) 052005. https://doi.org/10.1088/1757-899X/928/5/052005

[20] F.F. Ali, A.S. Al-Rawi, A.M. Aljumialy, Limestone residues of sculpting factories utilization as sorbent for removing Pb (II) ion from aqueous solution, Results Chem., 4 (2022) 100621. https://doi.org/10.1016/j.rechem.2022.100621

[21] R.S. Hwidi, T.N. Izher, F.N. Saad, Characterization of limestone as raw material to hydrated lime, E3S web of conferences, Int. Conf. Civil Environ. Eng., 34 (2018) 02042. https://doi.org/10.1051/3sconf/20183402042

[22] K.V. Kumar, Optimum sorption isotherm by linear and non-linear methods for malachite green onto lemon peel, Dyes Pigm., 74 (2007) 595-597. https://doi.org/10.1016/j.dyepig.2006.03.026

[23] S. Wadhawan, A. Jain, J. Nayyar, S.K. Mehta, Role of nanomaterials as adsorbents in heavy metal ion removal from waste water: A review, J. Water Process Eng., 33 (2020) 101038. https://doi.org/10.1016/j.jwpe.2019.101038

[24] H. Herna ndez-Cocoletzi, R.A. Salinas, E. A guila-Almanza, E. Rubio-Rosas, W.S. Chai, K.W. Chew, Natural hydroxyapatite from fishbone waste for the rapid adsorption of heavy metals of aqueous effluent, Environ. Technol. Innov., 20 (2020) 101109. https://doi.org/10.1016/j.eti.2020.101109

[25] H.A. Chanzu, J.M. Onyari, P.M. Shiundu, Brewers' spent grain in adsorption of aqueous Congo Red and malachite Green dyes: Batch and continuous flow systems, J. Hazard. Mater., 380 (2019) 120897. https://doi.org/10.1016/j.jhazmat.2019.120897

[26] A.M. Rashidi, A. Vahid, Arsenic speciation based on amine-functionalized bimodal mesoporous silica nanoparticles by ultrasound assisted-dispersive solid-liquid multiple phase microextraction, Microchem. J., 130 (2017) 137-146. https://doi.org/10.1016/j.microc.2016.08.013

[27] Y. Dai, D. Zhang, K. Zhang, Nitrobenzene-adsorption capacity of NaOH-modified spent coffee ground from aqueous solution, J. Taiwan Inst. Chem. Eng., 68 (2016) 232-238. https://doi.org/10.1016/j.jtice.2016.08.042

[28] M. Arjomandi, A review: analytical methods for heavy metals determination in environment and human samples, Anal. methods. Environ. Chem. J., 2 (2019) 97-126. https://doi.org/10.24200/amecj.v2.i03.73

[29] F.F. Ali, Adsorption of Toluidine blue dye from industrial wastewater on the remnants of tea leaf, Int. J. Chem. Tech. Res., 10 (2017) 497-506. https://www.sphinxsai.com/2017/ch_vol10_no3/abstracts/A(497-507)V10N3CT.pdf

[30] L.A. Ali, A.S. Farhood, F.F. Ali, Technique of batch adsorption for the elimination of malachite green dye from industrial waste water by exploitation walnut shells as sorbent, Indones. J. Chem., 17 (2017) 211-218. https://doi.org/10.22146/ijc.23063

[31] V.M. Muinde, J.M. Onyari, B. Wamalwa, Adsorption of malachite green dye from aqueous solutions using mesoporous chitosan-zinc oxide composite material, Environ. Chem. Ecotoxicol., 2 (2020) 115-125. https://doi.org/10.1016/j.enceco.2020.07.005

[32] M. Abewaa, A. Mengistu, T. Takele, Adsorption removal of malachite green dye from aqueous solution using Rumex abyssinicus derived activated carbon, Sci. Rep., 13 (2023) 14701. https://doi.org/10.1038/s41598-023-41957-x

[33] M.T. Hamed, Optimization study of the adsorption of malachite green removal by MgO nano-composite, nano-bentonite and fungal immobilization on active carbon using response surface methodology and kinetic study, Environ. Sci. Eur., 35 (2023) 26. https://doi.org/10.1186/s12302-023-00728-1

[34] D. Venkatesan, S. Um1sankar, V.L. Mangesh, Removal of Toluidine blue in water using green synthesized nanomaterials, South Afr. J. Chem. Eng., 45 (2023) 42-50. https://doi.org/10.1016/j.sajce.2023.04.006

[35] S. Jabeen, S. Alam, L.A. Shah, Removal of safranin-T and toluidine from water through gum Arabic /acrylamide hydrogel, Adsorp. Sci. Technol., 2022 (2022) 6100791. https://doi.org/10.1155/2022/6100791

Anal. Methods Environ. Chem. J. 7 (3) (2024) 127-158

AMECJ

Research Article, Issue 3
Analytical Methods in Environmental Chemistry Journal
Journal home page: www.amecj.com/ir

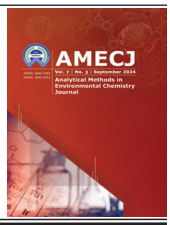

Analysis of pesticides in food: A review of applications on molecularly imprinted polymer nanoparticles by chromatographic methods

Ahmed Qasim Abdulhussein[*, a]

[a] *Department of Chemistry, Faculty of Science, University of Malaya, Kuala Lumpur, Malaysia*

ARTICLE INFO:

Received 25 Apr 2024
Revised form 5 Jul 2024
Accepted 17 Aug 2024
Available online 30 Sep 2024

Keywords:
Pesticides,
Analysis,
Molecularly imprinted polymers,
Food samples,
Ultra-high performance liquid chromatography-MS/MS,
Gas chromatography-mass spectrometry

ABSTRACT

Insecticides may build up in food and the environment, where even in deficient quantities, they can have a negative impact on ecosystems and human health. As a result, it's critical to establish a sensitive and trustworthy system for monitoring pesticides to ensure the safety of food and human health. On the other hand, chemical residues from controlling outbreaks in neighboring crop fields may degrade the quality of the food. Additionally, pesticides in the food matrix may signal environmental pollution. It is necessary to utilize extremely sensitive and selective procedures since many pesticides can be found simultaneously and because the amounts of these chemicals in food are often relatively low. Molecularly imprinted polymer nanoparticles (MIPs) were used as a sample preparation technique, and liquid or gas chromatography coupled to mass spectrometry (LC/GC-MS) was reported as the most important analytical technique. In this review, I present and discuss recent studies on the determination of pesticides in food matrices, with a particular emphasis on the use of molecularly imprinted polymer nanoparticles (MIP) for sample preparation and separation of pesticides in food matrices, followed by chromatographic analytical methods for detection such as Ultra-high performance liquid chromatography-MS/MS (UHPLC-MS/MS). Additionally, future perspectives and trends are also provided.

1. Introduction

The usage of pesticides has dramatically grown during the last few decades [1-3]. While using these materials aids in agriculture, many of them are found outside of the intended species, potentially contaminating food, water, and soil. Numerous pesticides, some of which have been linked to cancer, may cause dye functions in the brain and reproductive systems, even at low concentrations [1, 2, 4]. Therefore, the threats to food safety posed by the usage of these substances are a continual source of worry for people worldwide [5, 6]. Since World War II, there has been a rise in the use of pesticides in agriculture to enhance the global food supply. A wide range of pesticides from various organizations has developed considerably since then. The substances and their metabolites are found in all parts of the environment, including the air, water, and soil, as well as in crops, vegetables, and fruits. As a result, the use of pesticides and additional environmental harm caused by industrial emissions during pesticide manufacture [7]. Pesticides are among the most dangerous compounds that can be discovered in the environment. Due to their toxicity,

*Corresponding Author: Ahmed Qasim Abdulhussein
Email: ahmed.kosofi@yahoo.com
https://doi.org/10.24200/amecj.v7.i03.329

accumulation, and extensive natural persistence, they can contaminate fruits, vegetables, and waterways [8]. Their ability to cause cancer, birth defects, neurotoxicity, and neurobehavioral issues makes their presence in water considered a potential threat to both human health and ecosystems [9]. Hazardous pesticide residue levels must be controlled to protect public health and prevent pesticides from entering the environment, waterways, and food chains [10]. However, it is challenging to determine the exact quantities of pesticides in the environment and food due to their considerable regional fluctuation. Furthermore, government data regarding food contamination by pesticides is lacking in several countries. [11]. One of the most commonly utilized types of pesticides is organophosphorus insecticides. This class of pesticides affects both humans and animals. Esterases' toxicological effects are linked to their irreversible inactivation. [12]. Neonicotinoids are systemic insecticides that permeate all parts of the treated plants, including their pollen, nectar, guttation fluids, and the food those plants produce. They were developed to take the role of pesticides like organophosphate and carbamate [13]. These chemicals find essential applications in horticulture, wood conservation, vector control for pets and livestock, urban and residential pest control, and pest control for hundreds of crops in agriculture [14]. They are very efficient against difficult-to-observe sucking, boring, or feeding insects [15]. Unlike most other pesticides, neonicotinoids cannot be eliminated by washing food before consumption [16]. Neonicotinoids are less harmful to birds, animals, and insects than organophosphate and carbamate insecticides. Additionally, insects can be harmed by some breakdown products [17, 18]. Determining pesticide residues in complex samples (biological, dietary, environmental, etc.) requires careful sample preparation before instrumental analysis. Solid-phase extraction (SPE) [19, 20], liquid-liquid extraction (LLE) [21], and QuEChERS (rapid, easy, cheap, effective, robust, and safe) [22] are the most widely used methods for extracting pesticides. Magnetic dispersive solid-phase extraction (MDSPE), one of the SPE methods, has benefits over other methods. The sorbents may be quickly and easily separated using an external magnet rather than centrifugation and filtering. This allows for a fast and easy extraction procedure. Recently, some magnetic nanoparticles from various matrices, including Fe_3O_4 [22-25], $ZnFe_2O_4$ [26], $NiFe_2O_4$ [27], and GO [28], have been created for the MDSPE of organophosphates and neonicotinoids as shown in Table 1. Magnetic mixed metal hydroxide (MMH), in addition to the materials listed above, is currently regarded as an appealing magnetic material due to its ease and speed of manufacture, structural stability, and favorable magnetic characteristics [29]. Since MDSPE's extraction effectiveness depends on the sorbent material's affinity for the target analyte, adding certain functional groups to the materials might increase selectivity. Various techniques, including high-performance liquid chromatography (HPLC) [30, 31], gas chromatography-mass spectrometry (GC-MS/MS) [32, 33], and liquid chromatography-tandem mass spectrometry (LC-MS/MS) [34-36] have been used in the past to analyze pesticides. The most popular of these techniques is LC-MS/MS. To maintain their high sensitivity, routine analyses of pesticides in environmental waters need to be quicker, cheaper, and have a lower detection limit than what is now practiced. Scanner electron microscopy (SEM), Fourier transform infrared (FTIR) spectroscopy, vibrating sample magnetometer (VSM), and X-ray diffraction (XRD) were used to characterize the resulting magnetic MIPs [37]. MIPs are synthetic polymeric substances with recognition sites created intentionally and can selectively rebind a target molecule [38, 39]. MIPs are promising candidates for applications in various fields, such as diagnosis/drug delivery, sensors, catalysts, chromatographic-based separation, and sample pretreatment/preparation [40-42]. This is due to their benefits, such as simple preparation, good stability, low cost, high selectivity, sensitivity, chemical inertness, solubility in water and most organic solvents, and physical robustness. Conventional strategies for MIP production require large amounts of organic or toxic solvents. They also

require significant amounts of time and energy. To overcome these challenges, molecular imprinting technologies (MITs) based on green chemistry principles have been applied to develop novel MIPs[43]. Creating a MIP is based on the cross-linking agent and a functional monomer being chemically polymerized together in the presence of a template molecule (Fig. 1). An imprinted polymer is produced after the imprinted molecule has been eliminated. This polymer's structure and the functional groups' position on the monomer units produce high-affinity sites for the template molecule. The polymerization occurred between the functional monomer and templates (pesticides) via hydrogen-bonding interaction between the nitro, amino, or cyano groups in templates and the O–H groups in the functional monomer. Thus, it is simple to extract and clean pesticide residues from the determined matrices. MIPs have been proven to help develop sensors specific to desired analytes of interest and in enantiomeric separations, catalysis, solid-phase extraction, drug delivery, and chromatography [44-46]. Recently, Arabi et al. (39) offered 14 criteria for green MITs that might be remembered using the word "GREENIFICATION" as a mnemonic device. These guidelines include producing the least amount of trash possible, employing environmentally friendly, renewable chemicals, creating quicker imprinting times, and extending the usage of solvent-free imprinting techniques. Using dummy-template or multi-template molecules, bio-based monomers, ionic liquids, deep eutectic solvents, pure aqueous porogen, and ultrasound- or microwave-assisted reactions are other examples of green techniques [40, 41, 47, 48]. Bagheri et al. created fake MIPs for the MSPE of acrylamide in food samples utilizing propanamide and chitosan as dummy templates and bio-based functional monomers, respectively. The polymerization was accomplished at room temperature without using organic solvents [49]. This new MIP's quick equilibrium kinetics and high adsorption capacity decreased the analysis time and increased the aqueous applicability.

In this context, this review aims to present and discuss the studies published between 2017 and 2023 dealing with pesticide determination in the food matrix. Particular focus was given to MIPs sample preparation methods and separation/detection application of the developed methods worldwide.

2. Molecular Imprinting Technology (MIT)

Molecular imprinting technology (MIT) has created considerable interest in various applications, including chromatographic separation, catalysis, biosensors, and synthetic antibodies. Molecular imprinting is a well-established and straightforward method for creating molecularly imprinted polymers (MIPs) [48] as a result of the demand for fast, reliable, and cost-effective analytical procedures to ensure food protection, molecularly imprinted polymers (MIPs) as attractive materials have garnered considerable attention. They can be designed specifically to bind template target molecules with high selectivity. MIPs are synthesized by concurrently polymerizing functional monomers and cross-linkers in the presence of template target molecules. Following the removal of template target molecules, recognition cavities in the highly cross-linked polymer matrix are developed complementary in shape, size, and spatial arrangement to the template molecules [50]. MIPs have significantly advanced food analysis due to their unique properties. MIP is a frequently used

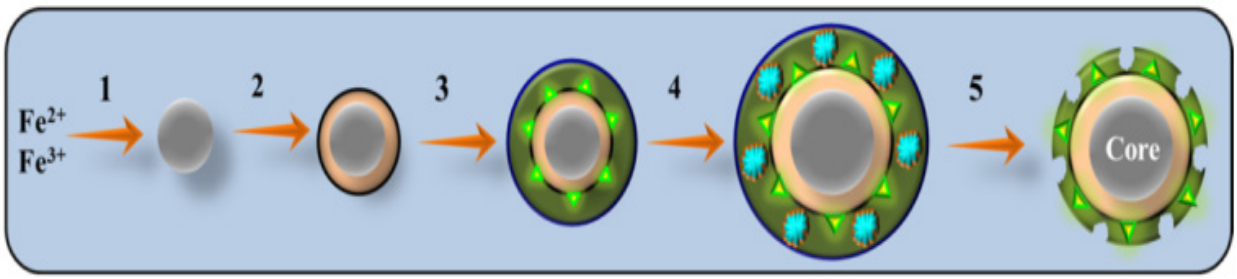

Fig. 1. Magnetic MIP nanoparticles-based extraction method [50]

technique in the field of sample preparation. Because of the complicated interactions between food matrix components and trace levels of target compounds, the output of analytical instruments is highly dependent on the sample treatment method. However, this is a component of analysis development that is commonly disregarded. To support the analysis of food samples, researchers must develop applicable sample preparation methodologies. MIPs have been used to prepare samples as sorbents [40]. Compared to conventional adsorbents such as C18 silica gel, MIPs have many evident advantages, including improved loading capacities, enhanced selectivity, and higher recovery performance during the retention procedure. Numerous studies have repeatedly demonstrated that using MIPs to prepare food samples can result in significant detection limits and recoveries. Until now, the majority of cases have included the use of MIPs in conjunction with traditional sample preparation procedures such as solid-phase microextraction (SPME) and solid-phase extraction (SPE) [51]. Recent improvements in MIPs combined with magnetic bead extraction have greatly improved sample processing and pre-treatment methods, enabling the integration of sample preparation with new analysis equipment such as biosensing/microfluidic platforms [52]. While MIP technology has tremendous potential for food analysis, commercial success has been relatively limited thus far. Only a few commercial examples of MIPs are utilized as sample preparation adsorbents, and no MIP-based biosensors are commercially available. Various challenges have limited the commercialization of MIPs, including incomplete template deletion, insignificant selectivity, and limitations in mass-producing MIPs. Efficient methods for preparing MIPs should be established to allow MIPs to significantly improve properties and accelerate the adoption of MIPs methods in the food sector [53].

3. Molecular Imprinting Methods

3.1. Synthesis of MIPs

MIPs can be created in several ways. The most frequent imprinting is non-covalent imprinting, where interactions between templates and functional monomers in a per-polymerization mixture are established, as illustrated in (Fig. 2) [54]. Non-covalent imprinting technologies include bulk polymerization, precipitation polymerization, core-shell imprinting, mini-emulsion polymerization, and solid-phase imprinting. The imprinting technique selected will depend on the kind of template used, the size and form of the desired MIP, such as (nanoparticles, thin films, etc.), and the planned application of the MIP as well as in the creation of food samples[55]. It is usually produced in bulk before applying the MIPs approach to a solid-phase structure. In contrast, MIP-based biosensors frequently apply thin layers to the sensor's surface. While non-specific binding should be minimized, MIPs with many binding sites and an enormous surface area are ideal for both purposes [54]. Due to its simplicity, bulk polymerization is the most often utilized procedure for creating MIP sorbents for sample extraction. However, the method produces particles with no binding sites and high batch-to-batch variation [44, 56]. The method is also complicated to process, includes many templates, and is vulnerable to template leakage. Due to their improved, well-defined size and surface-area-to-volume ratio, MIP nanoparticles are now being developed with a focus on biosensors, food, and sample preparation [57]. Precipitation polymerization is a practical method for imprinting nanoparticles, established through monomer research. It makes it possible to create pure nanoparticles, has control over particle size, and has high yields [40]. The method uses a cross-linker and diluted monomer solution to dilute the template, producing a high dilution factor. MIP gradually precipitates out of the solution after synthesis. Precipitation polymerization permits the imprinting of biomolecules like proteins in a tiny quantity of surfactant. However, the method is limited to great abundance templates [58]. The creation of MIPs has demonstrated the flexibility of emulsion polymerization. This method emulsifies the template, cross-linkers, and functional monomers in an aqueous phase. The dispersion phase is subsequently stabilized by restricting diffusion through the continuous phase and creating tiny, stabilized homogeneous-sized emulsion droplets.

High yields of monodispersed nanoparticles are produced by the process, although limited binding capacity might result from surfactant residues that prevent the analyte from being recognized upon rebinding [59]. Polymerization utilizing a solid phase effectively imprints minute molecules, endotoxins, and even whole viruses. Before chemical or photo-induced polymerization, the template compound is mixed with the monomers, initiator, and cross-linker and attached to a solid support, frequently glass beads or silica gel with a diameter of up to 1 m [60]. The method provides various significant benefits over existing methods for producing MIP nanoparticles. This concerns how easily the template can be removed, allowing it to be reused for more reactions. The resultant MIPs nanoparticle is also monoclonal, creating just one or two recognition sites per nanoparticle. Also, the technique may be used as an affinity column to distinguish between MIPs with a high affinity and those with a low affinity or those that are not imprinted [61]. Many other linker chemistries may be used to join the template to the support. For instance, MIPs for trypsin were created by covalently bonding the protein to its inhibitor and p-amino benzamidine in a glass bead template, as displayed in (Fig. 3) [62]. Compared to the binding cavity, this caused the MIPs nanoparticles to have a more consistent size and orientation. The huge surface area of the nanoparticles allows for rapid MIP binding kinetics and makes it easier for the analyte to get to the MIP. Moreover, adding a shell layer or changing the surface of nanoparticles might lessen their tendency to aggregate. Besides, the core of the imprinted nanoparticle may be composed of any precursor nanoparticles, including silicon oxide, iron oxide (magnetite), quantum dots, or polymers, which can give MIP nanoparticles extra functionality [63]. Pérez-Moral et al. (2007) devised the surface-initiated live radical polymerization approach to imprinting an MIP with a polymer-based core [64]. Magnetic nanoparticles were formed via iron chloride coprecipitation, resulting in magnetic core nanoparticles. After that, a SiO_2 shell layer was created by salinizing with tetraethyl orthosilicate (TEOS). The MIP layer was then grafted onto the core shell to allow biotin binding [60]. The ease with which these nanoparticles may be removed from food matrixes has boosted interest in using molecularly imprinted magnetic core-shell nanoparticles for effective sample separation. Quantum dots are commonly used as a substrate for molecular imprinting to create fluorescence-based sensors [65]. The core nanoparticles for imprinting are likewise silver and gold nanoparticles. MIPs made of silica and containing silver nanoparticles were developed to use the unique optical properties of silver nanoparticles, known as metal-enhanced fluorescence [66]. A core for imprinting MIPs can also be made of gold nanoparticles because of their unique UV absorbance properties, as shown in (Fig. 4) [67]. Core-shell imprinted polymers that include numerous functional components have shown promise by combining the distinctive qualities of many nanoparticle systems. Han et al. 2014 developed hybrid Fe_3O_4-CdTe quantum dot core-shell imprinted nanoparticles capable of detecting and binding 4-nonylphenol. The scientific community has been attracted to hollow shell imprinting, in which the particle's center is extracted after imprinting [68]. Several research groups have focused on methods for imprinting thin films. They are beneficial in biosensors like electrochemical sensors, where the surfaces may be produced by electro-polymerization. In situ, electro-polymerization is a form of electrode surface imprinting [69]. One notable advantage of this technology is that it allows for fine control of the polymer thickness via different factors, such as current density and applied voltage, resulting in a more uniform coating of the MIP on the electrode surface [70]. The polymer deposition region may also be accurately controlled. Combining an electrochemical transducer with non-conducting imprinted polymers can be accomplished by in situ electro-polymerization of monomers in the presence of aniline or ethylene-dioxy thiophene. On the other hand, electro-spraying or spin coating can immobilize the imprinted polymers on the electrode's surface. Other imprinted polymers, such as nanoparticles, can be linked via carbon electrode paste, ink casting, gels, and membranes [71].

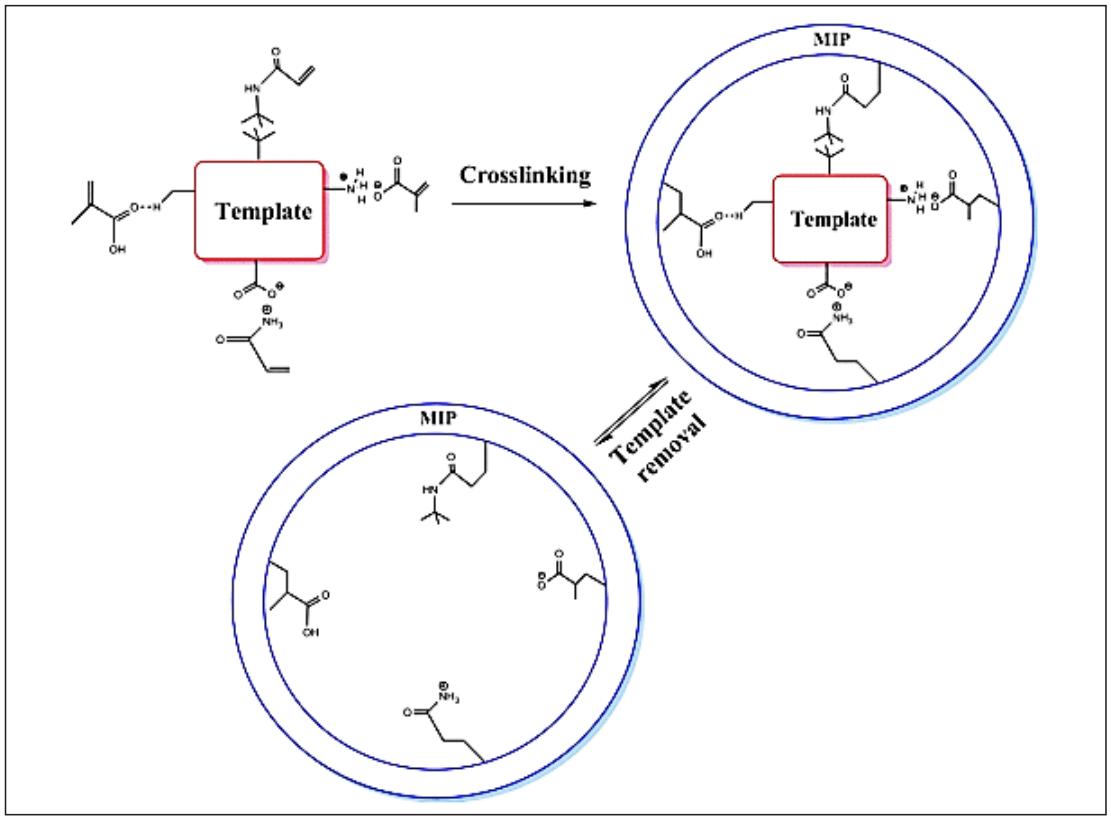

Fig. 2. Synthesis of molecular imprinting polymer nanoparticles [50]

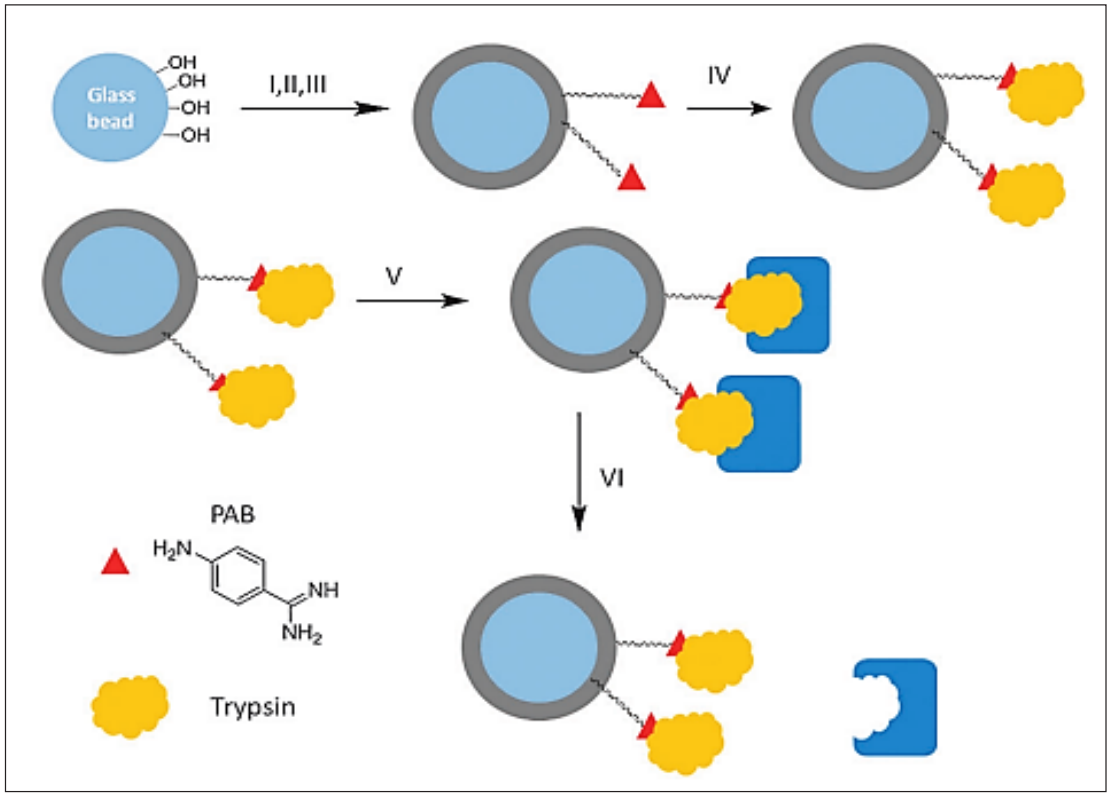

Fig.3. Schematic representation of the solid-phase synthesis of MIP-NPS. I: 3-Aminopropyl)triethoxysilane (APTES); II: glutaraldehyde; III: p-aminobenzamidine (PAB); IV: trypsin; V: pre polymerisation mixture; VI: release of thermoresponsive MIP-NPS (temperature change from 37 ̊C to room temperature) [59].

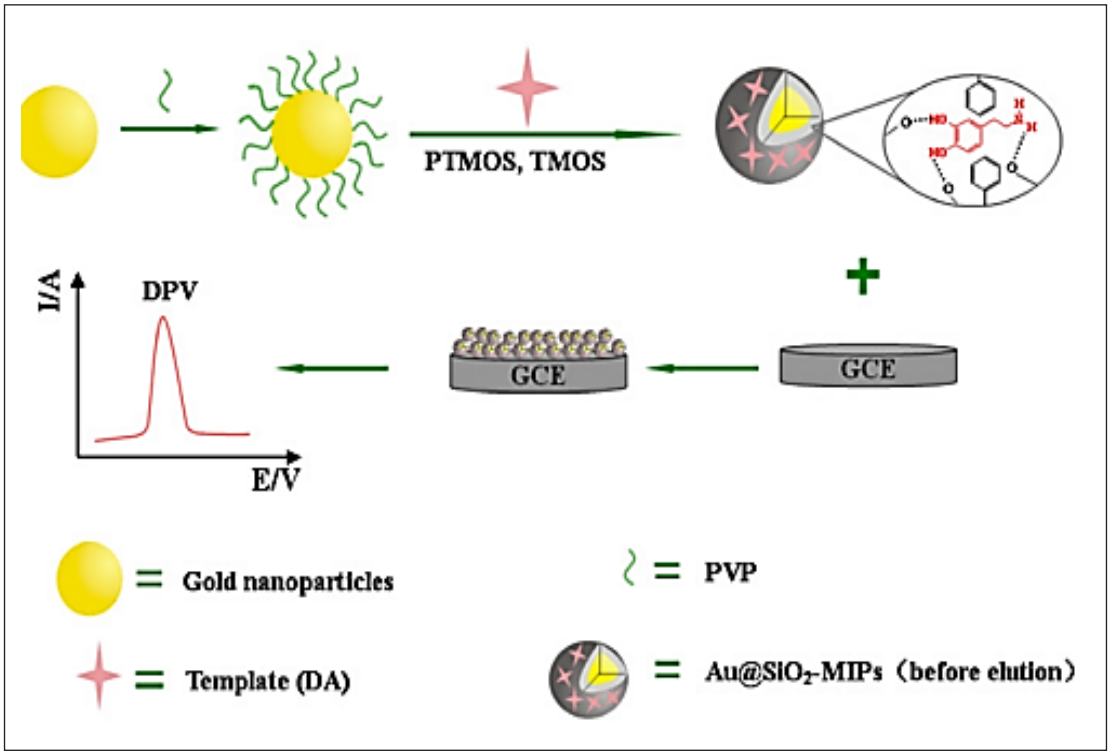

Fig. 4. Preparation procedure of the AuNPs@SiO_2-MIPs [64]

3.2. Design of MIPs

MIP development for new templates is often time-consuming and involves trial and error. Numerous experimental factors must be examined, including the shape and concentration of the monomer, the template, and the cross-linker [72]. When using temperature-responsive monomers or temperature-sensitive templates, it is equally necessary to examine the temperature at which the polymerization was carried out. MIPs have been designed using chemometrics, molecular modeling, combinatorial techniques, and experimental methods [73]. Chemometric-based design approaches have been shown on a variety of templates. It focuses on statistical analysis, allowing MIPs to be generated from the results of experiments. By simulating essential imprinting parameters, molecular modeling has become prominent as a technique for rationally constructing MIPs [74]. For example, a model including Monte Carlo simulations and analytical data was given to establish MIPs rationally [73]. The binding energy was calculated using the Hawtree Flock technique, which led to the selection of methacrylic acid as the monomer and ethylene glycol dimethyl acrylate as the cross-linker for imprinting [75]. Hawari et al. (2013) utilized 3D simulation to assess the binding of several monomers to pinene, a volatile substance emitted by ripening mangos [76]. Using computational chemistry in MIP design can speed up MIP synthesis with fewer reagents. On the other hand, it is still difficult to effectively simulate larger macromolecules. In 2011, researchers used molecular docking, one of the few examples of macromolecule MIP modeling, to simulate macromolecule-monomer interactions [77].

3.3. MIP characterization

The possibility of an MIP is associated with certain cavities that encourage a high level of contact with the intended insecticides. In most works, a non-imprinted polymer (NIP) is synthesized under identical circumstances as the MIP but without the template [78]. This control polymer has no imprint and is investigated in parallel with the MIP characterization. Because the same monomers, porogen, and interactions are used, the nature of the interactions formed between an MIP and a template

is the same as that between an NIP and a template. The difference between the two sorbents is the strength of these interactions. The strength of the interactions is more significant on the MIP than on the NIP if well-defined cavities are formed during the polymerization process because the template can be held by various sites (sum of the interactions) owing to the spatial complementarities between the template and the cavities [79]. The initial assessment of the synthesized MIPs may involve describing the surface of the MIP/NIP by SEM in terms of the form and size of the particles [80]. The porosity of MIP/NIP may also be determined and compared using the BET adsorption technique. The optimal monomer, the template/monomer ratio, and other parameters were chosen using binding assays that include introducing a specified quantity of MIP/NIP in the presence of a known amount of an OPP and then measuring, after a determined period, the amount retained by the MIP and the NIP [81]. In these circumstances, the solvent utilized is extremely near to or identical to the solvent used for polymer synthesis, promoting the same interactions as those generated during the polymerization process to create the imprint. The adsorption isotherm obtained from these binding studies also permits the number of binding sites and their affinity towards the template molecules and, in certain circumstances, structural analogs to be defined to be calculated using different models (Langmuir, Freundlich, Langmuir-Freundlich) [82]. Binding tests were also performed in a pure solvent that was highly comparable to the nature of the sample matrix, such as aqueous buffer, pure water, or acetonitrile, for further study of pesticides in aqueous or acetonitrile vegetable extracts, respectively [83, 84] as presented in Table 2. These binding examines were also conducted in heptane, the solvent used to dilute oil samples [85]. This method provides a more accurate assessment of the retention potential and selectivity that may be expected in actual samples. Similarly, by performing binding examinations on multiple solvents, the solvent with the best selectivity may be chosen to dilute the sample or sample extracts [86]. On the other hand, in the SPE technique [87], the solvent that provides the lowest affinity can be selected as the eluting medium. HPLC measurements were also used to examine how the types of solvents affected the retention characteristics. This technique was employed to assess the solvent that facilitates retention and the selectivity towards various analogs [88].

4. Sample Preparation

Sample preparation is crucial in the process of conducting a chemical analysis. The best sample preparation methodology should be easy to use, effective, selective, affordable, and work with a variety of instrumental procedures [89]. Analyzing the sample directly in a chromatographic system is impossible because environmental samples have a very complex composition and include analytes at low concentrations. Isolation, concentration, and analyte purification (clean-up) are required steps in sample preparation. The selection of the sample preparation technique is influenced by the analyte's physicochemical characteristics (such as its acid-base properties, stability, volatility, and solubility in water and organic solvents), the sample's nature (such as its aggregate state, purity, fat, and oil content), and the analytical technique used to analyze the sample [52].

4.1. Sample Preparation in Pesticides Analysis

Pesticide residue analysis in foods entails sample preparation and instrumental determination. At the same time, analytical instruments continue to advance rapidly in technologies [90]. Typically, interferences from food matrices affect their detection limits, detector noise, and final quantification [91]. Thus, sample preparation is the bottleneck for performing an efficient and reliable study of trace pesticide residues. The sample preparation procedure is designed to separate trace amounts of analytes from various complex matrices while minimizing interferences from the food matrix. Sample collection/homogenization, extraction, and clean-up are common sample treatment steps. The separation and clean-up steps

are critical for successfully analyzing pesticide residues [90]. Liquid-liquid extraction (LLE) is possibly the oldest and most widely used of all sample preparation techniques. Before LLE, solid samples are mechanically ground, mixed, agitated, chopped, crushed, macerated, minced, pressed, or pulverized to produce fine and homogeneous particles. Repeated extractions with an immiscible organic solvent are performed on homogenized solid or liquid samples. Before the final analysis of extraction solvents and analytes, the extracts are centrifuged, concentrated, and purified using the similarity concept. Due to its simplicity, robustness, and performance, liquid-liquid extraction (LLE) is a well-established process for routine sample preparation [92]. Supercritical-fluid extraction (SFE) is a relatively new technology that utilizes supercritical fluids to extract target analytes from solid samples rapidly. Supercritical fluids can permeate the solid matrix and dissolve analytes because their physicochemical properties vary from liquid and gas phases. Thus, supercritical fluids may be used instead of organic solvents when preparing samples for pesticide residue analysis. Organic solvent modifiers are used to increase the polarity of extraction solvents to eliminate pesticide residues that are moderately polar or polar [93]. Since its introduction in the mid-1970s, solid-phase extraction (SPE) has been the most commonly used sample treatment process for insecticide residue analysis in food [51]. Before usage, the extract is passed through the cartridge and adsorbed on the solid phase components. It is then conditioned and activated with water and an organic solvent. After pre-washing with organic solvents, the interferences are removed while the analytes remain on the sorbents. Following this cleaning step, the target components can be eluted with additional organic solvents to yield extracts [19]. Due to the fact that SPE requires small solvent volumes, simple experimental procedures, quick sample processing, and standard experimental equipment, it has been widely accepted as a viable alternative to LLE for sample treatment methods, particularly for cleaning and enriching organic compounds water samples. SPE is typically conducted by selectively retaining target components on sorbent packed in a disposable extraction mini-column. Numerous sorbents have been created to clean/pre-concentrate pesticide residues in foods to ensure adequate analyte absorption [94]. A solid-phase micro-extraction (SPME) approach is another alternative to traditional sample preparation methods. Modern insecticide residue analysis patterns necessitate simplifying sample preparation and reducing operation time and organic solvent. Solid-phase micro-extraction (SPME) was initially introduced as an SPE invention that is widely commercialized nowadays. SPME, like SPE, depends on the equilibrium of the analyte partition between the stationary phase and the sample [52]. This means that the analytes are absorbed in the solid phase and then desorbed utilizing either the thermal energy generated by the GC injection port or the solvent elution of the HPLC mobile phase during the subsequent chromatographic determination. SPME is a sample preparation method incorporating sampling, extraction, concentration, and injection into a single step [95, 96]. SPME is a beneficial alternative analytical approach to many conventional procedures because it significantly reduces and complicates organic solvents. While SPME is capable of quickly obtaining equilibrium adsorption, it is affected significantly by matrix contaminants. Typically, the impacting variables of SPME have been optimized. In comparison to SPE, SPME is an automated, one-step, straightforward, and solvent-free extraction method. The primary advantages of SPME are its superior analytical efficiency and ease of use [97]. Additionally, it is free of the plugging and channeling issues associated with solid-phase extraction. However, SPME remains laborious, as achieving equilibrium between the fiber and the sample solution takes a long time and requires numerous strict extraction conditions. Additionally, the fibers used in SPME are expensive and sensitive [98]. A method known as liquid phase micro-extraction (LPME)) has been created for miniaturized liquid phase

extraction [99]. During the LPME, the target components are moved from an aqueous phase (also called donor phase) to several microliters of a water-insoluble solvent (also called extractant or acceptor) [100]. Based on the sample treatment method, the LPME of pesticides in foods may be classified into three basic categories: dispersive liquid-liquid micro-extraction (DLLME), hollow-fiber LPME (HF-LPME), and single-drop micro-extraction (SDME). Compared to standard sample preparation methods for pesticide analysis in food samples, the LPME approach removes the SPE phase, eliminates the clean-up step, simplifies the sample treatment process, minimizes solvent usage, and lowers the analysis cost [20]. The target molecules are frequently extracted and concentrated in a bit of injection solution to improve the sensitivity of the analysis. This uses a significant amount of organic solvent and necessitates lengthy laboratory methods and expensive equipment. In 1976, Watanabe and colleagues developed micelle-mediated extraction (MME) and cloud point extraction (CPE) to improve the extraction methods [101]. When non-ionic surfactants are concentrated above their critical micelle concentration, micelles develop, and they become cloudy at their cloud-point temperature, which is often higher than their critical temperature. The cloudy solution is then extracted into an aqueous and a surfactant-rich phase, the latter containing only small amounts of analytes. Due to the viscosity of the concentration analytes for chromatographic injection, they may be dissolved in a minimal volume of mobile phase or organic solvent. Since different surfactants have different extraction efficiencies, the surfactants must be optimized for adequate analyte extraction [101]. CPE has a range of benefits over other extraction methods. It is simple to use, requires only a small amount of non-volatile surfactant, and is relatively non-flammable. Furthermore, CPE combines extraction and enhancement into a single step. As a result, CPE was developed as a feasible alternative to separation technologies. However, certain surfactants in CPE can interfere with the HPLC-UV to determine the analyte [102]. QuEChERS, a more modern and now widely used sample treatment method, was established in 2003 [103]. This approach is based on microscale extraction with ACN, water absorption and liquid-liquid partitioning with MgSO4 and NaCl, and d-SPE clean-up with a primary-secondary amine (PSA) sorbent. Mixing the separation and clean-up procedures into a single step significantly decreases the quantity of mixing, solvent transfers, evaporation/condensation, filtration, and solvent exchanges necessary for chromatographic analysis. QuEChERS is an acronym that stands for quick, easy, cheap, effective, rugged, and safe [22]. Compared to conventional LLE, the advantages of QuEChERS include a more straightforward and faster process and less organic solvent use. Since the QuEChERS approach considerably facilitates the separation and clean-up steps during the sample treatment procedure and generates quantitative results, it has a promising future in analyzing insecticide residues in foods [104]. It was done using molecularly imprinted polymers (MIPs), which are made by co-polymerizing a monomer and a cross-linker with a template analyte. The template is removed, followed by the polymer containing complementary recognition sites. There are recognition sites in the polymer that are structurally, chemically, and physically compatible with the template molecules [105]. Due to their ability to bind preferentially to the template (target component) and comparable structures, MIPs exhibit excellent molecular recognition and a high affinity for template molecules [53]. MIPs can, therefore, be utilized as adsorbents to identify and enrich pesticide residues in foods specifically. For instance, molecularly imprinted polymers were created when suspension polymerizing methacrylic acid polymers with ethylene dimethacrylate in the presence of a carbaryl template and its metabolite. These polymers were then packed into a pre-column to make it possible to isolate analytes from complex matrices without the need for extensive sample preparation and cleanup [106]. The sample preparation techniques previously outlined apply to studying different pesticide residues, and MIPs are

made to analyze analogous chemicals. Pesticide residues in food samples have been successfully examined using MIPs [38]. As a result, MIPs need to be low-cost, easy to prepare, have a higher population of homogeneous binding sites, produce clean extracts with high selectivity, and have excellent physicochemical stability in various solvents and laboratory conditions [107].

4.2. Application of MIPs in Food Sample Preparation

The dynamic impacts of food matrixes and the low concentration of target components make sample preparation a substantial bottleneck in the analytical procedure. The processes for sample treatment have recently seen advancements in their selectivity. MIPs have been used as adsorbents during sample treatment and are frequently advised. The ability of MIPs to concentrate analytes and selectively extract the target ingredient from bulk samples is their key competitive advantage. They provide more sensitive and focused detection by overcoming the non-specific affinity of traditional adsorbents such as C18-bonded silica gel [108]. Additionally, MIPs provide the following benefits: high sample load efficiency, ideal physical resilience, high stability, and strong resistance to high temperatures, as well as being simple to prepare, inert to organic solvents, as well as acidic and basic solutions, and affordable. MIPs are mostly used with popular sample treatment techniques like SPE and SPME. Recent advancements in magnetic MIP nanoparticle technology have made it possible to employ MIPs in conjunction with magnetic bead extraction, greatly simplifying sample-handling operations as shown in (Fig. 5) [109, 110].

4.2.1.MIP-based SPE

SPE based on MIP is the method most frequently used to prepare food samples because of its simplicity, speed, minimal solvent consumption, and capacity to clean unique analytes. In the standard MIP-SPE technique, the imprinted bulk polymer is packed in a cartridge, separation well plate (for high throughput analysis), or column. MIPs in different forms, such as nanoparticles and

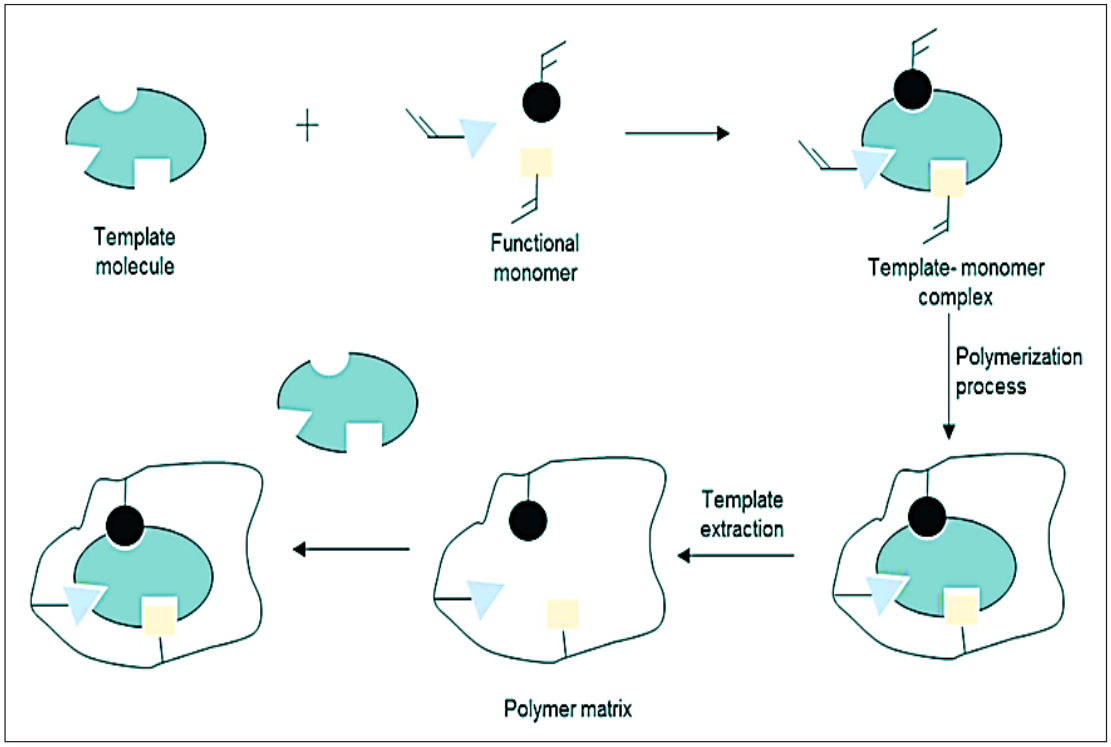

Fig. 5. Schematic diagram of the imprinting process [101].

thin films, have lately been employed as adsorbents in SPE [111]. The "natural phase" mode for food samples dissolved in a low polarity solvent and the "reverse phase" mode for aqueous food samples have been considered two distinct approaches to extract analytes utilizing MIPs. Target components interact with the adsorbent matrix in a shape-specific method to cause the adsorption of the target components onto an MIP adsorbent to occur in the "natural phase" mode. While interfering molecules pass through the separation column with excellent selectivity with ease, increased mobile phase intensity results in analyte elution [112]. In contrast, the target molecules in aqueous samples are then adsorbed onto the MIP adsorbent through hydrophobic interactions when the "reverse phase" mode is employed. Interfering elements can be removed from the target molecule after solvent cleaning. The analyte can be eluted once the column has been sufficiently cleaned with a solvent. The washing solvent can remove non-specific binding without affecting the MIP alone's selective interactions with the target components in food samples [113]. It may be possible to eliminate cleaning with washing solutions in some circumstances, such as when the elution step is highly selective for the target component and does not elute non-specifically bound compounds. This is especially advised for aqueous samples since using a non-polar solvent during the cleaning process might have an adverse effect on miscibility [110]. In previous studies, MIP-SPE was used to remove food samples' antibiotics, insecticides, and mycotoxins [114, 115]. In addition to MIPs created via bulk polymerization, nano-based core-shell type molecularly imprinted sorbents have been used for food analysis. As an example, Wang et al. (2014) used hollow core-shell spheres that were molecularly imprinted to extract estradiol from milk samples [116].

4.2.2.MIP-Based SPME

SPME is a sample treatment method that uses a syringe with a stainless steel microtubing needle and fused silica fiber tips coated with an organic adsorbent [117]. This coated silica fiber may travel forward and backward with the syringe plunger. Several benefits of SPME's distinctive design include the lack of organic solvents, accelerated sample processing, automation ease, and cheap cost [118, 119]. However, SPME shares the same problem as traditional SPE: a lack of selectivity. SPME has demonstrated better sensitivity and selectivity by applying an adsorbent MIP coating to the fiber tips. One of the most intriguing concepts to emerge in recent years is the fusion of MIP and sol-gel technology to create MIP extraction methods compatible with water [120]. In a sol-gel coating of MIP, Wang et al. (2013) utilized polyethylene glycol as the functional monomer and diazinon as the template. The researchers showed that diazinon and its analogs could be determined selectively in green pepper, cabbage, lettuce, cucumber, and eggplant samples. The extraction capacity was significantly higher than that of industrial fibers and unimprinted polymers, owing to the very porous surface, selective adsorption, heat stability, and superior chemical resistance [120]. Recently, Zhao et al. (2015) proved how temperature-sensitive MIPs may be connected to SPME, as displayed in (Fig. 6) [121]. With HPLC connected to SPME coated with MIP, they successfully extracted and tested ofloxacin from milk. Unique molecularly imprinted SPME fibers with the capacity to renew their selective binding sites through progressive polymeric network disintegration were also found with temperature-sensitive MIPs [122]. When using this reusable MIP fiber, the separation of triazole fungicides such as tebuconazole, metconazole, and triadimenol from grape juice samples was highly exact and accurate [123].

4.2.3.Magnetic MIP Nanoparticles-based Extraction

Another sample treatment approach based on magnetic MIP nanoparticles has recently drawn much interest. Since magnetic MIPs generally include a magnetic core and a MIP layer on the shell, they have magnetic susceptibility and good selectivity for target molecules, as shown in (Fig 1)

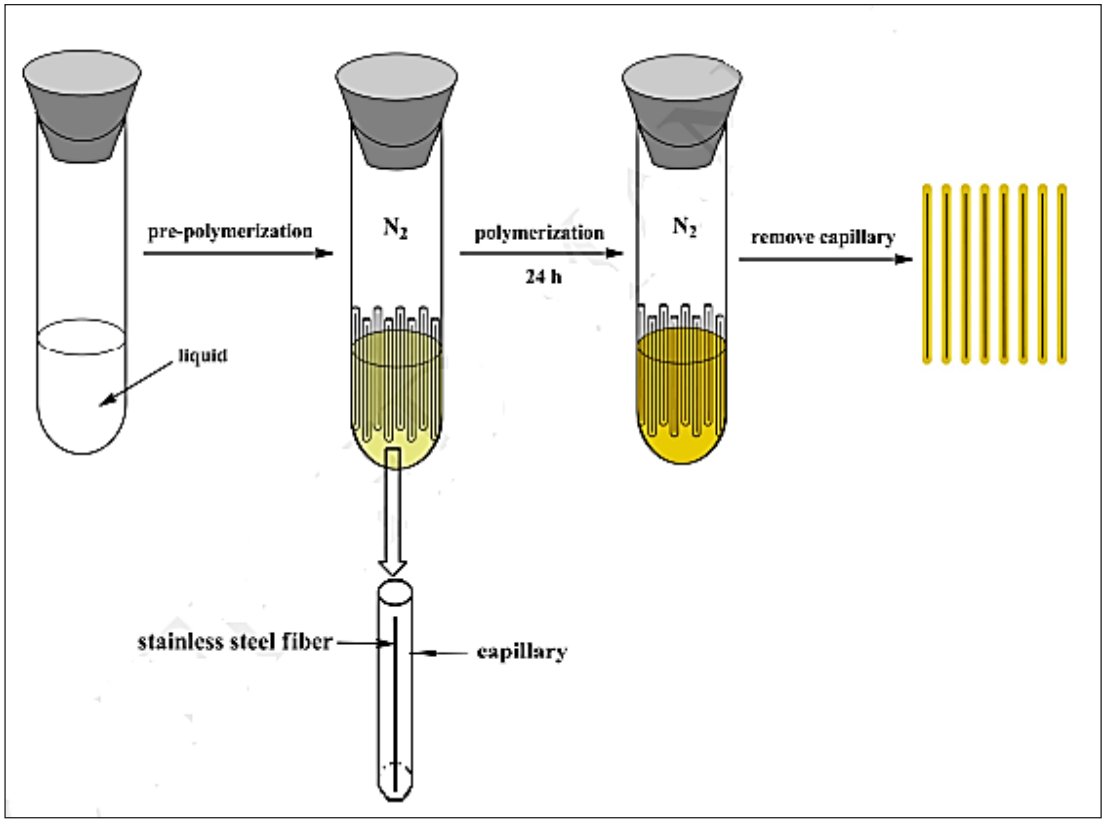

Fig. 6. Synthesized of MIP as SPME coating on the modified SSF in a capillary [112].

[124]. Magnetic adsorbents MIP can be dispersed directly in food samples to remove analytes during separation. A magnet is then utilized to separate the nanoparticles and analytes from the solution. The combination of magnetic nanoparticles and MIP technology has proven a highly effective technique for sample pre-treatment and analysis due to the outstanding target compound-adsorbent interaction and the ease with which magnetic nanoparticles may be removed from sample matrices [40]. Magnetic MIP nanoparticle extraction is quickly utilized to concentrate food contaminants such as pesticides, herbicides, antibiotics, endocrine-disrupting compounds, and growth hormones in complex sample matrices such as honey, milk, fruit juices, eggs, and meat products. Magnetic MIPs revealed sample recoveries ranging from 75% to 96% on average for diverse pollutants. The magnetic MIP approach required much less sample preparation time since extraction and clean-up were simplified by isolating the magnetic polymers in the sample matrix [107, 125, 126]. The utilization of new magnetic hollow nanoparticles with an etched core for quick enrichment of triazines and precise identification in food samples has been demonstrated [127]. Furthermore, a magnetic MIP nanoparticle adsorbent was established for the separation of imidacloprid pesticide residues from honey and eggplant samples, with an extraction recovery of 87.1-95.6% and selectivity for imidacloprid significantly higher than that of structurally related analogs acetamiprid and thiamethoxam [126].

5. Quantitative Analysis Methods

Previously, quantitative analysis was carried out using immunoassay techniques such as liquid chromatography (LC) and evaporative light scattering detection (ELSD) in conjunction with chemiluminescent nitrogen detection (CLND). However, techniques such as gas chromatography combined with mass spectrometry, liquid

chromatography, electrochemical detection, ultraviolet (UV), and fluorescence have advanced. These techniques are the most extensively utilized because they are more linear, exact, and sensitive, and they can analyze tiny sample volumes in food matrices at the same time [4]. Only molecules that can absorb UV light are detected by UV rays, and the absorbed energy is proportional to the concentration of the molecules of interest across a wide concentration range. As a result, analogs of the target molecule can absorb the same UV area [128]. Fluorescence and electrochemical detection are more sensitive than UV detection, but their applications are limited since they contain substances with electroactive or fluorescent groups. As a result, extraction of the chemicals will be required, altering the physical-chemical characteristics of the pesticides evaluated and adding time to the process [128]. However, by combining capillary GC with the unparalleled specificity of the MS, GC-MS analyses low-polarity compounds. Despite having low polarity, some of these molecules are too large to analyze without decomposition. Additionally, this technique cannot test many pesticides because they are non-volatile, thermolabile, and polar [128]. In terms of quantitative analysis, several methods mentioned above have limitations. However, with ongoing advancements in the hyphenation of analytical methods, liquid chromatography-tandem mass spectrometry (LC-MS/MS) has emerged as the most successful method for pesticide component analysis. Due to its unparalleled capacity for high throughput analysis, selectivity, and sensitivity, it has been used to classify and quantify novel pesticide targets in food samples and degradation products/metabolites [129]. Various analytical techniques have been employed to separate and identify pesticides in food. It is crucial to utilize analytical methods that offer excellent selectivity and sensitivity due to the low concentration of these chemicals and the incredible complexity of the matrix. The most used methods for analyzing multiple residues of pesticides in bee products are Gas Chromatography-Electron Ionization-Mass Spectrometry (GC-EI-MS) and Liquid Chromatography-Electrospray Ionization-Tandem Mass Spectrometry (LC-ESI-MS/MS) [129]. The features of the targeted pesticides play a significant role in selecting the separation method. While gas chromatography can identify volatile, semi-volatile, and thermally stable compounds, liquid chromatography can identify non-volatile and/or thermally unstable compounds [130]. Table 3 provides an overview of studies on pesticides in food published in the literature between 2017 and 2022, utilizing liquid or gas chromatography to separate these substances.

5.1. Gas chromatography

A potent method for quantitatively identifying low amounts of pollutants in complicated matrices is gas chromatography (GC) with quadruple mass spectrometry detection [6, 131]. It has been widely used to detect pesticides in food. For the examination of the food matrix, GC has been coupled with several detection methods, including (i) MS [132, 133]; (ii) MS/MS [134]; (iii) NPD [135, 136]; (iv) ECD [137, 138]; (v) AED [139]; and (vi) FPD [133, 140]. Mass spectrometry offers structural formation in a multi-residue study and is the most selective pesticide detector. This is because it gives unequivocal confirmation, which is crucial. When specific ions or their transitions are chosen, MS enables the simultaneous detection and identification of co-eluting substances [141, 142]. Mass spectrometry is frequently used to identify several pesticide classes in the food matrix. The most popular mode, selected-ion monitoring (GC-SIM/MS), has increased sensitivity due to its capacity to identify particles. In this method, the analyte's three strongest ions are chosen, one for quantification and the other for confirmation. It is possible to select more than two ions for confirmation; however, doing so can reduce the method's sensitivity. In the full-scan mode, the target analyte is confirmed and quantified using all of the ions generated by the MS. Standard MS libraries, such as the National Institute of Standards and Technology (NIST), which include more than 150,000 mass spectra

of standard organic compounds, can be achieved the reliability of compound identification [143, 144]. Although gas chromatography is frequently mentioned as the most powerful separation tool, it requires a derivatization step for non-volatile and thermally unstable compounds. This adds more handling and response time, which may affect repeatability and recovery rates [131, 145, 146]. The selection of the GC column is a critical step in pesticide analysis. The stationary phase should be chosen based on the polarity of the insecticides. As shown in Table 3, non-polar columns (5% phenyl 95% dimethylpolysiloxane) are the most widely employed for pesticide analysis in honey [134, 147, 148]. However, medium-polar (50% phenyl, 50% dimethylpolysiloxane) and medium to high-polar (50% Cyanopropylphenyl Polysiloxane) columns have also been employed [60, 113]. The number of pesticides to be determined concurrently can also be used to optimize other column characteristics like length, inner diameter, or film thickness. Contrary to LC-MS, GC-MS was formerly the technology most frequently employed to analyze residues in food products [95, 96]. The examination of thermally unstable pesticides used HPLC the most successfully. Today's pesticides are more polar, thermally unstable, or challenging to evaporate, making them more amenable to liquid chromatography analysis [43, 149, 150].

5.2. Liquid chromatography

Pesticides in food have also been extensively analyzed using liquid chromatography (LC), particularly for thermally labile chemicals. Although the most effective and appropriate detector for this type of analysis is mass spectrometry [10, 151, 152]. In addition to this mentioned above, variable wavelength [153], diode array (DAD) [154, 155,156], and spectrofluorimetric [133] have also been utilized as detector types. However, these other types of detectors are often only employed to analyze a small number of pesticides or classes of pesticides. Pesticides at low concentrations in complex matrices can be detected using liquid chromatography-tandem mass spectrometry. This system is crucial for structural information, decreases matrix interference, and increases sensitivity. in which utilizes multiple reactions monitoring (MRM) mode to improve the accuracy of the results [155]. Furthermore, in recent years, the LC-MS/MS technique has been widely employed to identify the presence of target analytes in commercial food and related samples, as shown in Table 2. Using high-resolution Orbitrap mass spectrometry and ultra-high-performance liquid chromatography, Gómez and Pérez [157] created a method that could analyse 350 compounds from three different classes of contaminants (pesticides, biopesticides, and veterinary drugs) in just 14 minutes. Nevertheless, despite all the benefits that the current detection techniques offer, it is still necessary to use an appropriate sample preparation method because matrix effects can negatively affect detection by creating significant noise and altering ionization efficiency, which leads to a reduction in sensitivity [141].

6. Matrix effect

Pesticide residue analysis in food matrices is typically tricky owing to their deficient concentrations and the interference of the complex matrix [158,159]. The matrix effect might result in an increased or reduced analyte signal from extracts obtained in the presence of a matrix compared to extracts obtained without a matrix [135]. Typically, two methodologies are used to investigate the matrix effect. One possibility is to compare the slopes of standards in a solvent to the slopes of matrix-matched standards. The matrix impact (%) is determined using the equation [(slope of standards in matrix-slope of standards in solvent/ slope of standards in solvent) x100]. The matrix impact is considered low when the values are between -20% and +20%, medium when between -50% and -20% or +20% and +50%, and higher when they are lower or higher than +50% [158]. A further method involves comparing the areas of standard solutions prepared within a matrix with those prepared in a solvent multiplied by 100. If the result is 100%, there is no matrix influence;

otherwise, values higher or lower than 100% indicate enrichment or suppression of the ionization by the matrix component [155]. To reduce the impact of the matrix, the authors created analytical curves in the food matrix extract concentration, which increased the analyte concentration and signal. However, it increases matrix effects and causes ion suppression in the ionization source, resulting in poorer signals with higher noise [130]. Therefore, diluting the extracts, which was Blascoetal's method [160], is an alternative approach to reducing the matrix effect. When samples were diluted, recoveries were higher. Studies have revealed that the floral origin of food can impact the matrix effect. Adopting matrix-matched standards is necessary to reduce the quantitative mistakes caused by matrix effects [158].

Table 1. Nano sorbent removes pesticides and other organic compounds from food matrices and biological fluids.

Target molecule	*Nano adsorbents	References
Malathion	$ZnFe_2O_4$	[26]
Methamidophos, Malathion, Parathion, and Diazinon	$NiFe_2O_4$	[27]
Diazinon, Fenitrothion, Chlropyrifos, Profenofos	GO	[28]
Diazinon, Malathion, and Chlorpyrifos	Fe_3O_4@SiO_2	[47]
Chlorpyrifos	MOFs & COFs	[54]
Thiamethoxam	Fe_3O_4@MIPs	[57]
Carbendazim	Nano Fe_3O_4 particles	[62]
Dimethoate	MIP-Quantum dots	[64]
Carbofuran	MIP-MWCNT	[69]
Dimethoate	**MIP-CNTs-Fe_3O_4@Au/CPE	[70]
Dimethoate	Activated carbon	[76]
Imidacloprid	CNT	[81]
Carbofuran	MIP-SPR sensor	[83]
Dimethoate	MIP-GO-AuNPs/ MIP-SPR	[94]
Dimethoate	AuNPs-Electrochemical sensor	[98]
Carbofuran	AuNPs-Colorimetric sensor	[102]
Dimethoate	AuNPs-FRET	[114]
Carbofuran	MIP-Electrochemical sensor	[123]
Dimethoate, Imidacloprid, and Methamidophos	MOFs	[129]
Dimethoate and Carbofuran	Fe_3O_4@SiO_2	[134]
Imidacloprid	Activated carbon	[137]

*Nano adsorbents// GO: Graphene Oxide, MOFs: Metal-organic frameworks, COFs: Covalent organic frameworks, MIP-MWCNT: Poly(acrylic acid)-MWCNT nanocomposite, CNT: Carbon nanotube, SPR: Surface plasmon resonance and FRET: Fluorescence resonance energy transfer

**MIP-GO-AuNPs/ MIP-SPR: MIP-GO-AuNPs/Electrochemical microfluidic chip MIP-SPR sensor

Table 2. MIPs are involved in extraction methods, synthesis conditions of MIPs for the determined pesticides, and selected compounds in real samples in previous studies.

Extraction Method	Chemical compounds	Synthesis	Monomer/CL/ Porogen/ Initiator	Matrix	Ref.
MIP-MDSPE	Material A	Precipitation Polymerisation	ATA/EGDMA/Water/APS	Tangerine, Chinese celery, Red grape, Cherry tomato,	[147]
MIP-SPE	Parathion Methyl, Fenamiphos, Diazinon, and Malathion	MIP film on steel blades	MAA/EGDMA/ 1-octanol/DMPA	Water and Apple juice	[47]

MIP-MSPE	Material B	Bulk Polymerisation	MAA/4-VP/EGDMA/ MoH/ AIBN	Cabbages	[35]
MIP-MISPE	Chlorpyrifos	Bulk Polymerisation	GBDA/GDPEA/Water/ IRGACURE 184	Water	[148]
MIP-SPR	Dimethoate and Carbofuran	Photo polymerisation	MATrp monomer /EGDMA/ Ethyl alcohol/AIBN	Water	[143]
MIP-SPE	Butyl benzyl phthalate, Diethyl phthalate, Dibutyl phthalate, and Dimethyl phthalate	Precipitation Polymerisation	MAA/EGDMA/MoH/AIBN	Tea	[140]
MIP-MISPE	Atrazine, Terbuthylazine, Acetochlor and Alachlor	Bulk Polymerisation	MAA/EGDMA/Toluene/ AIBN	Cannabis bud	[141]
MIP-SPE	Carbendazim	Precipitation Polymerisation	MAA/EGDMA/ACN/AIBN	Water, Fruits, and Vegetables	[142]
MIP-SPE	Azamethiphos and Chlorpyrifos	Bulk Polymerisation	MAA/EGDMA/ACN/ACPA	Mineral water and Grape	[143]
MIP-SPE	Material C	Bulk Polymerisation	APTES/PMTOS/Water:EoH/ NH4OH solution	Almond oil	[76]
MIP	Thiamethoxam	Precipitation polymerization	VBA/EGDMA/DMF/AIBN	Grain	[145]
MIP-SPE	Imidacloprid and Acetamiprid	Precipitation Polymerisation	MAA/EGDMA/Toluene/ AIBN	Tea	[146]
MIP	Pyriproxyfen, Deltamethrin and Etofenprox	Precipitation Polymerisation	MAA/EGDMA/Chloroform/ AIBN	Apple juice	[147]
MIP-SPE	Thiamethoxam and Thiacloprid	Bulk Polymerisation	2-VP/EGDMA/DMF/AIBN	Light and dark honey	[23]
MIP-SPE	Nitenpyram and Imidacloprid	Bulk Polymerisation	MAA/EGDMA/DMF/AIBN	Light and dark honey	[24]
MIP-SPE	Imidacloprid	Bulk Polymerisation	AA/EGDMA/MoH/AIBN	Eggplant and Honey	[114]
MIP	Imidacloprid	Bulk Polymerisation	MAA/EGDMA/ACN/AIBN	Chili and Tomato	[148]
MIP	Imidacloprid	Bulk Polymerisation	VBA/EGDMA/DMF/AIBN	Rice	[149]
MIP-SPE	Imidacloprid	Bulk Polymerisation	MAA/EGDMA/Water/AIBN	Apple	[150]
MIP-SPE	Imidacloprid	Bulk Polymerisation	MAA/EGDMA/PVA/AIBN	Water and Apple	[151]
MIP	Chemiluminescence	Bulk Polymerisation	AP/EGDMA/DMF/AIBN	Vegetables	[152]
MIP	Imidacloprid	Precipitation Polymerisation	MAA/EGDMA/MoH/AIBN	Strawberry and Apple	[153]
MIP-SPE	Trichlorfon, Dimethoate, Imidacloprid	Bulk Polymerisation	MAA/EGDMA/ O,O′-dimethyl thiophosphoryl chloride/AIBN	Lettuce and Cucumber	[154]
MIP	Imidacloprid	Emulsion Polymerisation	MAA/EGDMA/ACN/AIBN	Water	[155]
MIP	Material D	Precipitation Polymerisation	MAA/EGDMA/ACN/AIBN	Cauliflower, Radish, Pear	[156]
MIP-SPE	Imidacloprid	Precipitation Polymerisation	MAA/EGDMA/DMF/AIBN	Fruit juice	[157]
MIP	Parathion	Precipitation Polymerisation	AA/EGDMA/DMSO/AIBN	Vegetables	[158]

MIP-SPE	Material E	Precipitation Polymerisation	MAA/EGDMA/MoH/AIBN	Fruit juice	[159]
MIP	Parathion	Precipitation Polymerisation	MA-Bt/EGDMA/1,4-dioxane/AIBN	Water	[57]
MIP	Pyriproxyfen	Precipitation Polymerisation	AA/EGDMA/MoH/AIBN	Strawberry	[160]
MIP-DSPE	Chlorpyriphos	Bulk Polymerisation	MAA/EGDMA/MoH/AIBN	Waters, Soils and Vegetables	[36]
MIP	Tolfenpyrad	Bulk Polymerisation	2-VP/EGDMA/DMF/VTMS	Lettuce	[132]
MIP	Dinotefuran	Precipitation Polymerisation	MAA/EGDMA/MoH/AIBN	Cucumber and Soil	[42]
MIP-SPE	Material F	------	Fe_3O_4@C@UiO-66	Water and juices	[133]
MIP-SPE	Material G	------	MIH@MIL-101(Cr)-NH2-TDES	Honey and Tea	[134]

Materials; MIP: Molecularly imprinted polymer, MISPE: Molecularly imprinted solid-phase extraction, SPE: Solid-phase extraction, MDSPE: Magnetic dispersive solid-phase extraction, CL: Crros-linker, ATA: 3-amino-1,2,4- triazole, EGDMA: Ethylene glycol dimethylacrylate, APS: Ammonium peroxodisulfate, MAA: Methacrylic acid, DMPA: 2,2- dimethoxy-2-phenylacetophenone, 4-VP: 4-vinyl pyridine, AIBN: 2,2-azobis (isobutyronitrile), MoH: Methanol, GBDA: Glyoxalbis diallyl acetal, IRGACURE 184: 1-hydroxycyclohexyl phenyl ketone, VTMS: vinyltrimethoxysilane, MATrp monomer: N-methacryloyl-L-tryptophan methyl ester, SPR: Sensor chip nanofilms, CAN: Acetonitrile, ACPA: 4-cyanovaleric acid, APTES: 3-aminopropyl triethoxysilane, PTMOS: Phenyltriethoxysilane, DMF: N,N-dimethylformamide, VBA: 4-vinylbenzoic acid, AA: Acrylic acid, EoH: Ethanol, 2-VP: 2-vinylpyridine, VBA: P-vinylbenzoic acid, PVA: Polyvinyl alcohol, AP: Acephate, DMSO: Dimethyl sulfoxide, MA-Bt: Methacryloyl benzotriazole, VTMS: Vinyltrimethoxysilane

Material A: Azinphos-methyl, Parathion methyl, Azinphos-ethyl, Fenitrothion, Diazinon, Parathion ethyl, profenofos, and Chlorpyrifos

Material B: Methyl-parathion, Parathion, Paraoxon, Fenitrothion, Quinalphos, Isazophos, Chlorpyrifos-methyl, Chlorpyrifos, Fenthion, Methidathion, Profenofos, and Triazophos

Material C: Dimethoate, Fenthion sulfoxide, Fenthion sulfone, Methidathion, Malathion, Fenitrothion, Diazinon, Pirimiphos-methyl, Fenthion and Chlorpyrifos-ethyl

Material D: Ethoprophos, Parathion-methyl, Malathion, Triazophos, Fenthion, Fenamiphos and 2-methylimidazole

Material E: Chlorpyrifos, Haloxyfop-R-methyl, Oxadiazon, Diniconazole, Clodinafop-propargyl, Fenpropathrin, and Fenoxprop-P-ethyl

Material F: Diniconazole, Epoxiconazole, Hexaconazole, Imazaquin, Metalaxyl, Myclobutanil, Prothioconazole and Triticonazole

Material G: Hexachlorocyclohexane, Dichlorodiphenyl dichloroethylene and Dichlorodiphenyl dichloroethane

Table 3. Methods of separation and detection for pesticide determination in food matrix by gas and liquid chromatography.

Pesticides	Column	Mobile Phase	Detection	LOD	R (%)	Ref.
Imidacloprid	C18 (50-4.6 mm, 1.8 µm)	ACN: Water	ESI/MS/MS	0.03-0.10 (µg kg^{-1})	102-114	[158]
Azinphos-methyl, Parathion methyl, Azinphos-ethyl, Fenitrothion, Diazinon, Parathion ethyl, Profenofos,	C18-PFP (4.6 mm x 250 mm, 5 mm)	ACN: Water	HPLC-PDA	0.062-0.195 (µg kg^{-1})	81.3-110.0	[147]
Parathion Methyl, Fenamiphos, Diazinon, Malathion, and Chlorpyrifos	C18 (4.6 mm, 1.8 µm)	MoH: Water	ESI/MS/MS	0.002-0.48 (µg kg^{-1})	87.8-115.0	[47]
Dimethoate and Carbofuran	C18 (4.6 mm, 1.8 µm)	Water	LC–MS-TOF	16.92-20.47 (ng L^{-1})	101-104	[149]
Butyl benzyl phthalate, Diethyl phthalate, Dibutyl phthalate, and Dimethyl phthalate	Zorbax Eclipse XDB-C8 column (3.5 µm, 2.1 mm×50 mm)	ACN: Water	LC-ESI-MS	0.23-13.9 (µg kg^{-1})	78-102	[150]

Carbendazim	C18 ODS-3 (5 µm particle size, 4.6 mm × 250 mm, Japan)	ACN: Water	UHPLC-DAD	0.005-0.01 (µg kg^{-1})	84.32-99.14	[152]
Czamethiphos and Chlorpyrifos	A Phenomenex® C18 (250 mm × 4.60 mm, 5 µm)	MoH: Acetic acid	HPLC/UV	0.36-1.5 (µg kg^{-1})	92.3-105.7	[153]
Pesticides A	Accucore PFP (150 x 2.1 mm, 2.6 mm)	MoH: Water	LC-MS/MS	0.1-1.2 (µg kg^{-1})	81-95	[154]
Imidacloprid and Acetamiprid	BEH C18 (1.7 mm, 2.1 mm x 100 mm)	ACN	HPLC-MS-MS	0.5-1.5 (µg kg^{-1})	93.4-95.8	[156]
Pyriproxyfen, Deltamethrin and Etofenprox	C18 (250 mm × 4.60 mm, 5 µm)	EoH: Water	HPLC-UV	0.005-0.001 (µg kg^{-1})	76.18-97.12	[114]
Thiamethoxam and Thiacloprid	UHPLC (100 mm × 2.1 mm, 2.6 µm)	MoH: Water	UHPLC-MS/MS	0.045-0.070 (µg kg^{-1})	95.3-106.5	[23]
Nitenpyram and Imidacloprid	UHPLC (100 mm × 2.1 mm, 2.6 µm particle size)	MoH: Water	UHPLC-MS/MS	0.03-0.09 (µg kg^{-1})	94.3-108	[24]
Imidacloprid	Zorbax Eclipse Plus C-18 (Agilent) (3 x 100 mm, 3.5 µ)	MoH: Water	LC-MS/MS	0.05 (µg kg^{-1})	87.1-96.2	[114]
Imidacloprid	Agilent-C18 (4.6 × 250 mm i.e., 5.0 µm)	EoH: Water	HPLC-UV	0.1 (µg kg^{-1})	75-83.8	[159]
Imidacloprid	A Symmetry® C18 analytical (4.6×250 mm, 5 µm)	ACN: water	HPLC-UV	0.048 (µg kg^{-1})	77.6-96.5	[160]
Imidacloprid	120 EC - C18 (3.0 × 50 mm, particle size 2.7 µm)	MoH: Water	LC/Q-TOF/MS	2.6-3 (µg kg^{-1})	93.7-101.6	[141]
Chemiluminescence	Waters Sunfire™ C18 (4.6 × 150 mm, 5 µm)	MoH: Water	HPLC-MS/MS	0.86 (µg kg^{-1})	88.7-96.8	[142]
Imidacloprid	C18 (250 mm × 4.60 mm, 5 µm)	MoH: Water	LC-MS/MS	0.05-0.1 (µg kg^{-1})	85.47-101.5	[145]
Pesticides B	Agilent-C18 4.6 × 250 mm, 5.0 µm	MoH: Water	HPLC-MS/MS	0.02-0.45 (µg kg^{-1})	82.5-123.0	[146]
Imidacloprid	100 mm × 2.1 mm, 2.6 µm particle size	MoH: Water	UHPLC-MS/MS	0.18-0.62 (ng L^{-1})	92.4	[157]
Pyriproxyfen	Ultra IBD 5-m 250 × 4.6 mm long C18 column	ACN/ water/ MoH	HPLC-DAD	4.93 $x10^{-5}$ (µg kg^{-1})	97.3	[151]
Tolfenpyrad	100 mm × 2.1 mm, 2.6 µm particle size	ACN: Water	LC-MS/MS	1.7 (µg kg^{-1})	90.5-98.8	[132]
Pesticides C	Chiralcel OD-RH (150 mm × 4.6 mm i.d., 5 µm, Daicel, China)	ACN: Water	LC-MS/MS	0.1-0.35 (ng L^{-1})	83.68-95.99	[133]
Pesticides D	GC (30 m × 0.25 mm i.d., 0.25 µm)	-----	GC-MS	1.62-13.9 (ng L^{-1})	81.5-13.4	[35]
Chlorpyrifos	GC (30 m × 0.25 mm i.d., 0.25 µm)	-----	GC-MS	0.05 (µg kg^{-1})	88.0-92.8	[148]

Atrazine, Terbuthylazine, Acetochlor and Alachlor	A Phenomenex ZB5 MSi (30 m with a 5 m guard, 0.25 mm i.d., 0.25 µm)	-----	GC-MS	0.05-0.1 (µg kg^{-1})	76.4-85.0	[111]
Trichlorfon, Dichlorvos, Dimethoate, Imidacloprid, and Methamidophos	RTX-1701 (30.0 m × 0.25 mm × 0.25 µm)	-----	GC-MS	0.14-0.9 (µg kg^{-1})	87.7-92.5	[134]
Pesticides E	GC (30 m × 0.25 mm i.d., 0.25 µm)	-----	GC-MS	0.04-0.06 (ng L^{-1})	81.7-98.5	[139]
Pesticides G	GC (30 m × 0.25 mm i.d., 0.25 µm)	-----	GC-MS	0.07-0.85 (ng L^{-1})	81.7-109.3	[14]

LOD: Limit of detection, MS: Mass spectrometry, MS/MS: Tandem mass spectrometry, ToF: Time of flight, ESI: Electrospray ionization, UV: Ultraviolet detector, HPLC: High-performance liquid chromatography, UHPLC: Ultra high-performance liquid chromatography, DAD: Diode-Array Detection, PDA: Photometric Diode Array, CAN: Acetonitrile, Ethanol: EoH, ethanol: MoH.
Pesticides A: Dimethoate, Fenthion sulfoxide, Fenthion sulfone, Methidathion, Malathion, Fenitrothion, Diazinon, Pirimiphos-methyl, Fenthion, and Chlorpyrifos-ethyl
Pesticides B: Ethoprophos, Parathion-methyl, Malathion, Triazophos, Fenthion, Fenamiphos and 2-methylimidazole
Pesticides C: Diniconazole, Epoxiconazole, Hexaconazole, Imazaquin, Metalaxyl, Myclobutanil, Prothioconazole and Triticonazole
Pesticides D: Methyl-parathion, Parathion, Paraoxon, Fenitrothion, Quinalphos, Isazophos, Chlorpyrifos-methyl, Chlorpyrifos, Fenthion, Methidathion, Profenofos, and Triazophos
Pesticides E: Chlorpyrifos, Haloxyfop-R-methyl, Oxadiazon, Diniconazole, Clodinafop-propargyl, Fenpropathrin,
Pesticides G: Hexachlorocyclohexane, Dichlorodiphenyl dichloroethylene and Dichlorodiphenyl dichloroethane

7. Conclusion

MIPs have been established to meet the demand for easy-to-use, affordable, durable polymers that may take the position of receptors in natural antibodies. Initial attempts to use MIPs were plagued by several issues severely restricting their application. Most notably, binding was delayed in some situations due to extensive diffusion paths. Big analytes were permanently trapped inside the MIP (or, worse, leached from the polymer during the analysis). The usage of MIPs was one of the most significant advances in the sector. They could be used to reduce diffusion paths and the permanent entrapment of template molecules. However, initially, irregularly shaped MIPs had poor reproducibility; binding was poorly understood, and applying the technique to a different analyte was frequently difficult. In recent years, this field has made significant advances to address these challenges. To fine-tune the size and form of MIPs, several approaches, such as bulk polymerization, precipitation polymerization, emulsion polymerization, inverter polymerization, or the incorporation of a solid core, have been used. Furthermore, several polymerization methods have been developed that allow the polymerization endpoint to be controlled. Another intriguing strategy that might be beneficial is to modify the cavity after it has been imprinted. However, care must be taken during the modification to avoid destroying the imprinting effect. With all these improvements, MIPs are more desirable for industrial applications, and MIPs are being used more frequently. In particular, because it acts as an automated reactor for MIPs synthesis, developing the solid-phase imprinting approach revolutionizes the area of MIPs. Template molecules are immobilized on glass beads installed in the reactor for that purpose, enabling reuse. This makes it possible to scale up MIP production and improve repeatability significantly. MIPs are extensively suitable and compatible for integration in a wide range of applications, have high stability, and can be kept for extended periods of time. As a result, rapid advancement and improvement in nanosized MIPs are anticipated. Regarding analytical methods, UHPLC and tandem mass spectrometry are excellent due to regulatory agency regulations that demand even lower limitations. These detectors satisfy these requirements regarding excellent selectivity and sensitivity and precise identification of analytes at very low detection limits. Furthermore, a more significant number of pesticides can be analyzed concurrently. Another significant trend is the advancement of MIPs

approaches. Some studies have described the simultaneous analysis of over a hundred pesticides from various chemical classes. It was made feasible by developing equipment with exceptional selectivity and sensitivity. We are optimistic that the future will improve the MIP approach in food applications.

8. Acknowledgments

The author would like to thank the University Malaya, Malaysia (BKP Grant RP018B-14AFR and IIRG002A-19SAH) for their help and financial support. The author thanks the Department of Chemistry, Faculty of Science, University Malaya, for using their facilities. The author states that they do not have any known competing financial interests or personal ties that may have influenced the work disclosed in this study.

9. References

[1] T. Neufeld, I. Eshkenazi, E. Cohen, J. Rishpon, A micro flow injection electrochemical biosensor for organophosphorus pesticides, Biosens. Bioelectron., 15 (2000) 323-329. https://doi.org/10.1016/S0956-5663(00)00073-7

[2] D.G. Varsamis, E. Touloupakis, P. Morlacchi, D.F. Ghanotakis, M.T. Giardi, D.C. Cullen, Development of a photosystem II-based optical microfluidic sensor for herbicide detection, Talanta, 77 (2008) 42-47. https://doi.org/10.1016/j.talanta.2008.05.060

[3] E. Llorent-Martínez, P. Ortega-Barrales, M. Fernández-de Córdova, A. Ruiz-Medina, Trends in flow-based analytical methods applied to pesticide detection: A review, Anal. Chim. Acta, 684 (2011) 30-39. https://doi.org/10.1016/j.aca.2010.10.036

[4] D. Sharma, A. Nagpal, Y.B. Pakade, J.K. Katnoria, Analytical methods for estimation of organophosphorus pesticide residues in fruits and vegetables: A review, Talanta, 82 (2010) 1077-1089. https://doi.org/10.1016/j.talanta.2010.06.043

[5] G.-F. Pang, C.-L. Fan, Y.-M. Liu, Y.-Z. Cao, J.-J. Zhang, B.-L. Fu, X.-M. Li, Z.-Y. Li, Y.-P. Wu, Multi-residue method for the determination of 450 pesticide residues in honey, fruit juice and wine by double-cartridge solid-phase extraction/gas chromatography-mass spectrometry and liquid chromatography-tandem mass spectrometry, Food Addit. Contam., 23 (2006) 777-810. https://doi.org/10.1080/02652030600657997

[6] D.I. Kolberg, O.D. Prestes, M.B. Adaime, R. Zanella, Development of a fast multiresidue method for the determination of pesticides in dry samples (wheat grains, flour and bran) using QuEChERS based method and GC–MS, Food chem., 125 (2011) 1436-1442. https://doi.org/10.1016/j.foodchem.2010.10.041

[7] Y. Bai, L. Zhou, J. Wang, Organophosphorus pesticide residues in market foods in Shaanxi area, China, Food Chem., 98 (2006) 240-242. https://doi.org/10.1016/j.foodchem.2005.05.070

[8] K. Abir, R.R. Abdul, A.I. Mohamad, B. Daniel, B. Hélène, J. Farouk, Multiresidue method for determination of 67 pesticides in water samples using solid-phase extraction with centrifugation and gas chromatography-mass spectrometry, Am. J. Anal. Chemi., 2012 (2012). https://doi.org/10.4236/ajac.2012.33034

[9] R.A. Oni, M. Sharma, R.L. Buchanan, Survival of salmonella enterica in dried Turkey Manure and persistence on spinach leaves, J. food protect., 78 (2015) 1791-1799. https://doi.org/10.4315/0362-028X.JFP-15-047

[10] Ż. Bargańska, M. Ślebioda, J. Namieśnik, Pesticide residues levels in honey from apiaries located of Northern Poland, Food Control, 31 (2013) 196-201. https://doi.org/10.1016/j.foodcont. 2012.09.049

[11] N. Arnal, G. Morel, C.A. Marra, M. Astiz, Pro-apoptotic effects of low doses of dimethoate in rat brain, Toxicol. Appl. Pharmacol., 363 (2019) 57-63. https://doi.org/10.1016/j.taap.2018.11.013

[12] S. Martínez-Morcillo, M. Pérez-López, F. Soler-Rodríguez, A. González, The organophosphorus pesticide dimethoate decreases cell viability and induces changes

in different biochemical parameters of rat pancreatic stellate cells, Toxicol. In Vitro, 54 (2019) 89-97. https://doi.org/10.1016/j.tiv.2018.09.011

[13] W. Hu, Q. Chen, H. Li, Q. Ouyang, J. Zhao, Fabricating a novel label-free aptasensor for acetamiprid by fluorescence resonance energy transfer between NH2-NaYF4: Yb, Ho@SiO2 and Au nanoparticles, Biosens. Bioelectron., 80 (2016) 398-404. https://doi.org/10.1016/j. bios.2016.02.001

[14] J.-M. Bonmatin, C. Giorio, V. Girolami, D. Goulson, D. Kreutzweiser, C. Krupke, M. Liess, E. Long, M. Marzaro, E.A. Mitchell, Environmental fate and exposure; neonicotinoids and fipronil, Environ. Sci. Pollut. Res., 22 (2015) 35-67. https://doi.org/10.1007/s11356-014-3332-7

[15] D. Goulson, An overview of the environmental risks posed by neonicotinoid insecticides, J. Appl. Ecol., 50 (2013) 977-987. https://doi.org/10.1111/1365-2664.12111

[16] W. Chen, K. Sun, R. Zheng, H. Zeng, S. Zhang, C. Xia, Z. Yang, H. Li, X. Zou, J. He, Cancer incidence and mortality in China, 2014, Chin. J. Cancer Res., 30 (2018) 1. https://doi.org/10.21147/j.issn.1000-9604.2018.01.01

[17] M. Tomizawa, J.E. Casida, Neonicotinoid insecticide toxicology: Mechanisms of selective action, Annu. Rev. Pharmacol. Toxicol., 45 (2005) 247-268. https://doi.org/10.1146/annurev.pharmtox.45.120403.095930

[18] M. Arjomandi, H. Shirkhanloo, A review: Analytical methods for heavy metals determination in environment and human samples, Anal. Methods Environ. Chem. J., 2 (2019) 97-126. https://doi.org/10.24200/amecj.v2.i03.73

[19] L. Gao, L. Liu, Y. Sun, W. Zhao, L. He, Fabrication of a novel azamacrocycle-based adsorbent for solid-phase extraction of organophosphorus pesticides in tea drinks, Microchem. J., 153 (2020) 104364. https://doi.org/10.1016/j.microc.2019.104364

[20] S. Teimoori, H. Shirkhanloo, A.H. Hassani, M. Panahi, N. Mansouri, An immobilization of aminopropyl trimethoxysilane-phenanthrene carbaldehyde on graphene oxide for toluene extraction and separation in water samples, Chemosphere, 316 (2023) 137800. https://doi.org/10. 1016/j.chemosphere.2023.137800

[21] J. Hassan, M. Sarkouhi, Miniaturized counter current liquid–liquid extraction for organophosphorus pesticides determination, Arab. J. Chem., 9 (2016) 38-42. https://doi.org/10.1016/j.arabjc.2013.02.003

[22] M.K. Abbasabadi, F. Hosseini, Nanographene oxide modified phenyl methanethiol nanomagnetic composite for rapid separation of aluminum in wastewaters, foods, and vegetable samples by microwave dispersive magnetic micro solid-phase extraction, Food Chem., 347 (2021) 129042. https://doi.org/10.1016/j.foodchem.2021.129042

[23] S. Jullakan, O. Bunkoed, S. Pinsrithong, Solvent-assisted dispersive liquid-solid phase extraction of organophosphorus pesticides using a polypyrrole thin film–coated porous composite magnetic sorbent prior to their determination with GC-MS/MS, Microchim. Acta, 187 (2020) 1-10. https://doi.org/10.1007/s00604-020-04649-1

[24] A.Q. Abdulhussein, A.K.M. Jamil, N.K.A. Bakar, Magnetic molecularly imprinted polymer nanoparticles for the extraction and clean-up of thiamethoxam and thiacloprid in light and dark honey, Food Chem., 359 (2021) 129936. https://doi.org/10.1016/j.foodchem.2021.129936

[25] A.Q. Abdulhussein, N.K. Abu Bakar, H.I. Kafeenah, A.K. Mohd Jamil, Highly selective magnetic dual-template molecularly imprinted polymer for simultaneous removal and clean-up of nitenpyram and imidacloprid from light and dark honey, Int. J. Environ. Anal. Chem., (2021) 1-19. https://doi.org/10.1080/03067319.2021.1966698

[26] M. Mehdipour, M. Ansari, M. Pournamdari, L. Zeidabadinejad, M. Kazemipour, Selective

extraction of malathion from biological fluids by molecularly imprinted polymer coated on spinel $ZnFe_2O_4$ magnetic nanoparticles based on green synthesis, Sep. Sci. Technol., 56 (2021) 1899-1909. https://doi.org/10.1080/01496395.2020.1803912

[27] D. Chen, S. Ma, X. Zhang, X. Wang, M. Gao, J. Li, H. Wang, Enhanced extraction of organophosphorus pesticides from fruit juices using magnetic effervescent tablets composed of the NiFe2O4@SiO2@PANI-IL nanocomposites, RSC Adv., 11 (2021) 1668-1678. https://doi. org/10.1039/D0RA09100F

[28] M. Nasiri, H. Ahmadzadeh, A. Amiri, Organophosphorus pesticides extraction with polyvinyl alcohol coated magnetic graphene oxide particles and analysis by gas chromatography-mass spectrometry: Application to apple juice and environmental water, Talanta, 227 (2021) 122078. https://doi.org/10.1016/j.talanta.2020.122078

[29] J. Gamonchuang, R. Burakham, Surfactant-coupled titanium dioxide coated iron-aluminium mixed metal hydroxide for magnetic solid phase extraction of bisphenols in carbonated beverages, Heliyon, 7 (2021) e06964. https://doi.org/10.1016/j.heliyon.2021.e06964

[30] M. Arabi, A. Ostovan, A.R. Bagheri, X. Guo, J. Li, J. Ma, L. Chen, Hydrophilic molecularly imprinted nanospheres for the extraction of rhodamine B followed by HPLC analysis: A green approach and hazardous waste elimination, Talanta, 215 (2020) 120933. https://doi.org/10.1016/j. talanta.2020.120933

[31] S. Teimoori, H. Shirkhanloo, A.H. Hassani, M. Panahi, N. Mansouri, Rapid extraction of BTEX in water and milk samples based on functionalized multi-walled carbon nanotubes by dispersive homogenized-micro-solid phase extraction, Food Chem., 421 (2023) 136229. https://doi.org/10.1016/j.foodchem.2023.136229

[32] O.P. Luzardo, N. Ruiz-Suarez, P.F. Valeron, M. Camacho, M. Zumbado, L.A. Henríquez-Hernández, L.D. Boada, Methodology for the identification of 117 pesticides commonly involved in the poisoning of wildlife using GC–MS-MS and LC–MS-MS, J. Anal. Toxicol., 38 (2014) 155-163. https://doi.org/10.1093/jat/bku009

[33] S. Teimoori, H. Shirkhanloo, A. Hassani, M. Panahi, N. Mansouri, New extraction of toluene from water samples based on nano-carbon structure before determination by gas chromatography, Int. J. Environ. Sci. Technol., 20 (2023) 6589-6608. https://doi.org/10.1007/s13762-023-04906-9

[34] O.P. Luzardo, M. Almeida-González, N. Ruiz-Suárez, M. Zumbado, L.A. Henríquez-Hernández, M.J. Meilán, M. Camacho, L.D. Boada, Validated analytical methodology for the simultaneous determination of a wide range of pesticides in human blood using GC–MS/MS and LC–ESI/MS/MS and its application in two poisoning cases, Sci. Justice, 55 (2015) 307-315. https://doi.org/10.1016/j.scijus.2015.04.007

[35] L. Maldaner, I.C. Jardim, Determination of some organic contaminants in water samples by solid-phase extraction and liquid chromatography–tandem mass spectrometry, Talanta, 100 (2012) 38-44. https://doi.org/10.1016/j.talanta.2012.08.006

[36] N.J. Vickers, Animal communication: When I'm calling you, will you answer too?, Curr. biol., 27 (2017) R713-R715. https://doi.org/10.1016/j.cub.2017.05.064

[37] L. Liu, M. Yang, M. He, T. Liu, F. Chen, Y. Li, X. Feng, Y. Zhang, F. Zhang, Magnetic solid phase extraction sorbents using methyl-parathion and quinalphos dual-template imprinted polymers coupled with GC-MS for class-selective extraction of twelve organophosphorus pesticides, Microchim. Acta, 187 (2020) 1-12. https://doi.org/10.1007/s00604-020-04465-7

[38] S. Boulanouar, S. Mezzache, A. Combès, V. Pichon, Molecularly imprinted polymers for the determination of organophosphorus pesticides in complex samples, Talanta, 176

(2018) 465-478. https://doi.org/10.1016/j.talanta.2017.08.067

[39] S. Luo, J. Wu, X. Huang, Molecularly imprinted monolith-based portable in-tip microextraction device for field-specific extraction of triazine herbicides in aqueous samples followed by chromatographic quantification, J. Chromatogra. A, 1689 (2023) 463743. https://doi.org/10.1016/j.chroma.2022.463743

[40] M. Arabi, A. Ostovan, A.R. Bagheri, X. Guo, L. Wang, J. Li, X. Wang, B. Li, L. Chen, Strategies of molecular imprinting-based solid-phase extraction prior to chromatographic analysis, TrAC Trends Anal. Chem., 128 (2020) 115923. https://doi.org/10.1016/j.trac.2020. 115923

[41] A. Bazmandegan-Shamili, S. Dadfarnia, A.M.H. Shabani, M.R. Moghadam, M. Saeidi, MultiSimplex optimization of the dispersive solid-phase microextraction and determination of fenitrothion by magnetic molecularly imprinted polymer and high-performance liquid chromatography, J. Iran. Chem. Soc., 15 (2018) 1181-1189. https://doi.org/10.1007/s13738-018-1316-0

[42] C. Jamshidzadeh, H. Shirkhanloo, A new analytical method based on bismuth oxide-fullerene nanoparticles and photocatalytic oxidation technique for toluene removal from workplace air, Anal. Methods Environ. Chem. J., 2 (2019) 73-86. https://doi.org/10. 24200/amecj.v2.i01.55

[43] A. Faghihi-Zarandi, H. Shirkhanloo, C. Jamshidzadeh, A new method for removal of hazardous toluene vapor from air based on ionic liquid-phase adsorbent, Int. J. Environ. Sci. Technol., 16 (2019) 2797-2808. https://doi.org/10. 1007/s13762-018-1975-5

[44] L. Chen, S. Xu, J. Li, Recent advances in molecular imprinting technology: current status, challenges and highlighted applications, Chem. Soc. Rev., 40 (2011) 2922-2942. https://doi.org/10.1039/C0CS00084A

[45] M.F. Abdel-Ghany, L.A. Hussein, N.F. El Azab, Novel potentiometric sensors for the determination of the dinotefuran insecticide residue levels in cucumber and soil samples, Talanta, 164 (2017) 518-528. https://doi.org/10.1016/j.talanta.2016.12.019

[46] J. Rakhtshah, H. Shirkhanloo, N. Esmaeili, A rapid extraction of toxic styrene from water and wastewater samples based on hydroxyethyl methylimidazolium tetrafluoroborate immobilized on MWCNTs by ultra-assisted dispersive cyclic conjugation-micro-solid phase extraction, Microchem. J., 170 (2021) 106759. https://doi.org/10.1016/j.microc.2021.106759

[47] M. Arabi, A. Ostovan, J. Li, X. Wang, Z. Zhang, J. Choo, L. Chen, Molecular imprinting: Green perspectives and strategies, Adv. Mater., (2021) 2100543. https://doi.org/10.1002/adma. 202100543

[48] R. Viveiros, S. Rebocho, T. Casimiro, Green strategies for molecularly imprinted polymer development, Polymers, 10 (2018) 306. https://doi.org/10.3390/polym10030306

[49] A.R. Bagheri, M. Arabi, M. Ghaedi, A. Ostovan, X. Wang, J. Li, L. Chen, Dummy molecularly imprinted polymers based on a green synthesis strategy for magnetic solid-phase extraction of acrylamide in food samples, Talanta, 195 (2019) 390-400. https://doi.org/10.1016/j.talanta.2018.11.065

[50] L. Chen, X. Wang, W. Lu, X. Wu, J. Li, Molecular imprinting: perspectives and applications, Chem. Soc. Rev., 45 (2016) 2137-2211. https://doi.org/10.1039/C6CS00061D

[51] J. Hou, W. Xie, D. Hong, W. Zhang, F. Li, Y. Qian, C. Han, Simultaneous determination of ten neonicotinoid insecticides and two metabolites in honey and Royal-jelly by solid−phase extraction and liquid chromatography−tandem mass spectrometry, Food Chem., 270 (2019) 204-213. https://doi.org/10.1016/j.foodchem.2018.07.068

[52] E.A. Dil, A.H. Doustimotlagh, H. Javadian, A. Asfaram, M. Ghaedi, Nano-sized Fe_3O_4@SiO_2-molecular imprinted polymer as a sorbent for dispersive solid-phase microextraction of melatonin in the methanolic extract of Portulaca oleracea, biological, and water

samples, Talanta, 221 (2021) 121620. https://doi.org/10.1016/j.talanta.2020.121620

[53] S. Farooq, J. Nie, Y. Cheng, Z. Yan, J. Li, S.A.S. Bacha, A. Mushtaq, H. Zhang, Molecularly imprinted polymers' application in pesticide residue detection, Analyst, 143 (2018) 3971-3989. https://doi.org/10.1039/C8AN00907D

[54] X. Song, S. Xu, L. Chen, Y. Wei, H. Xiong, Recent advances in molecularly imprinted polymers in food analysis, J. Appl. Poly. Sci., 131 (2014). https://doi.org/10. 1002/app.40766

[55] A. Azizi, F. Shahhoseini, E.A. Langille, R. Akhoondi, C.S. Bottaro, Micro-gel thin film molecularly imprinted polymer coating for extraction of organophosphorus pesticides from water and beverage samples, Anal. Chim. Acta, 1187 (2021) 339135. https://doi.org/10.1016/j .aca.2021.339135

[56] Y. Ma, G. Pan, Y. Zhang, X. Guo, H. Zhang, Comparative study of the molecularly imprinted polymers prepared by reversible addition–fragmentation chain transfer "bulk" polymerization and traditional radical "bulk" polymerization, J. Mol. Recognit., 26 (2013) 240-251. https://doi.org/10.1002/jmr.2267

[57] J. Wackerlig, P.A. Lieberzeit, Molecularly imprinted polymer nanoparticles in chemical sensing – Synthesis, characterisation and application, Sens. Actuators B: Chem., 207 (2015) 144-157. https://doi.org/10.1016/j.snb.2014.09.094

[58] H. Wang, C. Huang, S. Ma, C. Bo, J. Ou, B. Gong, Recent advances of restricted access molecularly imprinted materials and their applications in food and biological samples analysis, TrAC Trends Anal. Chem., 147 (2022) 116526. https://doi.org/10.1016/j.trac.2022. 116526

[59] D. Vaihinger, K. Landfester, I. Kräuter, H. Brunner, G.E. Tovar, Molecularly imprinted polymer nanospheres as synthetic affinity receptors obtained by miniemulsion polymerisation, Macromol. Chem. Phys., 203 (2002) 1965-1973. https:// doi.org/10.1002/ 1521-3935(200209)203:13<1965::AID-MACP1965>3.0.CO;2-C

[60] R.J. Uzuriaga-Sánchez, S. Khan, A. Wong, G. Picasso, M.I. Pividori, M.D.P.T. Sotomayor, Magnetically separable polymer (Mag-MIP) for selective analysis of biotin in food samples, Food chem., 190 (2016) 460-467. https://doi.org/10.1016/j.foodchem.2015.05.129

[61] A. Poma, A. Guerreiro, M.J. Whitcombe, E.V. Piletska, A.P. Turner, S.A. Piletsky, Solid-Phase Synthesis of Molecularly Imprinted Polymer Nanoparticles with a Reusable Template–Plastic Antibodies, Adv. Funct. Mater., 23 (2013) 2821-2827. https://doi.org/10. 1002/adfm.201202397

[62] S. Ambrosini, S. Beyazit, K. Haupt, B.T.S. Bui, Solid-phase synthesis of molecularly imprinted nanoparticles for protein recognition, Chem. Commun., 49 (2013) 6746-6748. https://doi.org/10.1039/C3CC41701H

[63] M.B. Gawande, A. Goswami, T. Asefa, H. Guo, A.V. Biradar, D.-L. Peng, R. Zboril, R.S. Varma, Core–shell nanoparticles: synthesis and applications in catalysis and electrocatalysis, Chem. Soc. Rev., 44 (2015) 7540-7590. https://doi.org/10.1039/C5CS00343A

[64] N. Pérez-Moral, A.G. Mayes, Molecularly imprinted multi-layer core-shell nanoparticles – A surface grafting approach, Macromol. Rapid Commun., 28 (2007) 2170-2175. https://doi.org/10.1002/marc.200700532

[65] H. Li, H. Guan, H. Dai, Y. Tong, X. Zhao, W. Qi, S. Majeed, G. Xu, An amperometric sensor for the determination of benzophenone in food packaging materials based on the electropolymerized molecularly imprinted poly-o-phenylenediamine film, Talanta, 99 (2012) 811-815. https://doi.org/10.1016/j.talanta.2012.07.033

[66] D. Aguilar-García, A. Ochoa-Terán, F. Paraguay-Delgado, M.E. Díaz-García, G. Pina-Luis, Water-compatible core–shell Ag@SiO2 molecularly imprinted particles for the controlled release of tetracycline, J. Mater. Sci., 51 (2016) 5651-5663. https://doi.org/10.1007/s10853-016-9867-x

[67] D. Yu, Y. Zeng, Y. Qi, T. Zhou, G. Shi, A novel electrochemical sensor for determination of

dopamine based on AuNPs@SiO_2 core-shell imprinted composite, Biosens. Bioelectron., 38 (2012) 270-277. https://doi.org/10.1016/j.bios.2012.05.045

[68] S. Han, X. Li, Y. Wang, C. Su, A core–shell Fe_3O_4 nanoparticle–CdTe quantum dot–molecularly imprinted polymer composite for recognition and separation of 4-nonylphenol, Anal. Methods, 6 (2014) 2855-2861. https://doi.org/10.1039/C3AY41924J

[69] V. Suryanarayanan, C.T. Wu, K.C. Ho, Molecularly imprinted electrochemical sensors, Electroanal., 22 (2010) 1795-1811. https://doi.org/10.1002/elan.200900616

[70] E. Pardieu, H. Cheap, C. Vedrine, M. Lazerges, Y. Lattach, F. Garnier, S. Remita, C. Pernelle, Molecularly imprinted conducting polymer based electrochemical sensor for detection of atrazine, Anal. Chim. Acta, 649 (2009) 236-245. https://doi.org/10.1016/j.aca.2009.07.029

[71] P.S. Sharma, A. Pietrzyk-Le, F. D'souza, W. Kutner, Electrochemically synthesized polymers in molecular imprinting for chemical sensing, Anal. Bioanal. Chem., 402 (2012) 3177-3204. https://doi.org/10.1007/s00216-011-5696-6

[72] Z. Song, J. Li, W. Lu, B. Li, G. Yang, Y. Bi, M. Arabi, X. Wang, J. Ma, L. Chen, Molecularly imprinted polymers based materials and their applications in chromatographic and electrophoretic separations, TrAC Trends Anal. Chem., 146 (2022) 116504. https://doi.org/10.1016/j. trac.2021.116504

[73] T. Curk, J. Dobnikar, D. Frenkel, Rational design of molecularly imprinted polymers, J. Soft Matter, 12 (2016) 35-44. https://doi.org/10.1039/C5SM02144H

[74] I.A. Nicholls, S. Chavan, K. Golker, B.C. Karlsson, G.D. Olsson, A.M. Rosengren, S. Suriyanarayanan, J.G. Wiklander, Theoretical and computational strategies for the study of the molecular imprinting process and polymer performance, molecularly imprinted polymers in biotechnology, Springer, pp. 25-50, 2015. https://doi.org/10.1007/10_2015_318

[75] M.S. Khan, P.S. Wate, R.J. Krupadam, Combinatorial screening of polymer precursors for preparation of benzo[α] pyrene imprinted polymer: an ab initio computational approach, J. Mol. Model., 18 (2012) 1969-1981. https://doi.org/10.1007/s00894-011-1218-x

[76] H. Hawari, N. Samsudin, A.M. Shakaff, Y. Wahab, U. Hashim, A. Zakaria, S. Ghani, M. Ahmad, Highly selective molecular imprinted polymer (MIP) based sensor array using interdigitated electrode (IDE) platform for detection of mango ripeness, Sens. Actuators B: Chem., 187 (2013) 434-444. https://doi.org/10.1016/j.snb.2013.01.045

[77] D.R. Kryscio, Y. Shi, P. Ren, N.A. Peppas, Molecular docking simulations for macromolecularly imprinted polymers, Ind. Eng. Chem. Res., 50 (2011) 13877-13884. https://doi.org/10.1021/ie201858n

[78] L.A. Pereira, S. Rath, Molecularly imprinted solid-phase extraction for the determination of fenitrothion in tomatoes, Anal. Bioanal. Chem., 393 (2009) 1063-1072. https://doi.org/10.1007/s00216-008-2511-0

[79] J. Xin, X. Qiao, Z. Xu, J. Zhou, Molecularly imprinted polymer as sorbent for solid-phase extraction coupling to gas chromatography for the simultaneous determination of trichlorfon and monocrotophos residues in vegetables, Food Anal. Methods, 6 (2013) 274-281. https://doi.org/10.1007/s12161-012-9432-4

[80] M. Zhou, N. Hu, S. Shu, M. Wang, Molecularly imprinted nanomicrospheres as matrix solid-phase dispersant combined with gas chromatography for determination of four phosphorothioate pesticides in carrot and yacon, J. Anal. Methods Chem., 2015 (2015) 85167. https://doi.org/10.1155/2015/385167

[81] J.-J. Du, R.-X. Gao, H. Yu, X.-J. Li, H. Mu, Selective extraction of dimethoate from cucumber samples by use of molecularly imprinted microspheres, J. Pharm. Anal., 5 (2015) 200-206. https://doi.org/10.1016/j.jpha.2014.10.004

[82] D. Zhang, D. Yu, W. Zhao, Q. Yang, H. Kajiura,

Y. Li, T. Zhou, G. Shi, A molecularly imprinted polymer based on functionalized multiwalled carbon nanotubes for the electrochemical detection of parathion-methyl, Analyst, 137 (2012) 2629-2636. https://doi.org/10.1039/C2AN35338E

[83] D. Davoodi, M. Hassanzadeh-Khayyat, M.A. Rezaei, S.A. Mohajeri, Preparation, evaluation and application of diazinon imprinted polymers as the sorbent in molecularly imprinted solid-phase extraction and liquid chromatography analysis in cucumber and aqueous samples, Food chem., 158 (2014) 421-428. https://doi.org/10.1016/j.foodchem.2014.02.144

[84] M.G. Santos, R.V. Vitor, F.L. Andrade, I. Martins, E.C. Figueiredo, Molecularly imprinted solid phase extraction of urinary diethyl thiophosphate and diethyl dithiophosphate and their analysis by gas chromatography–mass spectrometry, J. Chromatogra. B, 909 (2012) 70-76. https://doi.org/10.1016/j.jchromb.2012.10.015

[85] N. Martins, E.P. Carreiro, M. Simões, M.J. Cabrita, A.J. Burke, R. Garcia, An emerging approach for the targeting analysis of dimethoate in olive oil: The role of molecularly imprinted polymers based on photo-iniferter induced "living" radical polymerization, React. Funct. Polym., 86 (2015) 37-46. https://doi.org/10.1016/j.reactfunctpolym.2014.11.003

[86] I. Bakas, N.B. Oujji, G. Istamboulié, S. Piletsky, E. Piletska, E. Ait-Addi, I. Ait-Ichou, T. Noguer, R. Rouillon, Molecularly imprinted polymer cartridges coupled to high performance liquid chromatography (HPLC-UV) for simple and rapid analysis of fenthion in olive oil, Talanta, 125 (2014) 313-318. https://doi.org/10.1016/j.talanta.2014.03.020

[87] X. Zhu, J. Cai, J. Yang, Q. Su, Y. Gao, Films coated with molecular imprinted polymers for the selective stir bar sorption extraction of monocrotophos, J. Chromatogra. A, 1131 (2006) 37-44. https://doi.org/10.1016/j.chroma.2006.07.041

[88] Y. Lv, Z. Lin, T. Tan, W. Feng, P. Qin, C. Li, Application of molecular dynamics modeling for the prediction of selective adsorption properties of dimethoate imprinting polymer, Sens. Actuators B: Chem., 133 (2008) 15-23. https://doi.org/10.1016/j.snb.2008.01.067

[89] A. Faghihi-Zarandi, J. Rakhtshah, A rapid removal of xylene vapor from environmental air based on bismuth oxide coupled to heterogeneous graphene/ graphene oxide by UV photo-catalectic degradation-adsorption procedure, J. Environ. Chem. Eng., 8 (2020) 104193. https://doi.org/10.1016/j.jece.2020.104193

[90] K. Ridgway, S.P. Lalljie, R.M. Smith, Sample preparation techniques for the determination of trace residues and contaminants in foods, J. Chromatogra. A, 1153 (2007) 36-53. https://doi.org/10.1016/j.chroma.2007.01.134

[91] F. Calbiani, M. Careri, L. Elviri, A. Mangia, L. Pistara, I. Zagnoni, Development and in-house validation of a liquid chromatography–electrospray–tandem mass spectrometry method for the simultaneous determination of Sudan I, Sudan II, Sudan III and Sudan IV in hot chilli products, J. Chromatogra. A, 1042 (2004) 123-130. https://doi.org/10.1016/j.chroma.2004.05. 027

[92] M. Gaweł, T. Kiljanek, A. Niewiadowska, S. Semeniuk, M. Goliszek, O. Burek, A. Posyniak, Determination of neonicotinoids and 199 other pesticide residues in honey by liquid and gas chromatography coupled with tandem mass spectrometry, Food Chem., 282 (2019) 36-47. https://doi.org/10.1016/j.foodchem.2019.01.003

[93] R. Rial-Otero, E. Gaspar, I. Moura, J. Capelo, Gas chromatography mass spectrometry determination of acaricides from honey after a new fast ultrasonic-based solid phase micro-extraction sample treatment, Talanta, 71 (2007) 1906-1914. https://doi.org/10.1016/j.talanta.2006. 08.035

[94] S. Valverde, M. Ibáñez, J.L. Bernal, M.J. Nozal, F. Hernández, J. Bernal, Gas chromatography mass spectrometry determination of acaricides from honey after a new fast ultrasonic-based

solid phase micro-extraction sample treatment, Food chem., 266 (2018) 215-222. https://doi.org/10. 1016/j.talanta.2006.08.035

[95] M. Farré, Y. Picó, D. Barceló, Application of ultra-high pressure liquid chromatography linear ion-trap orbitrap to qualitative and quantitative assessment of pesticide residues, J. Chromatogra. A, 1328 (2014) 66-79. https://doi.org/10.1016/j.chroma.2013.12.082

[96] R. Ashouri, H. Shirkhanloo, A. Rashidi, S. Mirzahosseini, N. Mansouri, Dynamic and static removal of benzene from air based on task-specific ionic liquid coated on MWCNTs by sorbent tube-headspace solid-phase extraction procedure, Int. J. Environ. Sci. Technol., 18 (2021) 2377-2390. https://doi.org/10.1007/s13762-020-02995-4

[97] L.M. Ravelo-Pérez, J. Hernández-Borges, M.Á. Rodríguez-Delgado, Multi-walled carbon nanotubes as efficient solid-phase extraction materials of organophosphorus pesticides from apple, grape, orange and pineapple fruit juices, J. Chromatogra. A, 1211 (2008) 33-42. https://doi.org/10.1016/j.chroma.2008.09.084

[98] H. Barchanska, M. Danek, M. Sajdak, M. Turek, Review of sample preparation techniques for the analysis of selected classes of pesticides in plant matrices, Crit. Rev. Anal. Chem., 48 (2018) 467-491. https://doi.org/10.1080/10408347.2018.1451297

[99] M.A. Jeannot, F.F. Cantwell, Solvent microextraction into a single drop, Anal. Chem., 68 (1996) 2236-2240. https://doi.org/10.1021/ac960042z

[100] J.C. Pinheiro, E.C. Chao, Efficient laplacian and adaptive gaussian quadrature algorithms for multilevel generalized linear mixed models, J. Comput. Graph. Stat., 15 (2006) 58-81. https://doi.org/10.1198/106186006X96962

[101] A.Q. Abdulhussein, A.K. Mohd Jamil, N.K. Abu Bakar, Cloud point extraction (CPE) coupled with QuEChERS for extraction and clean up of neonicotinoid pesticide residues in honey, Int. J. Environ. Anal. Chem., 104 (2024) 1365-1380 . https://doi.org/10.1080/03067319.2022.2038146

[102] R. Kachangoon, J. Vichapong, R. Burakham, Y. Santaladchaiyakit, S. Srijaranai, Ultrasonically modified amended-cloud point extraction for simultaneous pre-concentration of neonicotinoid insecticide residues, Molecules, 23 (2018) 1165. https://doi.org/10.3390/molecules23051165

[103] M. Anastassiades, S.J. Lehotay, D. Štajnbaher, F.J. Schenck, Fast and easy multiresidue method employing acetonitrile extraction/partitioning and "dispersive solid-phase extraction" for the determination of pesticide residues in produce, J. AOAC Int., 86 (2003) 412-431. https://doi.org/10.1093/jaoac/86.2.412

[104] I. Hrynko, B. Łozowicka, P. Kaczyński, Comprehensive analysis of insecticides in melliferous weeds and agricultural crops using a modified QuEChERS/LC-MS/MS protocol and of their potential risk to honey bees (Apis mellifera L.), Sci. Total Environ., 657 (2019) 16-27. https://doi.org/10.1016/j.scitotenv.2018.11.470

[105] K. da Mata, M.Z. Corazza, F.M. de Oliveira, A.L. de Toffoli, C.R.T. Tarley, A.B. Moreira, Synthesis and characterization of cross-linked molecularly imprinted polyacrylamide for the extraction/preconcentration of glyphosate and aminomethylphosphonic acid from water samples, React. Funct. Polym., 83 (2014) 76-83. https://doi.org/10.1016/j.reactfunctpolym.2014.07.004

[106] J. Hantash, A. Bartlett, P. Oldfield, G. Dénès, R. O'Rielly, D. Roudiere, S. Menduni, Use of an on-line imprinted polymer pre-column, for the liquid chromatographic-UV absorbance determination of carbaryl and its metabolite in complex matrices, J. Chromatogra. A, 1125 (2006) 104-111. https://doi.org/10.1016/j.chroma.2006.05.054

[107] A. Azizi, F. Shahhoseini, C.S. Bottaro, Magnetic molecularly imprinted polymers prepared by reversible addition fragmentation chain transfer polymerization for dispersive solid phase extraction of polycyclic aromatic

hydrocarbons in water, J. Chromatogra. A, 1610 (2020) 460534. https://doi.org/10.1016/j.chroma.2019.460534

[108] M. Arabi, A. Ostovan, J. Li, X. Wang, Z. Zhang, J. Choo, L. Chen, Molecular imprinting: Green perspectives and strategies, Adv. Mater., 33 (2021) 2100543. https://doi.org/10. 1002/adma.202100543

[109] J. Ashley, M.-A. Shahbazi, K. Kant, V.A. Chidambara, A. Wolff, D.D. Bang, Y. Sun, Molecularly imprinted polymers for sample preparation and biosensing in food analysis: Progress and perspectives, Biosens. Bioelectron., 91 (2017) 606-615. https://doi.org/10.1016/j. bios.2017.01.018

[110] M. Lasáková, P. Jandera, Molecularly imprinted polymers and their application in solid phase extraction, J. Sep. Sci., 32 (2009) 799-812. https://doi.org/10.1002/ jssc.200800506

[111] D. Wang, X. Chen, J. Feng, M. Sun, Recent advances of ordered mesoporous silica materials for solid-phase extraction, J. Chromatogra. A, 1675 (2022) 463157. https://doi.org/10. 1016/j.chroma.2022.463157

[112] L. Liu, M. Yang, M. He, T. Liu, F. Chen, Y. Li, X. Feng, Y. Zhang, F. Zhang, Magnetic solid phase extraction sorbents using methyl-parathion and quinalphos dual-template imprinted polymers coupled with GC-MS for class-selective extraction of twelve organophosphorus pesticides, Microchim. Acta, 187 (2020) 1-12. https://doi.org/10.1007/s00604-020-04465-7

[113] A. Andrade-Eiroa, M. Canle, V. Leroy-Cancellieri, V. Cerdà, Solid-phase extraction of organic compounds: A critical review (Part I), TrAC Trends Anal. Chem., 80 (2016) 641-654. https://doi.org/10.1016/j.trac.2015.08.015

[114] R. Chauhan, J. Singh, T. Sachdev, T. Basu, B. Malhotra, Recent advances in mycotoxins detection, Biosens. Bioelectron., 81 (2016) 532 - 545. https: // doi. org/ 10. 1016/ j. bios. 2016.03.004

[115] S. Khan, T. Bhatia, P. Trivedi, G. Satyanarayana, K. Mandrah, P.N. Saxena, M.K.R. Mudiam, S.K. Roy, Selective solid-phase extraction using molecularly imprinted polymer as a sorbent for the analysis of fenarimol in food samples, Food Chem., 199 (2016) 870-875. https://doi.org/10.1016/j.foodchem.2015.12.091

[116] X. Wang, Q. Tang, Q. Wang, X. Qiao, Z. Xu, Study of a molecularly imprinted solid-phase extraction coupled with high-performance liquid chromatography for simultaneous determination of trace trichlorfon and monocrotophos residues in vegetables, J. Sci. Food Agric., 94 (2014) 1409-1415. https://doi.org/10.1002/jsfa.6429

[117] H. Hashemi-Moghaddam, D.J. Jedi, Solid-phase microextraction of chlorpyrifos in fruit samples by synthesised monolithic molecularly imprinted polymer fibres, Int. J. Environ. Ana. Chem., 95 (2015) 33-44. https://doi.org/10.1080/03067319.2014. 983495

[118] G. Vas, K. Vekey, Solid-phase microextraction: a powerful sample preparation tool prior to mass spectrometric analysis, J. Mass Spectrometry, 39 (2004) 233-254. https://doi.org/10. 1002/jms.606

[119] M. Zhang, J. Zeng, Y. Wang, X. Chen, Developments and trends of molecularly imprinted solid-phase microextraction, J. Cchromatogra. Sci., 51 (2013) 577-586. https://doi. org/10.1093/chromsci/bms260

[120] Y.-L. Wang, Y.-L. Gao, P.-P. Wang, H. Shang, S.-Y. Pan, X.-J. Li, Sol–gel molecularly imprinted polymer for selective solid phase microextraction of organophosphorous pesticides, Talanta, 115 (2013) 920-927. https://doi.org/10.1016/j.talanta.2013.06.056

[121] T. Zhao, X. Guan, W. Tang, Y. Ma, H. Zhang, Preparation of temperature sensitive molecularly imprinted polymer for solid-phase microextraction coatings on stainless steel fiber to measure ofloxacin, Anal. Chim. Acta, 853 (2015) 668-675. https://doi.org/10.1016/j.aca. 2014.10.019

[122] J. Xu, S. Ambrosini, E. Tamahkar, C. Rossi, K. Haupt, B. Tse Sum Bui, Toward a universal method for preparing molecularly imprinted polymer nanoparticles with antibody-like

affinity for proteins, Biomacromol., 17 (2016) 345-353. https://doi.org/10.1021/acs.biomac.5b01454

[123] H. Sabik, J. Fortin, N. Martin, Identification of pyrazine derivatives in a typical maple syrup using headspace solid-phase microextraction with gas chromatography–mass spectrometry, Food Chem., 134 (2012) 1711-1711. https://doi.org/10.1016/j.foodchem.2011.07.132

[124] L. Chen, B. Li, Application of magnetic molecularly imprinted polymers in analytical chemistry, Anal. Methods, 4 (2012) 2613-2621. https://doi.org/10.1039/C2AY25354B

[125] N. Karaseva, T. Ermolaeva, B. Mizaikoff, Piezoelectric sensors using molecularly imprinted nanospheres for the detection of antibiotics, Sens. Actuators B: Chem., 225 (2016) 199-208. https://doi.org/10.1016/j.snb.2015.11.045

[126] N. Kumar, N. Narayanan, S. Gupta, Application of magnetic molecularly imprinted polymers for extraction of imidacloprid from eggplant and honey, Food Chem., 255 (2018) 81-88. https://doi.org/10.1016/j.foodchem.2018.02.061

[127] A. Wang, H. Lu, S. Xu, Preparation of magnetic hollow molecularly imprinted polymers for detection of triazines in food samples, J. Agric. Food Chem., 64 (2016) 5110-5116. https://doi.org/10.1021/acs.jafc.6b01197

[128] P.A.S. Tette, L.R. Guidi, M.B. de Abreu Glória, C. Fernandes, Pesticides in honey: A review on chromatographic analytical methods, Talanta, 149 (2016) 124-141. https://doi.org/10.1016/j.talanta.2015.11.045

[129] L. Wiest, A. Buleté, B. Giroud, C. Fratta, S. Amic, O. Lambert, H. Pouliquen, C. Arnaudguilhem, Multi-residue analysis of 80 environmental contaminants in honeys, honeybees and pollens by one extraction procedure followed by liquid and gas chromatography coupled with mass spectrometric detection, J. Chromatogr. A, 1218 (2011) 5743-5756. https://doi.org/10.1016/j.chroma.2011.06.079

[130] M.W. Kujawski, Ż. Bargańska, K. Marciniak, E. Miedzianowska, J.K. Kujawski, M. Ślebioda, J. Namieśnik, Determining pesticide contamination in honey by LC-ESI-MS/MS – Comparison of pesticide recoveries of two liquid–liquid extraction based approaches, LWT-Food Sci. Technol., 56 (2014) 517-523. https://doi.org/10.1016/j.lwt.2013.11.024

[131] A. Tabrizi, F. Golbabaei, H. Shirkhanloo, M. Jafarizaveh, K. Azam, R. Yarahmadi, Evaluation of the adsorption capacity of nano-graphene and nanographene oxide for xylene removal from air and their comparison with the standard adsorbent of activated carbon to introduce the optimized one, J. Health Safe. Work, 6 (2016) 25-34. https://jhsw.tums.ac.ir/article-1-5415-en.html

[132] F.H. Salami, M.E.C. Queiroz, Microextraction in packed sorbent for the determination of pesticides in honey samples by gas chromatography coupled to mass spectrometry, J. Chromatogr. Sci., 51 (2013) 899-904. https://doi.org/10.1093/chromsci/bms187

[133] G. Amendola, P. Pelosi, R. Dommarco, Solid-phase extraction for multi-residue analysis of pesticides in honey, J. Environ. Sci. Health Part B, 46 (2010) 24-34. https://doi.org/10.1080/03601234.2010.515170

[134] S. Panseri, A. Catalano, A. Giorgi, F. Arioli, A. Procopio, D. Britti, L. Chiesa, Occurrence of pesticide residues in Italian honey from different areas in relation to its potential contamination sources, Food Control, 38 (2014) 150-156. https://doi.org/10.1016/j.foodcont.2013.10.024

[135] M.A. Farajzadeh, M.R.A. Mogaddam, H. Ghorbanpour, Development of a new microextraction method based on elevated temperature dispersive liquid–liquid microextraction for determination of triazole pesticides residues in honey by gas chromatography-nitrogen phosphorus detection, J. Chromatogr. A, 1347 (2014) 8-16. https://doi.org/10.1016/j. chroma.2014.04.067

[136] D.R. López, D.A. Ahumada, A.C. Díaz, J.A. Guerrero, Evaluation of pesticide residues in honey from different geographic regions of

Colombia, Food Control, 37 (2014) 33-40. https://doi.org/10.1016/j.foodcont.2013.09.011

[137] Z. Du, M. Liu, G. Li, Novel magnetic SPE method based on carbon nanotubes filled with cobalt ferrite for the analysis of organochlorine pesticides in honey and tea, J. Sep. Sci., 36 (2013) 3387-3394. https://doi.org/10.1002/jssc.201300710

[138] F.M. Malhat, M.N. Haggag, N.M. Loutfy, M.A. Osman, M.T. Ahmed, Residues of organochlorine and synthetic pyrethroid pesticides in honey, an indicator of ambient environment, a pilot study, Chemosphere, 120 (2015) 457-461. https://doi.org/10.1016/j.chemosphere.2014.08. 032

[139] S.O. Salihu, Synthesis and antimicrobial activity of schiff bases derived from 5-chlorosalicylaldehyde with substituted aniline, Appl. Chem., 101(2016) 43578-42581. http://repository.futminna.edu.ng:8080/jspui/handle/123456789/5955

[140] C. Yu, B. Hu, Sol–gel polydimethylsiloxane/poly(vinylalcohol)-coated stir bar sorptive extraction of organophosphorus pesticides in honey and their determination by large volume injection GC, J. Sep. Sci., 32 (2009) 147-153. https://doi.org/10.1002/jssc. 200800486

[141] M.W. Kujawski, J. Namieśnik, Levels of 13 multi-class pesticide residues in Polish honeys determined by LC-ESI-MS/MS, Food Control, 22 (2011) 914-919. https://doi.org/10.1016/j.foodcont.2010.11.024

[142] M. Mohammadi Asl, Simultaneity comparative evaluation of toluene removal from the air by adsorption and UV semi-degradation-based adsorption procedure, Int. J. Environ. Sci. Technol., 21 (2024) 6677-6694. https://doi.org/10.1007/s13762-024-05503-0

[143] Y.R. Tahboub, M.F. Zaater, T.A. Barri, Simultaneous identification and quantitation of selected organochlorine pesticide residues in honey by full-scan gas chromatography–mass spectrometry, Analytica Chimica Acta, 558 (2006) 62-68. https://doi.org/10.1016/j.aca.2005.11. 004.

[144] M. Jafarizaveh, H. Shirkhanloo, F. Golbabaei, A. Tabrizi, K. Azam, M. Ghasemkhani, Nobel method for xylene removal from air on nano activated carbon adsorbent compared to NIOSH approved carbon adsorbent**,** J. Health Safe. Work, 6 (2016) 23-30. http://jhsw.tums.ac.ir/article-1-5374-en.html

[145] C. Pirard, J. Widart, B.K. Nguyen, C. Deleuze, L. Heudt, E. Haubruge, E. De Pauw, J.-F. Focant, Development and validation of a multi-residue method for pesticide determination in honey using on-column liquid–liquid extraction and liquid chromatography–tandem mass spectrometry, J. Chromatogr. A, 1152 (2007) 116-123. https://doi.org/10.1016/j.chroma.2007.03.035

[146] M. Fernández, Y. Picó, J. Manes, Analytical methods for pesticide residue determination in bee products, J. Food Prot., 65 (2002) 1502-1511. https:// doi.org/ 10.4315/ 0362-028X-65.9.1502

[147] G.P. de Pinho, A.A. Neves, M.E.L.R. de Queiroz, F.O. Silvério, Optimization of the liquid–liquid extraction method and low temperature purification (LLE–LTP) for pesticide residue analysis in honey samples by gas chromatography, Food Control, 21 (2010) 1307-1311. https://doi.org/10.1016/j.foodcont.2010.03.006

[148] O. Chienthavorn, K. Dararuang, A. Sasook, N. Ramnut, Purge and trap with monolithic sorbent for gas chromatographic analysis of pesticides in honey, Anal. Bioanal. Chem., 402 (2012) 955-964. https://doi.org/10.1007/s00216-011-5468-3

[149] B. Albero, C. Sánchez-Brunete, J.L. Tadeo, Analysis of pesticides in honey by solid-phase extraction and gas chromatography−mass spectrometry, J. Agric. Food Chem., 52 (2004) 5828-5835. https://doi.org/10.1021/jf049470t

[150] K. Wille, M. Claessens, K. Rappé, E. Monteyne, C.R. Janssen, H.F. De Brabander, L. Vanhaecke, Rapid quantification of pharmaceuticals and pesticides in passive samplers using ultra high performance liquid chromatography coupled to high resolution

mass spectrometry, J. Chromatogr. A, 1218 (2011) 9162-9173. https://doi.org/10.1016/j.chroma.2011.10.039

[151] Y. Al Naggar, G. Codling, A. Vogt, E. Naiem, M. Mona, A. Seif, J.P. Giesy, Organophosphorus insecticides in honey, pollen and bees (*Apis mellifera* L.) and their potential hazard to bee colonies in Egypt, Ecotox. Environ. Safe., 114 (2015) 1-8. https://doi.org/10.1016/j.ecoenv.2014.12.039

[152] P. Jovanov, V. Guzsvány, M. Franko, S. Lazić, M. Sakač, B. Šarić, V. Banjac, Multi-residue method for determination of selected neonicotinoid insecticides in honey using optimized dispersive liquid–liquid microextraction combined with liquid chromatography-tandem mass spectrometry, Talanta, 111 (2013) 125-133. https://doi.org/10.1016/j.talanta.2013.02.059

[153] M. Li, J. Zhang, Y. Li, B. Peng, W. Zhou, H. Gao, Ionic liquid-linked dual magnetic microextraction: A novel and facile procedure for the determination of pyrethroids in honey samples, Talanta, 107 (2013) 81-87. https://doi.org/10.1016/j.talanta.2012.12.056

[154] J. Vichapong, R. Burakham, S. Srijaranai, In-coupled syringe assisted octanol–water partition microextraction coupled with high-performance liquid chromatography for simultaneous determination of neonicotinoid insecticide residues in honey, Talanta, 139 (2015) 21-26. https:// doi.org/ 10.1016/ j.talanta.2015.02.033

[155] M.R. Sampaio, D. Tomasini, L.V. Cardoso, S.S. Caldas, E.G. Primel, Determination of pesticide residues in sugarcane honey by QuEChERS, and liquid chromatography, J. Brazil. Chem. Soc., 23 (2012) 197-205. https://doi.org/10.1590/S0103-50532012000 200002 .

[156] D. Debayle, G. Dessalces, M.F. Grenier-Loustalot, Multi-residue analysis of traces of pesticides and antibiotics in honey by HPLC-MS-MS, Anal. Bioanal. Chem., 391 (2008) 1011-1020. https://doi.org/10.1007/s00216-008-2003-2

[157] M.L. Gómez-Pérez, P. Plaza-Bolaños, R. Romero-González, J.L. Martínez-Vidal, A. Garrido-Frenich, Comprehensive qualitative and quantitative determination of pesticides and veterinary drugs in honey using liquid chromatography–Orbitrap high resolution mass spectrometry, J. Chromatogr. A, 1248 (2012) 130-138. https://doi.org/10.1016/j.chroma.2012.05.088

[158] D. Tomasini, M.R. Sampaio, S.S. Caldas, J.G. Buffon, F.A. Duarte, E.G. Primel, Simultaneous determination of pesticides and 5-hydroxymethylfurfural in honey by the modified QuEChERS method and liquid chromatography coupled to tandem mass spectrometry, Talanta, 99 (2012) 380-386. https://doi.org/10.1016/j.talanta.2012.05.068

[159] K.M. Kasiotis, C. Anagnostopoulos, P. Anastasiadou, K. Machera, Pesticide residues in honeybees, honey and bee pollen by LC–MS/MS screening: Reported death incidents in honeybees, Sci. Total Environ., 485 (2014) 633-642. https://doi.org/10.1016/j.scitotenv.2014.03.042

[160] C. Blasco, M. Fernández, Y. Picó, G. Font, Comparison of solid-phase microextraction and stir bar sorptive extraction for determining six organophosphorus insecticides in honey by liquid chromatography–mass spectrometry, J. Chromatogr. A, 1030 (2004) 77-85. https://doi.org/10.1016/j.chroma.2003.11.037